Self-powered biosensors for water quality monitoring: sensor design and signal treatment

(Alternative Format Thesis)

Gonzalez, Dolores

Award date:
2021

Awarding institution:
University of Bath

Self-powered biosensors for water quality monitoring: sensor design and signal treatment

Dolores González Olías

A thesis submitted for the degree of Doctor of Philosophy

University of Bath Department of Chemical Engineering

December 2020

Table of contents

Abstract

Increasing water pollution is limiting the availability of safe water sources worldwide. Reducing pollution requires *in situ*, online and continuous monitoring of water quality, to identify the source and fate of these contaminants. To do so, improvements on the stability and autonomy of current sensing technologies are necessary. This PhD Thesis proposes to meet these goals using microbial fuel cell (MFC) sensors with a cathodic sensing element. Specifically, the detection of pesticides in water with a MFC with an algal biocathode receptor is evaluated. The current output correlates with the dissolved oxygen (DO) concentration in the catholyte, an indicator of photosynthetic activity in the algal biofilm. The MFC sensor could detect the EU limit concentration of 0.1 µg L^{-1} of atrazine in 2.6 h. Two electrode materials, graphite felt and indium tin oxide (ITO), were investigated to evaluate the effect of porosity and transparency in the performance. The MFCs with graphite felt showed shorter response times and better sensitivity, as a result of a ten times greater baseline output than with ITO.

To improve the portability, robustness and affordability of MFC sensors, a ceramic based, soil-MFC (CSMFC) with an algal biocathode was designed as an early warning device to detect pesticides in water. The detection of single toxic events of 0.1 µg L^{-1} of the herbicides Diuron and glyphosate was statistically significant ($\alpha = 0.01$) based on changes in accumulated charge and accumulated variance, in five days before and after the toxic event. The correlation of the signal with DO reversed at 9 mg L^{-1} due to the detrimental effect of oxygen on the anode at higher DO. To solve this, the volume of the CSMFC was increased and the algal biocathode eliminated. The CSMFC was tested to detect hypoxia in water bodies by monitoring the cathodic reduction rate of oxygen. The CSMFC sensors responded instantaneously to changes in DO in a linear range from 0 to 6 mg L^{-1}.

To reduce maintenance of the sensors in the field, a single-point calibration method was developed based on a design of experiments (DoE), to correlate the DO with the CSMFC signal, showing an error of 0.05 mg L^{-1}.

The CSMFC sensors were also tested for early detection of eutrophic events. The photosynthetic pattern, an indication of algal activity, was captured in the signal

output, with a correlation with DO in the catholyte of R^2=0.85 in the day and R^2=0.52 in the night, up to an algal optical density (Abs=750 nm) of 0.2. A screening DoE design concluded that nitrates, which are present in eutrophic waters, compete with oxygen for the cathodic reduction, reducing the sensitivity of the sensor to photosynthetic activity, particularly at low DO.

The long-term autonomy of the soil MFC signal output was also investigated. The presence of algae in the catholyte provides a continuous source of organic matter to the anode biofilm. The system sustained an increasing voltage from 1 to 15 mV continuously, for a year.

All experiments were carried out without feeding or maintenance of the sensors, showing the potential autonomy of these devices.

Acknowledgements

I would like to thank the Biofuel and Biosensors group for their help and support during these three years. Special thanks to my supervisors Mirella Di Lorenzo and Petra Cameron for their guidance and feedback, and for being always available to help me. Thanks to Prof. Chris Chuck for letting me use his equipment and for his help during the first year. I would also like to acknowledge the help given by Brigite, Fernando, Cassie, Bob, Greg, Angela, Vio, Andrew and Laura, that has made possible the completion of this work.

I want to thank the WISE committee for giving me the chance to make a contribution towards a sustainable future through my PhD. Special thanks to Tom and Debbie for taking care of us at all moments.

Thanks to Alba Rodriguez and Merryl for being the best students ever. Your help was invaluable and made a great difference in this thesis.

Jamie, I can't stress enough how much you helped me through my last year, both in my career and personal life. I am grateful for all the efforts you made to help me finish the experiments, and for reminding me that science is fun and exciting.

Thanks to my friends in the UK, particularly Simbi, Levke, Mat and Jackie, who always supported me through the toughest moments and accompanied me in the best ones. Cohort 3 will always be with me.

A mis padres.

Dissemination

Published papers

Olías L.G., Cameron P., Di Lorenzo M. “Effect of Electrode Properties on the Performance of a Photosynthetic Microbial Fuel Cell for Atrazine Detection”, Frontiers in Energy Research, 7 pp. 1-11 (2019).

Olías L.G., Fernandez A., Cameron A., Di Lorenzo M. “A novel soil microbial fuel cell-based biosensor for dissolved oxygen monitoring in water”, Electrochimica Acta vol.362 137108 (2020).

Olías L.G., Di Lorenzo M. “Microbial Fuel Cell biosensors for in field monitoring of water quality”. RSC Advances, 11, 16307-16317 (2021).

Conference proceedings

Olías L.G., Fernandez A., Cameron P., Di Lorenzo M. “Use of a soil microbial fuel cell-based biosensor for early detection of eutrophic events”. Submitted to MDPI Proceedings.

Olías L.G., Di Lorenzo M. “In situ monitoring of dissolved oxygen in water with a hybrid photosynthetic soil microbial fuel cell biosensor”. Proceedings of EFC2019 European Fuel Cell Technology & Applications Conference - Piero Lunghi Conference December 9-11, (2019), Naples, Italy.

Olías L.G., Di Lorenzo M. “Investigating the use of Photosynthetic Sediment Microbial Fuel Cells for pesticide detection in water”. 3th International MEEP Symposium Proceedings, (2019), Lucerne, Switzerland.

Conference posters

Olías L.G., Fernandez A. Di Lorenzo M. “Soil Microbial Fuel Cell for environmental dissolved oxygen monitoring”. Poster presentation at C3Bio Conference, (2019), University of Bath, Bath (UK).

Olías L.G., Fernandez A. Di Lorenzo M. “Comparison of ITO and Carbon Felt cathodes for self-powered biosensors for water quality monitoring”. Electrochemical Conference on Energy and the Environment: Bioelectrochemistry and Energy Storage, (2019), Glasgow, UK.

Olías L.G., Cameron P., Hofman, J. Di Lorenzo M. “Self-powered biosensors for water quality monitoring”. Poster presentation at the 4th EU-ISMET, (2018), Newcastle upon Tyne, UK.

Olías L.G., Hofman, J.,Cameron P. “Biosensor development and signal processing for real-time water quality monitoring”. Presentation at 19th UK-IWA Young Water Professionals Conference, (2018), Cranfield University, Cranfield, UK.

Awards

- STFC Batteries Sponsorship for Bath Summer School in Electrochemistry (2017).
- Best Poster Presentation, WISE CDT Summer School (2018).
- SRUK Summer Studentship for a 3-month student research project (2019).
- SCELSE Summer School Scholarship: course and travel expenses (2019).
- EPSRC Travel Award: 2000 £ (2020).

List of Figures

List of Tables

Nomenclature

Symbol	Definition	Units
A	Electrode projected surface area	m^2
A_{an}	Anode projected surface area	m^2
DO_{sat}	Saturated dissolved oxygen	mg L^{-1}
D_{med}	Diffusion coefficient of mediator	m^2 s^{-1}
E_{an}	Anode potential	mV
E_{cat}	Cathode potential	mV
E_{cell}	Cell voltage	mV
E_{emf}	Electromotive force	mV
E_{KA}	Potential at j=jmax/2	V
E_{OM}	Potential outer membrane	V
F	Faraday constant	C mol_{-1}
I	Current density	mA m^{-2}
I_b	Baseline of current density in the light	mA m^{-2}
I_c	Limiting current density	mA m^{-2}
I_{db}	Current density baseline in the dark	mA m^{-2}
I_{dnb}	Current density baseline after the event in the dark	mA m^{-2}
I_{max}	Maximum current density	mA m^{-2}
I_{nb}	Baseline of current density after the event in the light	mA m^{-2}
J_{sc}	Short-circuit current density	mA m^{-2}
j	Exchange current density	A m^{-2}
j_{max}	Maximum exchange current density	A m^{-2}
K_A	Half saturation constant of electron acceptor	e^-meq cm^{-3}
k_{bio}	Conductivity of mediator	Ω^{-1} cm^{-1}
K_s	Half-saturation constant	mg L^{-1}
L_f	Biofilm thickness	cm
m_{105}	Weight after drying at 105 ˚C	g
m_{550}	Weight after ignition at 550 ˚C	g
OCP	Open Circuit Potential	mV
OCV	Open Circuit Voltage	mV
P_d	Power density	mW m^{-2}
P_{max}	Maximum power density	mW m^{-2}
q_{max}	Maximum specific rate of substrate utilisation	e^-meq mg^{-1}
R	Ideal gas constant	J mol^{-1} K^{-1}
R_{ext}	External resistance	Ω
R_{int}	Internal resistance	Ω
$R_Ω$	Ohmic resistance	Ω
S_A	Concentration of electron acceptor	e^-meq cm^{-3}
T	Temperature	°C
t_A	Time at injection point A	h
t_C	Time at new baseline C	h
t_D	Time at recovery baseline D	h
t_{lag}	Lag time	h
t_r	Response time	h
t_{rec}	Recovery time	h
V	Voltage	mV
V_{max}	Maximum voltage	mV
X_f	Concentration of active biomass	mg cm^{-3}
d	Distance between electrodes	m
ΔE/ΔI	Slope of the polarisation curve	Ω
$ΔG_r$	Gibbs free energy	kJ mol^{-1}
α	Charge transfer coefficient	-
$η_a$	Anode overpotential	mV
$η_c$	Cathode overpotential	mV

Acronyms

ANOVA	Analysis of variance
ATP	Adenosine tri phosphate
AWW	Artificial wastewater
BBM	Bold Basal Medium
BOD	Biological oxygen demand
CC	Carbon cloth
CE	Counter electrode
COD	Chemical oxygen demand
CoTMPP	Tetramethoxyphenyl porphyrin cobalt (II)
CP	Carbon paper
CSMFC	Ceramic soil microbial fuel cell
CV	Cyclic voltammetry
Cyt-C	Cytochrome C
$DC_{control}$	Double chamber control
DC_{toxic}	Double chamber toxic
DET	Direct electron transfer
DNA	Deoxyribonucleic acid
DO	Dissolved oxygen
DO_m	Measured dissolved oxygen
DO_p	Predicted dissolved oxygen
DoE	Design of experiments
EET	Extracellular electron transfer
EU	European Union
$FADH_2$	Flavin adenine dinucleotide
FTO	Fluoride titanium oxide
GC	Gas chromatography
GF	Graphite felt
HPLC	High performance liquid chromatography
IR	Inhibition ratio
ITO	Indium titanium oxide
LED	Light emitting diode
LOD	Limit of detection
LOI	Loss of ignition
LSM	Linear squares model
LSV	Linear sweep voltammetry
MEA	Membrane electrode assembly
MET	Mediated electron transfer
MFC	Microbial fuel cell
MS	Mass spectroscopy
NADH	Nicotinamide adenine dinucleotide
OFAT	One factor at the time
ORR	Oxygen reduction reaction
p-MFC	Photosynthetic microbial fuel cell
$p\text{-}MFC_{GF}$	Photosynthetic microbial fuel cell with graphite felt cathodes
$p\text{-}MFC_{ITO}$	Photosynthetic microbial fuel cell with ITO cathodes
PSII	Photosynthetic system II
PTFE	Polytetrafluoroethylene
RE	Reference electrode
RMSE	Root of mean squared error
RSS	Residual sum of squares
SCE	Standard calomel electrode
SEM	Scanning electron microscopy
SHE	Standard hydrogen electrode
SMFC	Soil microbial fuel cell
$SMFC_{1cm}$	Soil microbial fuel cell in 1 cm of soil
$SMFC_{3cm}$	Soil microbial fuel cell in 3 cm of soil
$SMFC_{Algae}$	Soil microbial fuel cell with algal catholyte

$SMFC_{Control}$	Soil microbial fuel cell with non-algal cathoyte
SR	Rate of signal reduction
TOC	Total Organic Carbon
TSS	Total sum of squares
VFA	Volatile fatty acids
WE	Working electrode
WFD	Water Framework Directive
WW	Wastewater
WWTP	Wastewater treatment plan

Chapter 1

1. Introduction

1.1 The water quality crisis

Population growth, rapid urbanisation, intensified food production and industrial development increase water pollution globally [1]. More than 80% of the wastewater resulting from these activities is discharged into rivers and seas without any treatment, resulting in more than one billion people exposed to unsafe water sources [2].

Unprecedent levels of water pollution pose unknown consequences for biota and human health, that need to be identified and managed [3]. In-field monitoring of highly persistent and globally spread contaminants sets exceptional challenges for detection methods. Detection of infrequent extreme events, such as sudden discharges or heavy rainfall, requires increased frequency of data acquisition and spatial coverage of sensing technologies [4].

Current water monitoring techniques comprise remote and field tests. Remote sensing technologies include visible, infrared, near-infrared, ultraviolet, radar, microwave, laser-acoustic and laser-fluorescence. These, provide wide coverage and high precision imaging capability, but suffer from high costs, interferences caused by aquatic plants and weather, and slow data collection [5, 6].

Field tests involve *in situ* determination of global indicators of water quality such as pH, conductivity, temperature and dissolved oxygen (DO). These tests are frequently performed in rivers, but intermittently in lakes and groundwater [7]. Temperature, pH, and conductivity sensors are low-cost and easy to implement.

DO sensors, whether optical or electrochemical, are relatively more expensive and require regular maintenance [8].

Other indicators, like nitrates and phosphates, emerging contaminants or mining products are usually determined using lab-bench analytical methods, i.e. gas/liquid chromatography or mass spectroscopy [9]. While accurate and sensitive, analytical methods are offline, expensive, time consuming, require specialised equipment and highly trained technicians, and do not detect the bioavailability and accumulation of pollutants in living organisms [10,11]. These features are generally assessed with bioassays and biosensors [10].

Bioassays evaluate the impact of a water sample, containing one or more pollutants, on living organisms. The toxicity, acute or chronic, is evaluated based on indicators, such as growth rate or fluorescence [11]. Bioassays are suitable for non-specific monitoring of water toxicity. Selectivity, sensitivity and response time depend on the characteristics of the bioreceptor, improving with simpler and smaller organisms such as bacteria or algae. Bioassays, however, are time consuming and not portable, hence not suitable for *in situ* monitoring of water quality [11].

Biosensors are analytical devices that combine a bioreceptor with a transducer to produce a signal that can be correlated with the identity and quantity of a pollutant [12] (Figure 1.1). The main difference with bioassays is that, in biosensors the transducer is external to the sensing element and the assay is faster. As such, biosensors can be classified by the bioreceptor or the method of signal transduction [10].

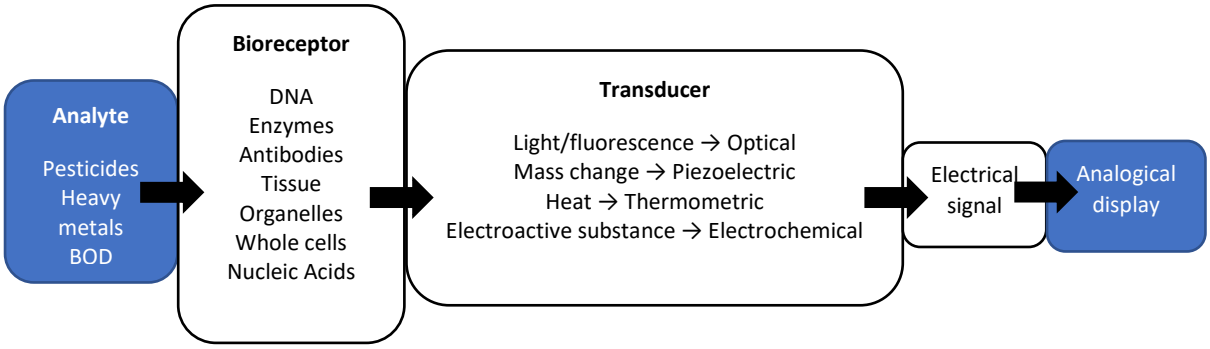

Figure 1.1 *Flow of information in a biosensor. The analyte reacts with the specific sensing element (bioreceptor) inducing a change from normal conditions. The change is traduced into a signal (transducer) and turned into an electrical signal.*

Table 1.1 shows that, amongst the available sensing techniques, biosensors, particularly whole-cell biosensors, are the most promising technology for continuous and *in situ* environmental water quality monitoring, thanks to comparatively better portability, bioreceptor stability and simplicity in signal transduction. Extraction and purification of the sensing element is also not required, as is an *in vivo* test. Whole cells contain multiple sensing elements, such as enzymes and organelles, that can be targeted simultaneously in a toxic event, producing a complex signal with lower selectivity than other biosensors based on single sensing elements [13].

Table 1.1**. Comparison of current methods for water quality monitoring.**

Method	Type	Advantages	Disadvantages	Ref.
Analytical	HPLC GC GC-MS Capillarity Electrophoresis Colorimetric methods Flame atomic absorption spectrometry	Accuracy Sensitivity Specificity	Time consuming Sample pre-treatment Expensive equipment Lab-based Single compound No synergic effect Skilled personnel	[14] [15] [12]
Bioassay	Fish Invertebrates Microbes Algae	Mixtures Synergistic effect Biological impact Detection range Bioavailability	Low specificity and sensitivity Difficult to handle Slow response Ethically objectionable Can be expensive Low reproducibility	[11]
Biosensor	Electrochemical Optical Piezoelectric	Sensitivity Bioavailability Portable	Needs transducer Long-term stability Power supply Bioreceptor stability	[10] [16]

Electrochemical whole-cell biosensors can be portable and could operate autonomously in the field, but the long-term performance, autonomy and reusability of the sensors need to be improved to achieve efficient field-based water quality monitoring. Microbial Fuel Cell (MFC) sensors are a relatively novel type of whole-cell electrochemical biosensors that could solve these issues.

1.2 Microbial Fuel Cell sensors

A microbial fuel cell (MFC) is a galvanic cell comprising two electrodes, anode and cathode, immersed in an electrolyte, where chemical energy is converted into electrical energy by the action of electroactive bacteria. The magnitude and shape

of the MFC signal output is closely related to the bacterial metabolism, becoming a direct indicator of the impact of toxicants in microorganisms [17] (Figure 1.2).

At the anode, always biotic, organic carbon is oxidised to CO_2, electrons and protons or else, CO_2 is photocatalytically reduced to sugars [18]. At the cathode, either abiotic or biotic, migrated charged species reduce an oxidant (i.e. oxygen, nitrate, ferricyanide, manganese oxide) [19]. As the overall electrochemical process is exothermic, the signal output is self-powered, reducing the energy input required to operate the sensor. Additionally, because a transducer is not needed, the design of a MFC sensor is relatively simpler than other biosensors.

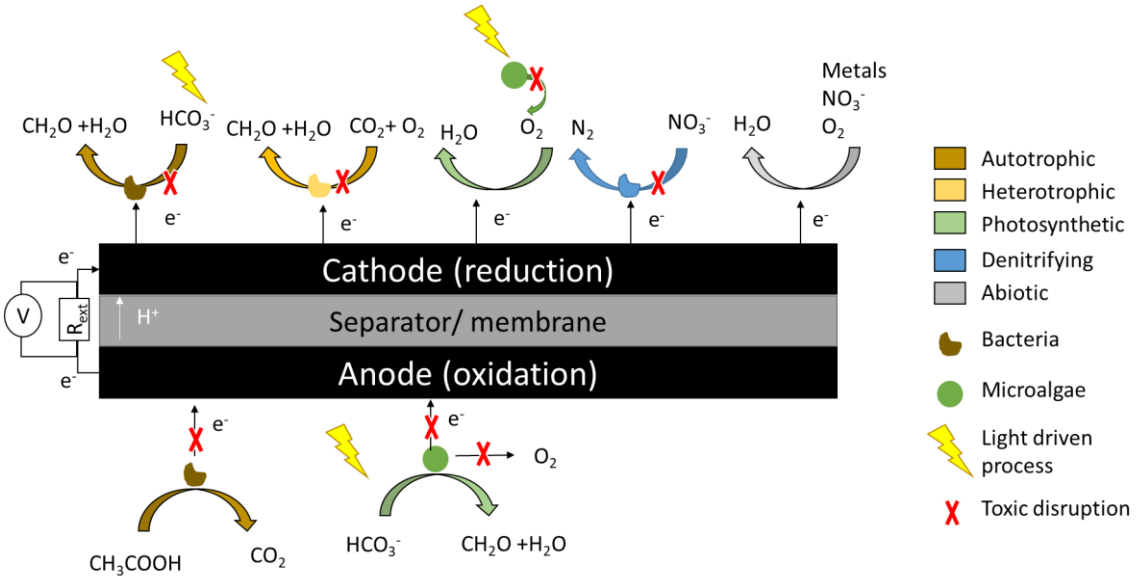

Figure 1.2 *Principles of operation of an MFC sensor. When the toxicant is in contact with the biofilm, a change in the electrical response is recorded. The biofilm is the sensing element containing the bioreceptor and the transducer.*

The field of MFC sensors is rapidly developing, with important improvements in long-term stability and performance over the past few years [18]. However, most of these studies are investigations of lab-based designs under controlled conditions. Practical designs, suitable for in field applications, as well as the performance evaluation of the sensor operating in real conditions, are required to fully develop MFC sensors for environmental water quality monitoring. Additionally, calibration models that can cope with high uncertainty and variability of the sensors signal are needed. This PhD thesis is an effort to overcome the limitations holding

back the use of MFC sensors, for long-term and unattended water quality monitoring in the environment.

1.3 Aims and objectives

The aims of this PhD are to design an MFC sensor for continuous, *in situ* water quality monitoring in real scenarios, and to provide methods of data analysis to improve the interpretation and prediction power of the signal generated by the sensor. The specific objectives to achieve these aims are:

- Objective 1: To proof the concept of a MFC sensor for pesticide detection with a cathodic algal biofilm as bioreceptor.
- Objective 2: To adapt and improve the experimental procedures and the performance indicators to implement the MFC sensors in the environment.
- Objective 3: To design a portable MFC sensor for continuous and unattended monitoring of dissolved oxygen in water bodies.
- Objective 4: To implement a factorial Design of Experiments (DoE) to characterise the MFC sensor response.
- Objective 5: To develop a statistical model with DoE to improve the prediction power of the sensor.
- Objective 6: To enhance the long-term autonomy of the MFC sensors.

1.4 Outline of the Thesis

Chapter 1 introduces the causes for the critical loss of water quality worldwide. The characteristics of water pollution are discussed, identifying the main challenges for environmental water monitoring. Next, a summary of current sensing techniques highlights the design limitations to overcome for online and in field operation of the sensors.

Chapter 2 presents a thorough review of the state-of-the-art research in MFC sensors for in field water quality monitoring. The most relevant performance indicators for environmental applications are discussed, followed by a summary of MFC sensors operated in real scenarios.

Chapter 3 explains the fundamentals of energy generation in a MFC sensor. It includes a discussion of the different mechanisms for extracellular electron transfer in bacteria, differentiating between direct and mediated extracellular electron transport. The electrochemical principles, energy balance and most common chemical reactions are described. The chapter ends with an overview of the electrochemical techniques used to characterise the MFC energy balance.

Chapter 4 provides the principles of Design of Experiments (DoE), the methodology implemented in this work to calibrate the sensor and study the influence of environmental factors in the signal. The steps to perform a factorial DoE on a MFC sensor are provided as a guideline to understand the experimental procedures of Chapters 7 and 8.

Chapter 5 describes the proof of concept of a MFC sensor, with a cathodic algal bioreceptor, for atrazine detection in water (Objective 1). Disturbances in the photosynthetic activity of algae are detected *via* oxygen reduction at the cathode. The performance of two cathode materials, carbon felt and indium-titanium oxide, are compared in terms of sensitivity, response time and signal recovery to toxic events of atrazine. Chapter 5 also introduces the analysis of the signal output based on the inhibition ratio to eliminate the need for a stable signal baseline (Objective 2).

Chapter 6 presents a novel, floating, ceramic-based, soil MFC (CSMFC) with an algal biocathode to detect pesticides in water *via* oxygen reduction reaction (Objective 1 and 3). Variations in photosynthetic DO due to toxicity are traduced into changes in the electrical signal output. The response, recovery and autonomy of the CSMFC sensor signal to 0.1 µg L^{-1} of the herbicides Diuron and glyphosate is evaluated. The study concludes with the characterisation of the signal features and a comparison of the performance indicators suitable for field based MFC sensors (Objective 2).

Chapter 7 presents a novel CSMFC design for continuous monitoring of dissolved oxygen in water (Objective 3). The influence of the most relevant environmental indicators: temperature, pH, conductivity and dissolved oxygen is assessed using a 4-factor DoE (Objective 4). Furthermore, a single-point calibration model, based on the 4-factor DoE regression model, is proposed to reduce the need for re-

calibration during field operation (Objective 5). The use of the CSMFC as early warning system for hypoxic events is evaluated.

In Chapter 8, the CSMFC sensors are evaluated for early detection of eutrophication, by monitoring algal activity through changes in photosynthetic dissolved oxygen (Objective 3). The calibration model developed in Chapter 7, is validated in this study highlighting its limitations to accurately predict the sensors output in this particular case (Objective 5). Chapter 8 also introduces a saturated DoE as a screening tool to identify the most important operational and design factors affecting the performance of the sensor (Objective 4).

The long-term stability of soil MFCs is addressed in Chapter 9 (Objective 6). Enrichment of the soil in algal biomass is presented as an option to ensure a continuous supply of organic matter in unattended operation. The effect of adding algae in the catholyte is assessed in terms of current output and soil organic content, in a year-long study.

Finally, Chapter 10 provides a summary on the key findings in this Thesis and offers guidance for future studies.

1.5 References

[1] E. Boelee, G. Geerling, B. van der Zaan, A. Blauw, and A. D. Vethaak, “Water and health: From environmental pressures to integrated responses,” *Acta Trop.*, vol. 193, no. March, pp. 217–226, 2019.

[2] “SDG 6 Synthesis Report 2018 on Water and Sanitation,” 2018.

[3] B. Petrie, R. Barden, and B. Kasprzyk-Hordern, “A review on emerging contaminants in wastewaters and the environment: Current knowledge, understudied areas and recommendations for future monitoring,” *Water Res.*, vol. 72, pp. 3–27, 2014.

[4] UNICEF and WHO, “Progress on household drinking water, sanitation and hygiene 2000-2017: Special focus on inequalities,” 2019.

[5] Z. Dai *et al.*, “In-situ oil presence sensor using simple-structured upward open-channel microbial fuel cell (UOC-MFC),” *Biosens. Bioelectron. X*, vol. 1, no. 2, p. 100014, 2019.

[6] H. B. Glasgow, J. A. M. Burkholder, R. E. Reed, A. J. Lewitus, and J. E. Kleinman, “Real-time remote monitoring of water quality: A review of current applications, and advancements in sensor, telemetry, and computing technologies,” *J. Exp. Mar. Bio. Ecol.*, vol. 300, no. 1–2, pp. 409–448, 2004.

[7] European Environmental Agency, “Assessment of information gaps in existing monitoring” Copenhagen, 2008.

[8] Y. Wei, Y. Jiao, D. An, D. Li, W. Li, and Q. Wei, “Review of dissolved oxygen detection technology: From laboratory analysis to online intelligent detection,” *Sensors (Switzerland)*, vol. 19, no. 18. pp.1-38, 2019.

[9] S. N. Zulkifli, H. A. Rahim, and W. J. Lau, “Detection of contaminants in water supply: A review on state-of-the-art monitoring technologies and their applications,” *Sensors and Actuators, B: Chemical*, vol. 255. pp. 2657–2689, 2018.

[10] J. Livage, “Micro-algal biosensors,” *Anal. Bioanal. Chem.*, vol. 401, no. October, pp. 581–579, 2011.

[11] S. H. A. Hassan, S. W. Van Ginkel, M. A. M. Hussein, R. Abskharon, and S.-E. Oh, “Toxicity assessment using different bioassays and microbial biosensors,” *Environ. Int.*, vol. 92–93, pp. 106–118, 2016.

[12] M. Mascini, “A Brief Story of Biosensor Technology,” *Biotechnol. Appl. Photosynth. Proteins Biochips, Biosens. Biodevices*, Chapter 2. pp. 4–10, 2006.

[13] L. Su, W. Jia, C. Hou, and Y. Lei, “Microbial biosensors: A review,” *Biosensors and Bioelectronics*, vol. 26, no. 5. pp. 1788–1799, 2011.

[14] A. Sassolas, B. Prieto-Simón, and J. Marty, “Biosensors for Pesticide Detection: New Trends,” *Am. J. Anal. Chem.*, vol. 03, no. 03, pp. 210–232, 2012.

[15] B. J. Vanderford *et al.*, “Results of an Interlaboratory Comparison of Analytical

Methods for Contaminants of Emerging Concern in Water," *Anal. Chem.*, vol. 86, pp. 774–782, 2014.

[16] Vigneshvar S, Sudhakumari CC, Senthilkumaran B and Prakash H "Recent Advances in Biosensor Technology for Potential Applications – An Overview". *Front. Bioeng. Biotechnol.* 4:11, 2016.

[17] M. Di Lorenzo, T. P. Curtis, I. M. Head, S. B. Velasquez-Orta, and K. Scott, "A single chamber packed bed microbial fuel cell biosensor for measuring organic content of wastewater," *Water Sci. Technol.*, vol. 60, no. 11, pp. 2879–2887, 2009.

[18] R. W. Bradley, P. Bombelli, S. J. L. Rowden, and C. J. Howe, "Biological photovoltaics: intra- and extra-cellular electron transport by cyanobacteria" *Biochem. Soc. Trans.*, vol. 40, no. 6, pp. 1302–1307, 2012.

[19] D. Ucar, Y. Zhang, and I. Angelidaki, "An overview of electron acceptors in microbial fuel cells," *Front. Microbiol.*, vol. 8, no. April, pp. 1–14, 2017.

Chapter 2

2. Literature review

To illustrate the degree of development and evaluate the potential of MFC sensors for environmental applications, Chapter 2 presents a thorough review of the state-of-the-art research, focusing on field based MFC designs for water quality monitoring. The most relevant performance indicators for environmental applications are discussed, followed by a summary of MFC sensor designs operated in real scenarios.

Statement of authorship

This declaration concerns the article entitled:

“Microbial fuel cells for in-field water quality monitoring”

Publication status: Published

Publication details: Olías L.G. and Di Lorenzo M. “Microbial fuel cells for in-field water quality monitoring”, RSC Advances,11,16307 (2021).

Author Contributions: L.G.: writing ,original draft preparation; MDL: supervision, review and editing.

Statement from candidate: This paper reports on original research I conducted during the period of my Higher Degree by Research candidature. In line with the regulations in QA7 Appendix 6 of the University of Bath, the abovementioned article has been stylistically integrated into the thesis, including: sections and figures numbering, typeface, margins and pagination.

Signed: Date:

2. Microbial Fuel Cells for environmental water quality monitoring

Lola Gonzalez Olias[1,2], Mirella Di Lorenzo[1,]*

[1] Centre for Biosensors, Bioelectronics and Biodevices (C3Bio) and Department of Chemical Engineering, University of Bath, Bath BA2 7AY, United Kingdom

[2] Water Innovation Research Centre (WIRC), University of Bath, Bath BA2 7AY, United Kingdom

Increasing pollution sets unprecedented challenges on water security that requires effective water quality monitoring to identify and control the source of contaminants. To provide an online and *in situ* status of water quality indicators, the development of sensing technologies, capable of autonomous and stable long-term operation is key. Microbial Fuel Cell (MFC) sensors have shown suitable long-term stability and autonomy to meet these requirements. MFC sensors have therefore attracted great attention in the last decade, with extensive results that were the object of several reviews. With the aim to provide direction to accelerate the implementation of MFC sensors, this review focuses on field applications, capturing key advances and limitations for long-term and unattended monitoring. In addition, the most relevant performance indicators for MFC sensors as early warning systems are identified, and algorithms to process the sensor signal for pollution events in environmental conditions are described. Finally, novel designs, materials and methods are proposed to solve some of the issues for practical implementation of MFC sensors in the environment.

Keywords: Early Warning System, Electrochemical Biosensors, Microbial Fuel Cell, Water Quality.

2.1 Microbial Fuel Cell as sensors for water quality monitoring

The first report of an MFC sensor dates back to 2003, when Kim et al. correlated the MFC signal with the organic content in the anolyte. The initial promising performance and long-term stability, up to 5 years [1] turned the attention towards MFC sensors, with various publications on detection of pH [2], volatile fatty acids (VFAs) [3, 4], pathogens [5], copper [6] chromium, iron, nitrate, and sodium acetate [7] ,cadmium [8], zinc [9] or pesticides [10], at constant organic loads and controlled environmental conditions. Although MFC sensors are already commercialised as benchtop detection devices for biological oxygen demand (BOD) and toxicity, widespread deployment of MFC sensors in the field remains a challenge.

To the best of our knowledge, the first study of an MFC sensor in the field was in 2007, to monitor uranium biodegradation in boreholes [11]. Here, the voltage output correlated with acetate, added to enhance uranium biodegradation. The sensor signal served as a proxy to monitor, and amend, the input of acetate to optimise uranium removal, over a period of 261 days. Acknowledging the particular suitability of MFC sensors for low income countries, in 2017 Velasquez et al. implemented low-cost sediment, and floating MFCs as early warning systems to detect faecal infiltration into a groundwater reservoir in Tanzania [12]. Although simple and effective, detection errors due to a high noise/signal ratio were important in this system. In the same year, Pasternak et al. designed a fully autonomous BOD sensor for anoxic waters. To reduce the signal noise, the output was converted into the frequency domain, as light and sound signals that worked as a detection beacon [13].

To push forward field applications, evaluation of the MFC sensor performance under field conditions is a must, yet the effect of materials, designs and operational conditions has been evaluated mostly in controlled conditions. Similarly, performance [14] and manufacturing [8] are assessed in a lab-based context.

The aim of this review is therefore to provide an overview of the most relevant findings and challenges of MFC sensors for practical environmental implementation. First, performance indicators for in field applications, which may

diverge from lab-based studies, are defined. MFC designs for environmental, off-grid monitoring of water quality are then discussed, focusing on enhancing robustness and long-term stability. Finally, the calibration methods and detection algorithms applicable in real scenarios are discussed.

2.2 Performance indicators for field based MFC sensors

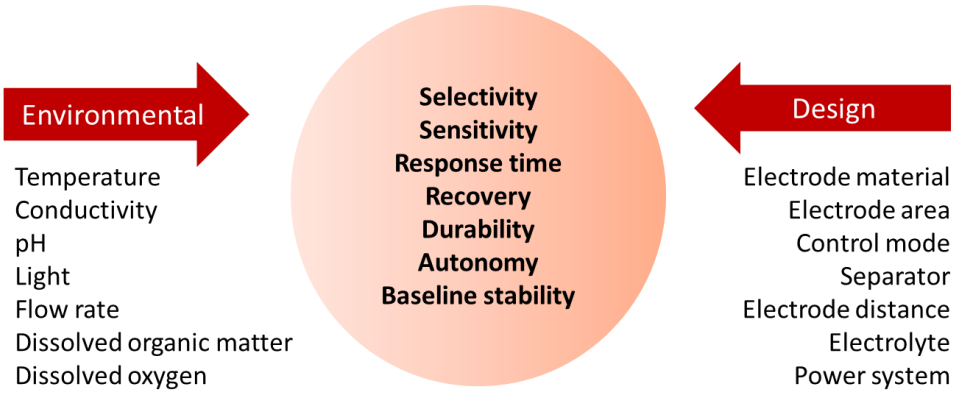

Figure 2.1 *Scheme of performance indicators and main influential factors.*

2.2.1 Selectivity

One of the major limitations in selectivity in MFC sensors, is the dependency of the anodic activity on the organic content in the anolyte. In lab-based studies, this issue is minimised by operating the system at saturating concentrations of BOD, generally using pumps, which is impractical for field applications [15, 16]. Soil based anodes [17] or solid anodic electrolytes (i.e. agar or alginate solidified medium) could circumvent this problem by supplying a long-lasting and constant, saturating concentration of organic matter to the anode [18]. Alternatively, performing the detection of toxicants under open circuit voltage (OCV) stabilises the anode potential, reducing its dependency on the organic content [19].

Regarding the choice of electrode, biocathodes are less prone to error than bioanodes [20]. In a biocathode, the combined shock of BOD and toxicants, change the signal in the same direction, having an additive effect. In bioanodes, the signals follow different directions and cancel each other, resulting in a confounded signal prone to error Type II [15].

Biocathodes are also subjected to error if the toxicant is abiotically reduced at the cathode [20, 21]. Simultaneous monitoring of both electrodes could improve the detection efficiency. An MFC sensor with two bioreceptors, a bioanode and a biocathode, was connected sequentially to obtain a time series signal with two components. This study obtained enhanced sensitivity and lower chance of false negatives with respect to single electrode, due to the additive but separately identified effect of each electrode in the overall signal [22].

Although selectivity is inherently poor in whole-cell biosensors, some degree of classification could be achieved based on the properties of the analyte and the bioreceptor. Analytes can be clustered by their redox properties. For example, due to its relative higher potential, Cr^{6+} was selectively reduced at the cathode of a sediment MFC from a mixture of Pb^{2+}, Zn^{2+}, Cu^{2+}, Ni^{2+}, Co^{2+}, Cd^{2+}, glucose, acetate and cellulose [23]. In this context, factors like pH, conductivity [11], electrode potential and external resistance [24] could be set to promote the electrochemical reaction that involves the analyte of interest.

Regarding bioreceptors, single culture biofilms are more selective than mixed cultures. Maintaining a pure culture is not feasible in the environment, however, a degree of selectivity towards electroactive bacteria is observed in biofilms colonising electrodes under applied potential. *Geobacter* spp. are naturally selected on a graphite electrode (80% population) in biofilms grown on sludge [25], anaerobic soil or marine sediment [11] at 0.4 V vs. Ag/AgCl. *Geobacter* and other strong electroactive bacteria generate electricity mostly from acetate and lactate, increasing the selectivity of the sensor to these compounds in mixtures [26].

The metabolic inhibition pathway of the pollutant could also be considered as a selection vector. Stein et al. classified the signal during a toxic shock, based on the enzymatic mode of action [27]. In another study, $CuSO_4$ and 1-cyclohexyl-2-pyrrolidone were independently detected in a mixture of volatile organic compounds by considering the inhibition point of the toxicant in the electron transport chain [28].

Photosynthetic and autotrophic bioreceptors are especially interesting to improve the sensor autonomy, as they rely on CO_2 and light, and are particularly suited to detect herbicides that specifically attack photosynthesis [29]. Depending on the

mode of action, the effect of herbicides can decrease or increase the signal output. Triazines, for example, block the electron flow in the photosynthetic chain by binding to the quinone Q_B in the PSII complex, which decreases the electron flow towards the electrode [10, 29]. On the other hand, Paraquat is a redox shuttle that facilitates electron transport across the membrane, increasing the current and signal output [30].

Selectivity can be further enhanced with an array of sensors with multiple functionalities. Integrating a Clark electrode with pH and optical probes and an MFC sensor, could selectively detect toxicants impacting photosynthesis, respiration [31] and fluorescence/bioluminescence [32].

2.2.2 Sensitivity

The sensitivity of a MFC sensor is defined as the change in electrical signal per unit change of analyte concentration, usually normalised by surface area of the sensing electrode [33]. This approach requires the determination of a dose-response curve under controlled conditions and a stable baseline throughout the determination of the curve [8]. Yet, a steady baseline is rarely observed in environmental conditions [34]. Less restrictive definitions, like the inhibition ratio (IR), that measures the difference in the short-term baseline before and after the toxic event, would be more appropriate to evaluate the sensitivity of MFC sensors in the field [35]. However, the lack of standardisation in the output metrics that define the IR (i.e. current, voltage, power) and time frame from minutes to hours (Tables 2.1 to 2.3), challenge the comparison of results. For example, measuring the IR based on the coulombic yield showed an improved sensitivity to chromium than the IR based on voltage (13 vs. 9 %) [36]. Regarding contact time, Shen et al. [6] reported an IR of 85% for 7 ppm of Cu^{2+} after 4 h at a flow rate of 1.3 mL min^{-1}, whereas the IR was 50% and 60% at 12 and 24 mL min^{-1}, respectively.

Several studies indicate that sensitivity improves at low external resistances, R_{ext}. Low R_{ext} force high currents that respond faster to the impact of a toxicant on the anodic activity [37, 38]. The optimal R_{ext} depends on the type of bioreceptor and toxicant. In a MFC, the IR was maximal at R_{ext}=680 Ω for Cd^{2+} and Pb^{2+}, and at R_{ext}=100 Ω for the pesticide Avermectin [39]. The discrepancy in the optimal R_{ext}

was attributed to the differences in anodic microbial communities enriched in the biofilm at different resistances.

Sensitivity is closely related to selectivity. When the anode of an MFC was challenged with 10 mg L^{-1} of $NaNO_3$, the IR was seven times larger at OCV than at closed circuit, due to selective oxidation of nitrate over acetate in the former case [19].

The use of biocathodes as the bioreceptor in MFC sensors is a promising option to improve sensitivity. Under the same enrichment and operational conditions, the sensitivity to formaldehyde was twice higher with a biocathode than a bioanode [20]. The sensitivity of biocathodes depends on the electrode potential during enrichment. The sensitivity of a biocathode enriched at -0.2 V vs Ag/AgCl was significantly superior than at 0 and -0.4 V vs. Ag/AgCl, which was attributed to a selective growth of *Nitrospirae* at -0.2 V over more diverse community at other potentials [40].

It is expected that prolonged exposure to toxicants exert a selective pressure on the microbial community towards toxicant tolerant organisms, reducing the sensitivity of the sensor [41]. After repeated shocks of 4- nonylphenol, a shift in the community towards toxicant tolerant bacteria was observed. The non-electrogenic degradation of 4-nonylphenol increased from 15 to 47 % after repeated shocks, reducing the sensitivity of the MFC sensor over time [65]. Similarly, a shift of the biofilm community to weak electrogenic bacteria was seen after prolonged exposed to Cr (VI), which decreased the electron conversion efficiency in the system [23].

2.2.3 Response time

Tables 2.1 and 2.2 report the response time of several field based MFC sensors. The variability of the designs challenges the comparison of results. For BOD detection in field operations, defining the response time as the time to reach the maximum height of the signal peak (i.e. voltage), would be appropriate as it does not rely on a steady baseline over time [35]. Yet this approach assumes a single maximum peak for each event, when multiple peaks and flat asymptotic curves are common signal features in real water samples [34]. Alternatively, the response time can be defined as the time to reach a threshold in the signal variance after the toxic

event. This threshold point would ideally be defined based on the variance of long-term historical datasets in non-toxic conditions [12].

Recently, Pasternak et al. measured the response time as the time to reach the minimum voltage required to switch on an LED beacon to warn of BOD infiltrations. The frequency of light emission correlated with the BOD concentration providing a straight forward detection tool [13].

In the case of cyclic signals, characteristic of photosynthetic MFCs, the response time can be defined as the time lag to reach a threshold of 50% of photosynthesis inhibition [43]. Alternatively, the signal can be linearised by transforming it into accumulated charge.

Overall, the response time improves at low R_{ext}, low flow rates [37]), high concentration of analyte [13, 48] and small ratio of electrode/bioreceptor area [45].

2.2.4 Detection limit

The limit of detection (LOD) is the minimum concentration of analyte that causes a significant change in the signal output. The lack of standardisation in the threshold (3:1 [16, 45] or 5:1 [46] signal to noise ratio) complicates the comparison of studies. A statistical approach, based on a time series, that measures the change of variance over time, might be a more appropriate method to determine the LOD, as it does not rely on a steady baseline.

The LOD can be improved by using oligotrophic biofilms, more sensitive to low concentrations of analyte [47], miniaturising the electrodes to reduce mass transport limitations, avoiding side reactions (i.e. oxygen cross-over to the anode) [48] or using several MFCs hydraulically connected in series [16].

2.2.5 Biosensor recovery

Reusability of the bioreceptor would greatly improve long-term unattended operation of the MFC sensors. The degree and time of recovery of the biofilm electroactivity, after exposure to the toxicant event in an MFC sensor is linked to flowrate, feed composition, nature and concentration of analyte [48] and the type of electrical control [41].

***Table 2.1**. Summary of characteristics and analytes detected with paper MFC sensors.*

Analyte	Paper	Anode	Inoculum	Cathode	Inoculation time	Power / $\mu W\ cm^{-2}$	R_{int} / Ω	Concentration	IR / %	Tr / min	Recovery	Ref
Cr (VI)	Filter paper 22 µm	4 electrodes (CI)	WW	4-layer PTFE/ CC 0.5 Pt	< 3h	3.5	547	10 mg L^{-1}	0.27	120		[49]
		CI				0.08		20 mg L^{-1}	0.34	8	60-80h	
								20 mg L^{-1}	6 x	8	60-80h	
	Membrane filter 0.22 µm	CI	MFC anode WW	CI	3h		1000				80h	[50]
Ni (II)												
NaCOCl	Filter paper 22 µm	4 electrode CI	WW	CC/ C/ Pt	< 3h	0.35	547	200 mg L^{-1}	0.325	120	N/A	[49]
								100 mg L^{-1}	0.22			
								50 mg L^{-1}	0.27			
NaAc								250 mg L^{-1}				
Formaldehyde	Fabriano paper	CNF/ G powder	Sludge /Ac		8 days	0.04	2200	0.10%	100	165		[51]
Formaldehyde	Whatman Filter paper	CI/ PEDOT:PSS	Shewanella MR-1	PEDOT: PSS/ Ag_2O	0.5-3 h	0.45	-	0.001	6.9			[52]
Atrazine	Filter paper	SWCNT (7 layers) +Ti nanolayer	Synechoc. PCC	Counter Pt wire	48h	0.4 µA[1]		10 µM	76±7			[30]
Diuron								0.5 µM	91±4			
Paraquat								0.7		120		

[1] *Chronoamperometry at 0 V vs. Ag/AgCl*

CI: carbon ink
CNF/G: Carbon nanofibers / Graphite
PEDOT: PSS: poly(3,4-ethylenedioxythiophene) polystyrene sulfonate
SWCNT: Single wall carbon nanotubes
WW: Wastewater
PTFE/CC: Polytetrafluoroethylene / Carbon cloth
R_{int}: Internal resistance

Table 2.2. *Summary of characteristics and analytes detected with sediment MFC sensors.*

Analyte	Sensing element	Anode	Inoculum / anolyte	Anode depth	Cathode	Catholyte	Electrode distance	Stat up / day	Linear range	Response time	Time / day	Ref.
DO	Cathode	GF	48.1% OM/LOI	5 cm	GF	Bulk	20 cm	10	0 - 9 mg L^{-1}	Real time	67	[53]
	Cathode	CP	11.6% OM/LOI	10 -15 cm	GF 5 sheets	Bulk	0 - 2 m	5	0-13 mg L^{-1}	Real time	142	[54]
COD	Both	GF	Bulk	2 cm	GF	Air	20 cm	15	300 mg L^{-1}	30 h	60	[12]
	Both		Bulk			Bulk				30 h		
	Both		8 mg L^{-1} (TOC)			Bulk				25 h (peak)		
	Both					SED						
Acetate	Anode	GC	Sand/silt	4 - 6 m	GC	Bulk	6 m	4 - 5	0 - 2.3 mM	Real time	110-261	[11]
Sediment	Anode	GF	< 35% OM/LOI	1 – 5 cm	GF	Bulk	10 – 15 cm	20	-	Real time	60	[55]
Cr (VI)	Cathode	CF	Lake	6 cm	CF	Bulk	10 cm	12	0.2 - 0.7 mg L^{-1}	18 min	18 - 37	[23]

DO: Dissolved oxygen
COD: Chemical oxygen demand
TOC: Total organic carbon
GF: Graphite felt
GC: Graphite cloth
CP: Carbon paper
OM/LOI: Organic matter by loss of ignition method

Table 2.3. *Summary of characteristics and analytes detected with floating MFC sensors.*

Analyte	Sensing element	Design	Separator	Anode	Inoculum / anolyte	Cathode	Startup/ day	Sensitivity	LOD / mg L^{-1}	Time	Stack	Ref.
Urine	Anode	Tubular	Terracotta	CFV	AS	CFV PTFE	5	0.021 Hz min	57.7	5 months	4	[13]
WWTP	Anode	Tubular (small boat)	Terracotta	CF	Denitrification tank	AC	15	-	-	3 years	16	[56]
	Anode	Tubular (big boat)	Terracotta	CF		AC	15	-	-		32	
	Anode	Flat large	PPE felt	CC		CC	30	-	-		1	
	Anode	Flat medium	PPE felt	CC		CC	30	-	-		4	
	Anode	Flat small	PPE felt	CC		CC	30	-	-		6	
Cu	Anode	Flat	NA	CF	Mixed field	MnO/ C			23.5 (LC_{50})	10 days	1	[44]
Oil	Cathode	Upward Open Channel circular	NA	CC	WW	CC/ Pt/C Teflon		32.1 mV mL^{-1}	0.5 mL		1	[90]

WWTP: wastewater treatment plant
PMS: Power management system
CFV: Carbon Fibre veil
PPE: Polyphenylene Ether
CC: Carbon cloth
AC: Activated carbon

Usually, the system's ability to recover after the toxic event is tested by restoring the baseline conditions, which implies feeding a non-contaminated media to the system [8, 16, 36]. Recovery under starvation and/or stagnant flow has also been reported [57] and should be highlighted for real applications.

When operated under flow, the biofilm recovery is faster at high flow rates due to rapid pollutant wash-off, that prevents bioaccumulation [44]. High concentrations of the target analyte typically reduce the recovery time [36]. Regarding the electrochemical control, Stein et al. achieved the quickest biofilm recovery at fixed R_{ext}, compared to galvanostatic or potentiostatic control, and hypothesised that a fixed R_{ext} allows bacteria to self-modulate current and potential to restore enzymatic activity and metabolic processes [38].

2.2.6 System stability

The stability of the baseline can be affected by natural changes in water temperature, conductivity, composition, organic matter and pH [55, 56]. Periodic trends like day/night variations in T, pH, light irradiance, tide and DO can be identified and separated from the global signal response [54, 56, 60]. Furthermore, it was observed that daily baseline oscillations in field tests are less pronounced with large electrodes, and the effect of temperature is reduced using high R_{ext}, possibly due to a sub-optimal loading [56]. The effect of pH variations could be minimised by using a solid electrolyte or soil with high buffer capacity [61]. Baseline normalisation accounts for these variations and allows to compare systems [16]. Baselines however, shift over time due to electrode biofouling [54], by-product precipitation [42, 62], cathodic catalyst deactivation [44], clogging [56] and corrosion, which implies frequent re-calibration, unfeasible in remote areas.

Strategies to stabilise the baseline include: covering abiotic cathodes with polytetrafluoroethylene (PTFE) to prevent biofouling [13]; operating the system under intermittent OCV, to avoid concentration gradients [44], or at high external loads, to improve the resilience of the anode to starvation periods [13]; using a large ratio of counter versus working electrode (i.e. cathode/anode) area [53], or an array of working electrodes sharing the same counter electrode [45]. The

optimum electrode surface area ratio can be determined through polarisation of the individual electrodes [57, 63] or capacitive tests [64].

2.2.7 Autonomous operation

Autonomy of MFC sensors requires passive feeding and *in situ* generation of power, to record and transmit the signal. Resilience of the hardware to environmental conditions is also crucial for autonomous, long-term operation.

The typical low organic content in water bodies is a challenge for MFC sensors. A shift in the carbon source from BOD to ubiquitous and readily available CO_2 can be done using autotrophic biofilms. Evidence of direct electron transport is not yet reported in these systems and it is believed that the electron transfer takes place *via* soluble redox mediators [65, 66], impractical for field operation. The use of a sacrificial anode, based either on metals like Mn [67] or solid electrolytes [18], has demonstrated stable and autonomous operation for several months.

Regarding solid anolytes, stable production of 111 and 105 µW over 2.5 months was achieved with gelatine and alginate hydrogels, in lab-bench experiments [68]. Long-term stable operation was also achieved with anolytes based on natural substrates, such as hummus, sawdust, peat and manure [69]. Substrate degradation rates can be customised varying the percentage of organic and inorganic carbon and clays. The combination of inert sawdust and bioactive hummus for example, provided the longest stable power output, of five months [69]. Algal assisted soil and sediment MFCs or plant MFCs, in which organics are replenished at the anode by the indirect action of photosynthesis [70], are particularly interesting for long-term operation.

Oxygen reducing biocathodes are promising bioreceptors for long-term, autonomous monitoring of heavy metals and organic pollutants in tap water [71]. The extended lifetime, up to eight months, high working potential (0.2 V vs. Ag/AgCl), lack of added nutrients and short response time of 1 min demonstrate the suitability of biocathodes as bioreceptors for autonomous biosensors [72].

The energy needed for potential control [28], charge pumps, maximum power point trackers, data loggers and data transmitters can be sustainably supplied by other MFCs [60, 73], solar panels [44] or wind turbines [67]. Due to low power output of

MFCs, fuel cells stacks or capacitors are used to boost power output to a minimum working voltage [56]. Stacks, however, incur on voltage reversal and energy losses [74]. Recently, an innovative energy management system comprising a storage capacitor, a switching integrated circuit and an inductor, harvested 3.02 μW and boost it to 3.3 V. Only one sediment MFC, generating 86.3 μW, powered several pH, DO and temperature sensors and long distance transmitters [75]. Similar to maximum power point trackers, this algorithm prevented voltage reversal, but with an energy consumption two orders of magnitude lower than the former.

Overall, the performance indicators (Table 2.4) are affected simultaneously by the same factors, meaning that the performance of an MFC sensor should be studied in a holistic manner, where all factors and indicators considered at the same time.

***Table 2.4**. Summary of indicators and main influential factors.*

Indicator	Operational vectors	Design solutions
Selectivity	Selective enrichment Toxicant redox potential Model of action Electrode potential	Solid electrolyte to keep high constant BOD Operate at high R_{ext} or OCV
Sensitivity	Baseline stability Electrode potential Sensing electrode Toxicant tolerance	Inhibition ratio standardisation Biocathodes/ dual sensing element Operate at low R_{ext}
Response time	Baseline Flow rate Concentration Electrode potential Electrode area	Statistical analysis of variance Transform time series signal into frequency High electrode area Low R_{ext}
Recovery	Flowrate Composition Potential control	Fixed Rext High flow rate Multiple electrodes with protective layers if not recoverable
Signal stability	Environmental variations Electrode potential Fouling	Identify periodic trends Normalise the baseline Solid state electrolyte with buffer and high BOD Use high Rext Cover abiotic electrodes to prevent fouling
Autonomy	Organic matter Stack Parasitic currents	Solid state electrolyte Power management system to use one MFC Solar or wind energy

2.3 MFC configurations for *in situ* monitoring of water quality

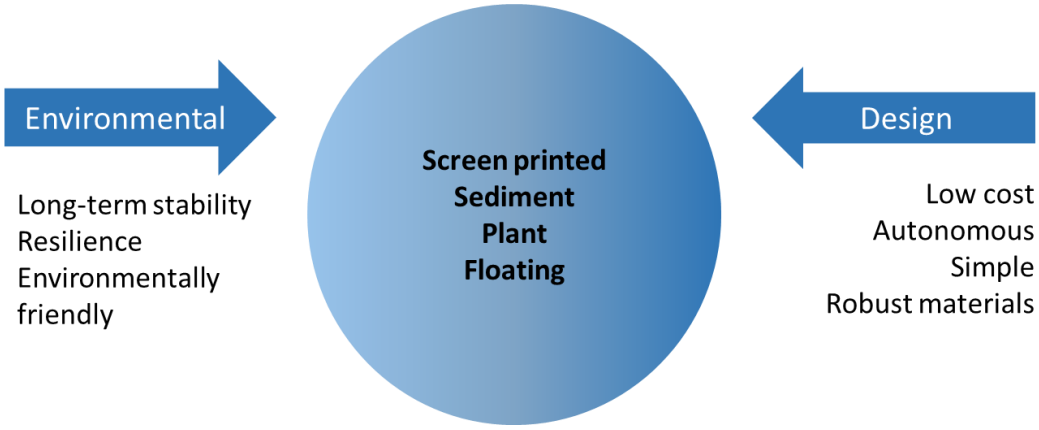

Figure 2.2. *Overview of the designs of MFC biosensors for field applications.*

2.3.1 Paper biosensors

Paper based MFC sensors are single use, cost-effective (0.43 £ per sensor [51]), and particularly suitable for field applications, thanks to their fast degradability and portability. Configurations are simple and easy to scale up (Figure 2.2). In these devices, electrolyte transport takes place within the molecular structure of the paper matrix, through capillarity, permeability and absorption. This simplifies the design, as the paper acts both as support and separator for electrodes [76]–[78]. The high ohmic resistance of paper, around 50 Ω [51], prevents short-circuiting of electrodes in close proximity allowing minimum electrode spacing [80, 81].

Addition of PTFE to bind the ink to the substrate, improves stability of the printed electrode [79], and crosslinking the fibres improves the stability of the paper [51].

Biofilm fixing is key to ensure the stability and portability of the paper MFC sensor. The 3-D microstructure of paper can be modified with conductive inks, to create a porous electrode with high surface area to hold the electroactive biofilm [52]. The result is an improved contact that reduces the enrichment time from days in carbon, to hours in paper based MFCs (Tables 2.1 and 2.2). Several strategies such as air drying of the biofilm and rehydration at the point of use [52], storage in the dark at 4˚C [30], entrapment or coating of the biofilm with chitosan [51], hydrogels [81] or polymers like alginate [30, 84] were proposed to overcome this issue.

An overview of the analytes detected with paper MFC sensors is shown in Table 2.1. The limit of detection for heavy metals is in the range of mg L^{-1}, while for pesticides it is the range of µg L^{-1}. Stacking several paper MFC sensors improves sensitivity due to a larger baseline. Paper MFC stacks can be compact and easily done by folding the paper [51].

Despite the fast degradability of paper, relative long-term continuous operation of paper MFC sensors could be realised, as studies showed biofilm recovery few hours after the toxic event (Table 2.1). Using ceramic instead of a paper matrix could improve the durability of screen-printed biosensors. The use of ceramics as separators is extensive in MFC for power generation, due to their adequate permeability, biofilm attachment, ion exchange capacity and durability properties [83], but is still unexplored as support for MFC sensors.

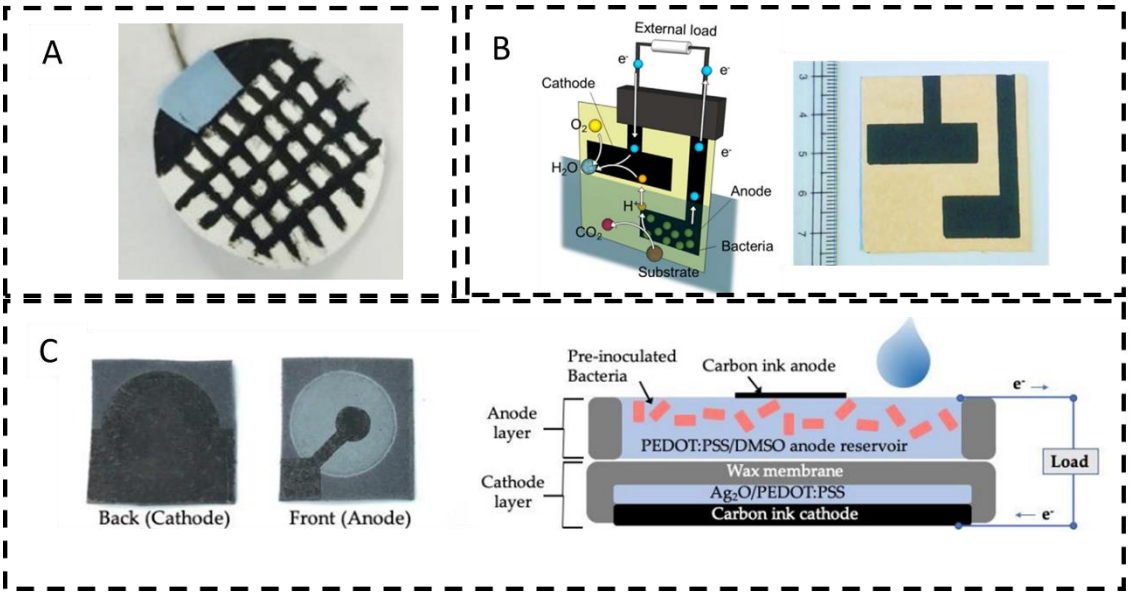

Figure 2.3. *Paper based MFC designs. Membrane-based online sticker for WW monitoring* [50]*. Screen printed biosensor for toxicity detection in water* [51]*. Paper MFC sensor with conductive reservoir for bacterial attachment* [52].

2.3.2 Sediment-based biosensors

Sediment MFC sensors consist of an anode, immersed in sediment and a cathode floating in the overlaying water. Sediment MFCs are particularly suitable to operate

in oceans, where the seafloor acts as the electron reservoir for the anode, and the high conductivity of seawater reduces the ohmic resistance [73].

Electrodes are commonly made of carbon felt, graphite rods or stainless steel. Both anode and cathode were reported as sensing elements for sediment MFC sensors (Table 2.2), although due to the lack of separator, the toxicant probably diffuse to both electrodes, working as a dual bioreceptor.

Sediment MFCs have been widely tested to monitor BOD in water bodies (Figure 2.4). A sediment MFC sensor was installed in boreholes, to control the supply of acetate for uranium biodegradation in groundwater [11] (Figure 2.4A). Velasquez et al. tested four designs to monitor BOD (Figure 2.4B), where the anode was either embedded in sediment or floating on the water [12]. In another study, the anode activity was used to warn of the excessive accumulation of organic matter in sediments, which causes oxygen depletion in the water above and greenhouse emissions [55]. In this study, seven horizontally and vertically spaced anodes (3 cm and 1 cm respectively) provided a profile of oxygen and availability of electron donors in the sediment (Figure 2.4C).

Sediment MFCs were also used to detect eutrophication [54] and stratification [53], and to monitor dissolved oxygen in environmental waters. Stratification in a shallow lake was detected with a multi-cathode sediment MFC (Figure 2.5A) [53]. The rate of cathodic oxygen reduction reaction dominated the sensors electrical output, providing a profile of oxygen in the water column. In another study, the signal of a sediment MFC operating in a coastal bay (Figure 2.5B), correlated directly with the variations in temperature and DO, and indirectly with tidal, irradiance, algal blooms and rainfall events [54]. The ohmic drop due to the distance between electrodes did not affect the signal, probably as a consequence of the high conductivity in seawater.

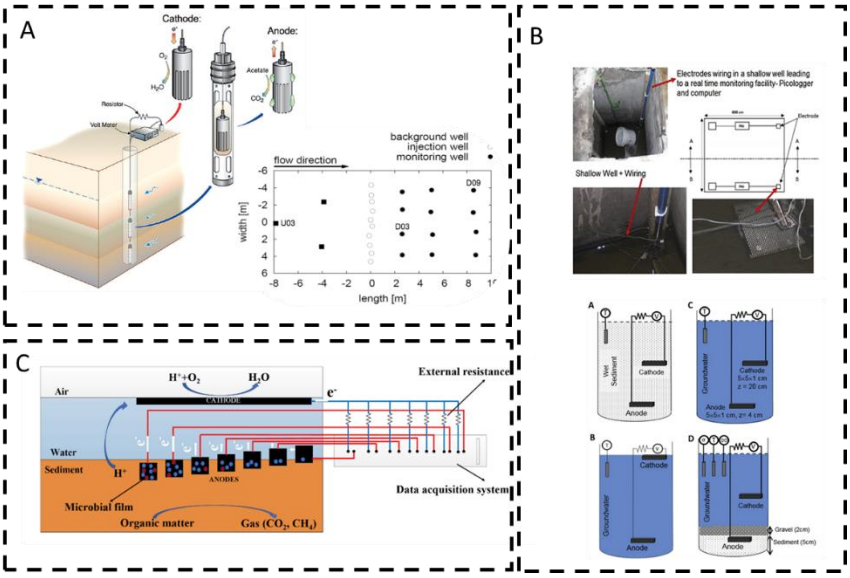

Figure 2.4 *Sediment MFCs for organic matter monitoring. (A) Monitoring of microbial activity for uranium remediation [11]. (B) An early warning tool for faecal infiltration on groundwater wells [12]. (C) Sediment bulking sensor* [55].

As reported in Table 2.2, the upper limit of DO detection in sediment MFCs is around 5 mg L^{-1} , larger than the minimum 2 mg L^{-1} necessary to sustain aquatic life [84]. Sediment MFC could therefore work as early warning systems for hypoxic events.

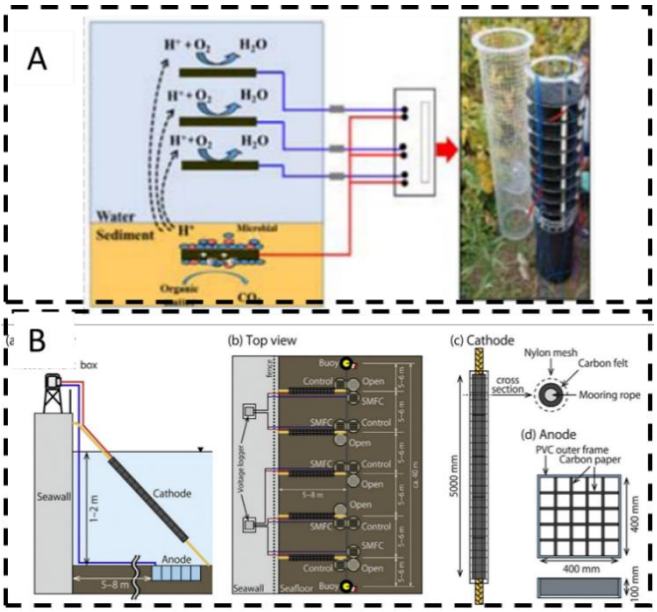

Figure 2.5. *Sediment MFCs for DO monitoring. (A) Monitoring of DO in a water column of a shallow lake with a sediment MFC with vertical cathode array* [53]. *(B) Multi-cathode SMFC deployed in an eutrophic bay* [54].

Sediment MFCs can also be used as early warning tools for toxicity, particularly to monitor oxidants at the cathode with higher potential than oxygen, like Cr (VI) [23].

Alternatively, plant MFCs have been recently proposed to monitor acid rain [85]. A plant MFC is a particular type of soil MFC, where the anode is enriched in organic matter excreted by the plant roots. In this study, the organic matter produced by the plant *Oryza sativa japonica* provided a sustainable source of electrons to the anode. When the plant was exposed to acid rain, modelled as a mixture of HNO_3 and H_2SO_4, the signal baseline dropped, with an IR of 77%. The signal recovered after two toxic events but was irreversibly lost after the third event, coinciding with the loss of green pigmentation in leaves due to the permanent damage of photosynthesis. The acid rain, plant MFC sensor showed a response time of 2 min. The current correlated with the change in the total organic carbon in the roots produced by the toxic event, suggesting a fast transfer rate of the perturbation from leaves to roots. These findings imply that plant MFCs can be very effective as field biosensors to monitor toxic compounds affecting photosynthesis [85].

The distance between electrodes in sediment MFCs limits their application in waters with low conductivity [54] due to high ohmic resistance. In Floating MFCs, on the other hand, electrode spacing is minimised thanks to the use of separator [48, 59] reducing the dependency of the sensors output on water conductivity.

2.4.3 Floating MFC biosensors

Floating MFCs are self-contained devices where the anode is submerged in water and the cathode can be either submerged or exposed to air. Floating MFCs were designed to monitor BOD [56], urine [13], oil spills [86] and toxic contamination [44] in freshwater bodies.

In these devices, the anode is generally exposed to high concentrations of oxygen that poison electroactive bacteria and reduce the energy efficiency of the sensor. Highly porous [87] or filamentous [88] anodes, are densely colonised by bacteria that consume the oxygen on the bulk interface, creating anaerobic areas at the electrode interface. Covering the anode with a thick, porous polymeric [44] or ceramic layer [60], or embedding the anode in soil [60], are proposed approaches to reduce the oxygen flux into the anode.

Several floating MFCs sensors were successfully implemented in the field (Table 2.3). Light and sound beacons were powered with a floating ceramic MFC in presence of urine (Figure 2.6A). A floating MFC sensor enriched in oligotrophic bacteria could sustain current to detect Cu in water with low organic content (Figure 2.6B) [44]. Several low-cost, floating configurations using ceramic separators were deployed to monitor BOD in the anoxic tank of a wastewater treatment plant (Figure 2.6C) [56]. In the last study, cathode colonisation by photosynthetic organisms was observed, opening opportunities to monitor oxygen, solar radiance and algal blooms.

In other study, oil spills were detected with a floating MFC (Figure 2.6D) with a cathodic sensing element. Reduction of oxygen at the cathode relied on diffusion of air into water, which was blocked when oil covered the water surface, provoking a drop in the signal output [86].

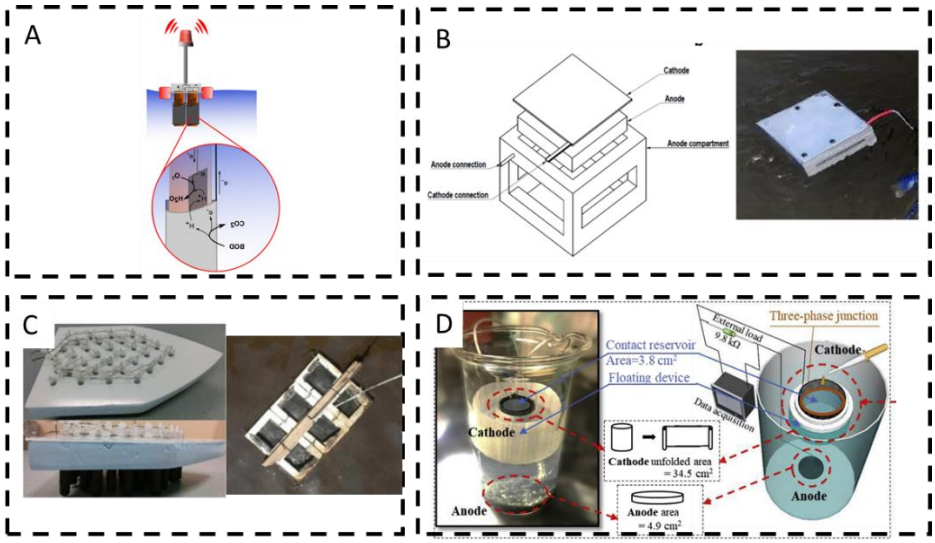

Figure 2.6. *Field based floating MFC sensors: (A) Detection of urine in water with a beacon EWS [13]. (B) Detection of metals in river water* [44]*. (C) Sludge monitoring with floating boats and flat MFC* [56]*. (D) Monitoring of oil spillages* [86]*.*

2.4.4 Algorithms to detect contamination

For unattended operation, re-calibration of the MFC sensors should be avoided. This can be done implementing models that account for drifts in the baseline. Calibration models are however seldom carried out in real conditions and are mostly run as one factor at the time, thus neglecting interferences between factors [23, 89]. Design of Experiments (DoE) is a statistical approach that identifies the most influential factors and provides a calibration model where both the main effects and their interactions are considered [90]. Machine learning tools provide interesting algorithms to predict the signal in non-steady conditions. Artificial Neural Networks were implemented to correlate the geometrical signal features a MFC sensor with the type and concentration of substrate, and presence of toxicants [91].

Algorithms to implement MFC sensors as decision making tools are classified as baseline methods and signal processing methods [92]. In baseline methods, the averaged deviation between the observed and predicted responses is measured over time and compared to a threshold value. If the averaged deviation is greater than the threshold value, an alarm is triggered. A drawback of baseline detection methods is that they cannot differentiate well between noise and signal. Data driven methods correlate signals of sensors spatially distributed to minimise the noise [93].

2.4.5 Outlook and future perspectives

Robustness, autonomy and low specificity make MFC sensors particularly suitable for early detection of global water pollution. As such, performance indicators for field applications should aim at reducing false alarms rather than accurately determining analyte concentrations. The procedures to obtain these indicators should be standardised to facilitate the comparison of different studies.

Overall, the key technological bottlenecks for environmental implementation of MFC sensors are to: decouple the signal components in a combined shock of BOD/toxicant; provide a steady, passive supply or organic matter to the anode, and stabilise the baseline with respect to environmental variations.

To solve these issues, a solid anolyte could provide long-lasting, slow-release source or electron donors. This would also reduce the dependency of the anodic activity on the organic content in the tested water. The applied external resistance also has an important influence on several indicators. A fixed R_{ext}/R_{int} ratio to achieve optimal selectivity, sensitivity, response time and stability, could be maintained implementing a feedback loop that accounts for variations in internal resistance over time.

Selectivity could be improved by integrating the MFC sensor in a multisensory platform with pH, DO, temperature and conductivity probes; and using biocathodes or sequential bioanode/biocathodes as bioreceptors.

Further research is needed to determine the recovery degree of the bioreceptor, as well as the biofilm resistance to multiple toxic events. Should the damage be irreversible, an array of biofilms covered with protective layers (i.e. alginate) of increasing thicknesses that slowly dissolves in water, could act like a time series array of sacrificial bioreceptors.

Regarding designs, paper MFCs are ideal for single use diagnostics. The stability of the sensor could be improved using more robust support materials like ceramics. For continuous monitoring, floating plant MFCs outstand for long-term monitoring thanks to the constant release of organics by the plant roots.

Recent advances in power management systems allow long-distance transmission of the sensors readings. The long-term stability of these systems under real environmental conditions needs further study. Long-term data sets of MFC sensors operating in the field must be generated to improve the signal treatment and decision algorithms, in order to minimise the errors as early warning tools in environmental waters. Equally, a holistic approach to calibrate the sensor (i.e. DoE) is recommended to account for the impact of variable environmental factors on the signal output.

2.4 References

[1] B. H. Kim, I. S. Chang, G. C. Gil, H. S. Park, and H. J. Kim, “Novel BOD (biological oxygen demand) sensor using mediator-less microbial fuel cell,” *Biotechnol. Lett.*, vol. 25, no. 7, pp. 541–545, 2003.

[2] Y. J. Shen, O. Lefebvre, Z. Tan, and H. Y. Ng, “Microbial fuel-cell-based toxicity sensor for fast monitoring of acidic toxicity,” *Water Sci. Technol.*, vol. 65, no. 7, pp. 1223–1228, 2012.

[3] A. Schievano *et al.*, “Single-chamber microbial fuel cells as on-line shock-sensors for volatile fatty acids in anaerobic digesters,” *Waste Manag.*, vol. 71, pp. 785–791, 2018.

[4] Y. Jiang, N. Chu, and R. J. Zeng, “Submersible probe type microbial electrochemical sensor for volatile fatty acids monitoring in the anaerobic digestion process,” *J. Clean. Prod.*, vol. 232, pp. 1371–1378, Sep. 2019.

[5] J. Hinks *et al.*, “Naphthoquinone glycosides for bioelectroanalytical enumeration of the faecal indicator Escherichia coli,” *Microb. Biotechnol.*, vol. 9, no. 6, pp. 746–757, 2016.

[6] Y. Shen, M. Wang, I. S. Chang, and H. Y. Ng, “Effect of shear rate on the response of microbial fuel cell toxicity sensor to Cu(II),” *Bioresour. Technol.*, vol. 136, pp. 707–710, 2013.

[7] B. Liu, Y. Lei, and B. Li, “A batch-mode cube microbial fuel cell based ‘shock’ biosensor for wastewater quality monitoring,” *Biosens. Bioelectron.*, vol. 62, pp. 308–314, Dec. 2014.

[8] M. Di Lorenzo, A. R. Thomson, K. Schneider, P. J. Cameron, and I. Ieropoulos, “A small-scale air-cathode microbial fuel cell for on-line monitoring of water quality,” *Biosens. Bioelectron.*, vol. 62, pp. 182–188, 2014.

[9] A. Khan *et al.*, “A novel biosensor for zinc detection based on microbial fuel cell system,” *Biosens. Bioelectron.*, vol. 147, no. September, p. 111763, 2020.

[10] J. Labro, T. Craig, S. A. Wood, and M. A. Packer, “Demonstration of the use of a photosynthetic microbial fuel cell as an environmental biosensor,” *Int. J. Nanotechnol.*, vol. 14, no. 1/2/3/4/5/6, p. 213, 2017.

[11] K. H. Williams, K. P. Nevin, A. Franks, A. Englert, P. E. Long, and D. R. Lovley, “Electrode-based approach for monitoring in situ microbial activity during subsurface bioremediation,” *Environ. Sci. Technol.*, vol. 44, no. 1, pp. 47–54, 2010.

[12] S. B. Velasquez-Orta, D. Werner, J. C. Varia, and S. Mgana, “Microbial fuel cells for inexpensive continuous in-situ monitoring of groundwater quality,” *Water Res.*, vol. 117, pp. 9–17, 2017.

[13] G. Pasternak, J. Greenman, and I. Ieropoulos, “Self-powered, autonomous Biological Oxygen Demand biosensor for online water quality monitoring,” *Sensors Actuators, B Chem.*, vol. 244, pp. 815–822, 2017.

[14] H. Lee, W. Yang, X. Wei, A. Fraiwan, and S. Choi, “A microsized microbial fuel cell based biosensor for fast and sensitive detection of toxic substances in water,” in *2015 28th IEEE International Conference on Micro Electro Mechanical Systems (MEMS)*, pp. 573–576, 2015.

[15] Y. Jiang *et al.*, “Enhancing signal output and avoiding BOD/toxicity combined shock interference by operating a microbial fuel cell sensor with an optimized background concentration of organic matter,” *Int. J. Mol. Sci.*, vol. 17, no. 9, Sep. 2016.

[16] M. W. A. Spurr, E. H. Yu, K. Scott, and I. M. Head, “A microbial fuel cell sensor for unambiguous measurement of organic loading and definitive identification of toxic influents,” *Environ. Sci. Water Res. Technol.*, vol. 6, no. 3, pp. 612–621, 2020.

[17] W. Logroño, A. Guambo, M. Pérez, A. Kadier, and C. Recalde, “A terrestrial single chamber microbial fuel cell-based biosensor for biochemical oxygen demand of synthetic ricewashed wastewater,” *Sensors (Switzerland)*, vol. 16, no. 1, 2016.

[18] T. Tommasi, G. P. Salvador, and M. Quaglio, “New insights in Microbial Fuel Cells: Novel solid phase anolyte,” *Sci. Rep.*, vol. 6, no. July, 2016.

[19] D. Wang *et al.*, “Open external circuit for microbial fuel cell sensor to monitor the nitrate in aquatic environment,” *Biosens. Bioelectron.*, vol. 111, no. March, pp. 97–101, 2018.

[20] Y. Jiang, P. Liang, P. Liu, D. Wang, B. Miao, and X. Huang, “Biosensors and Bioelectronics A novel microbial fuel cell sensor with biocathode sensing element,” *Biosens. Bioelectron.*, vol. 94, no. February, pp. 344–350, Aug. 2017.

[21] L. Huang, X. Chai, G. Chen, and B. E. Logan, “Effect of set potential on hexavalent chromium reduction and electricity generation from biocathode microbial fuel cells,” *Environ. Sci. Technol.*, vol. 45, no. 11, pp. 5025–5031, Jun. 2011.

[22] T. Zhao, B. Xie, Y. Yi, and H. Liu, “Sequential flowing membrane-less microbial fuel cell using bioanode and biocathode as sensing elements for toxicity monitoring,” *Bioresour. Technol.*, vol. 276, no. January, pp. 276–280, 2019.

[23] S. Zhao *et al.*, “A novel early warning system based on a sediment microbial fuel cell for in situ and real time hexavalent chromium detection in industrial wastewater,” *Sensors (Switzerland)*, vol. 18, no. 2, 2018.

[24] A. Prévoteau and K. Rabaey, “Electroactive Biofilms for Sensing: Reflections and Perspectives,” *ACS Sensors*, vol. 2, no. 8. American Chemical Society, pp. 1072–1085, 25-Aug-2017.

[25] J. Kretzschmar, C. Koch, J. Liebetrau, M. Mertig, and F. Harnisch, “Sensors and Actuators B : Chemical Electroactive biofilms as sensor for volatile fatty acids : Cross sensitivity , response dynamics , latency and stability,” *Sensors Actuators B. Chem.*, vol. 241, pp. 466–472, 2017.

[26] M. Estevez-Canales, A. Berná, Z. Borjas, and A. Esteve-Núñez, “Screen-Printed Electrodes: New Tools for Developing Microbial Electrochemistry at Microscale Level,” *Energies*, vol. 8, no. 11, pp. 13211–13221, 2015.

[27] N. E. Stein, K. J. Keesman, H. V. M. Hamelers, and G. van Straten, “Kinetic models for detection of toxicity in a microbial fuel cell based biosensor,” *Biosens. Bioelectron.*, vol. 26, no. 7, pp. 3115–3120, Mar. 2011.

[28] P. Kannan *et al.*, “A novel microbial - Bioelectrochemical sensor for the detection of n-cyclohexyl-2-pyrrolidone in wastewater,” *Electrochim. Acta*, vol. 317, pp. 604–611, 2019.

[29] M. Tucci, M. Grattieri, A. Schievano, P. Cristiani, and S. D. Minteer, “Microbial amperometric biosensor for online herbicide detection: Photocurrent inhibition of Anabaena variabilis,” *Electrochim. Acta*, vol. 302, pp. 102–108, 2019.

[30] M. Tucci, P. Bombelli, C. J. Howe, S. Vignolini, S. Bocchi, and A. Schievano, “A storable mediatorless electrochemical biosensor for herbicide detection,” *Microorganisms*, vol. 7, no. 12, pp. 1–14, 2019.

[31] I. B. Tahirbegi *et al.*, “Fast pesticide detection inside microfluidic device with integrated optical pH, oxygen sensors and algal fluorescence,” *Biosens. Bioelectron.*, vol. 88, pp. 188–195, 2017.

[32] X. Qi, P. Liu, P. Liang, W. Hao, M. Li, and X. Huang, “Dual-signal-biosensor based on luminescent bacteria biofilm for real-time online alert of Cu(II) shock,” *Biosens. Bioelectron.*, vol. 142, no. April, p. 111500, 2019.

[33] J. Chouler and M. Di Lorenzo, “Water quality monitoring in developing countries; Can microbial fuel cells be the answer?,” *Biosensors*, vol. 5, no. 3. MDPI AG, pp. 450–470, 2015.

[34] Y. Feng, O. Kayode, and W. F. Harper, “Using microbial fuel cell output metrics and nonlinear modeling techniques for smart biosensing,” *Sci. Total Environ.*, vol. 449, pp. 223–228, 2013.

[35] Y. Jiang, X. Yang, P. Liang, P. Liu, and X. Huang, “Microbial fuel cell sensors for water quality early warning systems: Fundamentals, signal resolution, optimization and future challenges,” *Renew. Sustain. Energy Rev.*, vol. 81, pp. 292–305, Jan. 2018.

[36] V. Agostino *et al.*, “Environmental electroactive consortia as reusable biosensing element for freshwater toxicity monitoring,” *N. Biotechnol.*, vol. 55, no. September 2019, pp. 36–45, 2020.

[37] H. Moon, I. S. Chang, K. H. Kang, J. K. Jang, and B. H. Kim, “Improving the dynamic response of a mediator-less microbial fuel cell as a biochemical oxygen demand (BOD) sensor,” *Biotechnol. Lett.*, vol. 26, no. 22, pp. 1717–1721, 2004.

[38] N. E. Stein, H. V. M. Hamelers, and C. N. J. Buisman, “The effect of different control mechanisms on the sensitivity and recovery time of a microbial fuel cell based biosensor,” *Sensors Actuators, B Chem.*, vol. 171–172, pp. 816–821, 2012.

[39] Y. Yi, B. Xie, T. Zhao, Z. Li, D. Stom, and H. Liu, “Effect of external resistance on the sensitivity of microbial fuel cell biosensor for detection of different types of pollutants,” *Bioelectrochemistry*, vol. 125, pp. 71–78, 2019.

[40] C. Liao *et al.*, “Optimal set of electrode potential enhances the toxicity response of biocathode to formaldehyde,” *Sci. Total Environ.*, vol. 644, pp. 1485–1492, Dec. 2018.

[41] A. Adekunle, V. Raghavan, and B. Tartakovsky, “On-line monitoring of heavy metals-related toxicity with a microbial fuel cell biosensor,” *Biosens. Bioelectron.*, vol. 132, no. March, pp. 382–390, 2019.

[42] A. Godain, M. W. A. Spurr, H. C. Boghani, G. C. Premier, E. H. Yu, and I. M. Head, “Detection of 4-Nitrophenol, a Model Toxic Compound, Using Multi-Stage Microbial Fuel Cells,” *Front. Environ. Sci.*, vol. 8, no. January, 2020.

[43] S. Morin, B. Chaumet, and N. Mazzella, “A Time-Dose Response Model to Assess Diuron-Induced Photosynthesis Inhibition in Freshwater Biofilms,” *Front. Environ. Sci.*, vol. 6, no. November, pp. 1–9, 2018.

[44] A. Adekunle, C. Rickwood, and B. Tartakovsky, “Online monitoring of heavy metal–related toxicity using flow-through and floating microbial fuel cell biosensors,” *Environ. Monit. Assess.*, vol. 192, no. 1, 2020.

[45] Y. Jiang, P. Liang, P. Liu, X. Yan, Y. Bian, and X. Huang, “A cathode-shared microbial fuel cell sensor array for water alert system,” *Int. J. Hydrogen Energy*, vol. 42, no. 7, pp. 4342–4348, 2017.

[46] S. B. Quek, L. Cheng, and R. Cord-ruwisch, “ScienceDirect Microbial fuel cell biosensor for rapid assessment of assimilable organic carbon under marine conditions,” *Water Res.*, vol. 77, pp. 64–71, 2015.

[47] K. Hyun Kang, J. Kyung Jang, T. Hai Pham, H. Moon, I. Seop Chang, and B. Hong Kim, “A microbial fuel cell with improved cathode reaction as a low biochemical oxygen demand sensor,” *Biotechnol. Lett.*, vol. 25, pp. 1357–1361, 2003.

[48] L. Cheng, S. B. Quek, and R. Cord-ruwisch, “Hexacyanoferrate-Adapted Biofilm Enables the Development of a Microbial Fuel Cell Biosensor to Detect Trace Levels of Assimilable Organic Carbon (AOC) in Oxygenated Seawater,” vol. 111, no. 12, pp. 2412–2420, 2014.

[49] Z. Xu *et al.*, “Disposable self-support paper-based multi-anode microbial fuel cell (PMMFC) integrated with power management system (PMS) as the real time ‘shock’ biosensor for wastewater,” *Biosens. Bioelectron.*, vol. 85, pp. 232–239, 2016.

[50] Z. Xu *et al.*, “Flat microliter membrane-based microbial fuel cell as ‘on-line sticker sensor’ for self-supported in situ monitoring of wastewater shocks,” *Bioresour. Technol.*, vol. 197, pp. 244–251, 2015.

[51] J. Chouler, Á. Cruz-Izquierdo, S. Rengaraj, J. L. Scott, and M. Di Lorenzo, “A screen-printed paper microbial fuel cell biosensor for detection of toxic compounds in water,” *Biosens. Bioelectron.*, vol. 102, pp. 49–56, Apr. 2018.

[52] J. H. Cho, Y. Gao, and S. Choi, “A portable, single-use, paper-based microbial fuel cell sensor for rapid, on-site water quality monitoring,” *Sensors (Switzerland)*, vol. 19, no. 24, 2019.

[53] N. Song *et al.*, “Development of a sediment microbial fuel cell-based biosensor for simultaneous online monitoring of dissolved oxygen concentrations along various depths in lake water” *Sci. Total Environ.*, vol. 673, no. April, pp. 272–280, 2019.

[54] K. Kubota, T. Watanabe, H. Maki, G. Kanaya, H. Higashi, and K. Syutsubo, “Operation of sediment microbial fuel cells in Tokyo Bay, an extremely eutrophicated coastal sea,” *Bioresour. Technol. Reports*, vol. 6, pp. 39–45, 2019.

[55] C. Wang and H. Jiang, “Real-time monitoring of sediment bulking through a multi-anode sediment microbial fuel cell as reliable biosensor,” *Sci. Total Environ.*, vol. 697, p. 134009, 2019.

[56] P. Cristiani, I. Gajda, J. Greenman, F. Pizza, P. Bonelli, and I. Ieropoulos, “Long Term Feasibility Study of In-field Floating Microbial Fuel Cells for Monitoring Anoxic Wastewater and Energy Harvesting,” *Front. Energy Res.*, vol. 7, no. November, pp. 1–11, 2019.

[57] L. Gonzalez Olias, P. J. Cameron, and M. Di Lorenzo, “Effect of Electrode Properties on the Performance of a Photosynthetic Microbial Fuel Cell for Atrazine Detection,” *Front. Energy Res.*, vol. 7, no. October, pp. 1–11, 2019.

[58] J. You, X. A. Walter, J. Greenman, C. Melhuish, and I. Ieropoulos, “Stability and reliability of anodic biofilms under different feedstock conditions: Towards microbial fuel cell sensors,” *Sens. Bio-Sensing Res.*, vol. 6, pp. 43–50, 2015.

[59] N. E. Stein, H. V. M. Hamelers, and C. N. J. Buisman, “Bioelectrochemistry Stabilizing the baseline current of a microbial fuel cell-based biosensor through

overpotential control under non-toxic conditions," *Bioelectrochemistry*, vol. 78, no. 1, pp. 87–91, 2010.

[60] A. Schievano *et al.*, "Floating microbial fuel cells as energy harvesters for signal transmission from natural water bodies," *J. Power Sources*, vol. 340, pp. 80–88, 2017.

[61] H.-S. Lee, K. Lee, S.-S. Kim, and S.-H. Ko, "Effect of soil buffering capacity and citric acid in electrolyte on electrokinetic remediation of mine tailing soils," *J. Ind. Eng. Chem.*, vol. 9, no. 4, pp. 360–365, 2003.

[62] M. Okochi *et al.*, "Development of an automated water toxicity biosensor using Thiobacillus ferrooxidans for monitoring cyanides in natural water for a water filtering plant," *Biotechnol. Bioeng.*, vol. 87, no. 7, pp. 905–911, 2004.

[63] Y. Yang, L. Yan, J. Song, and M. Xu, "Optimizing the electrode surface area of sediment microbial fuel cells," *RSC Adv.*, vol. 8, no. 45, pp. 25319–25324, 2018.

[64] T. Ewing, T. Ha, and H. Beyenal, "Evaluation of long-term performance of sediment microbial fuel cells and the role of natural resources," *Appl. Energy*, vol. 192, pp. 490–497, 2017.

[65] H. T. Pham, "Biosensors based on lithotrophic microbial fuel cells in relation to heterotrophic counterparts : research progress , challenges , and opportunities," vol. 4, no. March, pp. 567–583, 2018.

[66] A. J. McCormick, P. Bombelli, R. W. Bradley, R. Thorne, T. Wenzel, and C. J. Howe, "Biophotovoltaics: Oxygenic photosynthetic organisms in the world of bioelectrochemical systems," *Energy and Environmental Science*, vol. 8, no. 4. pp. 1092–1109, 2015.

[67] Q. Chen *et al.*, "Harvest energy from thewater: A self-sustained wireless waterquality sensing system," *ACM Trans. Embed. Comput. Syst.*, vol. 17, no. 1, pp. 1–25, 2017.

[68] I. Ieropoulos, P. Theodosiou, B. Taylor, J. Greenman, and C. Melhuish, "Gelatin as a promising printable feedstock for microbial fuel cells (MFC)," *Int. J. Hydrogen Energy*, vol. 42, no. 3, pp. 1783–1790, Jan. 2017.

[69] A. Adekunle, V. Raghavan, and B. Tartakovsky, "Carbon source and energy harvesting optimization in solid anolyte microbial fuel cells," *J. Power Sources*, vol. 356, pp. 324–330, 2017.

[70] B. Neethu and M. M. Ghangrekar, "Electricity generation through a photo sediment microbial fuel cell using algae at the cathode," *Water Sci. Technol.*, pp. 1–9, 2017.

[71] A. Prévoteau, P. Clauwaert, F. M. Kerckhof, and K. Rabaey, "Oxygen-reducing microbial cathodes monitoring toxic shocks in tap water," *Biosens. Bioelectron.*, vol. 132, pp. 115–121, May 2019.

[72] M. Rimboud, A. Bergel, and B. Erable, "Multiple electron transfer systems in oxygen reducing biocathodes revealed by different conditions of aeration/agitation" *Bioelectrochemistry*, vol. 110, pp. 46–51, 2016.

[73] F. Zhang, L. Tian, and Z. He, "Powering a wireless temperature sensor using sediment microbial fuel cells with vertical arrangement of electrodes," *J. Power Sources*, vol. 196, no. 22, pp. 9568–9573, 2011.

[74] S. Chen, S. A. Patil, R. K. Brown, and U. Schröder, "Strategies for optimizing the power output of microbial fuel cells: Transitioning from fundamental studies to

practical implementation," *Appl. Energy*, vol. 233–234, pp. 15–28, 2018.

[75] T. Yamashita, T. Hayashi, H. Iwasaki, M. Awatsu, and H. Yokoyama, "Ultra-low-power energy harvester for microbial fuel cells and its application to environmental sensing and long-range wireless data transmission," *J. Power Sources*, vol. 430, no. December 2018, pp. 1–11, 2019.

[76] J. Winfield, P. Milani, J. Greenman and I. Ieropolous "Passive feeding in Paper Based Microbial Fuel Cells", *ECS Trans*. 85, 1193, 2018.

[77] C. Santoro, J. Winfield, P. Theodosiou, and I. Ieropoulos, "Supercapacitive paper based microbial fuel cell: High current/power production within a low cost design" *Bioresour. Technol. Reports*, vol. 7, no. June, 2019.

[78] R. Veerubhotla, D. Das, and D. Pradhan, "A flexible and disposable battery powered by bacteria using eyeliner coated paper electrodes" *Biosens. Bioelectron.*, vol. 94, pp. 464–470, 2017.

[79] I. Shitanda, S. Kato, Y. Hoshi, M. Itagaki, and S. Tsujimura, "Flexible and high-performance paper-based biofuel cells using printed porous carbon electrodes" *Chem. Commun.*, vol. 49, no. 94, pp. 11110–11112, 2013.

[80] G. Choi, D. J. Hassett, and S. Choi, "A paper-based microbial fuel cell array for rapid and high-throughput screening of electricity-producing bacteria," *Analyst*, vol. 140, no. 12, pp. 4277–4283, 2015.

[81] M. Sawa, A. Fantuzzi, P. Bombelli, C. J. Howe, K. Hellgardt, and P. J. Nixon, "Electricity generation from digitally printed cyanobacteria," *Nat. Commun.*, vol. 8, no. 1, 2017.

[82] I. Shitanda, K. Takada, Y. Sakai, and T. Tatsuma, "Compact amperometric algal biosensors for the evaluation of water toxicity" *Anal. Chim. Acta*, vol. 530, no. 2, pp. 191–197, 2005.

[83] L. Rago *et al.*, "A study of microbial communities on terracotta separator and on biocathode of air breathing microbial fuel cells," *Bioelectrochemistry*, vol. 120, pp. 18–26, 2018.

[84] R. Vaquer-Sunyer and C. M. Duarte, "Thresholds of hypoxia for marine biodiversity," *Proc. Natl. Acad. Sci. U. S. A.*, vol. 105, no. 40, pp. 15452–15457, 2008.

[85] T. Li *et al.*, "Swift Acid Rain Sensing by Synergistic Rhizospheric Bioelectrochemical Responses," *ACS Sensors*, vol. 3, no. 7, pp. 1424–1430, 2018.

[86] Z. Dai *et al.*, "In-situ oil presence sensor using simple-structured upward open-channel microbial fuel cell (UOC-MFC)," *Biosens. Bioelectron. X*, vol. 1, no. 2, p. 100014, 2019.

[87] X. A. Walter, J. Greenman, and I. A. Ieropoulos, "Oxygenic phototrophic biofilms for improved cathode performance in microbial fuel cells," *Algal Res.*, vol. 2, no. 3, pp. 183–187, Jul. 2013.

[88] T. Yamashita, N. Ookawa, M. Ishida, and H. Kanamori, "A novel open-type biosensor for the in-situ monitoring of biochemical oxygen demand in an aerobic environment," *Nat. Publ. Gr.*, no. July, pp. 1–2, 2016.

[89] Y. Zhang and I. Angelidaki, "A simple and rapid method for monitoring dissolved oxygen in water with a submersible microbial fuel cell (SBMFC)," *Biosens. Bioelectron.*, vol. 38, no. 1, pp. 189–194, 2012.

[90] L. G. Olias, A. Rodriguez, P. J. Cameron, and M. Di Lorenzo, "A soil microbial fuel

cell-based biosensor for dissolved oxygen," *Electrochim. Acta*, p. 137108, 2020.

[91] S. T. King, M. Sylvander, M. Kheperu, L. Racz, and W. F. Harper, "Detecting recalcitrant organic chemicals in water with microbial fuel cells and artificial neural networks," *Sci. Total Environ.*, vol. 497–498, pp. 527–533, Nov. 2014.

[92] S. Liu, R. Li, K. Smith, and H. Che, "Why conventional detection methods fail in identifying the existence of contamination events," *Water Res.*, vol. 93, pp. 222–229, 2016.

[93] S. Liu, K. Smith, and H. Che, "A multivariate based event detection method and performance comparison with two baseline methods," *Water Res.*, vol. 80, pp. 109–118, 2015.

Chapter 3

Understanding the biological and electrochemical processes behind the energy generation in a MFC is a must to control and optimise the system. This chapter describes the unique biological features of electroactive bacteria and the underlying mechanisms for electron transport in MFCs. It also includes an explanation of the electrochemical fundamentals and characterisation techniques to understand the energy generation in a MFC.

3. Fundamentals of extracellular electron transfer

The mechanism of self-powered biosensors is based on the ability for Extracellular Electron Transfer (EET) in microorganisms. This phenomenon was observed in 1911 when M.C. Potter generated current from yeast and bacteria during fermentation [1] and has since inspired researchers to elucidate the electron transport processes between organisms, or to an abiotic acceptor, at the molecular level.

3.1 Extracellular electron transport

All known biological strategies to sustain life involve a flow of electrons into the cell, to gain energy from the environment. Microbes select the metabolic route that provides a greater energy gain within their metabolic possibilities, choosing the available electron donor with the lowest electrical potential and electron acceptor with the highest electrical potential [2]. During respiration for example, electrons enter the electron transport chain from the Citric Acid Cycle, carried by NADH/$FADH_2$ and quinones. Electrons are then transferred through different

membrane bound proteins in the electron transport chain, driven by a potential difference [3]. This movement of electrons across the inner membrane generates a proton gradient that powers the generation of adenosine triphosphate (ATP), to be used in anabolic processes in the cell. When the final electron acceptor is outside the cell, some microbes, known as electroactive bacteria [4], can externalise electrons *via* quinones, cytochromes or NADH/$FADH_2$, a process known as extracellular electron transfer [5]. This is the mechanism taking place in MFCs to carry the electrons from bacteria to the electrodes.

Extracellular electron transport requires charged molecules to cross hydrophobic, non-conductive membranes (Figure 3.1). Electricigens have developed specific pathways to allow charged molecules to travel across these barriers. The known mechanisms for EET are classified as direct and mediated electron transfer, depending on whether the electron transfer from the cell to the electrode is on one or several steps.

3.1.1 Mechanisms for Direct extracellular Electron Transport (DET)

The mechanisms for DET in bacteria include direct contact of membrane bound proteins with the electrode, and excretion of pili appendages and long-distance nanowires. DET occurs more frequently in dissimilatory metal reducing bacteria with a thin peptidoglycan [6]. The exact mechanism of DET remains largely undefined but is believed to be *via* electron hopping [7] and/or metal-like delocalised charge [8]. The MtrABC complex in *Shewanella oneidensis MR-1* is the best known DET pathway, followed by the porin-cytochrome complex in *Geobacter sulfurreducens* [9].

3.1.1.1 MtrABC complex in Shewanella oneidensis MR-1

Figure 3.1A shows the machinery for EET in *S. oneidensis MR-1*. The MtrABC complex is composed of six multiheme cytochromes that transfer electrons from the cytoplasm to external metals like Fe (III). The electrons exit the respiratory electron transport chain from the quinone pool in the inner membrane (Q-QH_2), are oxidised by cytochrome Cym-A and then released into the periplasm, where they are carried by two Cyt-C: Fcc and a small tetrahedral cytochrome (STC), to the outer membrane. In the outer membrane, the decaheme MtrA cytochrome in the

MtrABC complex takes the electrons from these periplasmic carriers, transferring them to the MtrB porin across the membrane and to outside metals (or other electron acceptors) by decaheme cytochromes MtrC and OmcA. These last two cytochromes can form long appendixes that extend outside the cell, to micrometre distances, and make connections with other cells or electron acceptors. The *in vitro* measurement of the complexes conductance estimates that, 10–100 membrane cytochrome conduits could be sufficient to support the extracellular respiration rate of an entire cell [13].

3.1.1.2 Porin-cytochrome complex

In *G. sulfurreducens* it is hypothesised that an arrangement of porin-cytochrome transmembrane complexes carries the electrons form the periplasm to the outside of the cell (Figure 3.1B). Here, the electrons also exit the electron transport chain at the quinone pool, oxidised by cytochromes in the cytoplasmic membrane (ImcH and CbcL). Electrons are transferred to periplasmic mobile carriers and to the outer membrane, escaping the cell through these porin-cytochrome complexes [9].

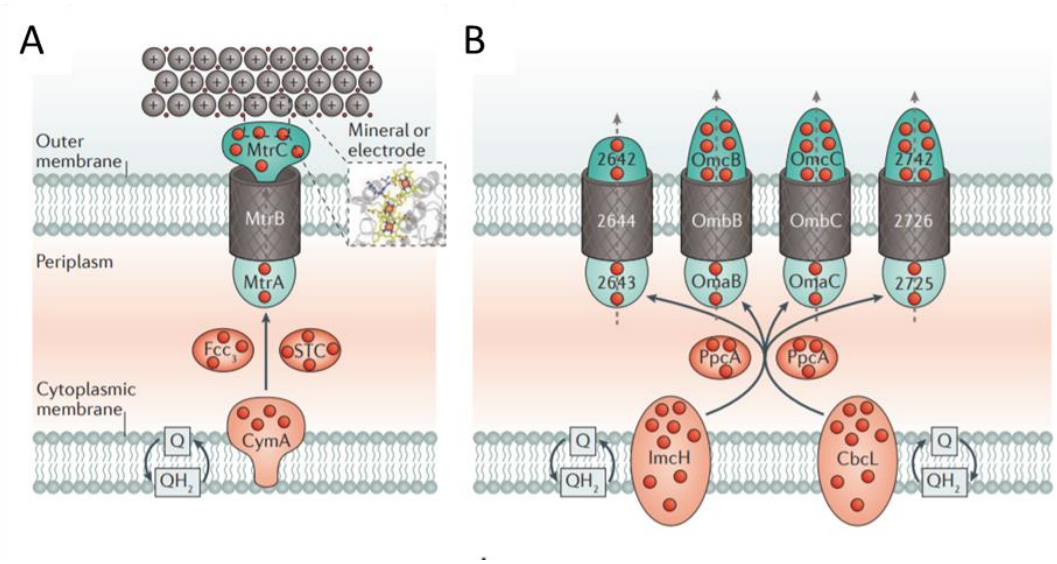

Figure 3.1. *Representation of extracellular secretion mechanisms for S. oneidensis (A) and (B) G. sufurreducens* [9].

3.1.1.3 Nanowires

In addition to membrane bound electron transport, *Geobacter* spp. form nanowires of protein filaments, anchored to the cell surface [10]. In *G. sulfurreducens* these

are assemblies of the pilin protein PilA86 which are hypothesised to be different to Mtr appendages but have similar functions [2].

These filaments are also observed in other bacteria. The sulphur reducing bacteria family *Desulfobulbaceae*, known as “cable bacteria”, form multicellular filaments that transfer electrons over centimetres, continuing from one cell to the next [11]. Cable bacteria are found in challenging environments (anoxic sediments, deep marine sediments), that force them to develop creative strategies to improve the access to electron acceptors [12]. The filaments are composed of tunnel-like cellular structures, called ridges, that are 70–100 nm wide and are formed between the cytoplasmic and outer membranes. The outer membrane might function as an insulator, to prevent leaking of the electrons outside the cells [9].

3.1.2 Mediated extracellular Electron Transport (MET)

Arguably all electron transport in bacteria is, to some extent, mediated. MET however refers to the use of soluble electron carriers to transport the electrons across the outer membrane to the electrode. MET allows distant cells to interact with the electrode and with other cells. Additionally, some electron shuttles chelate onto insoluble metals to transport them into the cell, increasing the availability of internal electron acceptors [13].

Redox mediators can be produced endogenously [14] or added externally [15].The use of externally added artificial mediators, such as methylene blue, neutral red, viologens, ferricyanide or naphthoquinone, is limited to lab studies, as their toxicity and cost constrains their use for field based applications [16].

Endogenous mediators, like riboflavin produced by *S. oneidensis MR-1*, shuttle electrons from the cell envelope (MtrC and OmcA) to mineral surfaces facilitating EET [17]. Figure 3.2 shows some of the known endogenous mediators involved in EET in bacteria.

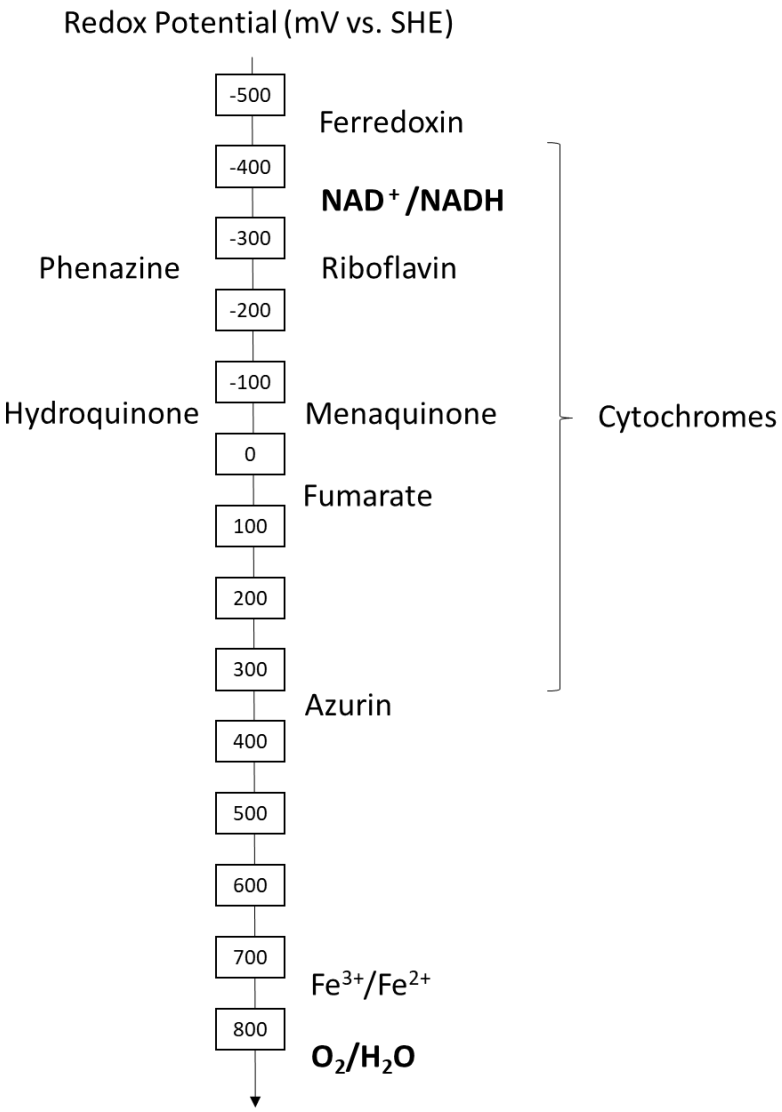

Figure 3.2. *Biological redox potentials of possible endogenous electron donors and acceptors in extracellular electron transport. Based on* [5].

Mediators are conjugated molecules, often pyridines and quinones, that exchange electrons with the environment driven by a potential gradient. In EET, the redox potential of mediators lies between the outer membrane potential and the anode potential, being oxidised by bacteria and reduced at the anode, in cycles. The process is however not self-sustaining due to loss of mediator by diffusion. To solve this, electricigens can immobilise redox active molecules at the electrode, by adsorption, forming biofilms, or with electrostatic forces [18]. Artificial adsorption [19] and electrodeposition [20] of mediators on electrodes have shown promising improvements on the stability of the bioreceptor.

EET in bacteria can be stimulated with a polarised electrode, leading to a wide range of diverse technologies: bioremediation [21], hydrogen production [22], energy supply for low power devices [23], robotics [24], biosensing [25] and electrosynthesis [26] .

3.2 Principles of Microbial Fuel Cells

In the particular case of MFC sensors, the anode is colonised by electroactive bacteria which, in the absence of a soluble electron acceptor in the nearby medium, transfer the electrons released during the oxidation of organic matter to the polarised electrode. The electrons migrate *via* a conductive wire to the cathode, whilst the protons- concomitantly excreted to balance the loss of electrons- migrate through the electrolyte to the cathode, where they reduce oxygen into water, liberating energy that can be traduced into electricity with a circuit (Figure 3.3).

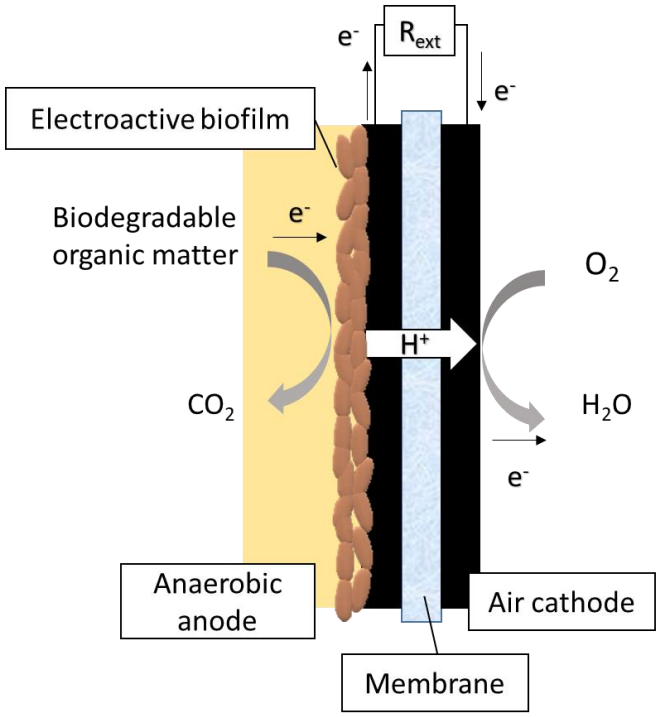

Figure 3.3. *Working principle of a microbial fuel cell. The anode is fed with organic matter (i.e. acetate or glucose) in anaerobic conditions. Through bacterial oxidation, electrons and protons are extracted from the substrate and released from the cells. These charged species are driven to the cathode by a electromotive driving force, to reduce oxygen.*

Although oxygen is the preferred electron acceptor due to its high potential and availability, there is a wide variety of electron acceptors: nitrates and sulphates, relevant in anoxic areas, sacrificial catholytes like $K_3[Fe(CN)_6]$, useful for lab-based studies, solid state metals such as MnO_2, or even biocathodes [27].

The energy gained in the MFC is proportional to the difference of redox potentials of the oxidant and reductant [28]:

$$W = \Delta G = -QE_{emf} = -nFE_{emf} \quad (3.1)$$

$$E_{emf} = E_{cat} - E_{an} \quad (3.2)$$

Where W is the useful work generated by the system, the Gibbs free energy (ΔG), in J mol $^{-1}$, Q is the charge exchanged, in C mol^{-1}, E_{emf} is the electromotive force driving the process, the potential difference of the anode, E_{an}, and cathode, E_{cath}, in V, n is the number of electrons per mol, and F is Faraday's constant (9.64853 × 10 C mol^{-1}), that relates mass to charge.

For the model case of acetate as electron donor and oxygen as acceptor in biological conditions (pH=7 pO_2=0.21, T=20 ˚C), with an equilibrium of 5 mM of CH_2COO^- and HCO_3, the E_{emf} is 1.1 V [29]:

$$Anode: 2HCO_3^- + 9H^+ + 8e^- \rightarrow CH_3COO^- + 4H_2O \qquad E = -0.296\,V \quad (3.3)$$

$$Cathode: O_2 + 4H^+ + 4e^- \rightarrow 2H_2O \qquad E = 0.805\ V \quad (3.4)$$

$$E_{emf} = 0.805 - (-0.296) = 1.1\ V \quad (3.5)$$

Electrode potentials differ from standard potentials because they depend on temperature and concentration of species, according to the Nernst equation:

$$E_{an} = {E_{an}}^0 + \frac{RT}{8F} ln\left(\frac{[CH_3COO^-]}{[HCO_3^-]^2[H^+]^9}\right) \quad (3.6)$$

$$E_{cat} = {E_{cat}}^0 + \frac{RT}{4F} ln\left(\frac{1}{pO_2[H^+]^4}\right) \quad (3.7)$$

Where E_x^0 is the standard potential, in V, R is the gas constant, 8.31 J mol^{-1} K^{-1}, T is temperature, in K.

The actual energy gained in the fuel cell (E_{cell}) is lower than the theoretical value E_{emf} due to losses in non-faradaic processes, activation energy of chemical reactions and heat. These inefficiencies, known as overpotentials, occur at the anode, cathode and the electrolyte.

3.2.1 Anode overpotentials

Anodic losses include the energy required to transport the electrons from the substrate to the electrode (Figure 3.4). These can be grouped in intracellular and extracellular losses [30].

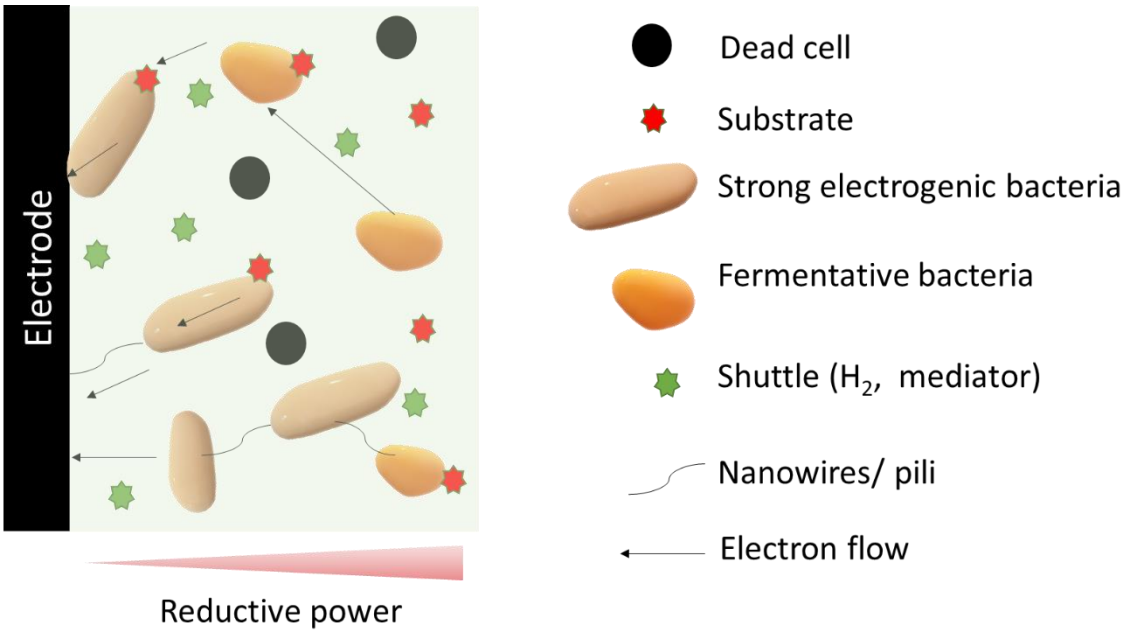

Figure 3.4. *Electron transport in a biofilm. Electron conduction takes place via DET and MET with the electrode and between cells, simultaneously.*

3.2.1.1 Intracellular losses

The energy invested in cellular, non-faradaic processes is determined as the potential difference between the electron donor and the exit point of electrons in the phosphorylation pathway (i.e. acetate to NADH/ quinone pool/ cytochromes). The remaining potential difference with the final electron acceptor is the available energy gain in the MFC, which is fully invested in ATP generation in non-

electrogenic conditions. To maximise the power output in the MFC, the anode potential is purposely set to the lowest possible value, whereas for sensing or bioremediation, anode potentials are set to maximise the sensitivity and selectivity.

Intracellular processes involve substrate uptake, oxidation of electron carriers and transfer of electrons to the outer membrane. Because substrate is generally added in excess, the system is rather limited by diffusion of electron shuttles or the electron transfer rate to the electrode [30]. The kinetics of the redox mediators are described by the Monod equation, expressed as a function of the electron shuttle concentration:

$$Turnover\ rate = q_{max} X_f L_f \frac{S_A}{S_A + K_A} \quad (3.8)$$

Where the turnover rate per surface area in e-m_{eq} cm^{-2}, the equivalent electron mass, depends on q_{max}, the maximum specific rate of substrate utilisation, in e-m_{eq} mg^{-1}; X_f is the concentration of active biomass in the biofilm in mg cm^{-3}; L_f is the biofilm thickness in cm; K_A is half-saturation electron-acceptor concentration, in e-m_{eq} cm^{-3}; and S_A is the electron-acceptor concentration in e-m_{eq} cm^{-3} [30].

The available electrons in an electrode are related to the Fermi level, and can be modelled as a combination of Nernst and Monod equations ([31]):

$$j = j_{max}\left(\frac{1}{1+\exp\left(-F(E-Eka)/RT\right.}\right) \quad (3.9)$$

Where j is the exchange current density in A m^{-2}, j_{max} is the maximum current density in A m^{-2}, E_{ka} is the potential at j= j_{max}/2 in V.

3.2.1.2 Extracellular losses

Extracellular losses to transfer electrons from the cell to the electrode are particularly relevant in thick biofilms where diffusion gradients rise (Figure 3.4). If the transfer is mediated, diffusion obeys *Fick's Law* [32]:

$$j = \frac{nFD_{med}\Delta C_{med}}{\Delta z} \quad (3.10)$$

Where D_{med} is the diffusion coefficient of the mediator in the matrix that depends on the Arrhenius equation, in m^2 s^{-1}; C_{med} is the concentration of mediator, mol m^{-3} and z is the distance between the mediator and the electrode, in m.

If the transfer of electrons in the biofilm to the interface is *via* DET, the current follows *Ohm's Law*:

$$j = \frac{-k_{bio}(E_{OM} - E_{interface})}{\Delta z} \quad (3.11)$$

where k_{bio} is the conductivity of the solid conductive matrix in Ω^{-1} m^{-1}; E_{OM} is the potential at the outer membrane and interface, in V and z is the distance between the cell and electrode, in m [30].

Equally, Butler Volmer's equation describes the direct electron transfer in the biofilm matrix and the transfer from membrane bound cytochromes in direct contact with the electrode:

$$j = j_0 exp\left[\frac{nF(1-\alpha)(E_{an} - E^{\circ})}{RT}\right] \quad (3.12)$$

Where, j_0 is the exchange current density at equilibrium, in A m^{-2} and α is the transfer coefficient [31].

Anodic losses decrease with increasing temperature, reducing the distance between the anode and bacteria and increasing the concentration of electron shuttles.

3.2.2 Cathode overpotentials

The Oxygen Reduction Reaction (ORR) is not only the preferred cathodic pathway in bioelectrochemical systems, but the key reaction in electrochemical oxygen sensors [32]. The ORR requires a large overpotential to break the oxygen bond (498 kJ mol^{-1}), which is the object of an extensive area of electrocatalysis. This chapter focuses only on carbon-based electrodes, the preferred option for long-term field deployment of MFC sensors. The ORR can take place via 4 or 2-electron pathway depending on the pH [33].

In acid media:

$$O_2\,(g) + 4H^+(aq) + 4e^- \rightarrow 2H_2O(l) \quad E^0 = 1.229\,V \quad (3.13)$$

$$O_2\,(g) + 2H^+(aq) + 2e^- \rightarrow H_2O_2(l) \quad E^0 = 0.67\,V \quad (3.14)$$

$$H_2O_2(l) + 2H^+(aq) + 2e^- \rightarrow H_2O(l) \quad E^0 = 1.77\,V \quad (3.15)$$

In alkaline media:

$$O_2\,(g) + 2H_2O(l) + 4e^- \rightarrow 4OH^-(aq) \quad E^0 = 0.401\,V \tag{3.16}$$

$$O_2\,(g) + H_2O(l) + 2e^- \rightarrow 4HO_2{}^-(l) \; + \; 4OH^-(aq) \; E^0 = -0.065\,V \tag{3.17}$$

$$HO_2{}^-(l) \rightarrow \; O_2\,(g) + \; 2OH^-(aq) \tag{3.18}$$

$$2H_2O_2(l) \rightarrow \; O_2\,(g) + 2H_2O(l) \tag{3.19}$$

For carbon electrodes without catalyst, the reduction of oxygen takes place at voltages lower than -1 V, therefore only peroxide through the two-electron reaction is formed [34]. In MFCs, the lack of catalysts, low conductivity of the electrolyte and neutral pH increases the overpotential of the ORR that occurs at < 0.5 V vs. Standard Hydrogen Electrode (SHE) [35].

3.3 Electroanalysis of bio-electrochemical systems

The use of electrochemical techniques is extensively used to determine the cause and extent of losses in bio-electrochemical systems. Voltammetry techniques stand out as non-invasive, fast and low-cost determination of overpotentials, transport processes and reaction rates in MFCs [36].

3.3.1 Polarisation curves

The polarisation test is a type of voltammetry assay that involves scanning the voltage and current from open circuit to short-circuit using a potentiostat or a variable resistor. When applied to an MFC, the measured cell voltage between electrodes decreases with increasing current, due to heat generation, as *Joule's Law* [13]:

$$E_{cell} = E_{emf} - \; IR_{int} = OCV - (\Sigma IR_a + \Sigma IR_c + IR_\Omega) \tag{3.20}$$

where OCV is the Open Circuit Voltage (mV) and IR_{int} (mV) is the sum of all internal activation, IR_a, concentration, IR_c and ohmic, IR_Ω energy losses.

Polarisation curves typically show three slopes corresponding to regions where different overpotentials dominate, namely activation (Zone 1), ohmic (Zone 2) and mass transport (Zone 3) limited regions (Figure 3.5).

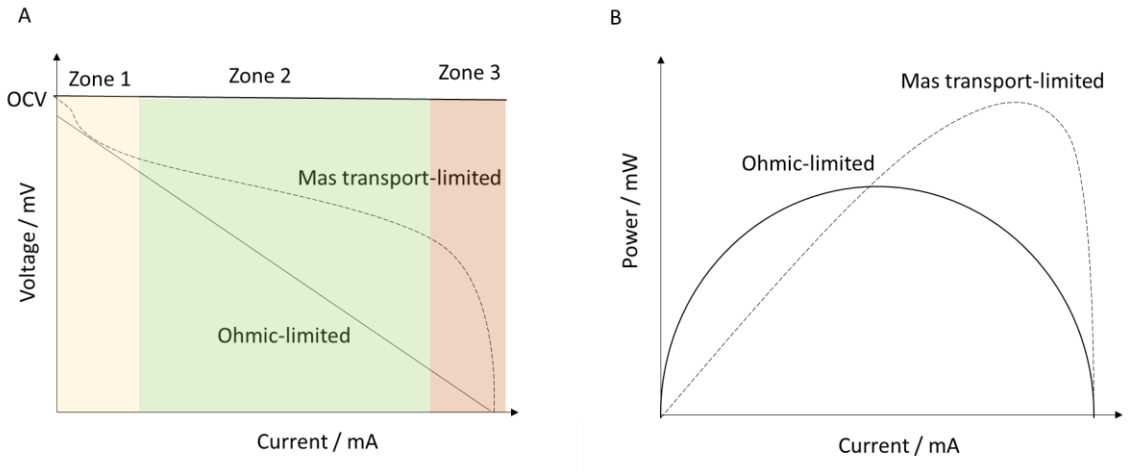

Figure 3.5. *(A) Polarisation curves showing the three distinctive regions for energy losses. (B) Power density curves of an ideal system (dashed line) and an ohmic limited, underperforming, system (black line).*

The difference between E_{emf} and OCV is the energy invested in parasitic internal currents. Oxygen crossover or presence of other electron acceptors in the anode, such as nitrates, decrease the OCV [37]. Equally, in biocathodes, organic matter acts as an alternative electron donor, decreasing the OCV. Diffusion and fluidic conductance increase parasitic currents, and can be reduced using membranes and air gaps [38].

At low current (Zone 1), the system incurs in activation losses, related to the electrode overpotentials and bacterial requirements previously described. The current drawn in this region is therefore an indication of the reaction rate, which can be determined with the Tafel plot [39]. Activation losses can be reduced by increasing the electrode surface area, biofilm coverage of the electrode to increase the transfer of electrons from cytochromes, use of catalysts and increasing temperature.

At midrange current (Zone 2), the energy is sufficient to overcome the activation overpotentials and transport of ionic species in the system becomes limiting. In this region, the system obeys *Ohm's Law*, hence the voltage and current follow an inverse linear relationship. The distance between electrodes, the presence of a separator and low conductivity of the electrodes and electrolytes increase ohmic losses. Reducing electrode spacing, the size of the MFC, increasing electrode to

membrane area ratio, using of current collectors with good electrical contact and operating at high temperature, contribute to reduce ohmic overpotentials [28]. The electrical contact between the biofilm and the electrode can also be improved increasing the electrode surface with carbon nanotubes [40], redox mediators [41] and conductive polymers such as polypyrrole [42] or osmium polymers [20].

Following *Ohm's Law*, the power output of the MFC is calculated as:

$$P_d = \frac{E_{cell}^2}{A_{An} R_{ext}} \quad (3.21)$$

Where E_{cell} is the recorded cell voltage at a fixed external resistance (mV), A_{an} is the area of the anode electrode (m^2) and R_{ext} is the applied external resistance (Ω).

MFCs often incur on substantial ohmic losses due to low conductivity of electrolytes and use of carbon-based electrodes. In these conditions, the power curve follows a symmetrical semicircle where the maximum power is far below the optimum current density achievable with low substrate usage efficiency. Ideally, power increases up to the maximum power point after which it decreases sharply due to mass transport limitations (Figure 3.5B).

At high currents (Zone 3), the reaction is fast, and mass transport limitations dominate the system. These have contributions from both the biological rate of substrate turnover and diffusion in the biofilm (Figure 3.4). The rate of electron transport is especially important in thick biofilms were bacteria are far from the electrode [43]. At the cathode, oxygen transport is the main limitation, especially in aqueous environments. Additionally, proton transport across the membrane is impeded by competition with other cations, which are normally orders of magnitude more concentrated in the electrolyte.

Polarisation requires that a pseudo-steady state is reached at each potential step, which is challenging in biological systems. Bacteria are unable to adjust to the external load if the scan rate is too fast and the system undergoes power overshoot, particularly at high currents, which underestimates both maximum power output and limiting current [44]. To determine if the waiting time between steps is sufficient to reach the steady state, the same profile should be obtained with a reverse scan (from low to high resistance) [45]. Additionally, to know the

limiting electrode in the system, individual electrode potentials can be measured against a reference electrode, along with the cell potential [28].

The internal resistance represents the sum of the overpotentials and is an important parameter to estimate the systems limitations. It is frequently approximated from the ohmic region of the polarisation curve, which is a valid approach when the system is ohmic limited, but is best calculated using impedance, which gives the contributions of the anode, cathode electrodes and ohmic resistance [46]. A high internal resistance implies a low short-circuit current, regardless of the OCV.

3.3.2 Cyclic voltammetry

Cyclic voltammetry (CV) is an electrochemical technique to study the reduction and oxidation processes of molecular species and the kinetics of a chemical reaction. In bio-electrochemical systems, CV is used to determine rate-limiting steps, reversibility of the reaction, overpotentials, limiting current and adsorption/diffusion processes [39]. CV is commonly performed using a potentiostat in a 3-electrode system, that comprises a working electrode (WE), counter electrode (CE) and reference electrode (RE) arranged as shown in Figure 3.6.

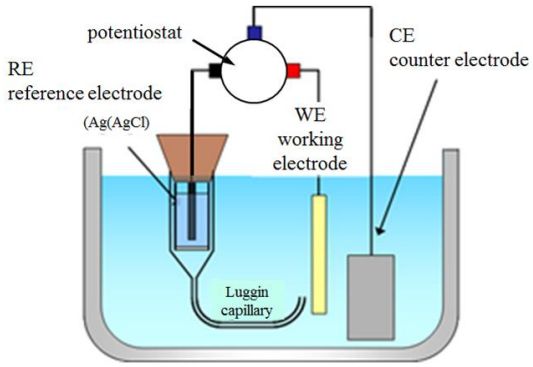

Figure 3.6. *Standard three-electrode set up for cyclic voltammetry. Wikipedia.*

The half reaction of interest, whether reduction or oxidation, takes place at the WE whereas the other half reaction occurs at the CE, that closes the electrical circuit. The CE must be stable and bigger than the WE to ensure that the counter half-

reaction, which is not of interest, do not affect the voltammogram trace. The WE potential is controlled and, therefore, must be referred to a stable reference potential in the system, provided by the RE. The electrodes are immersed in an electrolyte comprising a solvent and a supporting electrolyte, to increase the conductivity and reduce ohmic drop in the solution [47].

To study oxidation processes, the Fermi level of the electrode - the number of electrons available for the reaction - measured as potential, is raised from negative to positive values at a fixed scan rate. When the energy level of the WE overcomes the activation energy and overpotentials to start the reaction, current is produced. This point is known as onset potential and designates the activation energy [13].

In MFCs, the electrolyte is commonly growth medium containing redox active compounds that can give a signal in the voltammogram; thus, a blank scan is run in the media to extract the baseline signal from the biofilm signal. The background current, the non-faradaic contribution due to the double layer capacitance on the surface of the electrode, is also measured in the blank scanner and can be extracted in the post-analysis of the traces. Slow scan rates and low surface area prevent capacitive currents, increasing the sensitivity of the method to low current, faradaic processes. Slow scan rates also prevent false readings on the limiting current due to diffusion effects. Ideally, in each experiment the scan rate is set as the maximum where the limiting current does not change, which in practice often lies between 1 and 5 mV s^{-1} for biological systems [13].

The potential scan window should include all major reactions within the limit of stability of the solvent and cell membranes (i.e. -0.5 to 0.2 V vs Ag for *G.sulfurreducens* [48] and -0.7 to 0.4 V vs. SHE for *S.oneidensis* [17]).

3.3.2.1 Interpretation of CV in bioelectrochemical systems

Microbial electron transfer involves multiple reversible and irreversible reactions. Thicker biofilms induce long-range electron relays, cell-cell interactions and diffusion limitations that complicates the analysis and interpretation of results.

The simplest case is an irreversible reaction where the current density, *j*, is proportional to the diffusion of donors, the standard rate constant of the reaction and the electrode potential. Diffusion of donors is limiting in chemical reactions,

however in bioelectrochemical systems, the j_{lim} saturates at 5 mM, way below the diffusion limit of acetate oxidation estimated by the Levich equation [43].

If the final reversible step is sluggish, the j_0 should respond to a wide range of applied potentials which increase the electron transfer rate at the interface (Figure 3.7A). Should the irreversible enzymatic conversion be the limiting step, it will respond with a sharp increase followed by a plateau at higher potentials, because V_{max} depends on the enzymatic turnover rate, which is independent on the electrode potential (Figure 3.7B). Lastly, if the reversible pathway is limiting, faster scan rates will indicate the time for electrons to reach the surface [43].

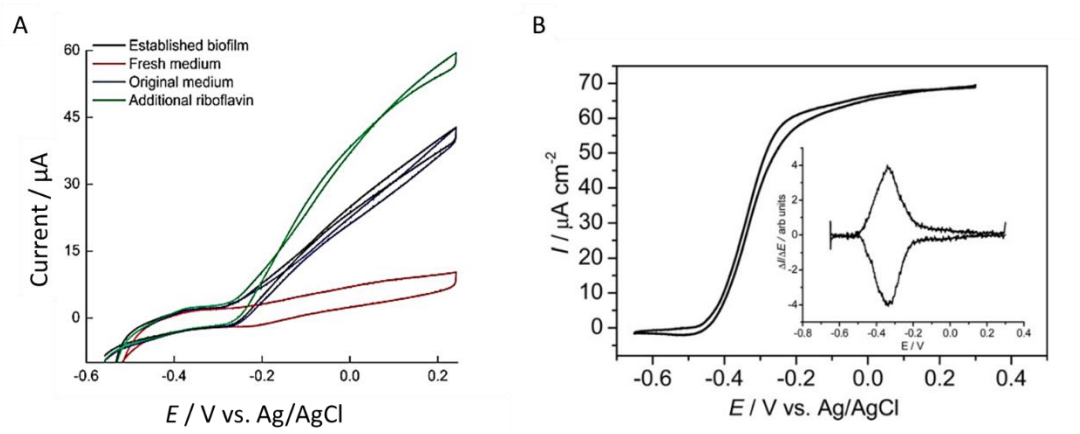

Figure 3.7. *Typical voltammograms of strong electricigens. (A) Voltammogram of S. oneidensis* [17]. *(B) G. sulfurreducens in turnover conditions* [48]*. Inset corresponds to the first derivative of the current with voltage.*

The nature of the EET, whether DET or MET, can be assessed from the diffusion or adsorption analysis with the Randles-Sevich equation [47], evaluating the change in redox couples in the voltammograms after replacing the medium or, alternatively, adding mediators that can improve the maximum current (Figure 3.7A) [17].

3.4 References

[1] M. C. Potter, “Electrical effects accompanying the decomposition of organic compounds,” *Proc. R. Soc. London. Ser. B, Contain. Pap. a Biol. Character*, vol. 84, no. 571, pp. 260–276, 1911.

[2] J. A. Gralnick and D. K. Newman, “Extracellular respiration,” *Mol. Microbiol.*, vol. 65, no. 1, pp. 1–11, 2007.

[3] L. Tao, M. Xie, G. G. Y. Chiew, Z. Wang, W. N. Chen, and X. Wang, “Improving electron: Trans -inner membrane movements in microbial electrocatalysts,” *Chem. Commun.*, vol. 52, no. 37, pp. 6292–6295, 2016.

[4] Y. Cao *et al.*, “Electricigens in the anode of microbial fuel cells: Pure cultures versus mixed communities,” *Microbial Cell Factories*, vol. 18, no. 1. 2019.

[5] F. Kracke, I. Vassilev, and J. O. Krömer, “Microbial electron transport and energy conservation - The foundation for optimizing bioelectrochemical systems,” *Front. Microbiol.*, vol. 6, no. JUN, pp. 1–18, 2015.

[6] L. E. Doyle and E. Marsili, “Weak electricigens: A new avenue for bioelectrochemical research,” *Bioresource Technology*, vol. 258. pp. 354–364, 2018.

[7] G. T. Feliciano, R. J. Steidl, and G. Reguera, “Structural and functional insights into the conductive pili of Geobacter sulfurreducens revealed in molecular dynamics simulations,” *Phys. Chem. Chem. Phys.*, vol. 17, no. 34, pp. 22217–22226, 2015.

[8] N. S. Malvankar *et al.*, “Structural basis for metallic-like conductivity in microbial nanowires,” *MBio*, vol. 6, no. 2, pp. 1–10, 2015.

[9] L. Shi *et al.*, “Extracellular electron transfer mechanisms between microorganisms and minerals,” *Nat. Rev. Microbiol.*, vol. 14, no. 10, pp. 651–662, 2016.

[10] G. Reguera, K. D. McCarthy, T. Mehta, J. S. Nicoll, M. T. Tuominen, and D. R. Lovley, “Extracellular electron transfer via microbial nanowires,” *Nature*, vol. 435, no. 7045, pp. 1098–1101, 2005.

[11] C. Pfeffer *et al.*, “Filamentous bacteria transport electrons over centimetre distances,” *Nature*, vol. 491, no. 7423, pp. 218–221, 2012.

[12] G. Wegener, V. Krukenberg, D. Riedel, H. E. Tegetmeyer, and A. Boetius, “Intercellular wiring enables electron transfer between methanotrophic archaea and bacteria,” *Nature*, vol. 526, no. 7574, pp. 587–590, 2015.

[13] F. Zhao, R. C. T. Slade, and J. R. Varcoe, “Techniques for the study and development of microbial fuel cells: An electrochemical perspective,” *Chem. Soc. Rev.*, vol. 38, no. 7, pp. 1926–1939, 2009.

[14] W. Habermann and E. H. Pommer, “Biological fuel cells with sulphide storage capacity,” *Appl. Microbiol. Biotechnol.*, vol. 35, no. 1, pp. 128–133, 1991.

[15] H. Bennetto, J. Stirling, K. Tanaka, and C. Vega, “Anodic reactions in microbial fuel cells,” *Biotechnol. Bioeng.*, vol. 25, no. 2, pp. 559–568, 1983.

[16] Z. Du, H. Li, and T. Gu, “A state of the art review on microbial fuel cells: A promising technology for wastewater treatment and bioenergy,” *Biotechnol. Adv.*, vol. 25, no. 5, pp. 464–482, 2007.

[17] E. Marsili, D. B. Baron, I. D. Shikhare, D. Coursolle, J. A. Gralnick, and D. R. Bond, “Shewanella secretes flavins that mediate extracellular electron transfer,” vol. 105, no. 10, pp. 6–11, 2008.

[18] S. Pirbadian *et al.*, “Shewanella oneidensis MR-1 nanowires are outer membrane and periplasmic extensions of the extracellular electron transport components,” *Proc. Natl. Acad. Sci. U. S. A.*, vol. 111, no. 35, pp. 12883–12888, 2014.

[19] Y. Li *et al.*, “Application of 2-hydroxy-1,4-naphthoquinone- graphene oxide (HNQ-GO) composite as recyclable catalyst to enhance Cr(VI) reduction by Shewanella xiamenensis,” *J. Chem. Technol. Biotechnol.*, vol. 94, no. 2, pp. 446–454, 2019.

[20] L. Darus *et al.*, “Redox-polymers enable uninterrupted day/night photo-driven electricity generation in biophotovoltaic devices,” *J. Electrochem. Soc.*, vol. 164, no. 3, pp. H3037–H3040, 2017.

[21] A. Domínguez-Garay, J. R. Quejigo, U. Dörfler, R. Schroll, and A. Esteve-Núñez, “Bioelectroventing: an electrochemical-assisted bioremediation strategy for cleaning-up atrazine-polluted soils,” *Microb. Biotechnol.*, vol. 11, no. 1, pp. 50–62, 2018.

[22] B. Ghasemi, S. Yaghmaei, K. Abdi, M. M. Mardanpour, and S. A. Haddadi, “Introducing an affordable catalyst for biohydrogen production in microbial electrolysis cells,” *J. Biosci. Bioeng.*, vol. 129, no. 1, pp. 67–76, 2020.

[23] T. Ewing, T. Ha, and H. Beyenal, “Evaluation of long-term performance of sediment microbial fuel cells and the role of natural resources,” *Appl. Energy*, vol. 192, pp. 490–497, 2017.

[24] I. Ieropoulos, C. Melhuish, J. Greenman, and I. Horsfield, “EcoBot-II: An artificial agent with a natural metabolism,” in *International Journal of Advanced Robotic Systems*, vol. 2, no. 4, pp. 295–300,2005.

[25] B. H. Kim, I. S. Chang, G. C. Gil, H. S. Park, and H. J. Kim, “Novel BOD (biological oxygen demand) sensor using mediator-less microbial fuel cell,” *Biotechnol. Lett.*, vol. 25, no. 7, pp. 541–545, 2003.

[26] K. P. Nevin, T. L. Woodard, A. E. Franks, Z. M. Summers, and D. R. Lovley, “Microbial electrosynthesis: Feeding microbes electricity to convert carbon dioxide

and water to multicarbon extracellular organic compounds," *MBio*, vol. 1, no. 2, 2010.

[27] D. Ucar, Y. Zhang, and I. Angelidaki, "An overview of electron acceptors in microbial fuel cells," *Front. Microbiol.*, vol. 8, no. APR, pp. 1–14, 2017.

[28] B. E. Logan *et al.*, "Microbial fuel cells: Methodology and technology," *Environmental Science and Technology*, vol. 40, no. 17. pp. 5181–5192, 2006.

[29] K. Rabaey, L. Angenent, U. Schroder, and K. Jurg, Eds., *Bioelectrochemical Systems: From Extracellular Electron Transfer to Biotechnological Application*. IWA Publishing, 2009.

[30] C. I. Torres, A. K. Marcus, H. S. Lee, P. Parameswaran, R. Krajmalnik-Brown, and B. E. Rittmann, "A kinetic perspective on extracellular electron transfer by anode-respiring bacteria," *FEMS Microbiol. Rev.*, vol. 34, no. 1, pp. 3–17, 2010.

[31] C. I. Torres, A. K. Marcus, P. Parameswaran, and B. E. Rittmann, "Kinetic experiments for evaluating the nernst-monod model for anode-respiring bacteria (ARB) in a biofilm anode," *Environ. Sci. Technol.*, vol. 42, no. 17, pp. 6593–6597, 2008.

[32] Y. Wei, Y. Jiao, D. An, D. Li, W. Li, and Q. Wei, "Review of dissolved oxygen detection technology: From laboratory analysis to online intelligent detection," *Sensors (Switzerland)*, vol. 19, no. 18, 2019.

[33] J. Mao, "Oxygen Reduction Reaction Electrocatalysis †," vol. 1, no. 9, pp. 8785–8789, 2019.

[34] H. Zhang, C. Lin, L. Sepunaru, C. Batchelor-McAuley, and R. G. Compton, "Oxygen reduction in alkaline solution at glassy carbon surfaces and the role of adsorbed intermediates," *J. Electroanal. Chem.*, vol. 799, pp. 53–60, 2017.

[35] F. Zhao, F. Harnisch, U. Schröder, F. Scholz, P. Bogdanoff, and I. Herrmann, "Challenges and constraints of using oxygen cathodes in microbial fuel cells," *Environ. Sci. Technol.*, vol. 40, no. 17, pp. 5193–5199, 2006.

[36] A. M. Bond *et al.*, *Electroanalytical Methods Guide to Experiments and Applications 2nd, revised and extended edition*. 2009.

[37] D. Wang *et al.*, "Open external circuit for microbial fuel cell sensor to monitor the nitrate in aquatic environment," *Biosens. Bioelectron.*, vol. 111, no. March, pp. 97–101, 2018.

[38] P. Ledezma, J. Greenman, and I. Ieropoulos, "MFC-cascade stacks maximise COD reduction and avoid voltage reversal under adverse conditions," *Bioresour. Technol.*, vol. 134, pp. 158–165, 2013.

[39] F. Zhao, R. C. T. Slade, and J. R. Varcoe, "Techniques for the study and development of microbial fuel cells: an electrochemical perspective," *Chem. Soc.*

Rev., vol. 38, no. 7, p. 1926, 2009.

[40] D. Odaci, A. Telefoncu, and S. Timur, “Pyranose oxidase biosensor based on carbon nanotube (CNT)-modified carbon paste electrodes,” *Sensors Actuators B*, vol. 132, pp. 159–165, 2008.

[41] A. Ruff, “Redox polymers in bioelectrochemistry: Common playgrounds and novel concepts,” *Curr. Opin. Electrochem.*, vol. 5, no. 1, pp. 66–73, 2017.

[42] Z. Yongjin, J. Pisciotta, R. B. Billmyre, and I. V. Baskakov, “Photosynthetic microbial fuel cells with positive light response,” *Biotechnol. Bioeng.*, vol. 104, no. 5, pp. 939–946, 2009.

[43] E. Labelle and D. R. Bond, “Cyclic voltammetry of electrode-attached bacteria.,” in *Bio-electrochemical Systems: from extracellular electron transfer to biotechnological application.*, Wiley-VCH Verlag, pp. 1–15, 2005.

[44] J. Winfield, I. Ieropoulos, J. Greenman, and J. Dennis, “The overshoot phenomenon as a function of internal resistance in microbial fuel cells,” *Bioelectrochemistry*, vol. 81, no. 1, pp. 22–27, Apr. 2011.

[45] V. J. Watson and B. E. Logan, “Analysis of polarization methods for elimination of power overshoot in microbial fuel cells,” *Electrochem. commun.*, vol. 13, pp. 54–56, 2011.

[46] Z. He and F. Mansfeld, “Exploring the use of electrochemical impedance spectroscopy (EIS) in microbial fuel cell studies,” *Energy Environ. Sci.*, vol. 2, no. 2, pp. 215–219, 2009.

[47] N. Elgrishi, K. J. Rountree, B. D. McCarthy, E. S. Rountree, T. T. Eisenhart, and J. L. Dempsey, “A Practical Beginner’s Guide to Cyclic Voltammetry,” *J. Chem. Educ.*, vol. 95, no. 2, pp. 197–206, 2018.

[48] K. Fricke, F. Harnisch, and U. Schröder, “On the use of cyclic voltammetry for the study of anodic electron transfer in microbial fuel cells,” *Energy Environ. Sci.*, vol. 1, pp. 144–147, 2008.

Chapter 4

To characterise the MFC sensor, the influence of environmental and design factors must be evaluated in a holistic approach such as Design of Experiments (DoE) rather than applying the one-factor-at-the-time (OFAT) approach. This Chapter introduces the principles of DoE, focusing on the use of factorial designs as an effective sequential method to study and characterise a system. A detailed mathematical description of the method is provided along with a practical example in the context of MFC sensors. Finally, the statistical background, simplifications and requirements of the model are discussed. The chapter is based on two main sources, provided as references. A discussion on the prior use of DoE in MFC systems is not included because these studies focus on the use of DoE for optimisation rather than prediction purposes.

4. Principles of Design of Experiments

MFC sensors are complex systems where operational and design factors may affect multiple features simultaneously. To better understand these systems, the influence of factors in the sensor response should be assessed taking into account possible interferences. This can be determined with Design of Experiments (DoE) method, an efficient statistical tool to systematically quantify the effect of several factors on an outcome.

DoE is versatile and can be used for optimisation and predictive purposes. In DoE, factors are classified as categorical (or qualitative), or numerical (or quantitative). Factor values are discretely set as high (+) and low (-) levels, corresponding to the limits of the range of study for numerical factors. For categorical factors, the assignment of levels is random but must be consistent throughout the analysis. The range of factor values should be wide enough to not pick up only noise, but

not too large to incur in important non-linearities. Each combination of factors and levels is called treatment and corresponds to one experiment.

Experiments must be run in random order and by different experimenters if possible, to avoid biases and autocorrelations in the results. Randomisation reduces the effect of unknown and unmeasurable factors in the system [1].

4.1 Factorial designs

For the particular case of a MFC sensor for water quality monitoring, the response variable could be voltage and the factors under study dissolved oxygen (DO) and temperature (T) (Table 4.1). This is a system with two factors at two levels and one outcome, hence the number of treatments in a full factorial design is 2^2, (which generalises to N^k for k factors at N levels).

***Table 4.1**. Standard order table for an MFC sensor with dissolved oxygen (DO) and temperature (T) factors and voltage response (V). Response values are simulated using prior knowledge in MFC systems.*

Experiment	**Factor 1 (T / ˚C)**	**Factor 2 (DO / mg L^{-1})**	**Outcome (V / mV)**
1	+ (30)	+ (10)	V1 (350)
2	+ (30)	- (1)	V2 (100)
3	- (10)	+ (10)	V3 (200)
4	- (10)	- (1)	V4 (20)

Where the factor levels are set in the range of 10-30 ˚C for T and 1-10 mg L^{-1} for DO and are coded as:

$$Center\ value = \frac{Low\ value + High\ value}{2} \tag{4.1}$$

$$Range = High\ value - Low\ value \tag{4.2}$$

$$Coded\ factor = \frac{Real - Center\ value}{\frac{1}{2} range} \tag{4.3}$$

If the OFAT approach was followed in this case, and only experiments 1,3 and 4 were run, we would get one estimate for each factor (Figure 4.1, thick arrows). Running the 4th experiment allows to get two estimates for each factor effect, duplicating the information (Figure 4.1, narrow arrows).

Figure 4.1 represents a factorial design in two (Figure 4.1A) and three factors (Figure 4.1B), known as cube plots. Note that in the latter, each side of the cube corresponds to a full factorial in two factors [2].

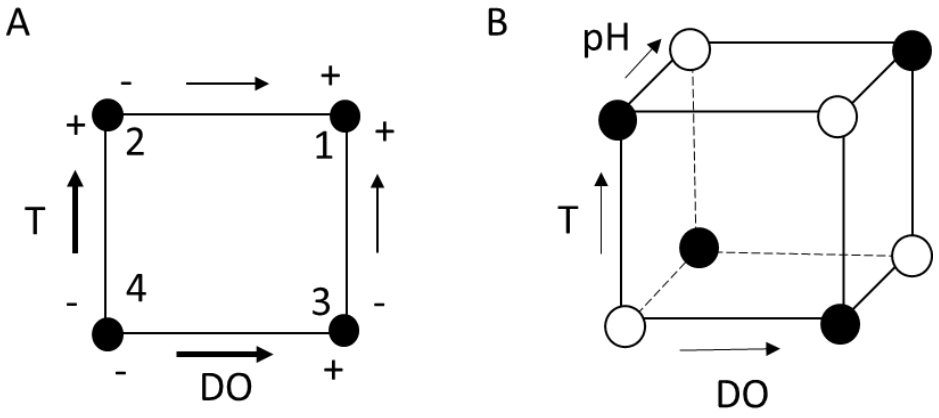

Figure 4.1. *Cube plot for two factors T and dissolved oxygen (DO) (A) and three factors T, DO and pH (B). Open and closed circles in B correspond to the half factorial experiments.*

The data from the 2-factorial DoE can be used to generate a Least Squares Model (LSM) to predict the voltage outcome as a function of T and DO:

$$V = interceipt + b_T T + b_{DO} DO + b_{DOT} DOT \quad (4.4)$$

Where the coefficients b_T, b_{DO} and b_{DOT} are calculated from Table 4.1 as follows:

b_T : Effect of temperature, in average, when T is increased from 10˚C to 30 ˚C:

$$At\ high\ DO \rightarrow V1 - V3 = 350 - 200 = 150$$

$$At\ low\ DO \rightarrow V2 - V4 = 100 - 20 = 80$$

$$b_T \rightarrow (150 + 80)/2 = 115$$

b_{DO} : The effect of DO, in average, when the DO is increased from 1 to 10 mg L^{-1}:

$$At\ high\ T \rightarrow V1 - V3 = 350 - 100 = 250$$

$$At\ low\ T \rightarrow V2 - V4 = 200 - 20 = 180$$

$$b_{DO} \rightarrow (250 + 180)/2 = 215$$

The effect of T is larger at high DO and the effect of DO is higher at high T, which is an indication of interaction between factors. Interaction implies that the effect of one factor depends on the level of the other factor and is symmetrical. An interaction term, b_{DOT}, is therefore needed in the LSM:

$$DO \rightarrow \frac{150 - 80}{2} = 35$$

$$T \rightarrow \frac{250 - 180}{2} = 35$$

The interaction plot is a straightforward tool to graphically assess the importance of the interactions, evidenced by the lines being unparallel (Figure 4.2A). Alternatively, the deviation from straight lines in contour plots give an idea of the interactions in the system (Figure 4.2B).

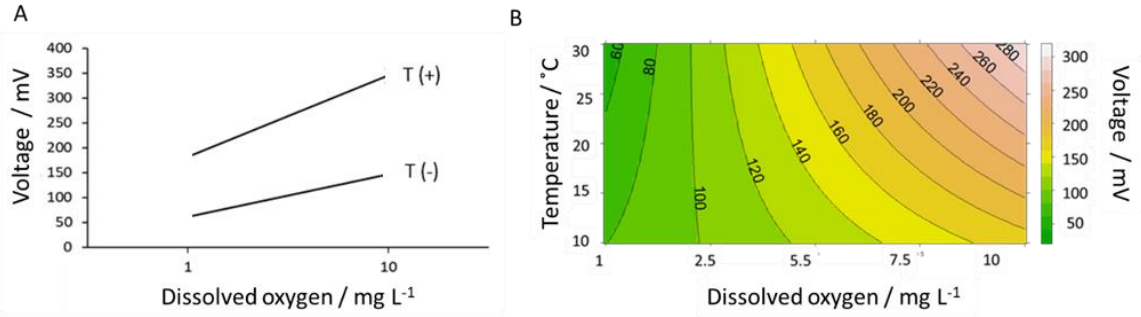

Figure 4.2. *(A). Interaction plot of T and DO on voltage. (B). Contour plot of T and DO with voltage as response.*

Substituting the values of the coefficients into the LSM we obtain the prediction of voltage, V, as a linear function of DO and T:

$$V = 167.5 + 57.5T + 107.5DO + 17.5DOT \qquad (4.5)$$

Where the intercept is the average of all outcomes and the coefficient of the factors represent the change in outcome when the factors are increased one unit. The factors are coded as 1 and -1, therefore an increase in 1 unit, from one to zero is half the total increase [1].

The representation of the coefficients of the linear model in a Pareto Plot (Figure 4.3) is useful to assess the relative importance of each factor [2].

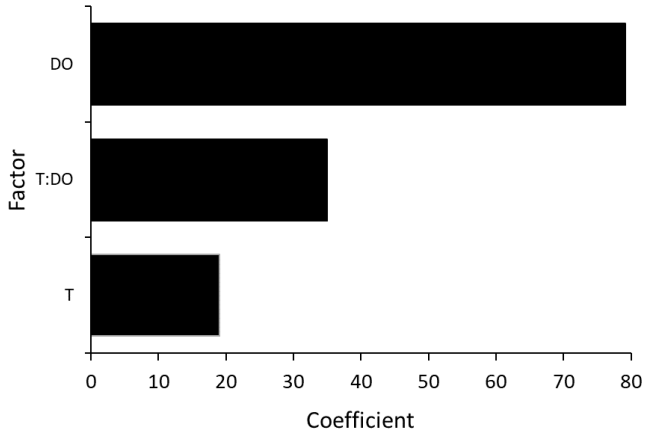

Figure 4.3. *Pareto plot showing the relative importance of the linear square model coefficients in T and DO.*

In a general approach with k factors and n experiments, the coefficients b_k are obtained with matrices:

$$\begin{bmatrix} y_1 \\ y_2 \\ \vdots \\ y_n \end{bmatrix} = \begin{bmatrix} x_{1,1}, x_{1,2}, \dots, x_{1,k} \\ x_{2,1}, x_{2,2}, \dots, x_{2,k} \\ \vdots \\ x_{n,1}, x_{n,2}, \dots, x_{n,k} \end{bmatrix} \begin{bmatrix} b_1 \\ b_2 \\ \vdots \\ b_k \end{bmatrix} + \begin{bmatrix} e_1 \\ e_2 \\ \vdots \\ e_n \end{bmatrix}$$

$$y = Xb + e$$

Substituting the data in Table 4.1 for the 2-factorial DoE in T and DO:

$$\begin{bmatrix} 350 \\ 100 \\ 200 \\ 20 \end{bmatrix} = \begin{bmatrix} +1, +1, +1, (+1)(+1) \\ +1, -1, +1, (-1)(+1) \\ +1, +1, -1, (+1)(-1) \\ +1, -1, -1, (-1)(-1) \end{bmatrix} \begin{bmatrix} b_0 \\ b_{DO} \\ b_T \\ b_{DOT} \end{bmatrix} + \begin{bmatrix} e_0 \\ e_{DO} \\ e_T \\ e_{DOT} \end{bmatrix}$$

$$X^T X = \begin{bmatrix} 4 & 0 & 0 & 0 \\ 0 & 4 & 0 & 0 \\ 0 & 0 & 4 & 0 \\ 0 & 0 & 0 & 4 \end{bmatrix}$$

$$X^T y = \begin{bmatrix} 670 \\ 430 \\ 230 \\ 70 \end{bmatrix}$$

$$b = (X^T X)^{-1} X^T y = \begin{bmatrix} \frac{1}{4} & 0 & 0 & 0 \\ 0 & \frac{1}{4} & 0 & 0 \\ 0 & 0 & \frac{1}{4} & 0 \\ 0 & 0 & 0 & \frac{1}{4} \end{bmatrix} \begin{bmatrix} 670 \\ 430 \\ 230 \\ 70 \end{bmatrix} = \begin{bmatrix} 167.5 \\ 107.5 \\ 57.2 \\ 17.5 \end{bmatrix}$$

Which gives the same coefficient values found in the graphical method described above. The error vector should be contained in a continuous convex plane with only one minimum, to obtain just one value of the coefficient that satisfies the above equations.

4.2. Fractional designs

It is obvious that running all the experiments in a DoE approach becomes prohibitive with increasing number of factors. Nonetheless, often only a few main factors and second order interactions are important while third and higher order interactions are commonly negligible or lay within the model's variance. Therefore, it is possible to run just a fraction of the experiments at the expense of losing information on high order interactions and still obtain a fair prediction of the data.

For example, a full three factorial requires eight experiments but is likely that the third and some second order coefficients are not significant. It would then be wise to run half factorial, assess the influence of the main factors and decide whether to run the other half or not. To design a half factorial in three factors, A, B and C, factor C is confounded with the interaction AB (standard order Table 4.2).

***Table 4.2**. Standard order table for a fractional factorial in three factors A, B and C.*

Exp	A	B	C=AB	AB	AC	BC	ABC	INT
1	**-**	**-**	**+**	**+**	**-**	**-**	**+**	**+**
2	**+**	**-**	**-**	**-**	**-**	**+**	**+**	**+**
3	**-**	**+**	**-**	**-**	**+**	**-**	**+**	**+**
4	**+**	**+**	**+**	**+**	**+**	**+**	**+**	**+**
5	-	-	-	+	+	+	-	+
6	+	-	+	-	+	-	-	+
7	-	+	+	-	-	+	-	+
8	+	+	-	+	-	-	-	+

Here, the columns of the first four rows are duplicated treatments. This means that running these four experiments gives a grouped outcome where the two paired coefficients are confounded:

$$\begin{bmatrix} y_1 \\ y_2 \\ y_3 \\ y_4 \end{bmatrix} = \begin{bmatrix} +1, -1, -1, +1 \\ +1, +1, -1, -1 \\ +1, -1, +1, -1 \\ +1, +1, +1, +1 \end{bmatrix} \begin{bmatrix} b_0 + b_{ABC} \\ b_A + b_{BC} \\ b_B + b_{AC} \\ b_C + b_{AB} \end{bmatrix} + \begin{bmatrix} e_1 \\ e_2 \\ e_3 \\ e_4 \end{bmatrix}$$

In this design, factor C is confounded, or aliased, with the second order interaction AB, A with AC and B with BC because their columns are indistinguishable. The intercept is aliased with the third order interaction ABC, because the multiplication of three factors gives the unity due to the imposed aliasing of C with AB. The remaining four experiments to complete the factorial are set by changing the sign of factor C, giving a unique set of treatments for each model coefficient.

Figure 4.1B shows the optimum choice of a subset of four experiments that provides more information and flexibility (black circles or white circles). With this arrangement, collapsing the cube into the sides produces a full factorial in two factors. This means that if one factor was found non-significant after running half factorial, then the DoE collapses on one side providing a full factorial in the other two factors and the experiment is finished [2].

In summar, a half factorial in a 3-factor DoE reduces the number of experiments from 8 to 4 at the expense of losing the second and third order interactions. This analysis can be extended to more factors with more complicated confounding patterns that are summarised in the so-called trade-off table (Table 4.3). This table

shows the confounding pattern as a function of the degree of reduction in experiments and the number of factors. The experiments are 2^{k-p}, where p is the reduction in the work with respect to the full factorial. For example, with eight experiments one can study three factors in a full factorial design, four factors in a half design, five factors in a quarter of a design, and up to seven factors with eight experiments (instead of 131), known as saturated or screening designs.

Table 4.3. *Trade-off table for fractional designs [1].*

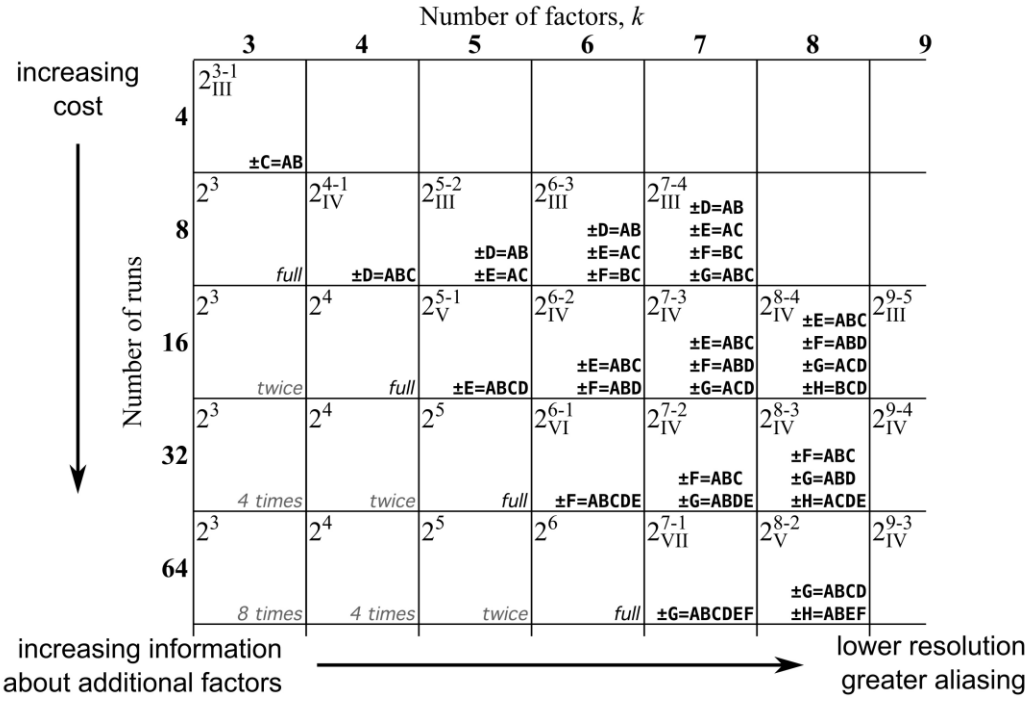

The generators for the aliasing pattern (each square in the trade-off table) are obtained following the same rationale explained for the three factors case. To define the aliasing pattern, the generators are rearranged as identity vectors, a unity vector obtained multiplying a vector for itself. In the case of five factors and eight experiments, the standard order table based on the trade-off table generators is (Table 4.4):

***Table 4.4**. Standard order of a saturated fractional design with five factors.*

Exp	A	B	C	D=AB	E=AC
1	**-**	**-**	+	**+**	**+**
2	**+**	**-**	+	**-**	**-**
3	**-**	**+**	+	**-**	**+**
4	**+**	**+**	+	**+**	**-**
5	-	-	-	+	+
6	+	-	-	-	-
7	-	+	-	-	+
8	+	+	-	+	-

The identity vector gives a relationship between the generators, which is known as defining relationship and is composed of words. Each defining relationship has 2^p words, where p is the reduction degree in the fractional design with respect to full design:

D=AB; DD=ABD=I
E=AC; EE=ACE=I

I=ABD=ACE=(ABD)(ACE)=BDCE → Defining relationship

word

To know the aliasing pattern of each factor, each letter is multiplied by the defining relationship:

A=BD=CE=ABDCE
B=AD=ACE=DCE
C=ABD=AE=BDE
D=AB=ACE=BCE
E=ABD=AC=BDC

From these sequences it is likely that three order and higher interactions are insignificant, and the aliasing can be simplified to:

A=BD=CE

B=AD

C=AE

D=AB

E=AC

Consequently, factor A is confounded with second order interactions and should not be one of the most important factors under study. In this design, main and second order interactions are confounded, which indicates the resolution of the design, which in this case is III (roman numbers in the trade-off table). The design resolution is equal to the length of the shortest word of the defining relationship.

In a resolution III or screening designs, main interactions are confounded with second order and third with fourth interactions. The resolution III design uses the less possible number of experiments to include the largest number of factors in the analysis and constitutes a practical first step to drop out non-significant factors.

In a resolution IV design, main interactions are confounded with third order effects, which are often negligible, and the coefficient describes mainly main interactions. The prediction of second order interactions is poor in this design as they are aliased with each other.

Resolution V designs are useful to characterise systems. Here the main effects are confounded with fourth order and second with third order interactions. This design provides the most accurate determination of main and second order interactions at the expense of the largest number of experiments. Resolution V designs are ideal for predictive models [1].

4.3. Model validation

To be able to use the model for predictive purposes, the confident intervals of the coefficient estimates should be determined, which requires the analysis of the variance of the data. Whether replicates are not essential in DoE, as the experiments are intrinsically duplicated, replicates at the centre points or replicates of the whole data set are recommended to define the variance in the system [3].

Variance is defined as the deviation of the mean, caused by the effect of factors on the response. It is partially explained by the model, but there is also an error component that must be quantified.

An LSM of a sample with one factor:

$$y = b_0 + b_1 x + e \tag{4.6}$$

Where b_1 is the slope where the model predicts a higher portion of the variability (RegSS), which is quantified with respect to a flat line at the mean value with no variability (Figure 4.4). The rest of the variability is unexplained (RSS) and both add up to the total variance (TSS). These contributions are calculated as:

$$\sum(y_T - \overline{y})^2 = \sum(y_{LSM} - \overline{y})^2 + \sum(y_T - y_{LSM})^2 \tag{4.7}$$

Or:

Total sum of squares (TSS)=Regression SS (RegSS) + Residual SS (RSS) (4.8)

Where $\bar{y}$ and $\bar{x}$ are mean values, x_T and y_T are the actual point measured and y_{LSM} is the predicted value by the model.

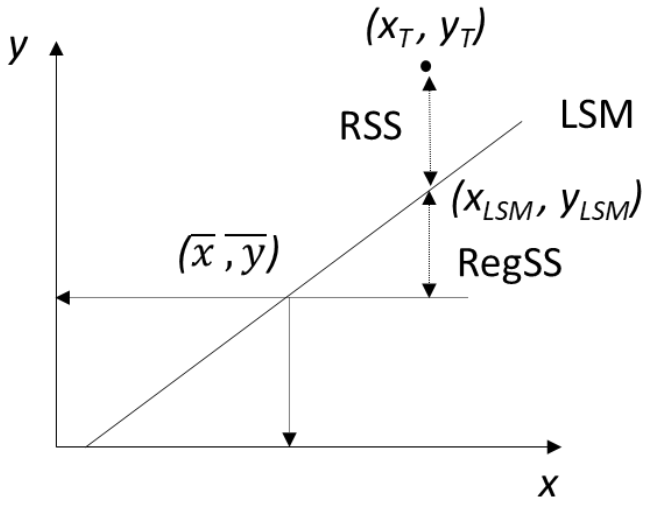

Figure 4.4. *Graphical representation of variance breakdown. Adapted from [1]..*

The percentage of the variability explained by the model with respect to the total variability is the correlation coefficient R^2= RegSS/TSS.

The determination of confidence intervals is particularly important for predictive purposes. Several assumptions are required to be able to calculate the confident intervals based on the variance of the coefficients [1,2]:

1. *All the error in the data belong to the response variable*: The explanatory variable *x* is assumed to be known and fixed. This assumption is frequently violated as *x* is measured during the experiment. However, the error precision of *x* is set by the instrument and is commonly insignificant.

2. *Linearity of the model*: required to use the LSM. Most processes are not linear but can be approximated by narrowing the range of study to a linear region or transforming the data into a linear expression. If non-linearity is unavoidable, the LSM can be replaced by non-linear models [3].

3. *Constant variance*: This is frequently violated in bioelectrochemical systems where the variance is time dependant and greatly varies with temperature. Non-constant variance is identified as a funnel shape when plotting residuals vs. predicted *y* or *x* (which are related by the least squares). Using weighted lest squares where the weight of residuals is pondered based on their magnification improves the homogeneity of variance.

4. *Normal error distribution*: this is an important assumption to verify that the true value lies within the confident intervals. Normality is checked with the qq-plot of the residuals. Deviation from the 45˚ line is commonly due to outliers. It also indicates that the analysis should have included more factors because a fraction of the data has a feature not included in the model. A screening design avoids this situation. If there is no information left in the residuals, the trend will follow the 45˚ line. Non-linearity can also skew the residuals which can be fixed by linearising or transforming the data.

5. *Independence of y and its error*: Independence of the data is required to use the central limit theorem. Independence of the observed data if often violated in slow processes with frequent data acquisition in time series. Plotting data over time and residuals over time and finding cyclic, cross-crossing and drifting patterns is an indication of non-independence. Randomisation of experiments in DoE should prevent autocorrelation.

4.4 References

[1] K. G. Dunn, “Process Improvement using Data,” *http://learnche.org/pid*, 2019. [Online]. Available: learnche.mcmaster.ca/pid.

[2] D. C. Montgomery, *Design and Analysis of Experiments*, 10th ed. Wiley-VCH Verlag, 2019.

[3] J. Lawson, *Design and Analysis of Experiments with R*. Utah, USA: CRC Press Taylor & Grancis Group, 2017.

RESULTS

Chapter 5

Chapter 5 introduces the novel use of algal biocathodes as sensing elements for pesticide detection in MFC biosensors. The concept is validated in a controlled lab environment, using a standard electrochemical reactor. In particular, an H-type double chamber cell with a polymeric proton exchange membrane (Nafion) is used. The membrane separates the electrolytes, to minimise the diffusion of algae and toxicant into the anode and the contamination of the cathodic biofilm with anodic heterotrophic bacteria, which could change the response of the algal biofilm to the toxicant. Nafion is prone to fouling and cracking and needs to be replaced in future studies for more sustainable and robust materials.

In this study, the anode is enriched in a standard manner using sludge as source of electroactive bacteria and acetate as carbon source. This is done to facilitate the comparison of the results with other studies run in similar conditions. The need for electrolyte replacement is however a limitation for unattended, in field operation. Instead, a solid anolyte like soil would provide long-term supply of organic matter to maintain the anodic reaction.

Atrazine is the tested pesticide because its effect in the photosynthetic activity is well characterised and has been used as model toxicant in biological assays, which can be used for comparison.

The alga *Scenedesmus obliquus* is chosen as bioreceptor for two reasons. Firstly, because there is extensive literature in the use of this organism for atrazine detection and secondly, it is widely used for tertiary treatment in wastewater treatment plants. The latter opens the possibility of using this sensor to detect toxicants at the inlet of the tertiary treatment, thus avoiding breakdown of the algal culture, which would incur in important economic losses. The cathode chamber is

however open to air, and it is therefore contaminated with other species. The SEM images of the cathodes shows a clear contamination of the biofilms with fungus and bacteria. Future studies on the use of algal biocathodes for self-powered biosensors should consider running the experiments in aseptic conditions and a closed cathode chamber to prevent contamination.

The algal biofilm generates oxygen, consumed in the cathodic reduction. When atrazine is injected in the catholyte, it induces a change in the photosynthetic oxygen evolution rate, which modifies the cathodic reduction reaction rate producing a change in the signal output.

To detect changes in the concentration of dissolved oxygen at a fast rate and minimise the response time of the sensor, the external resistance is chosen to provide the maximum current output without incurring in power overshoot.

Carbon felt and ITO are tested as cathode materials to evaluate their physical properties in the sensor's performance. This chapter also evaluates the recovery of the bioreceptor after the toxic event, a key aspect for practical implementation of MFC sensors for environmental monitoring. The study concludes that the porosity of carbon felt facilitates cell attachment and oxygen transport within the electrode, but the accumulation of oxygen in the electrode delays the response of the sensor to changes in algal metabolism.

This chapter has been published as detailed on the following page.

Statement of authorship

This declaration concerns the article entitled:

“Effect of Electrode Properties on the Performance of a Photosynthetic Microbial Fuel Cell for Atrazine Detection”

Publication status: Published

Publication details: Olías L.G., Cameron P., Di Lorenzo M. “Effect of Electrode Properties on the Performance of a Photosynthetic Microbial Fuel Cell for Atrazine Detection”, Frontiers in Energy Research, 7 pp. 1-11 (2019).

Author Contributions: Concept, L.G.; methodology, L.G., M.D.L.; experimentation, L.G.; writing—original draft preparation, L.G.; writing—review and editing, L.G., P.J.C., M.D.L.; supervision, P.J.C., M.D.L.; project administration, M.D.L.; funding acquisition, L.G., M.D.L.”.

Statement from candidate: This paper reports on original research I conducted during the period of my Higher Degree by Research candidature. In line with the regulations in QA7 Appendix 6 of the University of Bath, the abovementioned article has been stylistically integrated into the thesis, including: sections and figures numbering, typeface, margins and pagination.

Signed:

Date:

5. Effect of electrode properties on the performance of a photosynthetic microbial fuel cell for atrazine detection

Lola Gonzalez Olias,[1,2] Petra J. Cameron,[3] Mirella Di Lorenzo[1,]*

[1] Centre for Biosensors, Bioelectronics and Biodevices (C3Bio) and Department of Chemical Engineering, University of Bath, Bath BA2 7AY, United Kingdom

[2] Water Innovation Research Centre (WIRC), University of Bath, Bath BA2 7AY, United Kingdom

[3] Department of Chemistry, University of Bath, Bath BA2 7AY, United Kingdom

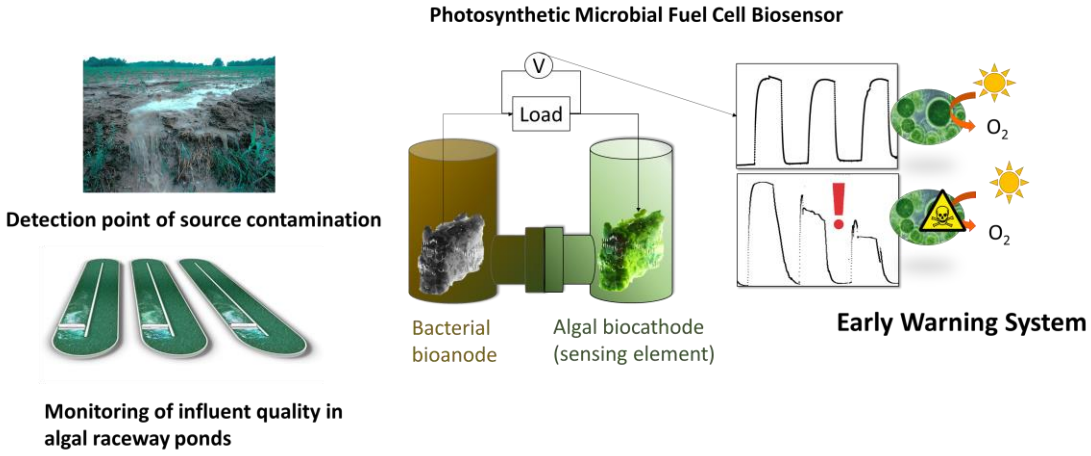

The growing use of herbicides in agriculture poses increasing concerns on the pollution of water systems worldwide. To be able to assess the presence of these compounds in water and limit their impact on human health and ecosystems, the development of effective *in situ* monitoring tools is key. Yet, many existing sensing technologies are not suitable for *in situ* and remote applications, due to challenges in portability, durability, cost and power requirements. In this study, we explore for the first time the use of an algal-assisted cathode in a photosynthetic microbial fuel cell (p-MFC) as a self-powered dissolved oxygen probe for herbicides detection in water. The cathode is enriched with the alga *Scenedesmus obliquus* and two different electrode materials are tested, graphite felt and indium tin oxide, which mainly differ in porosity, surface roughness and transparency. Despite the much larger specific surface area of graphite felt compared to indium tin oxide, the

current generated under light was only 10 times larger (109 ± 2µA vs. 10.5 ± 0.6 µA) and 8 times larger in the dark (37 ± 5 µA vs. 4.2 ± 0.6 µA). By generating a current output that correlates with the dissolved oxygen in the catholyte, the resulting p-MFCs could detect the EU atrazine concentration limit of 0.1 µg L^{-1}. The use of graphite felt led to shorter response times and better sensitivity, as a result of the greater current baseline. In both cases, the current baseline was recovered after exposure of the sensor to frequent toxic events, thus showing the resilience of the cathodic biofilm and the potential of the p-MFCs for early warning of herbicides pollution in water.

Keywords: Photosynthetic Microbial Fuel Cell, Biosensor, Water Quality, Algae, Atrazine, ITO, graphite felt.

5.1 Introduction

Worldwide, agricultural pollution is one of the major causes of degradation of water systems. Population growth, and the consequent increase in food demand, has led to an intensified use of pesticides and chemical fertilizers in agriculture that contaminate waters, posing serious risks to aquatic ecosystems and human health. In the EU, different directives, such as the Ground Water Directive, the Drinking Water Directive and the Water Framework Directive, regulate the maximum concentrations of individual pesticides and their degradation products in waters. To enforce these directives, reliable analytical methods for *in situ* monitoring of chemical pollutants in water are required [1].

Whole cell electrochemical biosensors represent a promising technology for water quality monitoring, leading to affordable technologies that can be used also in the most remote and poorest areas of the world, while moving away from the need of centralised analytical laboratories and the requirement of specialised personnel [2]. Particularly attractive is Microbial Fuel Cell (MFC) technology, which has also the potential benefit of self-powered operations [3].

Recently, the use of algae as the biorecognition element in photosynthetic MFC (p-MFC) based sensors has been reported [2]. Algae bring the benefits of great

susceptibility towards a wide range of pollutants, but are particularly interesting for herbicide detection, as these compounds specifically disrupt the activity of photosynthetic cells. In p-MFCs algae can be used at the anode or at the cathode and act respectively as the electron donor or as a source of electron acceptor. In the case of an algae-assisted anode, the presence of a pollutant interferes with the electrons generated, thus causing a change in the baseline current. On this basis, the detection of the herbicide atrazine [2], as well as other pollutants such as Zn, Cu [3] and formaldehyde [2] was recently demonstrated. In these systems, however, the stability of the signal output is greatly influenced by changes in pH and biological oxygen demand (BOD), which challenges their practical application in field. An algae-assisted cathode as sensing element would instead generate a more resilient signal to operational disturbances, with the result of a more reliable sensor [4]. In this case, the pollutant would cause a change in the photosynthetic generation of oxygen at the cathode, thus affecting the oxygen reduction reaction, and consequently the signal output [5]. As such, in this study we test for the first time the use of an algae-assisted cathode in a p-MFC based sensor for herbicide detection in water. We also investigate the role that the electrode properties have on the performance of the p-MFCs. In particular, two electrode materials, Graphite Felt (GF) and Indium Tin Oxide coated on Polyethylene Terephthalate (ITO/PET), are tested, which differ for surface area, roughness and transparency. ITO/PET is widely used in Clark based electrochemical biosensors [6, 7], where photosynthetic oxygen is transduced into current, yet, to the best of our knowledge, its use at the cathode in photosynthetic microbial fuel cells has not been investigated yet.

The electrode properties can play an important role in the reliability and sensitivity of the resulting sensor. The porosity and surface roughness would influence the distribution, thickness and stability of the cathodic biofilm [8]. On a porous electrode the biofilm is more resilient to detachment, however mass transport limitations may be introduced. Conversely, the biofilm that develops on a smooth planar surface is homogeneously exposed to bulk conditions, but it is more prone to detachment due to shear forces [9].

In this study, the cathode is inoculated with the microalgae *Scenedesmus obliquus.* This is a common eukaryotic alga, typically used for tertiary treatment in wastewater treatment plants, which has been previously tested for herbicide

detection [10]. Atrazine is used as the model herbicide, given its widespread use worldwide and the concerns about its high toxicity to aquatic life [11]. The electrochemical performance of the resulting systems is presented, and their ability to detect atrazine in water, due to changes in the dissolved oxygen, assessed.

5.2 Materials and methods

5.2.1 Materials

All reagents were purchased from Sigma Aldrich, unless otherwise specified.

Bold Basal Medium (BBM) was prepared by adding in 1 L of distilled water [12]: 0.25 g L^{-1} $NaNO_3$; 0.075 g L^{-1} $MgSO_4 \cdot 7H_2O$; 0.025 g L^{-1} NaCl; 0.075 g L^{-1} K_2HPO_4; 0.175 g L^{-1} KH_2PO_4; 0.025 g L^{-1} $CaCl_2 \cdot 2H_2O$; 0.011 g L^{-1} H_3BO_3; 1.0 mL of a trace elements solution (8.82 g L^{-1} $ZnSO_4 \cdot 7H_2O$, 1.44 g L^{-1} $MnCl_2 \cdot 4H_2O$, 0.71 g L^{-1} MoO_3, 1.57 g L^{-1} $CuSO_4 \cdot 5H_2O$, 0.49 g L^{-1} $Co(NO_3)2 \cdot 6H_2O$); a 1.0 mL EDTA solution (Na_2 5.0 g, KOH 3.1 g in 1 L of distilled water); and a 1.0 mL Fe solution (4.98 g $FeSO_4 \cdot 7H_2O$, 0.33 mL concentrated H_2SO_4 in 1 L of distilled water). The BBM was autoclaved (121 ˚C, 1 bar, 15min) prior to use. The final pH of the BBM solution was 6.75 ± 0.28 and the conductivity 0.97 ± 0.15 mS cm^{-1}.

Anaerobic sludge was provided by Wessex Water from a wastewater treatment plant in Avonmouth, UK. Artificial wastewater (AWW) was prepared as previously described [13] (pH=7.56 ± 0.21, conductivity 1.46 ± 0.35 mS cm^{-1}), with potassium acetate (9.8 g L^{-1}) as the carbon source, and autoclaved prior to use.

All aqueous solutions were prepared with reverse osmosis purified water.

The pH was measured with a pH-meter (Thermo Scientific Orion ROSS Ultra pH/ATC Triode, USA). Conductivity was measured with a conductivity benchtop cell (Orion, Thermo Scientific). The dissolved oxygen, DO, of the electrolytes was measured with a DO portable meter (RDO Orion 7003, Singapore). The chemical oxygen demand (COD) was determined by using a commercial reagent for high range samples (0-14000 ppm, HANNA Instruments HI 839800 COD reactor).

5.2.2 Algal culture

Scenedesmus obliquus (Dept. of Biology and Biochemistry, University of Bath, UK) was grown in 100 mL of autoclaved BBM, in triplicate, with no additional carbon source, in an incubator at 25 ˚C and a 12h/12h light/dark cycle, on white light (5 lm m^{-1}). The cultures were inoculated at a seeding concentration of $3.8 \cdot 10^5$ cells mL^{-1} and maintained within the exponential phase (Figure S5.1) by discontinuous dilution with BBM. Algal cell biomass was determined by flow cytometry (Guava Easy Cyte, Millipore) and the optical density (OD) by spectroscopy (Spectronic 200, Thermo Scientific) at 750 nm.

5.2.3 Configuration and operation of the photo-Microbial Fuel Cell sensor (p-MFC)

The photo-microbial fuel cell (p-MFC) consisted of a standard H-cell configuration made in glass. Each chamber had a total volume of 26 mL. The two chambers were separated by a Nafion 115 membrane, with an exposed area of 1.13 cm^2, and the two electrodes were kept at a fixed distance of 4 cm.

Carbon graphite felt (GF, Online Furnace Services Ltd., UK) was used as both the anode and cathode electrode, with a projected surface area of 13.6 cm^2 (2 x 2 x 0.7 cm^3). Prior to be used, the GF electrodes were acid treated to enhance both the hydrophilicity and the specific surface area of the graphite fibres, as previously described [14]. For comparison, Indium Tin Oxide, coated with Polyethylene Terephthalate Film (ITO/PET, 60 Ω cm^{-1}), was also tested as cathode. The ITO/PET electrodes had a projected surface area of 5 cm^2 (5 x 1 cm). The p-MFC with GF cathode is hereafter named as p-MFC_{GF}, while the device with ITO/PET as p-MFC_{ITO}.

The anode and cathode were connected with Ti wire (25 mm, Advent Research Materials, Oxford, UK) to an external resistance (R_{ext}) of 510 Ω to polarise the cells and to a data logger (PicoLog High Resolution Data Logger, Pico Technology) to monitor the voltage (V) over time. The voltage across the electrode terminals was measured every minute during normal operation and every 15 seconds during the toxic events.

The anolyte consisted of a 20% v/v AWW, inoculated with anaerobic sludge for a total COD of 7.41 ± 0.76 mg L^{-1} (n=3). The solution was purged for 10 min with N_2 prior to use. After the enrichment period (approximately 25 days), the anode was fed only on with AWW, which was replaced on a 4-day basis. During the operation, the anode chamber was sealed with a rubber septum to ensure anaerobic conditions and covered with aluminium foil to prevent the growth of photosynthetic microorganisms.

The catholyte consisted of the algal inoculum in BBM, prepared as detailed above, at a concentration of 4.4 x 10^5 cells mL^{-1}. The initial conditions of the catholyte were pH=7.22; Conductivity=0.871 mS cm^{-1}; Abs_{750}=0.176; DO=8.45 mg L^{-1}. The cathode chamber was open to air and operated under light/dark cycles of 12h/12h with LEDs lights (light intensity 1 mW cm^{-1}, 4.8 W m^{-3} warm white, 6000 K, Lighting Ever, UK.), placed at approximately 5 cm distance from the cathodes (Figure S5.2).

After the initial algal inoculation, tap water was added every two days to compensate for the evaporation losses. The catholyte was replaced by fresh algae (in the same seeding conditions) after 20 days of operation.

The p-MFC cells were operated in batch mode, thus allowing the pH and DO of the catholyte to rise along with the planktonic growth of algae, to mimic the conditions of stagnant eutrophic waters and raceway ponds. Dissolved oxygen, conductivity and pH were monitored during the start-up period. The temperature during operation was 23.9 ± 2.3 °C.

The current (I) was calculated according to Ohm's Law ($I = V/ R_{ext}$) and power (P) was calculated as P = I x V. The internal resistance was calculated from the slope of the middle section of the polarisation curves, as previously described [15]. Maximum power output was obtained from the power curve. For comparison with other studies, power density was normalised by the cathode projected surface area.

Polarisation tests were conducted by using a resistance box (RS Components, UK), from Open Circuit Voltage (OCV) to short-circuit across a loading range of 10 MΩ to 500 Ω, and a benchtop multi-meter (RS PRO RS-14 Digital Multimeter). Single electrode potentials were measured against an Ag/AgCl reference electrode (EDAQ, USA), which was placed inside the chamber of the electrode to be tested.

Cyclic Voltammetry (CV) measurements were performed in a three-electrode system by using a potentiostat (Autolab Metrohm Potstat 126N AUT85001). In these tests, the anode or the cathode served as the working electrode, a Pt wire (0.5 mm diameter) was used as the counter electrode and Ag/AgCl as the reference electrode. The CVs were carried out at a scan rate of 1 mV s^{-1}, swapping from 0.3 V to - 0.8 V when the cathode was investigated and from 0.6V to -0.8 V when the anode was tested, with 10 seconds of stabilisation.

Scanning electron microscopy (SEM) was performed as previously described [13] to visualise the biofilm on the electrodes. The resulting images were digitized using a JEOL SEM6480LV scanning electron microscope (JEOL, UK).

5.2.4 Simulating the toxic event

Atrazine was used as model substance for the toxic event because of its well-known inhibitory effects on algal photosynthetic activity [16]. This was simulated by adding the toxicant to the catholyte for a final concentration from 0.1 µg L^{-1} up to 10 mg L^{-1}, under agitation (45 rpm). The volume of toxicant injected was small enough to avoid significant changes in conductivity or pH (Figure S5.3). All experiments were performed in duplicate, unless otherwise specified, and at room temperature.

The p-MFC sensors response to atrazine was assessed in terms of response time, t_r, and recovery time, t_{rec}, calculated as:

$$t_{rec} = t_D - t_r \quad (5.1)$$

Where: t_r (h) is the response time, when the current output has reached 95% of its steady state (point C, Fig. S5.4) response after exposure to the pollutants; t_D (h) is the time when the initial baseline current is re-established, and it is assumed that the p-MFC has recovered from the toxicant event.

The rate of reduction of the signal, *SR,* in *(µA h^{-1})* was calculated as [17]:

$$SR = \frac{I_b - I_r}{t_r - t_A} \quad (5.2)$$

Where I_b is the current baseline under light before the event (µA); I_r is the current at t_r; *and* t_A is the time of injection of the toxicant.

The response was also assessed in terms of inhibition ratio (%) in both the short and long term, which was calculated as:

$$IR_{short\ term} = \frac{I_{nb} - I_b}{I_{nb}} \times 100 \quad (5.3)$$

$$IR_{long\ term} = \frac{I_{nb(long\ term)} - I_b}{I_{nb}(long\ term)} \times 100 \quad (5.4)$$

Where I_{nb} (µA) is the current baseline after the toxic event, either in the short or long term. A graphical description of these parameters is provided in Figure S5.4.

5.3 Results and discussion

5.3.1 Electrochemical performance of the p-MFCs

This study explores the use of a photosynthetic cathode as the sensing element in a photo microbial fuel cell (p-MFC) sensor for atrazine in water *via* the detection of dissolved oxygen changes in the catholyte. To evaluate the effect that the electrode porosity and transparency have on the sensing performance, two electrode materials were tested at the cathode: graphite felt (GF), used in p-MFC_{GF}; and ITO/PET (from here on simply referred to as ITO), used in p-MFC_{ITO}.

Firstly, the anode and cathode were enriched respectively with bacteria and algae. Figure 5.1A shows the current trend over time for the two p-MFCs. As shown, for the case of p-MFC_{ITO}, after only three days of operation, a photosynthetic pattern in the output current was observed, which was characterised by current increase under light and current decrease under dark conditions. In the case of p-MFC_{GF}, this light/dark current cycle started after seven days. This result suggests that that on the ITO electrode the cell attachment and biofilm formation is much more rapid than on GF, which could be a consequence of the higher hydrophilicity and lower porosity of ITO compared to GF [9, 18].

In both systems the formation of a green biofilm on the cathode surface was observed after the first week of operation. With p-MFC_{GF}, a growth curve, typical for anodic biofilm enrichment in microbial fuel cells [19], is observed during a period of over 20 days. After that, the catholyte was replaced with a fresh algal solution. This caused a drop in the current output followed by an increase until reaching a

higher steady-state current output (Figure 5.1A). As shown in Figure 5.1B and 5.1C, pH and DO of the catholyte quickly recovered after this change. For the case of p-MFC_{ITO}, replacing the catholyte on day 20 did not cause marked changes in the current output.

The exponential current increase is not as obvious for p-MFC_{ITO}, suggesting that, in this system, the cathode limits the reaction also at early stages of the enrichment, due to the lower surface area.

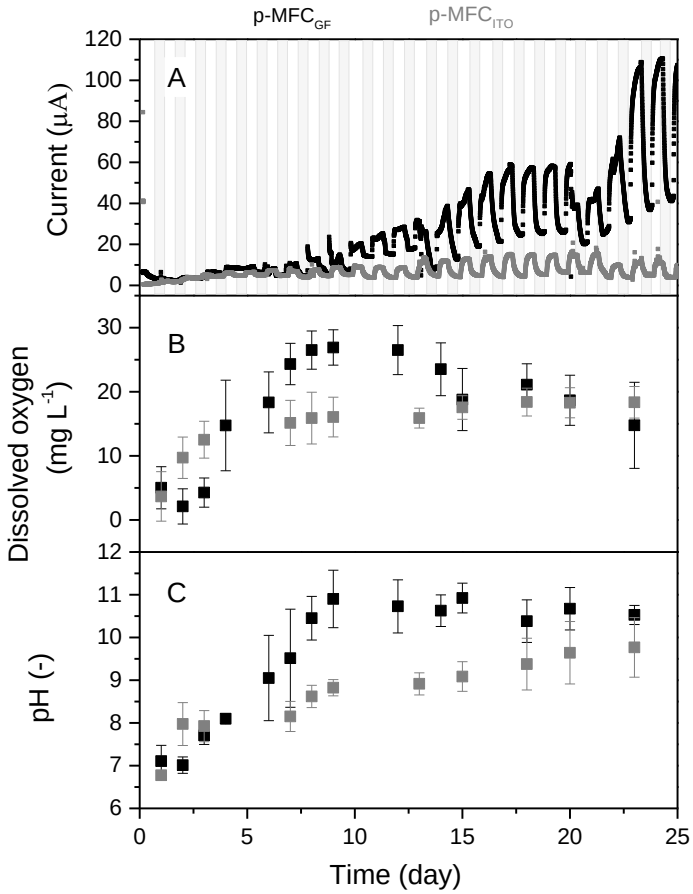

***Figure 5.1**. (A). Output current over time generated by the p-MFCs during the first 25 days of operation (start-up period). Data is the average of six replicates. Shadowed areas indicate the operation during the dark cycle. Figure S5.5 in the Supplementary Information shows data with error bars and data normalised by projected surface area. (B). Dissolved oxygen in the catholyte during the start-up period. (C). pH and conductivity evolution of the catholytes during start-up. In all the graphs, data related to p-MFC_{ITO} are reported in grey and data related to p-MFC_{GF} are reported in black.*

After 13 days, a steady-state current was reached for p-MFC_{ITO}, while for p-MFC_{GF} 23 days were necessary. The longer time required for p-MFC_{GF} may be the result of the much larger specific surface area available for cell attachment in the case of GF (3D electrode) compared to ITO (2D electrode) [9]. Despite the great difference in the specific surface area, the current obtained with p-MFC_{GF} was, however, only 10 times larger than p-MFC_{ITO} under light (109.4 ± 2.6 µA vs. 10.47 ± 0.63 µA) and 8 times larger under dark (36.8 ± 4.9 µA vs. 4.24 ± 0.57 µA). Similarly, the charge produced by p-MFC_{GF} during the first 24 days of operation was only 2.7 times larger than p-MFC_{ITO} (156 mC and 57 mC respectively). This result indicates that, in this system, ITO is much more efficient than GF as cathodic material for energy production. Nevertheless, maximising the power performance of the p-MFC would not necessarily lead to better sensing performance or better long-term stability.

During the dark cycle, the current baseline generated by p-MFC_{GF} increases over time, probably as a consequence of the oxygen produced and accumulated during the day**.** As shown in Figure 5.1B, the DO in the catholyte increases during the first days, to stabilise at a value of 16.4 ± 5.4 mg L^{-1} once a steady-state light/dark trend is reached, and an algal biofilm is developed at the cathode [20, 21]. The DO of the catholyte is influenced by multiple factors, i.e. light intensity [22], temperature [23], algae concentration [24] and pH [25]. Following the DO trend, the pH of the catholyte also increases with time to reach a value of 10.1 ± 0.5 at steady state (Figure 5.1C). The increase in the catholyte pH during operation, with respect to the algal catholyte grown as control (Figure S5.6), suggests that hydroxide is being produced [26].This high value of pH may be the reason why the levels of DO reported in this study are higher than what was previously observed in other p-MFCs (Table S5.1). Alkaline conditions at the cathode would prevent the growth of heterotrophic bacteria, which, although tolerate pH up to 10, grow optimally at neutral pH [27]. Consequently, high pH would limit the oxygen consumption in the catholyte not associated to electricity generation [28]. There is in fact a good correlation between DO and pH of the catholyte (R^2=0.8), with an increase of 0.14 mg L^{-1} of DO per unit of pH for both materials. On the other hand, the high pH of the catholyte could be the reason for the relative low power output obtained in this study (Figure S5.7) compared to similar studies (Table S5.1), because it affects the cathode potential [29].

In alkaline conditions, the theoretical OCV is 450 mV, in agreement with the value obtained in our study and other similar studies on GF (Table S5.1).

The electrochemical performance of the p-MFCs was assessed by measuring polarisation curves and cyclic voltammetry. To investigate whether the cathode is the limiting electrode under external load, polarisation studies were performed not only on the fuel cell but also on the individual electrodes. Since in this study the cathode is the sensing probe, it should be the limiting electrode, and in order to obtain a direct correlation between DO in the catholyte and current, the limiting reaction should be the cathodic oxygen uptake. To minimise any influence of DO variations, the polarisation tests were carried out once the current output reached a steady value during the light cycle (5 h after the start of the light cycle). Figure 5.2A reports the results obtained for both p-MFC configurations tested. Assuming that the rate of variation of the individual electrode potentials is an indicator of the limiting electrode [30], it can be concluded that in p-MFC_{ITO} the cathode limits the reaction in the whole potential window. This result is expected if the relative surface areas of the anode and cathode electrodes are considered. Moreover, SEM images of the cathodes in the two p-MFC configurations (Figure S5.8) show a much denser biofilm onto the ITO electrode surface, which may lead to greater oxygen diffusion limitations compared to GF. The open structure of the latter could facilitate oxygen transport through the fibres.

In p-MFC_{GF} both the anode and the cathode contribute to the overpotential (Figure 5.2B), which may be a consequence of the fact that the two electrodes are made of the same material and have the same projected area. Future studies should therefore assess the impact of a relatively larger anode area on the performance of this system.

The analysis by cyclic voltammetry of the GF cathode (Figure S5.9) reveals a mass transport limited process with an onset potential for oxygen reduction at -0.21 V vs Ag/AgCl and a maximum peak of current at around -0.5 V vs. Ag/AgCl, in agreement with previous studies [31, 32]. Such a negative potential is due to the high pH of the catholyte [29]. The maximum current for ITO is lower than for GF under similar DO concentration (around 10 mg L^{-1}) and diffusion limitations are not

as obvious in the CV of the ITO electrode, which also suggests that the reaction at ITO could be reducing other electron acceptors rather than oxygen.

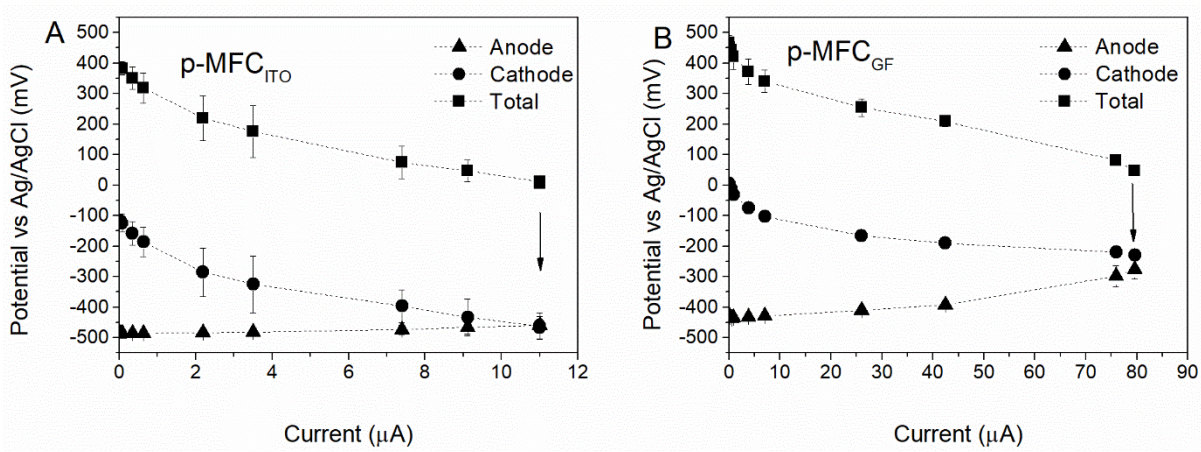

Figure 5.2. *Electrochemical characterisation of the p-MFCs by polarisation studies performed after 30 days of operation. A) p-MFC$_{ITO}$, B) p-MFC$_{GF}$. The fuel cells were left in OCV for two hours before the polarisation studies. These were carried out after five hours from the beginning of the light cycle, when the current reaches a steady value. Arrows indicate the potential and current value under the external resistance of 510 Ω.*

The signal output of the p-MFCs under operation corresponds to the maximum current, as determined by the polarisation tests in Figure 5.2. Under an external resistance of 510 Ω, the MFC$_{ITO}$ generated 11 μA and the p-MFC$_{GF}$ 80 μA (arrows in Figure 5.2). Low resistances benefit both sensitivity and range of detection [33], and maximises the rate of oxygen consumption [5]. Due to the high concentration of DO in our system, we assume that a stable diffusion gradient of oxygen from the catholyte to the electrode regardless of the reaction rate.

5.3.2 p-MFCs performance during the light cycle, influence of the DO on current output

In comparison with other studies on p-MFCs, the energy performance of the p-MFC sensors appears to be low (Table S5.1). The lack of catalyst at the cathode electrode, oxygen crossover to the anode, due to high values of DO reached in the catholyte, low conductivity of the electrolytes, and high cathodic pH are the most likely reasons for the higher internal resistance and hence, poorer performance of our system. On the other hand, for sensing purposes, stability and robustness of

the electrodes are more important than power output. Therefore, the use of a catalyst that may leach or deactivate over time is not advised. Likewise, if from one hand the high pH and relative low conductivity typical of algal systems, are detrimental for power production, these operational conditions are important to assess the suitability of the biosensor performance in real scenarios.

To assess the performance of the p-MFCs as DO sensor, the DO was monitored hourly over a 12 h light cycle and its value was correlated to the current generated.

As shown in Figure 5.3, during the light cycle, current output increases until a steady state value and then rapidly decreases once the light is off. In the case of p-MFC_{GF}, this trend is followed by the DO. The current output generated during 12 hours of light correlates well with the catholyte DO (R^2=0.96, Figure S5.10), with a sensitivity of 3.66 ± 0.35 µA L mg_{DO}^{-1} within the DO range 15 - 25 mg L^{-1} (Figure 5.3B).

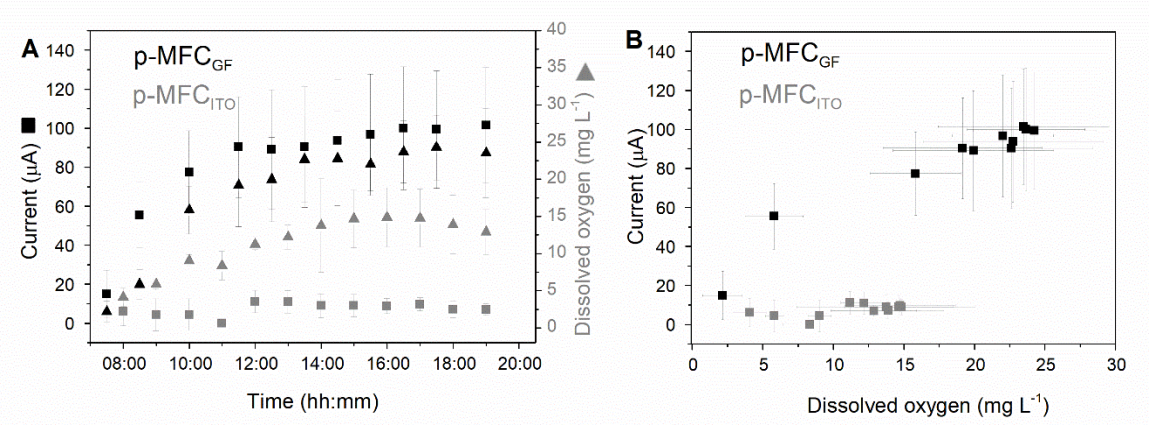

***Figure 5.3**. Investigating the relationship between dissolved oxygen in the catholyte and current generated by the p-MFCs under light. (A) Dissolved oxygen (triangles) and current (squares) evolution with time over the 12 h of light for p-MFC_{GF} (black) and p-MFC_{ITO} (grey) .(B) Correlation between the catholyte DO and the current, derived from (A). Data is the average of 6 replicates.*

In the case of p-MFC_{ITO}, there is no apparent correlation between current and DO (Figure 5.3B). This result could be either caused by the ITO saturation at lower concentrations of DO, due to the lower electrode area, or by the presence of other reduction mechanisms at the cathode *via* direct or mediated electron transfer from the biofilm [34], involving CO_2 reduction [35]. The latter would occur when oxygen

availability is limited at the electrode surface, as may be the case for the ITO electrode. The dense electrode coverage by the cathodic biofilm, observed from the SEM images, may in fact limit the access of bulk reactants to the electrode surface of ITO (Figure S5.8).

5.3.3 Response of the p-MFCs to atrazine

Atrazine, an herbicide commonly used to control grassy leaves and broadleaf weeds in crops, was tested as the model toxicant in this study. Concentrations of atrazine and its metabolites in groundwater and surface water rarely exceed 2 µg L^{-1} and are commonly below 0.1 µg L^{-1}, although concentrations may be higher in agricultural areas, where large amounts of pesticides are used [36]. In Europe, the Water Framework Directive limits the level of atrazine to 0.1 µg L^{-1} in environmental waters.

Since its mode of action towards freshwater algae is well understood, atrazine is frequently used as a model pollutant for the development of algal biosensors [6]. It binds specifically the Q_b site of the PSII within the photosynthetic electron transport chain of algae. The result is an inhibition of the light-induced oxygen produced by the algal cells [37]. In the p-MFCs, the presence of atrazine in the catholyte would produce a change in the current output caused by a drop in the photosynthetic oxygen [6]. Several studies report the inhibition of pesticides, including atrazine, on the oxygen production by *Sc. obliquus* [10, 38, 39].

Initially, the p-MFCs were exposed to a concentration of 0.1 µg L^{-1} to assess the suitability of the sensor to detect the threshold legal limit. Since point of source and groundwater concentrations are likely to be higher [40], concentrations up to 10 mg L^{-1} were also tested. The performance of the p-MFCs as sensor for atrazine detection was assessed in terms of rate of reduction, reproducibility, inhibition ratio, response time and recovery of the baseline signal over time.

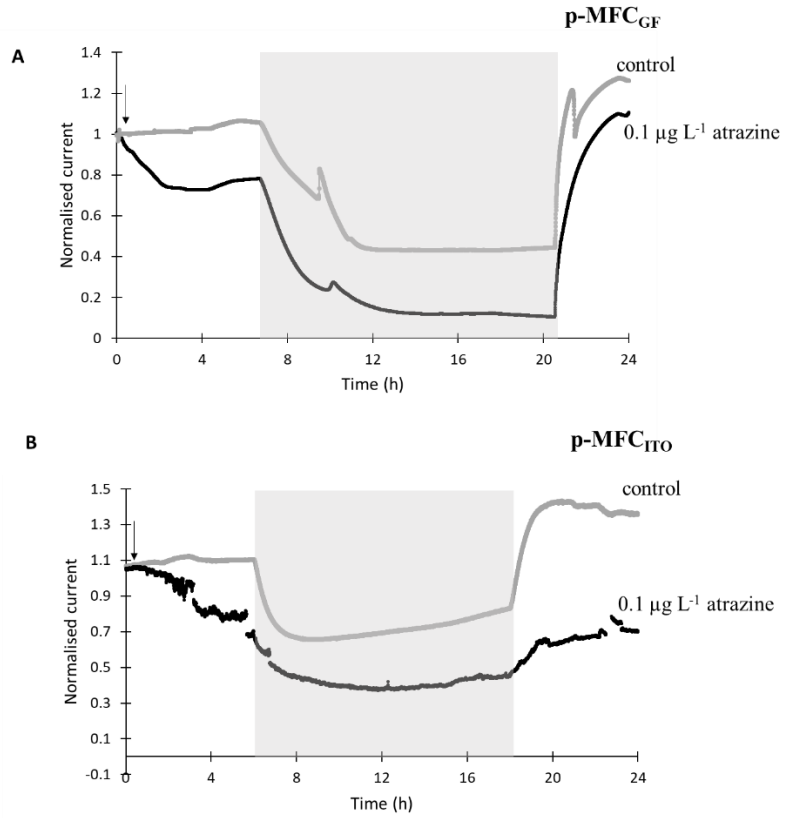

Figure 5.4**. Sensors response to 0.1 µg L^{-1} of atrazine for p-MFC$_{GF}$ (A) and p-MFC$_{ITO}$ (B) during the first 24 h after intoxication. The current output was normalised by the baseline current before the injection, Ib. Black lines correspond to the fuel cells exposed to atrazine and grey lines correspond to the control p-MFCs. The arrow indicates the point of atrazine injection. Error bars (referring to two replicates) are presented in Figure S5.12. Shadowed areas indicate the operation during the dark cycle.

Cyclic voltammetry tests at the anode before and after atrazine injection confirmed that the electrode performance was unaffected by the toxic event, and, therefore, that the response was caused by changes at the cathode only (Figure S5.11).

When the sensors were exposed to a concentration of 0.1 µg L^{-1} of atrazine (Figure 5.4), an IR$_{short\text{-}term}$ of 25.5% (p-MFC$_{GF}$, Figure 5.10SA) and 23.2% (p-MFC$_{ITO}$, Figure 5.4B), with a response time of 2.6 h (p-MFC$_{GF}$) and 3.6 h (p-MFC$_{ITO}$) was observed. The rate of reduction, SR, of p-MFC$_{GF}$ to atrazine was superior to p-MFC$_{ITO}$: 66.2 µA h^{-1} vs 0.6 µA h^{-1} (Figure S5.12). The larger current drop obtained with p-MFC$_{GF}$ is also associated to a larger drop in the DO of the catholyte. In this case, in fact, the DO dropped from 17.5 mg L^{-1} to 7.7 mg L^{-1} when exposed to 0.1 µg L^{-1} of atrazine. The DO in p-MFC$_{ITO}$ only dropped from 15 to 13 mg L^{-1}. The

reproducibility in p-MFC$_{GF}$, however, was poorer than p-MFC$_{ITO}$, as demonstrated by the larger error bars obtained (Figure S5.12B), which is probably due to trapped oxygen within the GF porous structure. Interestingly, when p-MFC$_{GF}$ was exposed to 8 µg L^{-1} (Figure 5.5), the photosynthetic pattern was lost on the next cycle showing the potential of the pMFC as shock sensor.

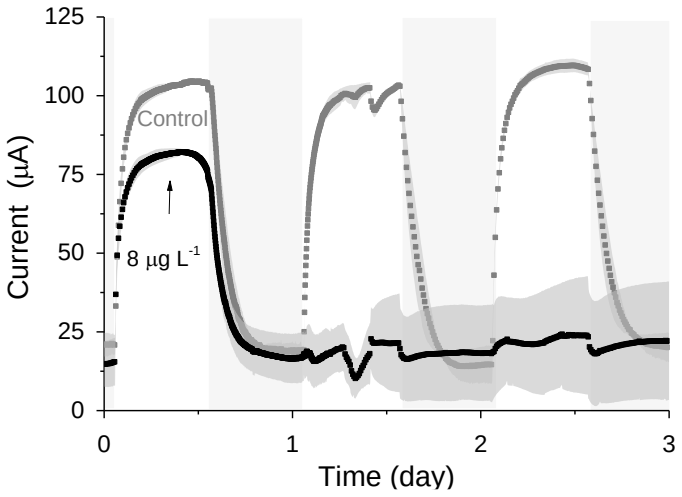

***Figure 5.5**. Response of p-MFC$_{GF}$ to 8 µg L^{-1} of atrazine. The arrow indicates the point of atrazine injection. Shadowed areas indicate the operation during the dark cycle. Data is the average of two replicates. Error bars represent the absolute error between the two replicates.*

Both p-MFC devices showed a response to atrazine concentrations in the mg L^{-1} range. When the systems were exposed to 0.5 mg L^{-1} an immediate drop in the signal was observed (Figures 5.6 and 5.7). p-MFC$_{GF}$ showed a higher SR rate (23.5 µA h^{-1}) compared to p-MFC$_{ITO}$ (0.715 µA h^{-1}), with IR$_{short\text{-}term}$ of 53% (Figure 5.6A) and 27.3 % (Figure 5.7A). Subsequent additions of atrazine in the cathode chamber caused further decreases in the current output, however, the IR$_{short\text{-}term}$ did not correlate with the concentration. Moreover, the extent of the current decay depended on the history of the sensor. For example, when p-MFC$_{ITO}$ was firstly exposed to 10 mg L^{-1} (Figure 5.7B) an IR$_{short\text{-}term}$ of 52 % was observed. Nonetheless, an IR$_{short\text{-}term}$ of only 8% to the same concentration was recorded with device previously exposed to the pollutant (Figure 5.7A), thus suggesting that the biofilm may develop resistance to the toxicant [41]. The acclimation of the biofilm to the toxic event means that a dose-response curve could not be representative

of the performance of this type of sensor. The current drop was however correlated with a concomitant drop in the DO of the catholyte thus, the low reproducibility of the sensor is due to an uneven response of the algae to the toxicant. Moreover, the anodic potential determines the saturation level of DO of the sensor. The lower the anodic potential, the larger the current output and the higher the saturating concentration of DO, resulting in better the sensitivity and detection range of the sensor.

The response time of the p-MFCs to atrazine was in the range of hours, instead of minutes as reported for other algae biosensors [6, 42]. Mass transfer limitations, especially within the porous structure of the GF cathode, and low electrode surface-area-to-volume-ratio, may be a reason for this [43].

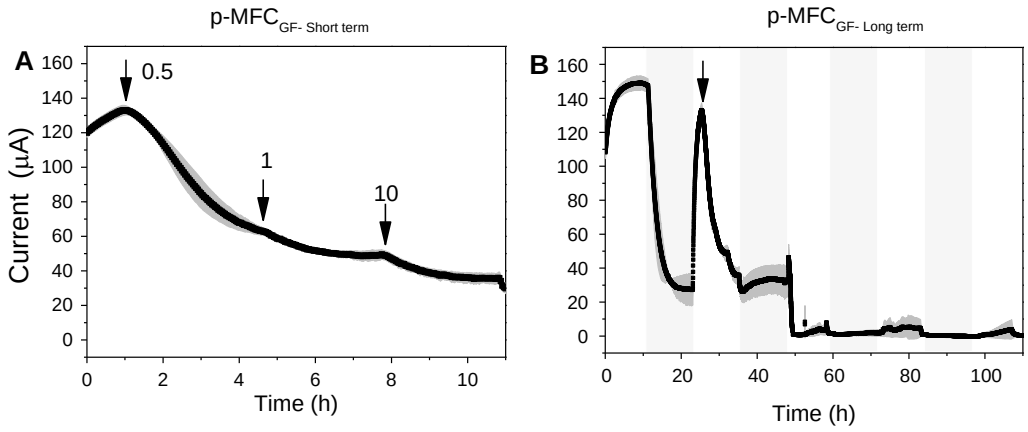

***Figure 5.6**. Response of p-MFC$_{GF}$ to atrazine injection in the mg L^{-1} range. (A) Short term response. (B) Long term response. The arrows indicate the point of atrazine injection. Shadowed areas indicate the operation during the dark cycle.*

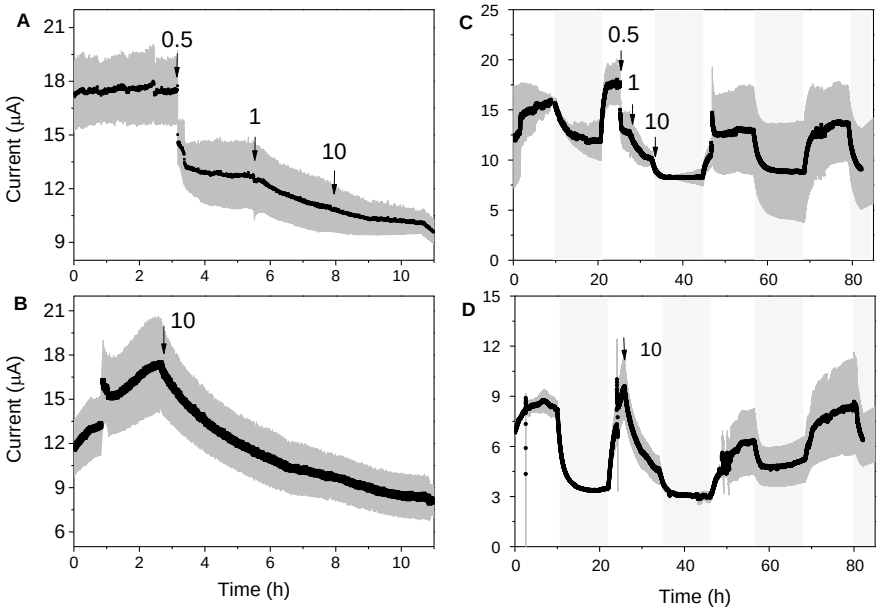

***Figure 5.7**. Response of the p-MFC$_{ITO}$ sensor to atrazine. (A) and (C) response to subsequent injections of atrazine for concentrations ranging between 0.5- 10 mg L^{-1}. (B) and (D) response to a single atrazine injection of 10 mg L^{-1}. (A) and (B) show the short-term response (i.e. up to 10 hours), while (C) and (D) the response up to 80 hours. Shadowed areas indicate the operation during the dark cycle.*

5.3.4 Recovery of the sensors after the toxic event

After exposure to 0.1 µg L^{-1} of atrazine, the baseline current generated by p-MFC$_{GF}$ recovered during the next dark/light cycle (Figure 5.4A). In the case of p-MFC$_{ITO}$, this recovery did not occur and a 36% decay in the current baseline was observed (Figure 5.4B). This result suggests that the p-MFC can be used as an early warning system to detect the limit concentration imposed by law. When p-MFC$_{GF}$ was exposed to higher concentrations of atrazine, however, the baseline current signal did not recover (Figure 5.6B), while p-MFC$_{ITO}$ (Figure 5.7C and D) recovered the baseline current in the next cycles without changing the electrolyte. The denser biofilm developed onto the ITO electrode (Figure S5.8) may protect it from the atrazine action. On the other hand, the uneven biofilm distribution on the GF electrode would facilitate atrazine access also to the cells closer to the electrode

surface. In addition, atrazine could be adsorbed on the GF structure and released also after the completion of the simulated toxic event.

The SEM images (Figure S5.8C and S5.8D) suggest that the cathodes exposed to atrazine may be contaminated by fungi [44, 45]. The toxic effect of atrazine towards photosynthetic species would allow pathogens and opportunistic species to thrive and change the consortia within the biofilm. Not only is this detrimental for the health of the bioreceptor, but also for the stability of the baseline over time.

Maintaining sterile conditions at the cathode, would probably minimise baseline fluctuations over time and lead to a more stable sensor. Nevertheless, this approach is incompatible with practical applications, where the cathodic probe would be exposed to the water samples to be analysed. Future studies should include in-depth analyses of the microbial and algal communities at the cathode to try and relate the sensor performance over time with the cathodic biofilm evolution.

5.4 Conclusions

Algae are the ideal bioreceptors for the development of herbicides biosensors, given their high sensitivity to these compounds. Yet, their practical use is still limited by the development of reliable and portable systems for effective *in situ* operations. In this work, we investigated for the first time the use of photosynthetic microbial fuel cells, with algae-assisted cathodes, for the detection of atrazine in water systems. Two cathode materials were tested, graphite felt and ITO to investigate the effect of the electrode properties on performance, and long-term exposure studies with this technology were reported. When both devices were exposed to the limiting concentration imposed by the Water Framework Directive of 0.1 µg L^{-1}, a detectable change in the photosynthetic pattern was obtained. In the case of p-MFC_{GF}, higher concentration of atrazine, however, highly affected the current generation light/dark cycle permanently, while p-MFC_{ITO} recovered the day/night cycle after the toxic events, for all concentrations tested.

The electrode porosity allows the built-up of a 3D cathodic biofilm, but the accumulation of oxygen within the fibres slows down the response time and affects the reproducibility of the sensor. On the other hand, the high cell density biofilm

generated by the ITO surface prevents oxygen access to the electrode, which leads to a low sensitivity to DO changes in water.

Based on our results, both p-MFCs could be used for point of source detection of a toxic event or as early warning system to avoid contamination in algal raceway ponds fed with wastewater.

Further studies are required to investigate the effect of environmental factors (i.e. temperature, pH, light intensity, flow rate) and particularly the cathode potential on the sensitivity, detection limit and range of application of the p-MFC system as DO sensor for environmental monitoring. The sensor performance in the co-presence of several other pesticides along with atrazine should be tested in future studies.

5.5 Acknowledgements

The authors thanks: the Water Informatics, Science and Engineering (WISE) Centre for Doctoral Training (CDT), funded by the UK Engineering and Physical Sciences Research Council (EP/L016214/1) to support Lola Gonzalez Olias's PhD Scholarship; Aidan Barry from the Department of Biology, University of Bath for supplying the algae strain and assisting with the culture growth.

5.6 Supplementary information

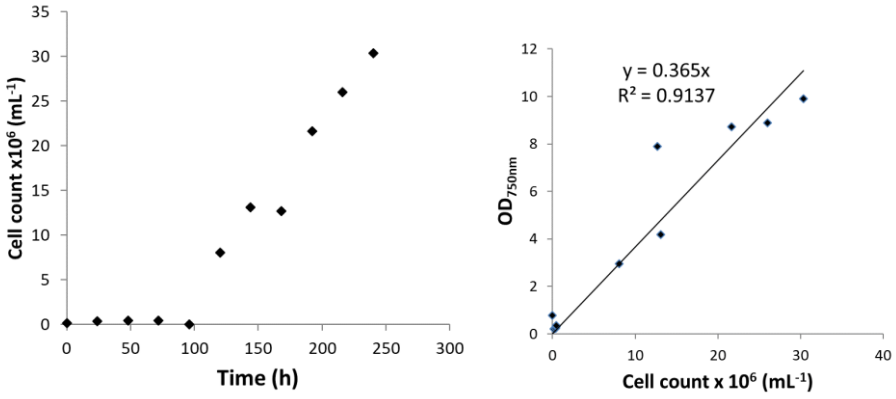

***Figure S5.1**. Growth curves of Sc. Obliquus on BBM in batch at 25℃ and 12h/12h white light regime of 5 lm m^{-1}. Cell count and OD were assessed on a daily basis for 10 days. The growth curve was not continued until steady state because after 10 days the culture started to clump, and OD measurements became unreliable.*

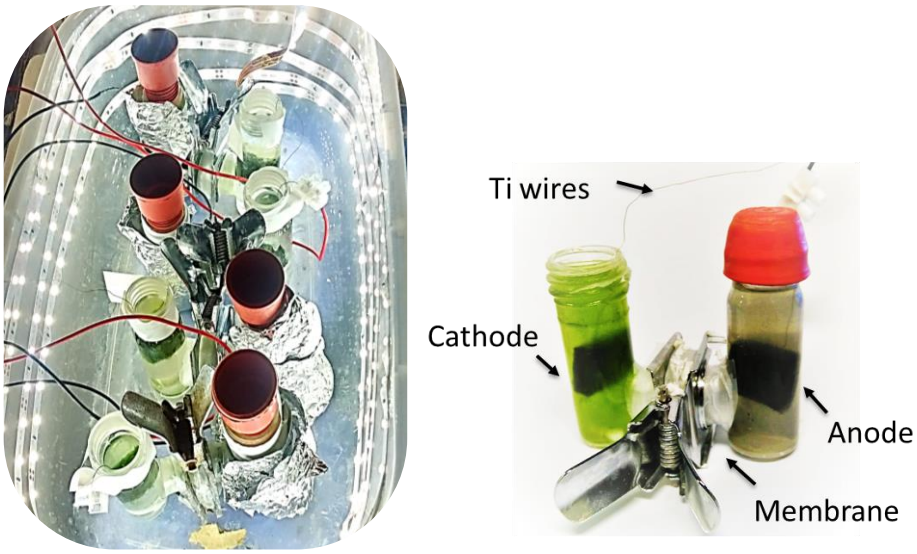

***Figure S5.2**. Experimental set up (left). Example of the H-cell p-MFC$_{GF}$ (right).*

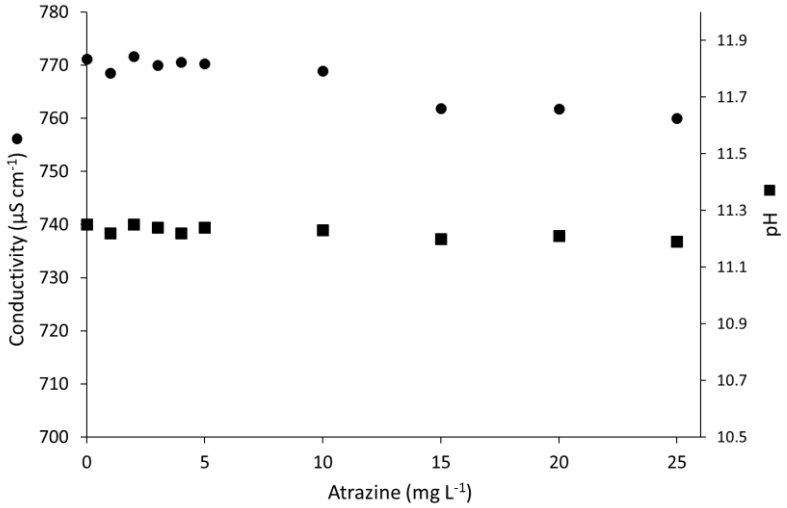

***Figure S5.3**. Catholyte pH and conductivity evolution over time after atrazine addition. The study was performed in a catholyte extracted from the cathode chamber after 20 days of operation.*

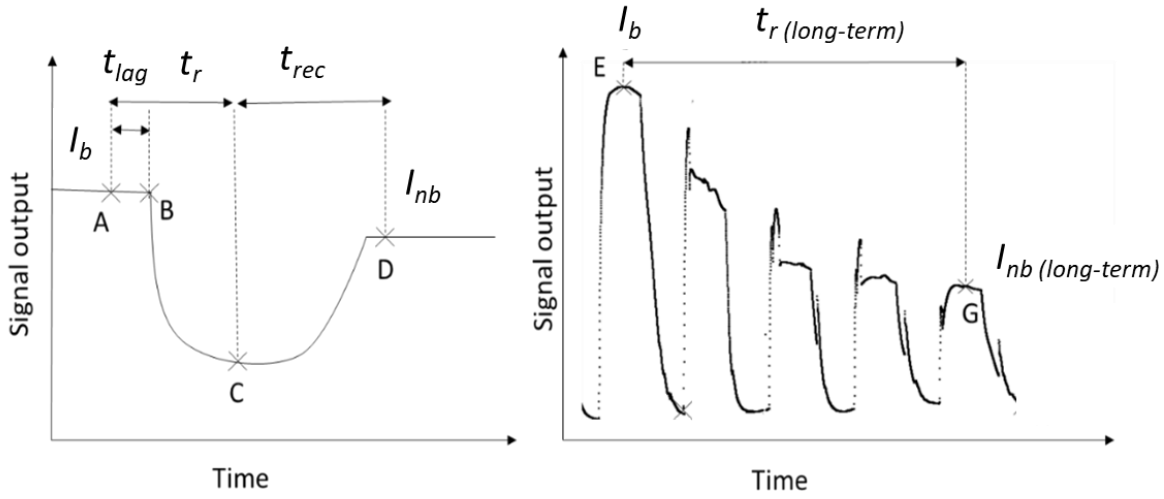

***Figure 5.4**. Example of the short-term response (left) and long-term response (right) of the p-MFCs to a toxic event. (A) is the moment of injection of the toxicant. (B) indicates the moment when a response is observed in the signal output. (C) is the moment when the current has reached the 95% of its steady state following the change in current. (D) is the point when the sensor has recovered from the toxicant event. (E) is the moment when the light baseline of the photosynthetic cycle stabilises. I_b is the current baseline in the light before the event, I_{nb} is the current baseline in the light after the event. t_{lag} is the lag period from the injection of the toxicant until it reached the biofilm. t_r is the response time of the sensor. t_{rec} is the recovery time of the sensor.*

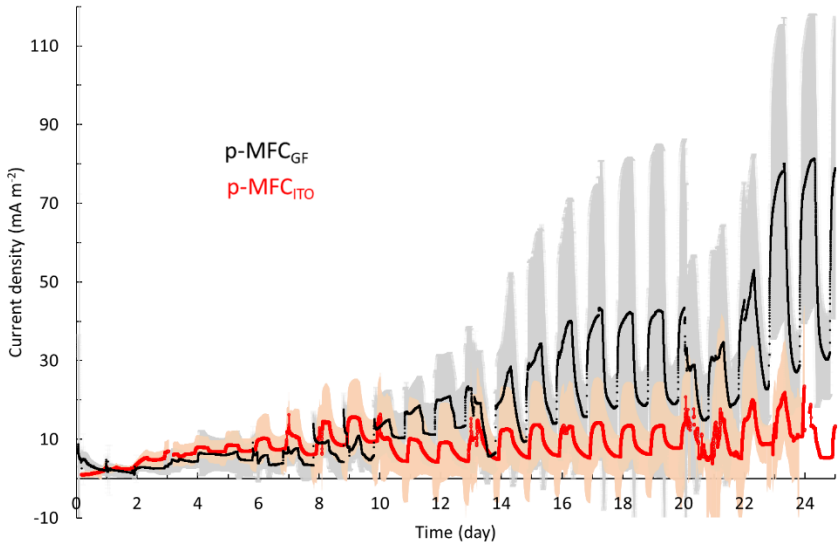

***Figure S5.5**. Start-up period of the p-MFCs with error bars. P-MFC$_{GF}$ corresponds to the black line and p-MFC$_{ITO}$ to the red line. Current density refers to the projected surface area. Error bars correspond to the standard deviation of 6 replicates.*

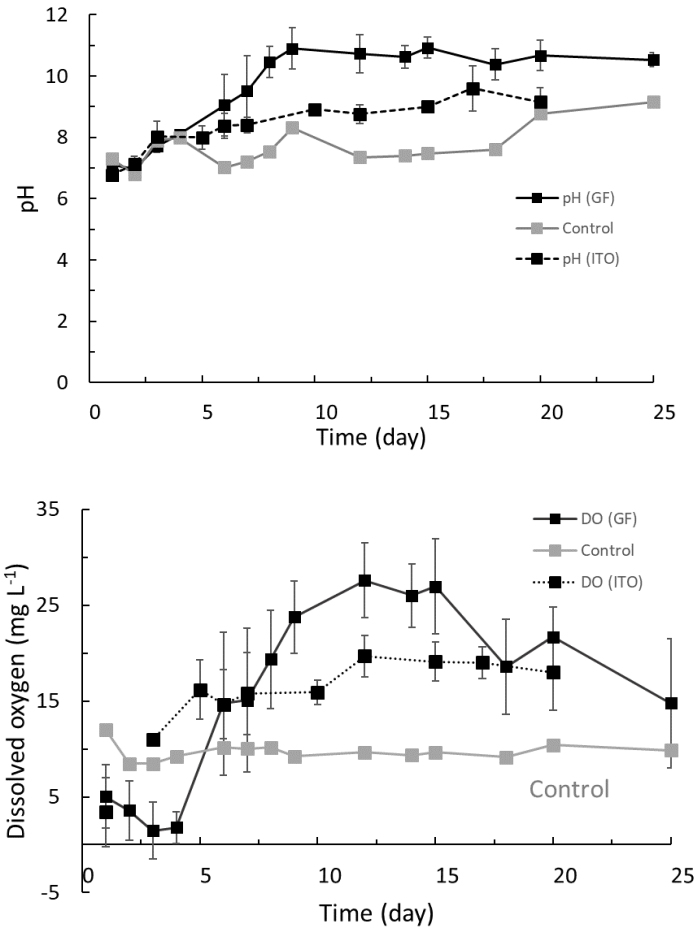

***Figure S5.6**. Values of pH and dissolved oxygen evolution in the catholyte during the start up. The control refers to a beaker with the catholyte solution only without the cathode, so that no electrochemical reactions would occur. In each case, the same starting algal solution was used as described in the Methods Section.*

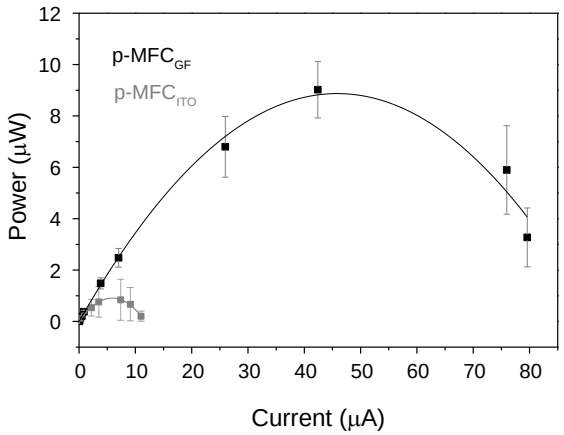

***Figure S5.7**. Power density curves of the p-MFC$_{GF}$ (black) and p-MFC$_{ITO}$ (grey). Data points are the average of two replicates. The power curve corresponds to the polarisation curves in Figure 5.2.*

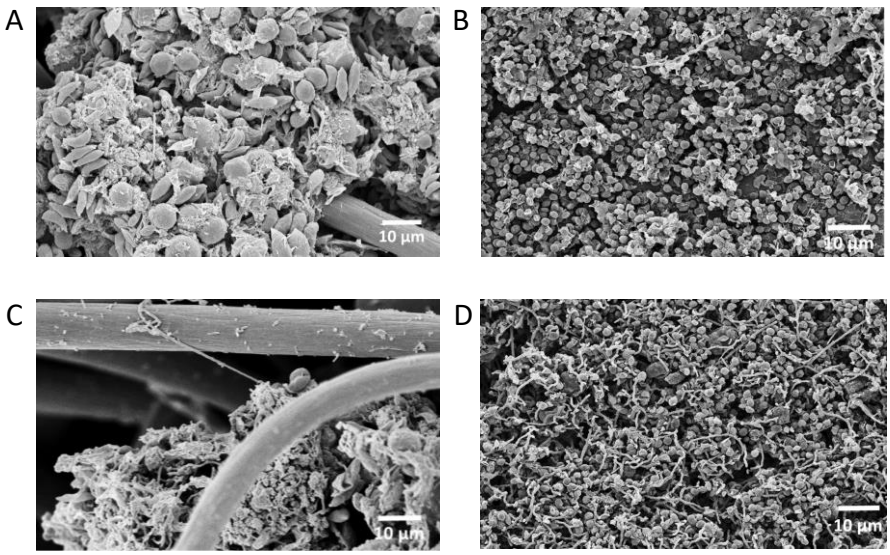

***Figure S5.8**. SEM images of the electrodes at 10 kW x1000 magnification. (A) and (B) refer to p-MFC$_{GF}$ and p-MFC$_{ITO}$ not exposed to atrazine. (C) and (D) refer to p-MFC$_{GF}$ and p-MFC$_{ITO}$ exposed to atrazine. The images were taken after three months of operation and one month after the first exposure to atrazine.*

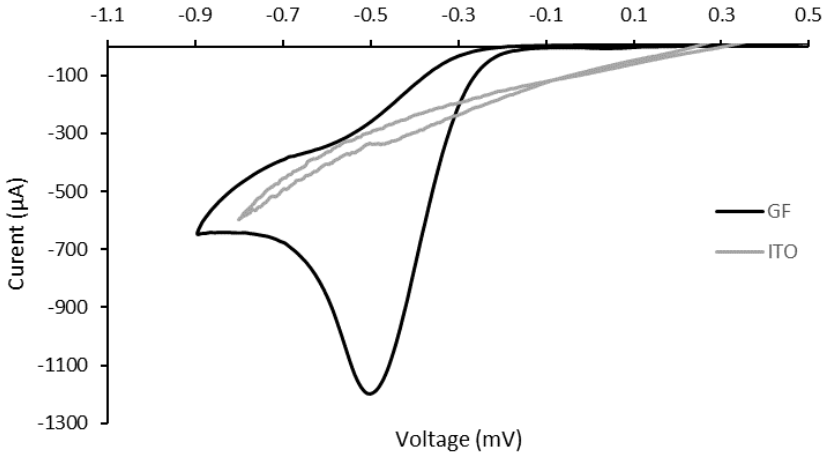

***Figure S5.9**. Cyclic voltammetry of the colonised cathodes at a scan rate of 1 mV s^{-1} vs. Ag/AgCl, under light. The curves are the third scan, representative of two replicates. Dissolved oxygen concentrations of the electrolyte are similar in both cases, around 10 mg L^{-1}.*

.

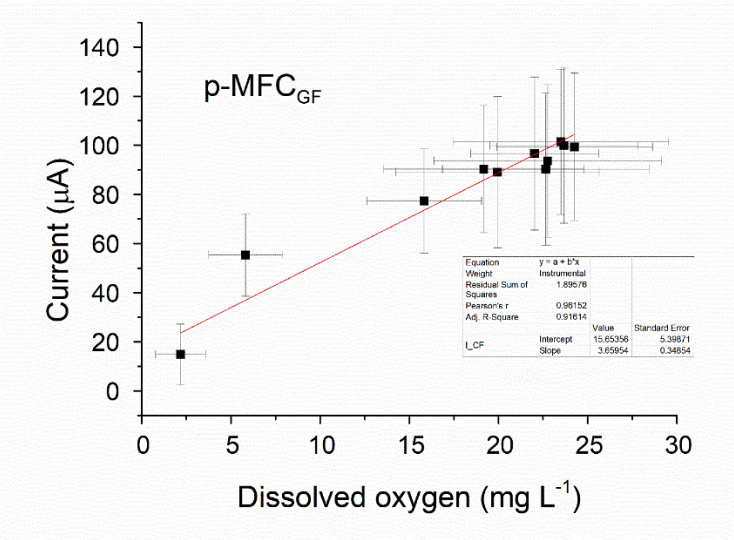

***Figure S5.10**. Linear fitting of cathodic DO with current for p-MFC$_{GF}$ on a 12h light cycle. The analysis was performed with OriginPro 9.*

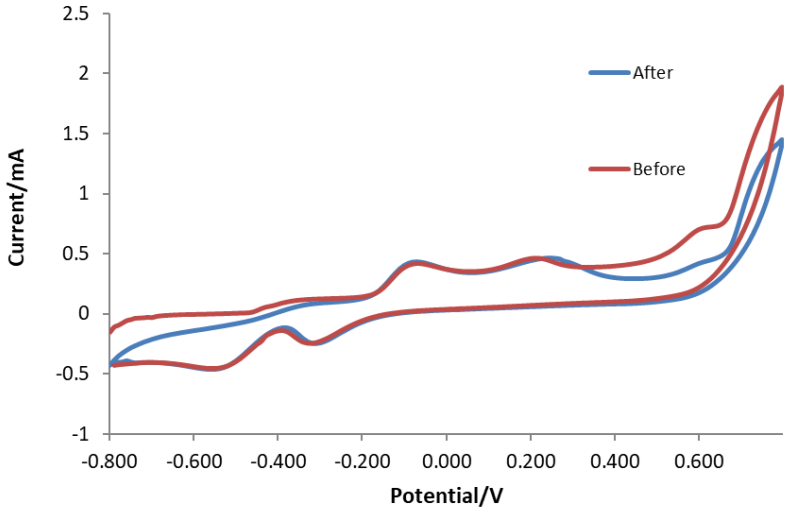

***Figure S5.11**. Cyclic voltammogram at the anode of the p-MFC before (red line), and after (blue line) the injection of atrazine. The tests were performed in a three-electrode set-up with Ag/AgCl as the reference electrode and Pt as the counter electrode.*

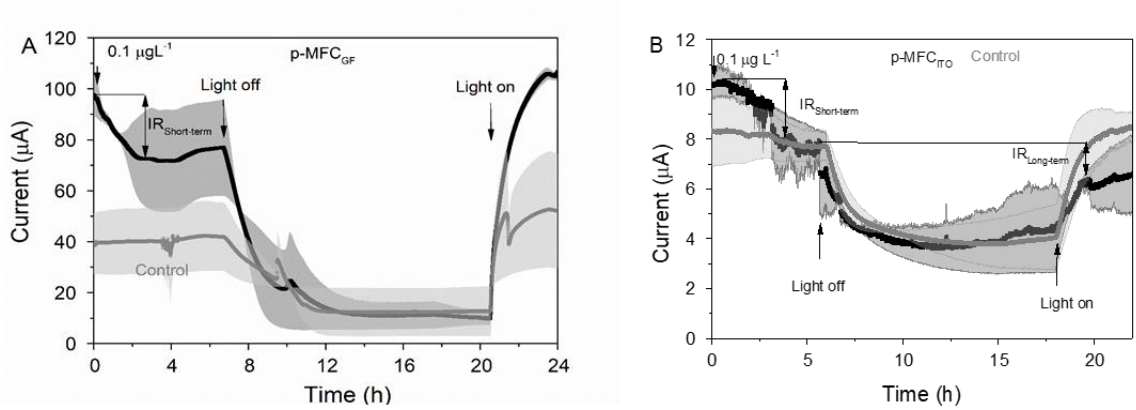

***Figure S5.12**. Response of the sensors to 0.1 µg L^{-1} of atrazine for p-MFC_{GF} (A) and p-MFC_{ITO} (B) during the first 24 h after intoxication. Black lines correspond to the intoxicated sensor and grey lines correspond to the control p-MFCs. Mean values and error bars (absolute error) correspond to two replicates.*

***Table S5.1**. Summary of performance of two-chamber p-MFC previously reported.*

Cathode material	**Cathodic algae**	**OCV (mV)**	**R_{int} (Ω)**	**Max power density / mW m^{-2}**	**pH**	**DO / mg mL^{-1}**	**Ref.**
Carbon cloth/10%Teflon	Mixed		9600	11.5	7.5	7.5	[25]
Carbon fibre cloth	*Ch. Vulgaris*	429	138	44.6	7	5.65	[26]
Carbon fibre cloth	*Ch. species*	379	158	39.75	7	5.22	[26]
0.5 mg/cm^2 platinum coated carbon paper	*Sc. Obliquus*	897	438	154	7	6.5	[10]
Carbon cloth 10%Teflon	*Ch. Vulgaris*	462	1300	14.4	7	6	[27]
GF	*Desmo-desmus sp. A8*	410	136	64.2		7.5	[18]
CC/Pt 0.1mg/cm^2	*Ch. Vulgaris*	805		2300		7.6	[28]
CP 0.5 mg/cm^2 Pt	*Sc. Obliquus*		673	34.2			[29]
ITO/PET	*Sc. Obliquus* / mixed	485	5230	1.52 ± 1.45	9	12	This study
GF acid treated	*Sc. Obliquus* / mixed	497	1866	6.63 ± 0.81	9	15	This study

5.7 References

[1] P. Lepom, B. Brown, G. Hanke, R. Loos, P. Quevauviller, and J. Wollgast, “Needs for reliable analytical methods for monitoring chemical pollutants in surface water under the European Water Framework Directive,” *Journal of Chromatography A*, vol. 1216, no. 3. pp. 302–315, 2009.

[2] J. Chouler, M. D. Monti, W. J. Morgan, P. J. Cameron, and M. Di Lorenzo, “A photosynthetic toxicity biosensor for water,” *Electrochim. Acta*, vol. 309, pp. 392–401, Jun. 2019.

[3] J. Labro, T. Craig, S. A. Wood, and M. A. Packer, “Demonstration of the use of a photosynthetic microbial fuel cell as an environmental biosensor,” *Int. J. Nanotechnol.*, vol. 14, no. 1/2/3/4/5/6, p. 213, 2017.

[4] Y. Jiang, P. Liang, P. Liu, D. Wang, B. Miao, and X. Huang, “Biosensors and Bioelectronics A novel microbial fuel cell sensor with biocathode sensing element,” *Biosens. Bioelectron.*, vol. 94, no. February, pp. 344–350, Aug. 2017.

[5] Y. Zhang and I. Angelidaki, “A simple and rapid method for monitoring dissolved oxygen in water with a submersible microbial fuel cell (SBMFC),” *Biosens. Bioelectron.*, vol. 38, no. 1, pp. 189–194, 2012.

[6] I. Shitanda, K. Takada, Y. Sakai, and T. Tatsuma, “Compact amperometric algal biosensors for the evaluation of water toxicity,” *Anal. Chim. Acta*, vol. 530, no. 2, pp. 191–197, 2005.

[7] J. Livage, “Micro-algal biosensors,” *Anal. Bioanal. Chem.*, vol. 401, no. October, pp. 581–579, 2011.

[8] K. Schneider *et al.*, “An investigation of anode and cathode materials in photomicrobial fuel cells An investigation of anode and cathode materials in photomicrobial fuel cells Authors for correspondence :,” *Philos. Trans. R. Soc. A Math. Phys. Eng. Sci.*, vol. 374, no. February, pp. 1–22, 2016.

[9] J. Li *et al.*, “Enhanced detection of toxicity in wastewater using a 2D smooth anode based microbial fuel cell toxicity sensor,” *RSC Adv.*, vol. 9, no. 15, pp. 8700–8706, 2019.

[10] J. Mofeed and Y. Y. Mosleh, “Toxic responses and antioxidative enzymes activity of Scenedesmus obliquus exposed to fenhexamid and atrazine, alone and in mixture,” *Ecotoxicol. Environ. Saf.*, vol. 95, pp. 234–240, 2013.

[11] S. Singh *et al.*, “Toxicity, degradation and analysis of the herbicide atrazine,” *Environ.*

Chem. Lett., vol. 16, pp. 211–237, 2018.

[12] R. Kakarla and B. Min, “Photoautotrophic microalgae Scenedesmus obliquus attached on a cathode as oxygen producers for microbial fuel cell (MFC) operation,” *Int. J. Hydrogen Energy*, vol. 39, no. 19, pp. 10275–10283, Jun. 2014.

[13] J. Chouler, I. Bentley, F. Vaz, A. O’Fee, P. J. Cameron, and M. Di Lorenzo, “Exploring the use of cost-effective membrane materials for Microbial Fuel Cell based sensors,” *Electrochim. Acta*, vol. 231, pp. 319–326, Mar. 2017.

[14] S. M. Martinez and M. Di Lorenzo, “Electricity generation from untreated fresh digestate with a cost-effective array of floating microbial fuel cells,” *Chem. Eng. Sci.*, vol. 198, pp. 108–116, 2019.

[15] W. Verstraete and K. Rabaey, “Critical Review Microbial Fuel Cells : Methodology and Technology †,” vol. 40, no. 17, pp. 5181–5192, 2006.

[16] M. Tucci, M. Grattieri, A. Schievano, P. Cristiani, and S. D. Minteer, “Microbial amperometric biosensor for online herbicide detection: Photocurrent inhibition of Anabaena variabilis,” *Electrochim. Acta*, vol. 302, pp. 102–108, 2019.

[17] Y. Feng, O. Kayode, and W. F. Harper, “Using microbial fuel cell output metrics and nonlinear modeling techniques for smart biosensing,” *Sci. Total Environ.*, vol. 449, pp. 223–228, 2013.

[18] P. Bombelli *et al.*, “Surface morphology and surface energy of anode materials influence power outputs in a multi-channel mediatorless bio-photovoltaic (BPV) system,” *Phys. Chem. Chem. Phys.*, vol. 14, no. 35, pp. 12221–12229, 2012.

[19] J. Lobato, A. González Del Campo, F. J. Fernández, P. Cañizares, and M. A. Rodrigo, “Lagooning microbial fuel cells: A first approach by coupling electricity-producing microorganisms and algae,” *Appl. Energy*, vol. 110, pp. 220–226, 2013.

[20] A. S. Commault, G. Lear, P. Novis, and R. J. Weld, “Photosynthetic biocathode enhances the power output of a sediment-type microbial fuel cell,” *New Zeal. J. Bot.*, vol. 52, no. 1, pp. 48–59, Jan. 2014.

[21] A. Colombo, S. Marzorati, G. Lucchini, P. Cristiani, D. Pant, and A. Schievano, “Assisting cultivation of photosynthetic microorganisms by microbial fuel cells to enhance nutrients recovery from wastewater,” *Bioresour. Technol.*, vol. 237, pp. 240–248, 2017.

[22] F. Zhao, Y. Zheng, Z. Wang, Z. Yang, Y. Xiao, and Y. Wu, “Light intensity affects the performance of photo microbial fuel cells with Desmodesmus sp. A8 as cathodic microorganism,” *Appl. Energy*, vol. 116, pp. 86–90, Mar. 2013.

[23] M. I. M. Mowjood and T. Kasubuchi, “Dynamics of dissolved oxygen (DO) in ponded water of a paddy field,” *Soil Sci. Plant Nutr.*, vol. 44, no. 3, pp. 405–413, 1998.

[24] Q. Hou, H. Pei, W. Hu, L. Jiang, and Z. Yu, “Mutual facilitations of food waste treatment, microbial fuel cell bioelectricity generation and Chlorella vulgaris lipid production,” *Bioresour. Technol.*, vol. 203, pp. 50–55, 2016.

[25] A. Colombo, S. Marzorati, G. Lucchini, P. Cristiani, D. Pant, and A. Schievano, “Assisting cultivation of photosynthetic microorganisms by microbial fuel cells to enhance nutrients recovery from wastewater,” *Bioresour. Technol.*, vol. 237, pp. 240–248, Aug. 2017.

[26] X. Ge *et al.*, “Oxygen Reduction in Alkaline Media: From Mechanisms to Recent Advances of Catalysts,” *ACS Catal.*, vol. 5, no. 8, pp. 4643–4667, 2015.

[27] Z. He, Y. Huang, A. K. Manohar, and F. Mansfeld, “Effect of electrolyte pH on the rate of the anodic and cathodic reactions in an air-cathode microbial fuel cell,” *Bioelectrochemistry*, vol. 74, pp. 78–82, 2008.

[28] L. Rago *et al.*, “Influences of dissolved oxygen concentration on biocathodic microbial communities in microbial fuel cells,” *Bioelectrochemistry*, vol. 116, pp. 39–51, 2017.

[29] H. Zhang, C. Lin, L. Sepunaru, C. Batchelor-McAuley, and R. G. Compton, “Oxygen reduction in alkaline solution at glassy carbon surfaces and the role of adsorbed intermediates,” *J. Electroanal. Chem.*, vol. 799, pp. 53–60, 2017.

[30] J. Babauta, R. Renslow, Z. Lewandowski, and H. Beyenal, “Electrochemically active biofilms: Facts and fiction. A review,” *Biofouling*, vol. 28, no. 8. pp. 789–812, 2012.

[31] L. Darus, Y. Lu, P. Ledezma, J. Keller, and S. Freguia, “Fully reversible current driven by a dual marine photosynthetic microbial community,” *Bioresour. Technol.*, vol. 195, pp. 248–253, Nov. 2015.

[32] M. Rimboud, E. Desmond-Le Quemener, B. Erable, T. Bouchez, and A. Bergel, “The current provided by oxygen-reducing microbial cathodes is related to the composition of their bacterial community,” *Bioelectrochemistry*, vol. 102, pp. 42–49, 2015.

[33] N. E. Stein, H. V. M. Hamelers, and C. N. J. Buisman, “Influence of membrane type, current and potential on the response to chemical toxicants of a microbial fuel cell based biosensor,” *Sensors Actuators, B Chem.*, vol. 163, no. 1, pp. 1–7, 2012.

[34] X. Wang *et al.*, “Sequestration of CO2 discharged from anode by algal cathode in microbial carbon capture cells (MCCs),” *Biosens. Bioelectron.*, vol. 25, no. 12, pp. 2639–2643, 2010.

[35] X. Cao *et al.*, “A completely anoxic microbial fuel cell using a photo-biocathode for cathodic carbon dioxide reduction,” vol. 2, no. 5, pp. 1754–5692, 2009.

[36] WHO, “Atrazine and Its Metabolites in Drinking-water; Background Document For Development of WHO Guidelines For Drinking-Water Quality,” *WHO/HSE/WSH/10.01/11*, 2010.

[37] L. J. C. (Editor) Jeuken, Ed., “Biophotoelectrochemistry: From Bioelectrochemistry to Biophotovoltaics,” vol. 158, Springer Nature, 2016.

[38] X. Zhu *et al.*, “Herbicides interfere with antigrazer defenses in Scenedesmus obliquus,” *Chemosphere*, vol. 162, pp. 243–251, 2016.

[39] A. Chalifour, A. LeBlanc, L. Sleno, and P. Juneau, “Sensitivity of Scenedesmus obliquus and Microcystis aeruginosa to atrazine: effects of acclimation and mixed cultures, and their removal ability,” *Ecotoxicology*, vol. 25, no. 10, pp. 1822–1831, 2016.

[40] K. Manamsa, E. Crane, M. Stuart, J. Talbot, D. Lapworth, and A. Hart, “A national-scale assessment of micro-organic contaminants in groundwater of England and Wales,” *Sci. Total Environ.*, vol. 568, pp. 712–726, 2016.

[41] S. Patil, F. Harnisch, and U. Schröder, “Toxicity response of electroactive microbial biofilms-a decisive feature for potential biosensor and power source applications,” *ChemPhysChem*, vol. 11, no. 13, pp. 2834–2837, 2010.

[42] I. B. Tahirbegi *et al.*, “Fast pesticide detection inside microfluidic device with integrated optical pH, oxygen sensors and algal fluorescence,” *Biosens. Bioelectron.*, vol. 88, pp. 188–195, 2016.

[43] M. Rimboud, M. Barakat, A. Bergel, and B. Erable, “Different methods used to form oxygen reducing biocathodes lead to different biomass quantities, bacterial communities, and electrochemical kinetics,” *Bioelectrochemistry*, vol. 116, pp. 24–32, 2017.

[44] L. V Lopez-Llorca and P. Hernandez, “Infection of the green alga Oocystis lacustris chod with the chytrid fungus Diplochytridium deltanum (Masters) Karling. An SEM study,” *Micron*, vol. 27, no. 5, pp. 355–358, 1996.

[45] L. V Lopez-Llorca, T. Carbonell, and J. Salinas, “Colonization of plant waste substrate by entomopathogenic and mycoparasitic fungi - A SEM study,” *Micron*, vol. 30, no. 4, pp. 325–333, 1999.

Chapter 6

The previous chapter describes the proof of concept of an algal biocathode as sensing element for pesticide detection in the context of self-powered biosensors. The study concludes that atrazine can be successfully detected with the MFC sensor by monitoring changes in the oxygen produced by the algal biocathode. The design used in Chapter 5 is, however, not suitable for environmental monitoring due to poor portability, robustness and durability of the device. Chapter 6 presents a novel ceramic soil MFC (CSMFC) sensor to solve these issues.

In a CSMFC sensor, the anolyte is soil, a solid substrate rich in organics and humic acids. According to literature, this long-lasting substrate can sustain the anodic electroactivity for several months. The Nafion membrane is changed for a ceramic separator made of terracotta. Terracotta is a non-specific porous cation exchange membrane. The separator is shaped as a vessel, to keep the soil enclosed in a floating container and improve the portability of the sensor. The volume of the vessel is small, to enhance the transport of algal biomass from the biocathode to the anode and enrich the soil in organic matter. It is hypothesised that microbes in soil consume the oxygen crossing from cathode to anode before it affects the electroactivity of the anodic biofilm.

The electrodes are made of carbon felt as it enhances biofilm attachment, crucial when the sensing element is exposed to flowing streams. The catholyte, enriched in a pure culture of *Scendesmus obliquus* to keep consistency with the previous chapter, is cultured in non-aseptic condition thus constituting a mixture of photosynthetic species and other unidentified organisms, as seen under the microscope.

The external resistance is increased with respect to the configuration in Chapter 5, to adjust it to the increase in internal resistance in the CSMFC, added by the terracotta vessel. Again, it is chosen at the highest current density without incurring into power overshoot, to maximise the rate of oxygen consumption and detect variations in the current output at a fast rate.

In this study, Diuron and glyphosate are chosen as model toxicants because of their relevance. Diuron is commonly used as model compound for toxicity assessments. It is a highly stable, urea-based molecule that binds the protein D1 in photosystem II, blocking the transfer of electrons across the photosynthetic electron transport chain and inhibiting oxygen evolution in algae. Glyphosate is currently the most frequently used herbicide for weed control worldwide. It is a non-specific glycine-based herbicide that blocks the aminoacid synthesis and reduces the production of plastoquinone and chlorophyll, involved in the photosynthetic apparatus, also affecting the photosynthetic oxygen production.

The characterisation of the photosynthetic signal output in Chapter 5 revealed high instability of the baseline, which challenges the use of metrics based on a stable baseline over time. To solve this issue, in this study the performance of the sensor is assessed by comparing the accumulated standard deviation and accumulated charge before and after 5 days of the toxic event. A perturbation in the signal at any point in the 5-day average induces a significant change in the parameters, thus proving an effective non-baseline dependant indicator of the presence of a toxicant in real environments.

This work is written and presented as a research publication to comply with the format of the rest of the thesis but has not been submitted for publication in peer-reviewed journals.

6. Floating ceramic soil microbial fuel cells sensors (CSMFC) for pesticide detection in water

Lola Gonzalez Olias,[1,2,3] Mirella Di Lorenzo[1,2]*

[1] Centre for Biosensors, Bioelectronics and Biodevices (C3Bio)

[2] Department of Chemical Engineering, University of Bath, Bath BA2 7AY, UK

[3] Water Innovation Research Centre (WIRC), University of Bath, Bath BA2 7AY, UK

Increasing water pollution derived from the use of pesticides, calls for efficient sensing technologies capable of online and *in situ* environmental monitoring of water quality. This study presents a Soil Microbial Fuel Cell with a photosynthetic biocathode, for detection of pesticides in environmental waters. The sensor consists of a ceramic vessel, containing a soil-based anode and an algal enriched cathode, which is placed on the outside of the vessel. In steady state, the signal strongly correlates with dissolved oxygen (DO) in water, positively at DO < 9 mg L^{-1} (R^2=0.86) and negatively at DO > 9 mg L^{-1} (R^2=0.70). The sensor signal responds to 0.1 µg L^{-1} of the herbicides Diuron and glyphosate. The change in the signal is significant for both toxicants ($p < 0.01$) when measured as the difference in the daily accumulated charge and the daily accumulated standard deviation, averaged in five days before and after the toxic event. Furthermore, the sensor responds significantly to a second toxic event of 50 µg L^{-1} of Diuron, suggesting the potential reusability of the photosynthetic bioreceptor. The sensor operated without addition of nutrients for three months, indicating the potential long-term unattended deployment of soil MFC sensors, with photosynthetic biocathodes, for pesticide detection in environmental waters.

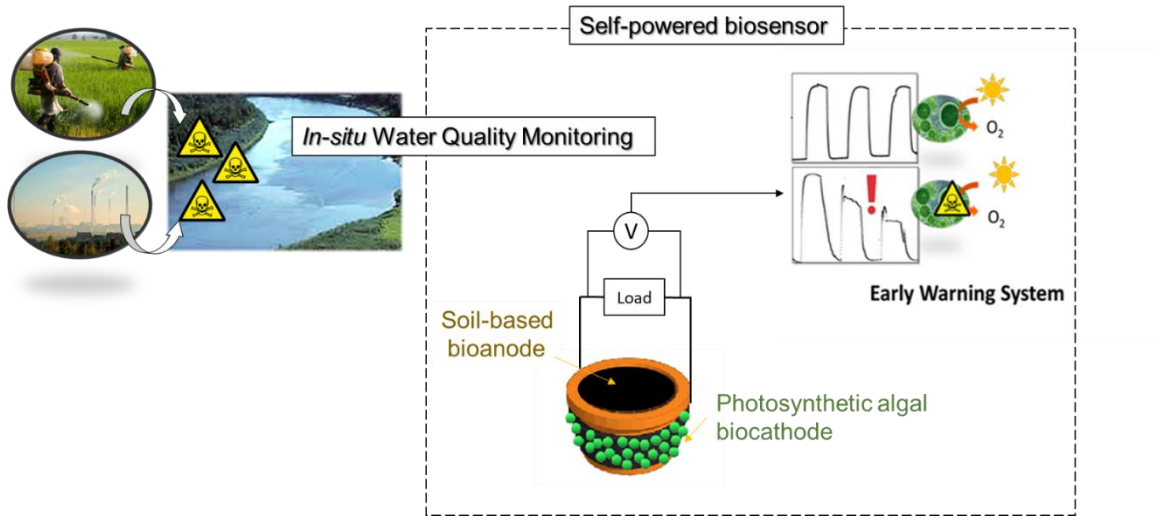

Keywords: Biosensor, Photosynthetic biocathode, Pesticides, Soil microbial fuel cell, Water quality.

6.1 Introduction

The intensive use of pesticides in agriculture and industry is nowadays necessary to cope with the increasing food demand [1]. Pesticides are toxic and persistent substances entering the environment from agricultural and wastewater discharges. Their long-term accumulation in the environment poses unknown consequences for ecosystems and human health [2]. During peak events, such as sudden discharges or heavy rainfall, the concentration of pesticides drastically increases [3]. The unpredictability of these events requires sensing technologies capable of continuous and *in situ* water quality monitoring. Yet, current detection methods are offline, lab-based analytical techniques unsuitable for this purpose [4]. Analytical methods also fail in determining the bioavailability of pesticides, which is best assessed with biosensors. Electrochemical algal biosensors stand out for field implementation due to relatively simpler and more portable designs. Microalgae are ideal bioreceptors for environmental sensing, as they are ubiquitous in nature, withstand harsh environmental conditions and are very sensitive to pollutants [5].

Current algal biosensors are however not ready for continuous deployment due to limitations on the long-term stability and autonomy of the device. These issues

could be solved by integrating algal biosensors with microbial fuel cells (MFCs). MFCs are fuel cells where the energy stored in an organic substrate is converted into electricity by electroactive bacteria. In MFCs, electricity generates as the result of organic matter oxidation at the anode and reduction of oxygen at the cathode [6]. When the MFC is immersed in the water under evaluation, the overall process can be rate-limited by the concentration of dissolved oxygen at the cathode. If the cathode is colonised by algae, that generates oxygen through photosynthesis, the signal will follow the photosynthetic cycle, with oxygen increasing in the day and decreasing in the night. Any disruption in the algal oxygen production, for example by the presence of a pesticide, would perturbate the sensors signal, acting as a detection device [7].

Among MFC sensors, floating Ceramic Soil based Microbial Fuel Cell (CSMFC) designs are promising for long-term, autonomous, performance for continuous, field monitoring of water quality [8]. In a CSMFC the anode is enclosed a ceramic vessel, that prevents the diffusion of oxygen from water. In the vessel, the anode is immersed in soil that provides a long-term supply of organic matter. At the cathode, located outside of the ceramic vessel, oxygen is reduced, closing the electrical circuit [9]. If the cathode is colonised by an algal biofilm, the signal output will indicate the status of photosynthesis by electrochemical reduction of oxygen evolution. A CSMFC sensor with an algal biocathode could therefore be used detect the presence of pesticides through dissolved oxygen monitoring.

This study investigates the effect of two herbicides, Diuron and glyphosate, on the signal output of a CSMFC sensor with a photosynthetic biocathode. Diuron is commonly used as model compound for toxicity assessments. It is a highly stable, urea-based molecule that binds the protein D1 in photosystem II, blocking the transfer of electrons across the photosynthetic electron transport chain and inhibiting oxygen evolution in algae [10]. Glyphosate is currently the most used herbicide for weed control worldwide. Is a non-specific glycine-based herbicide that blocks the aminoacid synthesis and reduces the production of plastoquinone and chlorophyll, involved in the photosynthetic apparatus, also affecting oxygen production [11].

In addition, stabilising the sensor signal to changes in organic matter in water is crucial to minimise detection errors. In this study, we hypothesise that soil provides a saturating, steady load of organic matter to the anode, that reduces the sensitivity of the signal to organic matter. The sensitivity of the signal to organic content in water is experimentally assessed by adding potassium acetate to the catholyte.

6.2 Materials and methods

All chemicals were supplied by Sigma Aldrich and without further purification. The CSMFCs were constructed as previously described [9]. Briefly, the ceramic vessels (3.5 x 4 x 2.7 x 0.3 cm^3) contained 15 g of soil of organic content of 16.88 ± 0.91 % by loss of ignition method (LOI [12]), pH of 6.07 ± 0.12 and conductivity of 1516 ± 32 µS cm^{-1}. The electrodes were made of acid treated graphite felt [13] with anode and cathode dimensions of 7 x 2 x 0.35 cm^3 (34.3 cm^2 projected area) (Figure 6.1 A-C). Algae were collected and enriched as previously described [7].

6.2.1 Enrichment of the CSMFC with algal biocathodes

For the enrichment of the CSMFCs with an algal biocathode ($CSMFC_{Algae}$), the sensors were integrated in a floating platform (Figure 6.1D) and placed in a container with a solution of approx. 10^6 cells mL^{-1} of algae in Bold Basal Medium (BBM), operated under a 12h / 12h on/off light cycle in a black box (light intensity of 40 mW cm^{-1}). As controls, CSMFCs were enriched in the same conditions but in BBM without algal inoculum ($CSMFC_{Control}$).

Once a visible biofilm formed on the cathode surface, the planktonic cells were removed from the catholyte. For this, the $CSMFC_{Algae}$ were placed in individual containers of 200 mL, with 100 mL of tap water, that was exchanged every day at the beginning of the light cycle. Ti wire (25 mm, Advent Research Materials, Oxford, UK) was used as current collector and to connect the electrodes to an external resistance (R_{ext}) of 11 kΩ. During operation, the voltage output (V) was recorded with a PicoLog (Pico Technology, UK) every minute.

6.2.2 Injections of diuron and glyphosate

To simulate a toxic event, 10 mL of glyphosate and Diuron were injected in the

catholyte of the $CSMFC_{Algae}$ under gentle agitation, approximately 6 h after the start of the light period. The catholyte was exchanged for tap water (pH=6.8, Conductivity= 1987 µS cm^{-1}) at the start of the next light cycle, 18 h after the injection. Tests were performed in triplicate. Two tailed t-test at 95% confidence was performed with R, to assess the statistical significance of the perturbations.

6.2.3 Influence of background organic content

Potassium acetate was used to model the influence of organic matter in water. To simplify the interpretation of the CSMFC signal, the effect of BOD was assessed in sensors without algal catholyte. The CSMFCs were enriched in 200 mL of tap water, for 30 days (Figure 6.1E) at R_{ext} =1 kΩ, to promote the electrochemical oxidation of organic matter. The external resistance was selected at the maximum power point based on preliminary tests. The anodes were enriched in soil with 62.5 ± 0.9 % carbon, measured by loss of ignition [14]. After two weeks of operation, the catholyte was exposed to injections of 1 mL of 1 M of potassium acetate, under gentle agitation. One injection was introduced every hour for 4 h and the signal was monitored for 24 h. During operation, the voltage output (V) was recorded with a data logger (EDAQ, USA) every minute.

6.2.4 Electrochemical characterisation

Polarisation tests were performed to identify the rate-limiting electrode in $CSMFC_{Algae}$ under operation. Electrode potentials were measured against an Ag/AgCl (3M NaCl, EDAQ, USA) reference electrode with a benchtop Multimeter (RS PRO RS-14 Digital Multimeter). Polarisation was performed by varying the external load in the range of 10 MΩ -100 Ω with a variable resistor (RS Components, UK), starting from Open Circuit Voltage (OCV) and waiting until signal stabilisation in each step. The current (I) was calculated according to *Ohm's Law* ($I = V/ R_{ext}$) and power (P) was calculated as $P = IV$.

To evaluate the effect of biofilm damage in the electrochemical response of the sensor, polarisation tests were performed on the $CSMFC_{Algae}$ before and after the toxic event. These were conducted using tap water as catholyte, without agitation and open to air.

The kinetic effects of anode and cathode biofilms were assessed with cyclic voltammetry (CV), using a potentiostat (Palmsense, Netherlands) and a 3-electrode system. The electrode colonised by a biofilm operated as the working electrode, a Pt wire as counter electrode and an Ag/AgCl as reference electrode. The CVs were run at a scan rate of 1 mV s^{-1}. For the cathode, the voltage was scanned from 0 V to - 0.8 V vs Ag/AgCl, in a 250 mL beaker with 200 mL of BBM as electrolyte without agitation, approximately five hours after the start of the light period. For the anodes, the CV were scanned from -0.8 to 0.8 V vs Ag/AgCl with the reference and counter electrodes embedded in the soil. All potentials are reported against an Ag/AgCl (NaCl 3M) reference electrode.

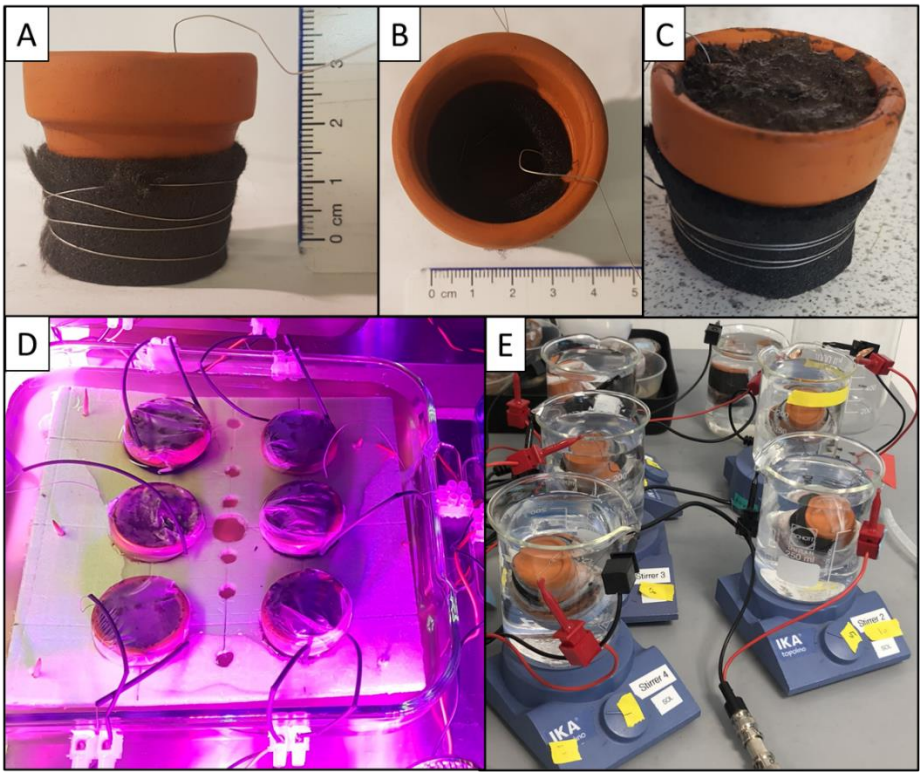

Figure 6.1. *Experimental set up. (A) Terracotta vessel with the cathode wrapped around with Ti wire. (B) Anode inside the ceramic vessel wrapped against the wall with Ti wire. (C) CSMFC with soil in the anode compartment. (D) Floating set up for the enrichment of the CSMFC cathodes on the algal solution. (E) Set up for the evaluation of the BOD on the CSMFC signal.*

The pH was measured with a pH-meter (Thermo Scientific Orion ROSS Ultra pH/ATC Triode, USA). Conductivity was measured with a conductivity benchtop

cell (Orion, Thermo Scientific), and dissolved oxygen was measured with a portable optical probe (RDO Orion 7003, Singapore).

6.3 Results and discussion

6.3.1 Enrichment of the CSMFC$_{Algae}$

Figure 6.2A shows a positive signal one day after the start of the operation. At this stage, the voltage output is likely produced by mediated electron transfer between planktonic bacteria and redox compounds in the soil, rather than by an electroactive biofilm, which generally takes longer to form [15]. During the enrichment period, the signal follows the concentration of algae and oxygen in the catholyte (Figure S6.1A). The photosynthetic pattern develops after 10 days of operation, indicating sufficient enrichment of the anode in electroactive bacteria to not rate-limit the process. At this point the signal develops a light-dependent cycle [7], with voltage increasing during the day and decreasing in the night. A maximum voltage of 78.5 ± 6.6 mV is reached in the CSMFC$_{Algae,}$ after 22 days at a DO of 14 mg L^{-1}. In contrast, the CSMFC$_{Control}$ shows a voltage output below 10 mV and no photosynthetic cycle, which suggests that the CSMFC$_{Algae}$ signal depends on the photosynthetic activity of the algae.

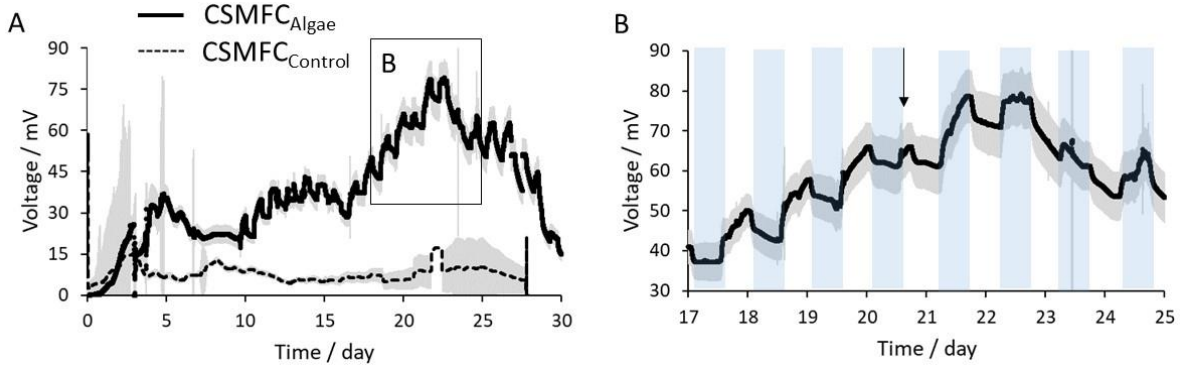

Figure 6.2. *(A) Signal development during the start-up period of the CSMFC$_{Algae}$ sensors. Shadowed areas represent the standard deviation of 12 replicates. (B) Detail of (A) showing the moment of reversal of the photosynthetic cycle with a black arrow. Error bars represent the standard deviation of CSMFC$_{Algae}$ (n=12) and CSMFC$_{Control}$ (n=3). Blue areas represent the dark cycle.*

After 22 days, the trend on the $CSMFC_{Algae}$ signal reverses, probably because the high concentration of oxygen accumulated in the catholyte diffuses into the anode, poisoning anaerobic electroactive bacteria [16]. In fact, Figure 6.3B shows that the signal of the $CSMFC_{Algae}$ correlates positively with DO at DO < 9 mg L^{-1} (R^2=0.86) and negatively at DO > 9 mg L^{-1} (R^2 = 0.70) indicating a strong dependency of the signal to oxygen.

The sensor baseline drastically dropped after 27 days of operation but recovered when the sensors were placed in individual containers. It is indeed possible that parasitic currents arose between the sensors as a result of fluidic conductance when they share the electrolyte [17].

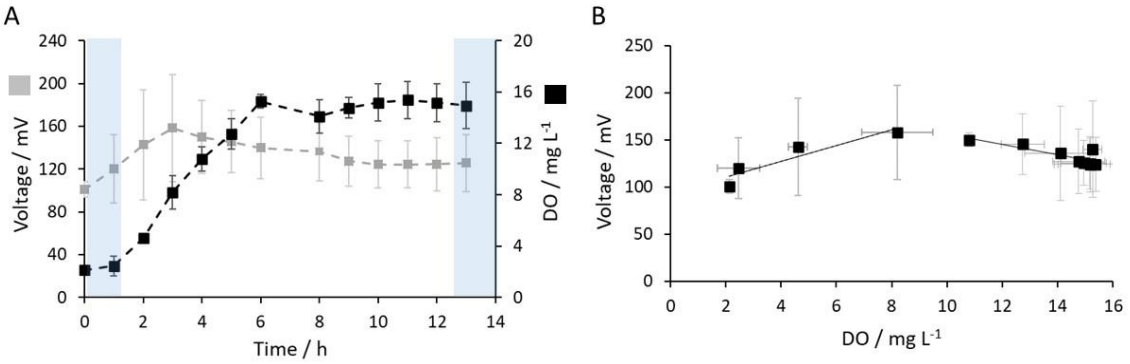

Figure 6.3. *(A) Time series of voltage output (grey squares) and dissolved oxygen (black squares) during the light cycle. (B) Correlation of voltage and DO in (A) showing an increasing trend up to DO= 9 mg L^{-1} and decreasing afterwards. Error bars are the standard deviation of three replicates. Shadowed areas represent the dark cycle.*

To eliminate the effect of planktonic cells on the sensor response, after 30 days of enrichment the $CSMFC_{Algae}$ were placed in individual containers, immersed in water of DO = 8.6 mg L^{-1}. The maximum power output obtained in these conditions was 2.88 ± 0.99 µW (0.84 mW m^{-2} projected area), substantially lower than reported for other algal assisted MFCs [18]. This is because the short distance between electrodes facilitates exposure of the anode to oxygen. The polarisation curves in Figure 6.4A evidence the anodic inefficiencies. First, the anodic open circuit potential (OCP) is around - 50 mV vs. Ag/AgCl. A high OCP partially indicates the presence of alternative electron acceptors [19]. An OCP as low as -450 mV is reported for anaerobic anodes [20], whereas OCPs around - 200 mV are

common in sediment MFC with algal cathodes [21], where oxygen and other electron acceptors, like nitrates or sulfides, are available. The cathodic OCP, around 300 mV, is yet similar to other algal biocathodes [20, 21] and higher than the OCP in abiotic cathodes, of - 100 mV in the same conditions (Figure S6.2). The three-fold increase in limiting cathodic current in the presence of a biofilm (Figure 6.4B), suggests that the increase in cathodic OCP in colonised electrodes is likely the result of a local rise in photosynthetic oxygen. Additionally, the similar onset potential of both colonised and abiotic cathodes, of -0.2 V, shown in Figure 6.4B, suggests that the biofilm does not catalyse the reduction and the improvement in the reaction is due to facilitated diffusion of oxygen to the cathode surface [21].

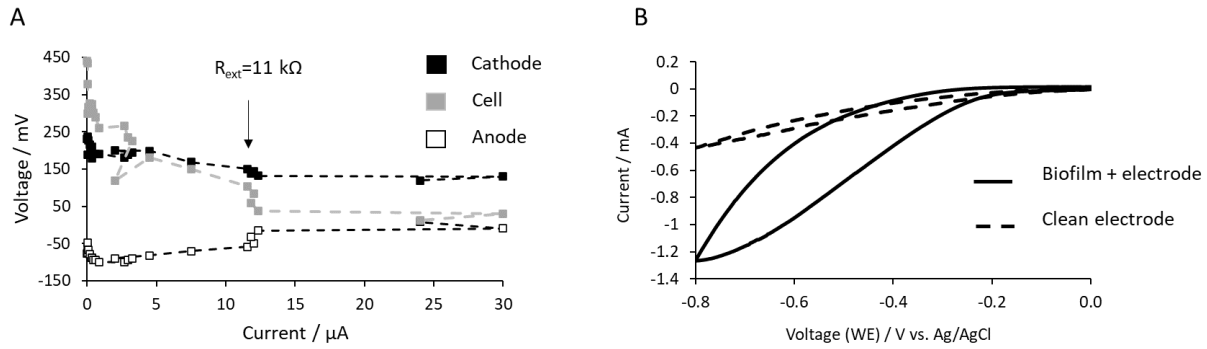

Figure 6.4. *(A) Polarisation curves of the SCMFC where grey squares represent the cell voltage, black square the cathode potential and open squares the anode potential. Data is one replicate of two representative samples shown in Figure S6.3. (B) Cyclic voltammograms of a colonised cathode (black line) and clean cathode (dotted line) in BBM medium.*

To improve the stability of the signal output, the external resistance was selected to prevent power overshoot (Figure 6.4A). Power overshoot is often observed in underperforming MFCs where the current reverses due to a sudden increase in internal resistance. Low conductivity of the electrolyte, lack of sufficient organics and presence of alternative electron acceptors could be the cause of power overshoot in our system [23].

Previous studies report a DO saturation for the cathode reaction around 8 mg L^{-1}, with the same anode and cathode electrode areas [24], indicating that oxygen supplied by algae, up to 20 mg L^{-1} in the light cycle, is sufficient to not limit the

reduction reaction in the whole range of current. The polarisation sweep of individual electrodes shows that, at R_{ext} =11 kΩ, the system is mainly anode limited and the signal is sensitive to changes in oxygen in the anode. Inhibition of photosynthetic oxygen production in algae would increase the signal output, as a consequence of decreased diffusion of oxygen in the soil from the bulk water.

6.3.2 Detection of pesticides with the CSMFC$_{Algae}$ sensors

Figure 6.5 shows the response of the CSMFC$_{Algae}$ sensors to a toxic event of the legal limit of 0.1 µg L^{-1} [25], of the pesticides Diuron (Figure 6.5A) and glyphosate (Figure 6.5B). As predicted, the signal output increases after the toxic event, in both cases. The change in voltage before and after intoxication is significant for Diuron but not for glyphosate, in the tested conditions (Figure 6.5C and D and Table 6.1). The enhanced sensitivity of algae to Diuron over glyphosate was also observed in other electrochemical algal biosensors [26]. As discussed, the increased voltage after exposure is probably due to reduced oxygen crossover into the anode, as a consequence of the decrease of DO in the catholyte [7]. While the perturbation is not apparent in the timeseries representation (Figure 6.5A and B), the change in the mean of daily accumulated charge (Figure 6.5E and F) and accumulated standard error (Figure 6.5G and H), averaged for five days before and after the toxic event, is significant for both pesticides.

The variance of these metrics is also significantly larger before and after the toxic event (Table 6.1). Moreover, the autocorrelation value of consecutive samples is R^2=0.2 (Figure S6.4) which means that the independency of the data assumption is not heavily violated. Lower autocorrelation could be obtained spacing out the sample frequency, but that would also increase the detection time [27].

Consequently, a decision algorithm to detect a toxic event could be based on the comparison of the variance of accumulated charge or accumulated standard error of a sample, with the equivalent in non-toxic conditions. This approach simplifies the statistical analysis, as it does not require the variance of the timeseries dataset to be constant or normally distributed [27].

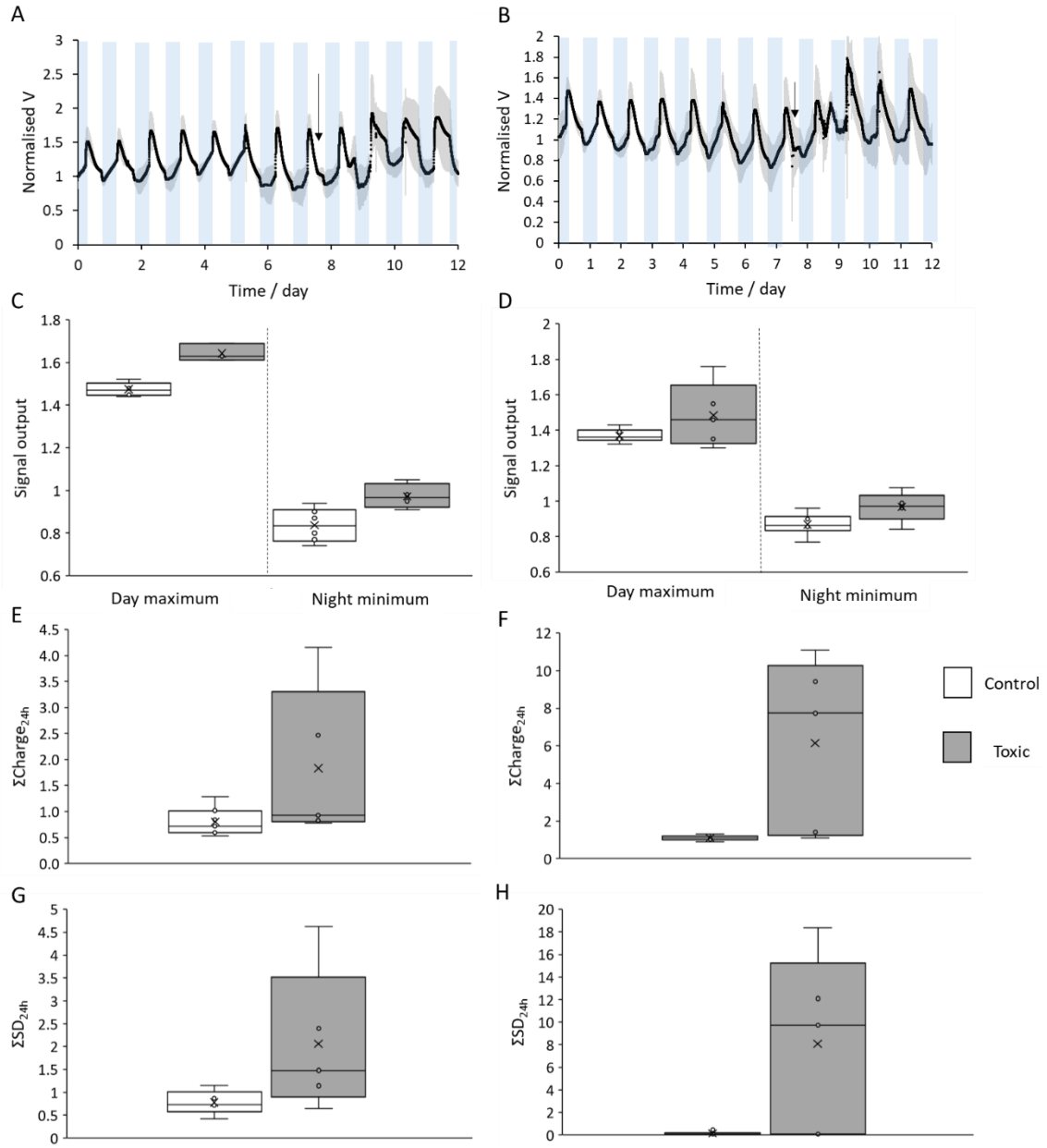

Figure 6.5. *Response of the CSMFC sensor to a toxic event of 0.1 µg L^{-1} of Diuron (A) and glyphosate (B). Data shown is the average of the voltage output of three replicates, normalised by the steady state voltage at the beginning of the day cycle in non-toxic conditions. Shadowed grey areas represent the standard deviation of the normalised sample and blue areas represent the night cycle. Boxplots of the maximum day voltage and minimum night voltage Diuron (C) and glyphosate (D). Boxplots of the accumulated charge in 24 h for Diuron (E) and glyphosate (F). Boxplots of the accumulated standard deviation for Diuron (G) and glyphosate (H). White boxes include data of 5 days before the toxic event and grey boxes include data 5 days after the toxic event. All values are calculated based on normalised voltage in (A) and (B).*

Table 6.1. *Summary of metrics derived from the data in Fig. 6.5A and 6.5B before and after the toxic event of 0.1 µg L^{-1} of Diuron and glyphosate. Values are normalised by the steady state voltage at the beginning of the light cycle, in non-toxic conditions.*

Pesticide	Metric	Avg. of 5 days before	Avg. of 5 days after
Diuron	Maximum day	1.43 ± 0.07	1.65 ± 0.04
	Minimum night	0.84 ± 0.07	0.97 ± 0.06
	Charge 24h	1.53 ± 0.50	3.99 ± 2.99
	Standard deviation 24 h	0.78 ± 0.26	2.41 ± 1.57
Glyphosate	Maximum day	1.37 ± 0.04	1.48 ± 0.18
	Minimum night	0.08 ± 0.06	0.97 ± 0.08
	Charge 24h	1.10 ± 0.14	6.14 ± 4.62
	Standard deviation 24 h	0.14 ± 0.04	8.07 ± 7.95

The reusability of the biosensor was evaluated exposing the CSMFCs to another injection of 50 µg L^{-1} of Diuron (Figure 6.6). The “non-toxic” conditions are set by the baseline reached few days after the first injection of 0.1 µg L^{-1} of Diuron. The change in the signal after the consecutive toxic event with respect to the non-toxic dataset is significant for all metrics (Table 6.2), suggesting that the CSMFC sensors can be reused for multiple toxic events.

Table 6.2. *Summary of metrics derived from Figure 6.6A before and after the toxic event of 50 µg L^{-1} of Diuron. Values are normalised by the steady state voltage at the beginning of the light cycle in non-toxic conditions.*

Pesticide	Metric	Avg. of 5 days before	Avg. of 5 days after
Diuron	Max V day	0.98 ± 0.15	1.80 ± 0.32
	Min V night	0.95± 0. 08	1.52 ± 0.40
	Charge 24h	1.59 ± 0.21	2.31 ± 0.85
	Standard deviation in 24h	1.15 ± 0.23	2.21 ± 0.98

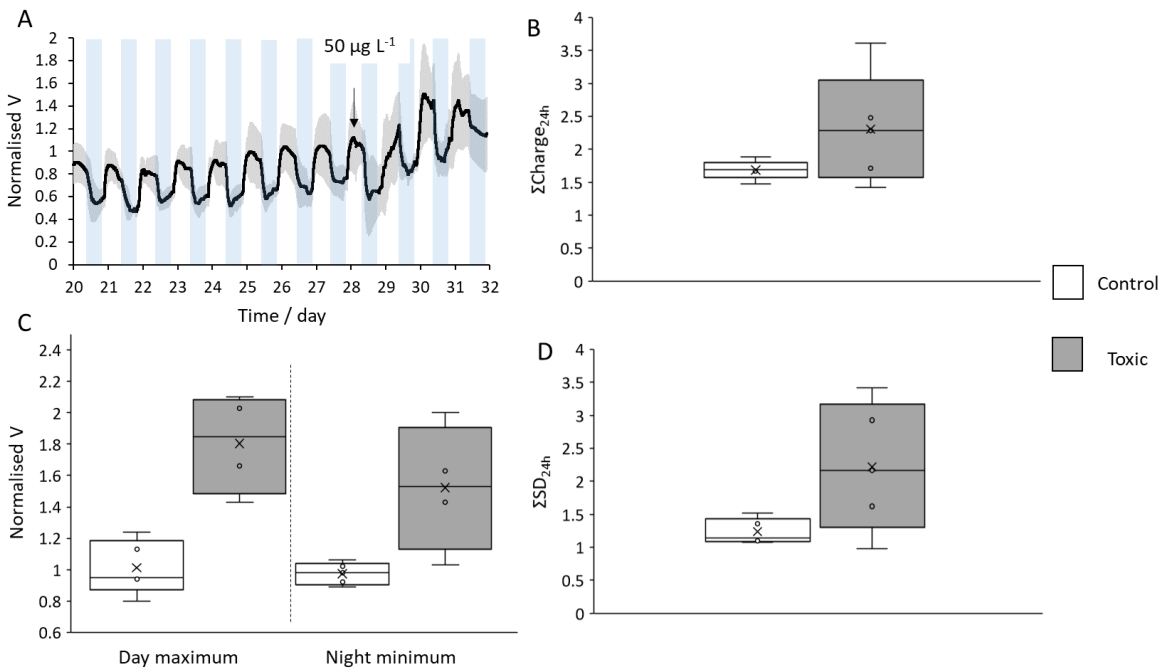

Figure 6.6. *(A) Response of the CSMFC sensor to a toxic event of 50 µg L^{-1} of Diuron. Data is the average of the voltage output of three replicates, normalised by the steady state voltage at the beginning of the day cycle in non-toxic conditions. Shadowed grey areas represent the standard deviation of the normalised sample and blue areas represent the night cycle. (B) Boxplots of the accumulated charge in 24 h. (C) Boxplots of the maximum day voltage and minimum night voltage (D). Boxplots of the accumulated standard deviation in 24 h. White boxes include data of 5 days before the toxic event and grey boxes include data 5 days after the toxic event. All values are calculated based on normalised voltage in (A).*

6.3.3 Influence of BOD on the CSMFC signal

To evaluate the impact of organic content in water in the sensor signal, new CSMFCs enriched in tap water (Figure S6.4) were challenged to varied concentrations of acetate in the catholyte. No significant short-term change in the signal after four injections of 5 mM of acetate each, 30 min apart, is observed in the first 3.5 hours from the first injection (Figure 6.7A). The signal output steadily increases after 4 hours from the first injection (Figure 6.7B), likely due to diffusion of acetate into the anodic chamber. Bacterial oxidation of acetate consumes oxygen in the anode, increasing both the electrochemical reaction rate and the anaerobic conditions [28].

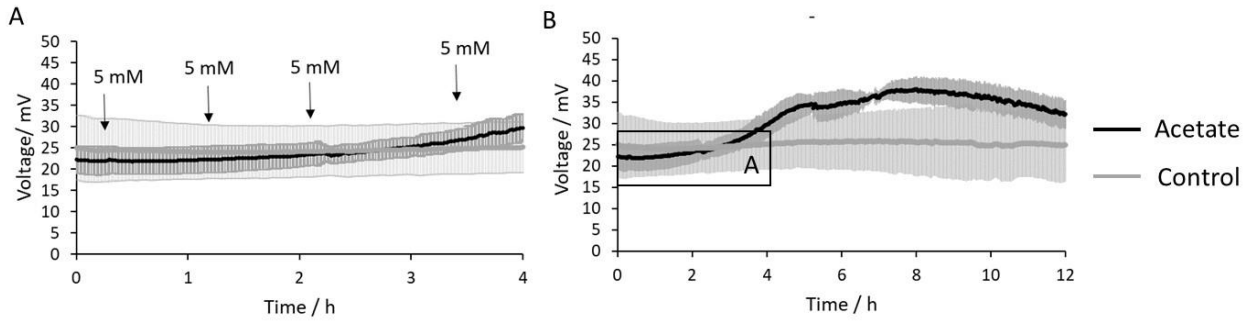

Figure 6.7. *(A) Short-term and (B) long-term effect of acetate on the CSMFC signal. Error bars correspond to the standard deviation of three replicates.*

The signal steadily increases, stabilising at a maximum voltage of 37.3 ± 3.3 mV, almost twice the initial baseline, after 6 h of operation. The signal then decays due to oxygen depletion in the catholyte exposed to acetate, from a DO of 8.9 ± 0.3 to 4.0 ± 1.3 mg L^{-1} after 24 h, in agreement with the correlation trend in Figure 6.3B with an inflexion point at 9 mg L^{-1}.The baseline was restored upon replacement of the catholyte with fresh tap water. It is worth noticing that the high conductivity of the acetate injection (1706 ± 1 µS cm^{-1}) did not have any instant effect on power performance, a possible consequence of having the anode surrounded by soil with high conductivity.

6.4 Conclusions

This work demonstrates the use of CSMFC to detect pesticides in water *via* changes in the photosynthetic oxygen evolved in algae. The signal correlates positively with DO up to 9 mg L^{-1} and negatively at higher values, probably due to oxygen crossover into the anode. The detection of 0.1 µg L^{-1} of herbicides Diuron and glyphosate was significant in terms of the accumulated charge and variance, but only to Diuron in terms of maximum day and minimum night voltage. A second injection of Diuron was successfully detected with the same bioreceptor, indicating the reusability of the sensing element for multiple shocks. Moreover, the soil-based anode prevents any organic matter in the water to produce sudden variations in the signal, reducing the noise in the signal. The system operated without addition of nutrients for three months, showing the potential of this technology for unattended monitoring of water quality.

6.5 Supplementary information

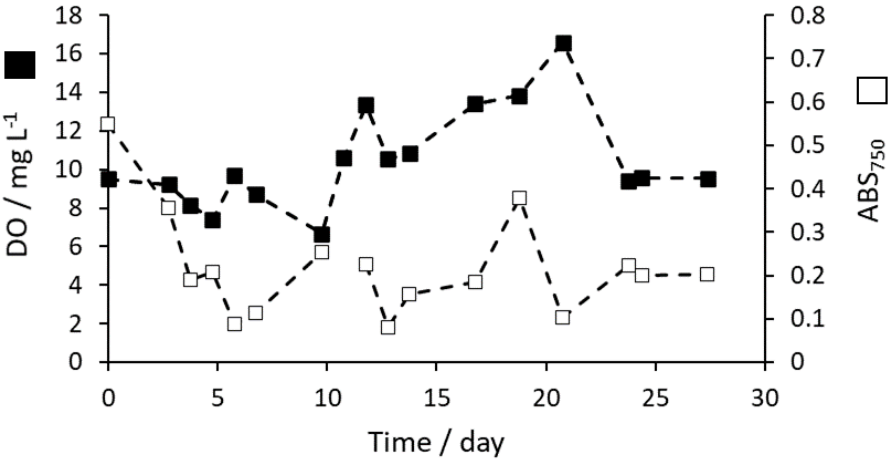

***Figure S6.1**. Conditions of dissolved oxygen (black squares) and absorbance (white squares) in the electrolyte during the enrichment period.*

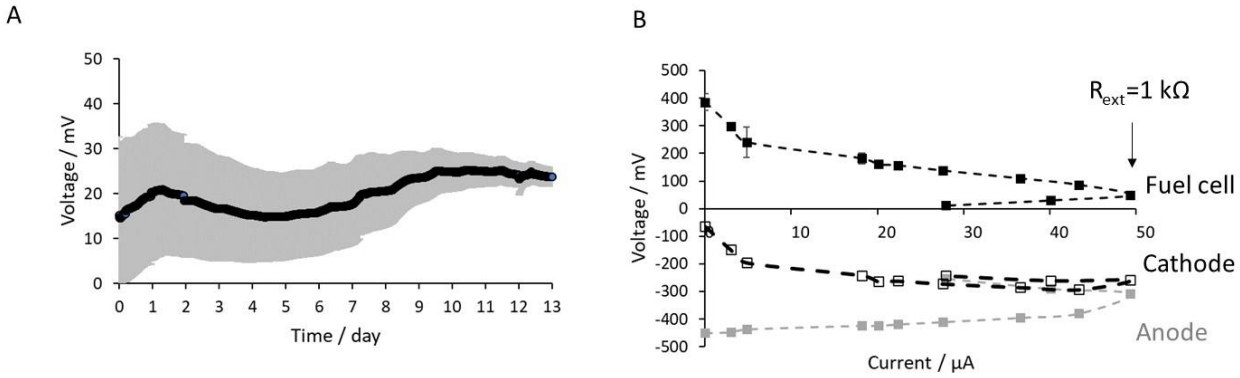

***Figure S6.2**. (A) Enrichment at R_{ext}= 1 kΩ and (B) polarisation curves of the CSMFC used to evaluate the effect of acetate in water on the signal output. Shadowed areas and error bars correspond to the standard deviation of three replicates.*

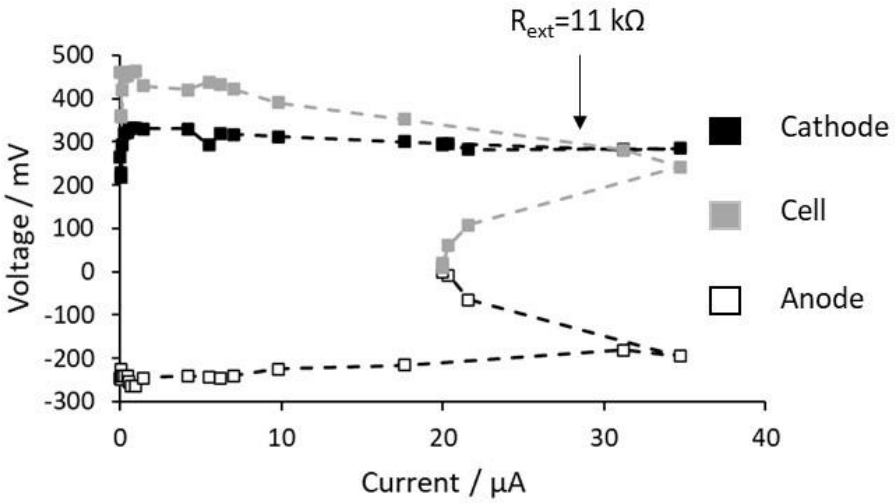

Figure S6.3. *Polarisation curve of the CSMFC suplementary to Figure 6.4.*

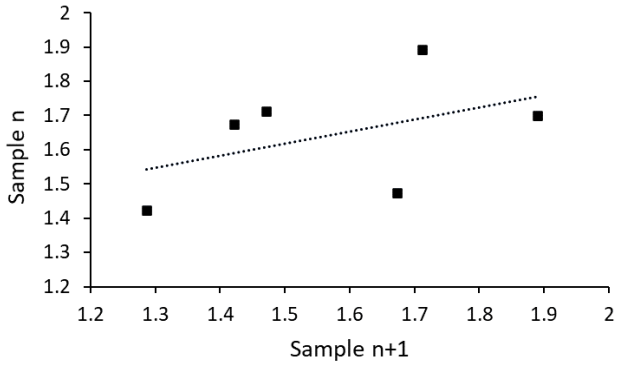

Figure S6.4. *Autocorrelation plot for accumulated charge.*

6.6 References

[1] "SDG 6 Synthesis Report 2018 on Water and Sanitation," 2018.

[2] B. Petrie, R. Barden, and B. Kasprzyk-Hordern, "A review on emerging contaminants in wastewaters and the environment: Current knowledge, understudied areas and recommendations for future monitoring," *Water Res.*, vol. 72, pp. 3–27, 2014.

[3] M. Lefrancq, A. Jadas-Hécart, I. La Jeunesse, D. Landry, and S. Payraudeau, "High frequency monitoring of pesticides in runoff water to improve understanding of their transport and environmental impacts," *Sci. Total Environ.*, vol. 587–588, pp. 75–86, 2017.

[4] P. Lepom, B. Brown, G. Hanke, R. Loos, P. Quevauviller, and J. Wollgast, "Needs for reliable analytical methods for monitoring chemical pollutants in surface water under the European Water Framework Directive," *Journal of Chromatography A*, vol. 1216, no. 3. pp. 302–315, 2009.

[5] J. Livage, "Micro-algal biosensors," *Anal. Bioanal. Chem.*, vol. 401, no. October, pp. 581–579, 2011.

[6] B. E. Logan *et al.*, "Microbial fuel cells: Methodology and technology," *Environmental Science and Technology*, vol. 40, no. 17. pp. 5181–5192, 01-Sep-2006.

[7] L. Gonzalez Olias, P. J. Cameron, and M. Di Lorenzo, "Effect of Electrode Properties on the Performance of a Photosynthetic Microbial Fuel Cell for Atrazine Detection," *Front. Energy Res.*, vol. 7, no. October, pp. 1–11, 2019.

[8] A. Schievano *et al.*, "Floating microbial fuel cells as energy harvesters for signal transmission from natural water bodies," *J. Power Sources*, vol. 340, pp. 80–88, 2017.

[9] L. G. Olias, A. Rodriguez, P. J. Cameron, and M. Di Lorenzo, "A soil microbial fuel cell-based biosensor for dissolved oxygen," *Electrochim. Acta*, p. 137108, 2020.

[10] H. Heldt, *Plant Biochemistry*, vol. 168, no. 4262. 1951.

[11] M. P. Gomes and P. Juneau, "Temperature and Light Modulation of Herbicide Toxicity on Algal and Cyanobacterial Physiology," *Front. Environ. Sci.*, vol. 5, no. August, pp. 1–17, 2017.

[12] M. H. McCrady, “STANDARD METHODS FOR THE EXAMINATION OF WATER AND WASTE-WATER (12th ed.),” *Am. J. Public Heal. Nations Heal.*, vol. 56, no. 4, pp. 684–684, 2008.

[13] S. M. Martinez and M. Di Lorenzo, “Electricity generation from untreated fresh digestate with a cost-effective array of floating microbial fuel cells,” *Chem. Eng. Sci.*, vol. 198, pp. 108–116, 2019.

[14] S. O. P. Sm *et al.*, “Standard Methods for the Examination of Water and Wastewater,” 2009.

[15] G. Liu, M.D. Yates, S. Cheng, D.F. Call, D. Sun, B.E. Logan, “Examination of microbial fuel cell start-up times with domestic wastewater and additional amendments,” Biores. Techno., vol. 102, 15, pp. 7301-7306, 2011.

[16] Z. He, J. Kan, F. Mansfeld, L. T. Angenent, and K. H. Nealson, “Self-sustained phototrophic microbial fuel cells based on the synergistic cooperation between photosynthetic microorganisms and heterotrophic bacteria,” *Environ. Sci. Technol.*, vol. 43, no. 5, pp. 1648–1654, 2009.

[17] J. Winfield, I. Ieropoulos, J. Greenman, and J. Dennis, “Investigating the effects of fluidic connection between microbial fuel cells,” *Bioprocess Biosyst. Eng.*, vol. 34, no. 4, pp. 477–484, May 2011.

[18] D. A. Jadhav, S. C. Jain, and M. M. Ghangrekar, “Simultaneous Wastewater Treatment, Algal Biomass Production and Electricity Generation in Clayware Microbial Carbon Capture Cells,” *Appl. Biochem. Biotechnol.*, vol. 183, no. 3, pp. 1076–1092, 2017.

[19] D. Wang *et al.*, “Open external circuit for microbial fuel cell sensor to monitor the nitrate in aquatic environment,” *Biosens. Bioelectron.*, vol. 111, no. March, pp. 97–101, 2018.

[20] F. Zhao, F. Harnisch, U. Schröder, F. Scholz, P. Bogdanoff, and I. Herrmann, “Challenges and constraints of using oxygen cathodes in microbial fuel cells,” *Environ. Sci. Technol.*, vol. 40, no. 17, pp. 5193–5199, 2006.

[21] A. S. Commault, G. Lear, P. Novis, and R. J. Weld, “Photosynthetic biocathode enhances the power output of a sediment-type microbial fuel cell,” *New Zeal. J. Bot.*, vol. 52, no. 1, pp. 48–59, 2014.

[22] I. Bardarov, M. Mitov, D. Ivanova, and Y. Hubenova, “Light-dependent processes

on the cathode enhance the electrical outputs of sediment microbial fuel cells ☆," *Bioelectrochemistry*, vol. 122, pp. 1–10, 2018.

[23] J. Winfield, I. Ieropoulos, J. Greenman, and J. Dennis, "The overshoot phenomenon as a function of internal resistance in microbial fuel cells," *Bioelectrochemistry*, vol. 81, no. 1, pp. 22–27, Apr. 2011.

[24] Y. Zhang and I. Angelidaki, "A simple and rapid method for monitoring dissolved oxygen in water with a submersible microbial fuel cell (SBMFC)," *Biosens. Bioelectron.*, vol. 38, no. 1, pp. 189–194, 2012.

[25] R. N. Carvalho, L. Ceriani, and A. Ippolito, "Development of the first Watch List under the Environmental Quality Standards Directive water policy," 2015.

[26] C. Durrieu, H. Guedri, F. Fremion, and L. Volatier, "Unicellular algae used as biosensors for chemical detection in Mediterranean lagoon and coastal waters," *Res. Microbiol.*, vol. 162, no. 9, pp. 908–914, 2011.

[27] K. G. Dunn, "Process Improvement using Data," *http://learnche.org/pid*, 2019. [Online]. Available: learnche.mcmaster.ca/pid.

[28] K. H. Williams, K. P. Nevin, A. Franks, A. Englert, P. E. Long, and D. R. Lovley, "Electrode-based approach for monitoring in situ microbial activity during subsurface bioremediation," *Environ. Sci. Technol.*, vol. 44, no. 1, pp. 47–54, 2010.

Chapter 7

Chapter 6 introduces a novel ceramic soil floating MFC sensor for pesticide detection in water bodies, with an algal biocathode as sensing element. The study revealed that the size of the terracotta vessel, used as electrode separator and anode chamber, is too small to prevent the influence of cathodic oxygen in the anodic electroactivity. As such, in this chapter the size of the vessel is increased from 30 to 140 cm^3 approx.

Chapters 5 and 6 show that the baseline signal generated by an algal bioreceptor is unstable due to daily variations in dissolved oxygen and long-term effects of the toxicant in the algal activity. To stabilize the signal, in Chapter 7 the cathode biofilm is eliminated to simplify the sensor's response and signal treatment. This study proposes a floating CSMFC sensor with an abiotic cathode to detect changes in the DO in water. This is a practical approach for early detection of hypoxia in water bodies, a frequent cause of ecosystem disruption in environmental waters.

In previous chapters, given the high oxygen content at the interface of the cathode due to the photosynthetic activity, the external resistance was chosen to maximise the oxygen reduction reaction rate to improve the detection time of the sensor. In this chapter, the DO of the water is constant at a value of approximately 8 mg L^{-1}. As such, here the external resistance is chosen to operate the sensor at the maximum power point, to increase the long-term stability of the anodic activity and reduce the diffusion layer thickness of oxygen at the interface of the cathode.

Based on the results of Chapter 5 and 6, in this study the anode electrode area is larger than the cathode area to prevent the former from limiting the electrical signal.

Chapter 7 finalises with a comparison of the influence of environmental factors using a one factor at the time approach and a holistic approach based on a design of experiments (DoE). The influence of environmental variables temperature, pH,

oxygen and water conductivity is investigated with a factorial DoE. This is an important contribution to understand the behaviour of the sensor signal in real conditions. The linear model obtained in the factorial design describes the trends of the signal variation with these factors. This work hypothesises that whether the absolute baseline varies over time, the trends are conserved. This chapter has been published as detailed on the following page.

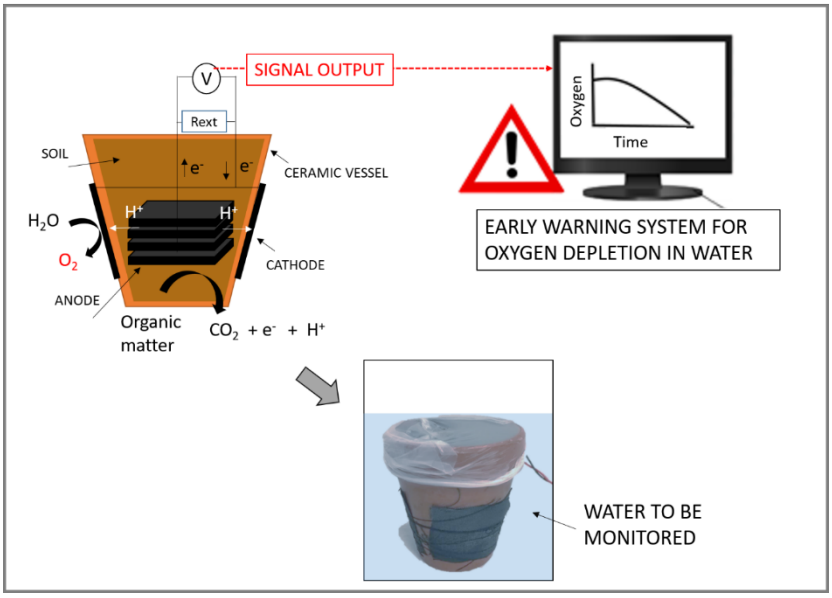

Statement of authorship

This declaration concerns the article entitled:

"A novel soil microbial fuel cell-based biosensor for dissolved oxygen monitoring in water"

Publication status: Published

Publication details: Olías L.G., Rodríguez A., Cameron A., Di Lorenzo M. "A novel soil microbial fuel cell-based biosensor for dissolved oxygen monitoring in water", Electrochimica Acta vol.362 137108 (2020). doi:10.1016/j.electata.2020.137108.

Authorship contributions:

Original ideal, conceptualization and sensor design, L.G.; experimental design, L.G., A.R., P.J.C, M.D.L.; experimentation, L.G., A.R.; writing-original draft, L.G.; editing, L.G., P.J.C., M.D.L.; supervision, M.D.L., P.J.C.

Statement from candidate: This paper reports on original research I conducted during the period of my Higher Degree by Research candidature. In line with the regulations in QA7 Appendix 6 of the University of Bath, the abovementioned article has been stylistically integrated into the thesis, including: sections and figures numbering, typeface, margins and pagination.

Signed:

Date:

7. A soil microbial fuel cell-based biosensor for dissolved oxygen monitoring in water

Lola Gonzalez Olias[1,2,] Alba Rodríguez Otero[1], Petra J. Cameron[3], Mirella Di Lorenzo[1,]*

[1] Centre for Biosensors, Bioelectronics and Biodevices (C3Bio) and Department of Chemical Engineering, University of Bath, Bath BA2 7AY, United Kingdom

[2] Water Innovation Research Centre (WIRC), University of Bath, Bath BA2 7AY, United Kingdom

[3] Department of Chemistry, University of Bath, Bath BA2 7AY, United Kingdom

Water pollution can cause depletion of dissolved oxygen (DO) in water systems with serious environmental and economic consequences. Online and continuous monitoring of DO can help prevent or minimise the risks associated with low DO values in water. Current DO sensors are, however, expensive and not suitable for continuous and autonomous in-field operation. In this study, we propose a novel and affordable Ceramic Soil Microbial Fuel Cell (CSMFC) for *in situ*, continuous and autonomous monitoring of DO in water. The system consists of a submersible ceramic vessel containing a soil-based anodic chamber, while the cathode, wrapped around the vessel, is used as the DO probe. The sensor signal, in terms of output voltage, correlates with the DO in water up to a saturating value of 4.5 ± 1.2 mg L^{-1}, at a maximum voltage output of 321 ± 29 mV (20 ℃, pH=7, 1.65 mS cm^{-1}) with a sensitivity in the linear range of 53.3 ± 22.6 mV L mg^{-1}. A factorial Design of Experiments (DoE) on pH, conductivity, DO and temperature shows that the sensor voltage response is mainly affected by temperature and DO, as well as by their mutual interaction. The resulting model was used to assess the DO in water samples, showing an error as low as 0.05 mg L^{-1}. The calibration model is normalised by the output voltage baseline, thus accounting for any variability in performance, within the same device during long-term operation and from one device to another, which is a challenge in microbial-based systems. As such, this work not only reports an innovative microbial fuel cell-based DO sensor, but also demonstrates the necessity of a DoE to effectively calibrate the sensor.

Keywords: Design of Experiments, Dissolved Oxygen Sensor, Soil Ceramic Microbial Fuel Cell, Water Quality.

7.1 Introduction

Worldwide, the uncontrolled release of pollutants from intensive agriculture and industrial activities poses serious risks to the environment. The effect of such pollutants in ecosystems can lead to hypoxia, a sudden drop in the dissolved oxygen below the critical value to sustain aquatic life of ca. 2 mg L^{-1}, with important environmental and economic consequences [1]. Online monitoring of dissolved oxygen (DO) in water can help detect and mitigate the impact of hypoxic events [2].The few commercially available sensors for environmental DO monitoring are, however, expensive and require regular maintenance [3]. Their use in the field is therefore restricted, particularly in developing countries.

Microbial Fuel Cell (MFC) technology could be an affordable option for long-term, online and in-field monitoring of DO [4]. An MFC is a fuel cell that uses microorganisms to directly convert the energy stored in an organic substrate into electricity. If the cathode of the MFC is immersed in the water to be analysed, it could be used as a dissolved oxygen probe [2]. In this case, the current output generated by the system would directly depend on the concentration of DO in the catholyte, as long as the oxygen reduction reaction at the cathode is the limiting step of the overall bioelectrochemical process [3, 5].

Sediment MFCs are particularly suitable for long-term and unsupervised operation due to their proven autonomy and stability over time [6]. In such systems, the electrochemical performance is greatly affected by the ohmic losses due to electrode spacing and the transport of organic content in the sediment, limiting the distance of application of this systems as DO sensors [7,8].

To overcome these limitations, we here propose a ceramic-based soil MFC (CSMFC), with an electrode spacing as short as 4 mm. We demonstrate, for the first time, the use of a CSMFC as a DO sensor. The signal output of the CSMFC sensor is influenced by the DO concentration, but also by other factors, such as pH, anode potential, salinity, the presence of competitive reductive species and temperature, and the interactions between them [9,10]. All of these factors must necessarily be considered in the sensor calibration. To demonstrate this, the calibration models obtained both with a one factor at the time (OFAT) approach

and a holistic approach, based on a design of experiments (DoE), are compared. To the best of the authors' knowledge, this is the first time that such a systematic analysis has been carried out on a microbial fuel cell-based sensor. The models resulting from this study, assessed in terms of goodness of fit and the best performing model, are validated in real water to prove the practical use of the CSMFC sensor.

7.2 Materials and methods

7.2.1 Materials

All reagents were purchased from Sigma Aldrich, unless otherwise specified. All aqueous solutions were prepared with reverse osmosis purified water.

Soil was collected at the outskirts of the University of Bath campus and cleared of leaves and stones prior to be used. The organic content of the soil right after collection, assessed with the loss of ignition method [11], was 16.88 ± 0.91 %.

7.2.2 Design of the CSMFC and operation

The CSMFC consists of a terracotta vessel (Little Bug Crafts, UK) of dimensions 7.4 cm (height) x 8 cm (upper diameter) x 4.8 cm (bottom diameter) x 0.4 cm (thickness), which serves as the electrode separator and provides structural support for the anode chamber. The anode was made of four pieces (3 x 3 x 0.7 cm^3) of graphite felt (GF, Online Furnace Services Ltd.), woven together with Ti wire (25 mm, Advent Research Materials, Oxford, UK). Prior to be used as the anode, the GF pieces were acid treated to enhance both the hydrophilicity and the specific surface area of the graphite fibres, as previously described [12]. The anode was then placed inside the terracotta vessel, buried in water saturated soil and sealed with parafilm. The cathode, made of two pieces (6 cm x 4 cm each) of plain carbon cloth (CC, Fuel Cell Store, USA), was wrapped around the outside of the ceramic vessel with non-conductive thread and woven with Ti wire as current collector.

During operation, the anode and cathode were connected to an external resistance (R_{ext}) and to a data logger (PicoLog High Resolution Data Logger, Pico

Technology) to monitor the voltage over time. During the process of enrichment of the anode with an electroactive biofilm, the CSMFCs were placed inside a 250 mL glass vessel containing 100 mL of reversed osmosis water, exposing only a third of the ceramic vessel and the bottom part of the cathode to water, to ensure full hydration and access to air of the cathode (Figure 7.1A). A R_{ext} of 10 kΩ was used in this case.

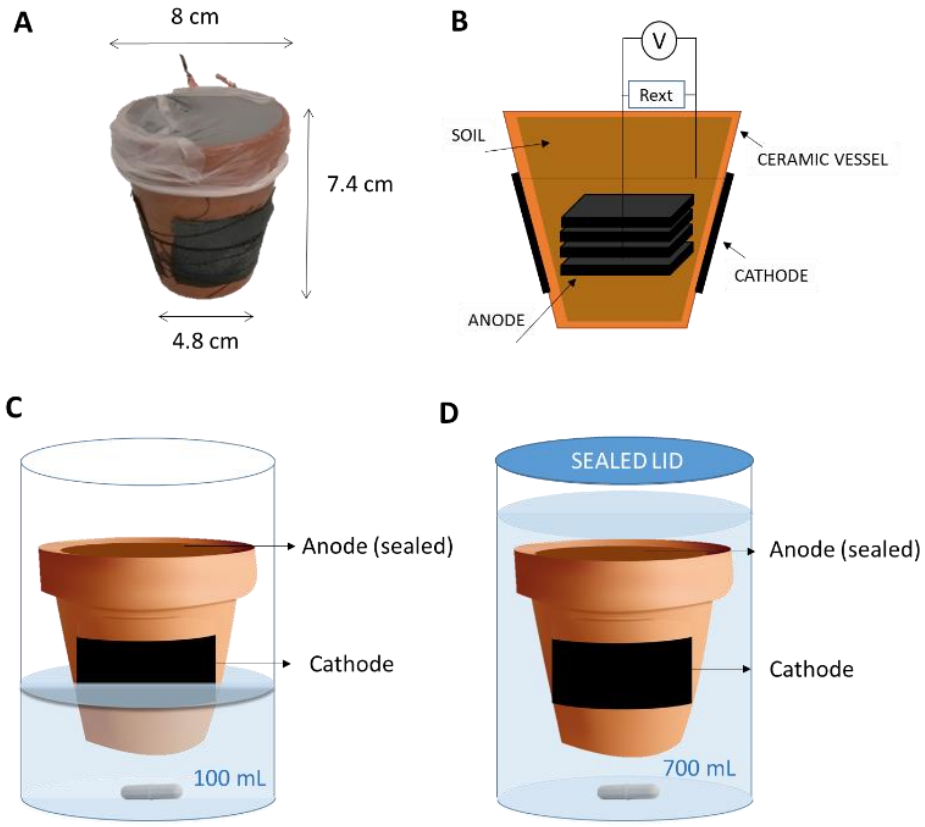

***Figure 7.1**. CSMFC used in this study and experimental set-up. (A) Actual photo and (B) schematic of the CSMFC. (C) Experimental set-up during the enrichment, with only half of the cathode submerged in the catholyte, and (D) during operation, with the cathode fully submerged in the catholyte.*

7.2.3 Electrochemical characterisation

Polarisation tests were conducted at different stages of the experiment to evaluate the energy performance of the CSMFC sensor over time. The tests were performed by applying an external load to the CSMFCs, varying within the range from 10 MΩ - 100 Ω with a resistance box (RS Components, UK), and starting from Open Circuit

Voltage (OCV). During the operation, the anode and cathode potential were measured with a benchtop multi-meter (RS PRO RS-14 Digital Multimeter). When required, an Ag/AgCl electrode (3M NaCl, EDAQ, USA) was placed in the soil, to monitor the anode potential, and another Ag/AgCl electrode was placed in the catholyte. The fuel cell voltage (V), measured across the electrode terminals, was monitored every minute during normal operation with the PicoLog data logger. The current (I) was calculated according to Ohm's Law ($I = V/ R_{ext}$) and power (P) was calculated as P = IV. The internal resistance was calculated from the maximum power point of the power curve.

7.2.4 Influence of factors on the CSMFC response

Both a one factor at the time (OFAT) approach and a design of experiments (DoE) were considered to evaluate the effect of DO, temperature, conductivity and pH on the voltage response of the CSMFC. With the OFAT approach, the value of one single factor (pH, temperature, conductivity) was set at the time, according to Table S7.1, while the remaining factors were kept at the centre levels. The resulting effect on the CSMFC response to varying DO levels was investigated. The relationship between the maximum voltage, V_{max}, and DO saturation values was obtained from the OFAT experiments by fitting the saturation curve with Equation 7.1:

$$V = V_{max}\left(\frac{DO}{K_s + DO}\right) \quad (7.1)$$

Where V (mV) is the voltage output, V_{max} (mV) is the maximum voltage at the saturation point, DO (mg L^{-1}) is the concentration of dissolved oxygen, and K_s (mg L^{-1}) is the half saturation constant.

The experiments for the DoE model were instead performed by simultaneously manipulating all the factors, following the run order sequence given in Table S7.2.

The range of values investigated are reported in Table 7.1, and were selected based on typical values in freshwater basins [13]. Conductivity was assessed across a broad range to investigate the use of this sensor in seawater.

***Table 7.1**. Range of study of the factors.*

Factor	Low value (-1)	High value (+1)
Temperature / ˚C	10	30
Conductivity / mS cm^{-1}	300	3000
Dissolved oxygen / mg L^{-1}	1	10
pH	5	9

For both the OFAT and DoE experiments, the coded values were obtained by using the following equations:

$$Coded\ value = \frac{Real\ value - Center\ value}{\frac{1}{2}\ range} \tag{7.2}$$

$$Center\ value = \frac{Low\ value + High\ value}{2} \tag{7.3}$$

$$Range = High\ value - Low\ value \tag{7.4}$$

To perform these tests, the CSMFC was immersed in a 1 L beaker filled with 700 mL of water under agitation, so that the cathode was fully submerged (Figure 7.1D). The beaker was covered with parafilm to prevent changes in the catholyte DO. Measurements were taken once the signal was stable (±10 mV) for at least 20 min after each change in the DO. In between experiments, the cells were left to stabilise in the configuration shown in Figure 7.1C.

The catholyte pH was measured with a pH-meter (Thermo Scientific Orion ROSS Ultra pH/ATC Triode, USA) and adjusted by adding appropriate amounts of 0.1 M HCl and NaOH 0.1 M. The catholyte conductivity was measured with a conductivity benchtop cell (Orion, Thermo Scientific) and adjusted by adding appropriate amounts of 1 M NaCl. The dissolved oxygen of the catholyte was measured with a DO portable meter (RDO Orion 7003, Singapore) and varied by purging nitrogen and/or oxygen. The operating temperature was controlled with a Thermoelectric Reptile Incubator (ExoTerra, UK). pH, conductivity and DO were measured before and after the experiment to account for variations.

7.2.5 Calibration of the CSMFC sensors

The output voltage from the CSMFC was correlated with the DO and T, the factors that mainly influenced the signal, by using the least squares equation arising from the refined 2-factorial design:

$$V = int + a\ DO + b\ T + a\ b\ DO\ T \quad (7.5)$$

Where the voltage V (mV) is the response variable and DO and T are the explanatory variables, in coded values. The standard order Table S7.3 shows the experimental runs to train the model and estimate the least squares coefficients a, b, ab and the intercept term, int, in Equation 7.5.

The response was obtained by fitting four different data sets: the OFAT dataset, the 4-factorial dataset and the respective baseline normalised responses. As a result, four linear least squares models were obtained respectively: OFAT, OFAT_n, DOE and DOE_n. The values for the OFAT experiments were obtained by interpolating the OFAT saturation curves at T=30 ˚C and T=10 ˚C for DO=1 mg L^{-1} and DO=10 mg L^{-1} (Table S7.4) whereas all the experiments of the 4-factorial (Table S7.2) were used in the DOE 2-factorial model. The normalised datasets were referred to the baseline conditions (pH=7; DO=5.5 mg L^{-1}; Conductivity=1.65 mS cm^{-1} and T= 20 ˚C), also denoted as zero level.

Rearranging Equation 7.5 to express DO as a function of V and T (Eq. 7.6), leads to the calibration expression of the CSMFC.

$$DO = \frac{V - int + bT}{(a + abT)} \quad (7.6)$$

Where the coded DO can be transduced into real DO using Equation 7.2. The coefficients a, b ab, obtained with the four different datasets lead to the four calibration models assessed in this study.

7.2.6 Testing and validation of the calibration models

The calibration models were evaluated based on the ANOVA analysis in terms of the adjusted R^2 (R^2_{adj}), which measures the variability of the data explained by the model; the F-value, which indicates how significant the model is; the predicted R^2

(R^2_{pred}) that estimates the predictive power of the model; and the significance of the coefficients, which are indicated by the p-value [14, 15].

The best performing calibration models were further tested under varying conditions of DO, from 0 to 9 mg L^{-1} and uncontrolled temperature on unused SCMFCs enriched as described above.

The models were subsequently validated in real water collected from a pond near the University of Bath campus (51°22'41.6"N 2°19'42.2"W). The water was characterised by a conductivity of 138 ± 11 µS cm^{-1} and a pH of 7.63 ± 0.02. The performance of the model to predict new data was assessed in terms of the root-mean-squared error (RMSE) [14]:

$$RMSE = \sqrt{\frac{(DO_p - DO_m)^2}{n}} \quad (7.7)$$

Where DO_p (mg L^{-1}) is the DO predicted with the calibration model, DO_m (mg L^{-1}) is the DO value obtained with the commercial DO probe, and n is the number of samples. The experiments were performed in triplicate unless stated otherwise and by two different experimenters to ensure independence of the data.

The statistical analyses, saturation curves fittings, Pareto Plots and surface response curves were performed by using the R software, adapting an existing code [14]. The validation of the model assumptions is included in the R code, which can be found in the Supplementary Data.

7.3 Results and discussion

The CSMFCs reached a stable signal after one month of enrichment, with no addition of nutrients or water to the anode chamber. The polarisation tests (Figure 7.2A), performed at this point, confirm that the output voltage is dominated by the cathode in the whole range of current investigated. The larger area of the anode with respect to the cathode, leads to a system that is limited by oxygen reduction at the cathode [16]. To avoid fast oxygen consumption, that would increase the thickness of the diffusion layer at the cathode and lead to inaccurate readings of the DO [2], the external resistance was fixed to 2 kΩ (Figure 7.2A) after enrichment.

Under this external resistance the CSMFC operates close to the maximum power point (Figure 7.2B), which has been proved to extend the lifetime of the CSMFC and stability of the anode potential [17].

The stability of the signal of a soil-based MFC greatly depends on the degree of hydration of the soil in which the anode is buried, since water enhances the transport of nutrients and ions in the soil [18]. In the CSMFC, the soil is kept moist thanks to the passive diffusion of water through the terracotta, which increases the stability of the signal, simplifies system maintenance and allows for unattended operation in the field. The maximum power output generated by the CSMFC, 20 mW m^{-2}, is comparable to the power obtained in an analogous system fed with acetate in growth medium [18, 19].

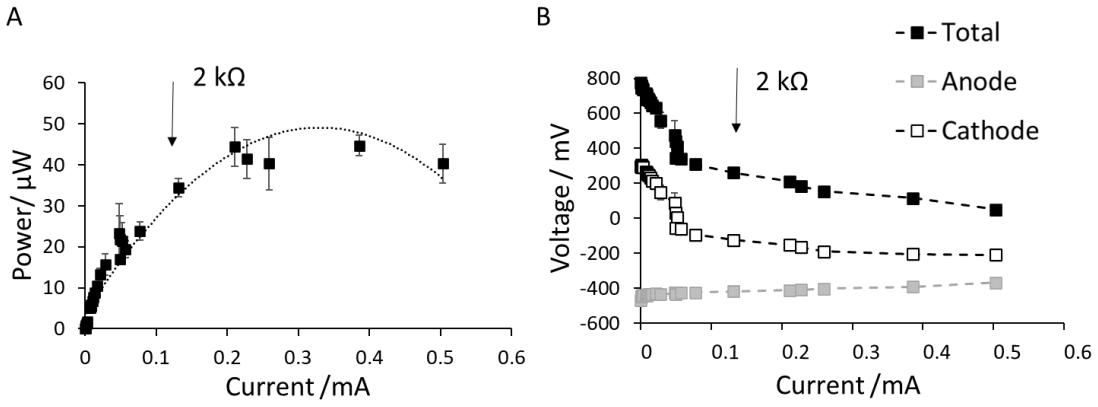

***Figure 7.2**. (A) Power curve after one month of enrichment. (B) Polarisation curves of anode (grey squares), cathode (white squares) and total cell (black squares) of the CSMFC exposed to air after one month of enrichment (T=20 ˚C). The arrows indicate the power conditions under operation at 2 kΩ. Error bars are the standard deviation of three replicates.*

7.3.1 Testing the CSMFCs as a DO sensor

The correlation between the electrochemical performance (current and voltage output) of the SCMFC and dissolved oxygen in the catholyte was investigated. As expected, the SCMFC showed better electrochemical performance at a high (10 mg L^{-1}) rather than low (1 mg L^{-1}) concentration of DO. This result further confirms that the current produced in the CSMFC is cathode limited (Figure S7.1).

The dose-response curve in Figure 7.3 shows how the output voltage generated by the CSMFC increases with DO up to a saturating concentration of approximately 5 mg L^{-1}. This saturation limit is lower than that observed for other MFC based DO sensors, with a reported saturating DO limit of 8 mg L^{-1} [7, 10, 17]. Nonetheless, to enhance both the affordability of the system and its stability over time, no expensive oxygen reduction reaction catalysts or membrane is used in this work [20]. Considering that the critical level of dissolved oxygen in water for aquatic life is 2 mg L^{-1} [21], the CSMFC can be used as an early warning tool to detect hypoxic events.

The CSMFC showed a response time of approximately 3.3 min to changes in the DO of the catholyte. The response time of the CSMFC sensor is in agreement with other MFC-based DO sensors [10]. This response is, however, ten times slower than that achieved by commercially available electrochemical DO sensors [3]. Still, contrary to most commercial DO sensors, the CSMFC can operate in field for continuous monitoring. As shown in Figure 7.3, the sensor response to a step-increase and a step-decrease in DO concentrations is consistent. This result demonstrates the reliability of the CSMFC sensor and its ability to detect different scenarios (i.e. corresponding to either depletion or increase of DO in water).

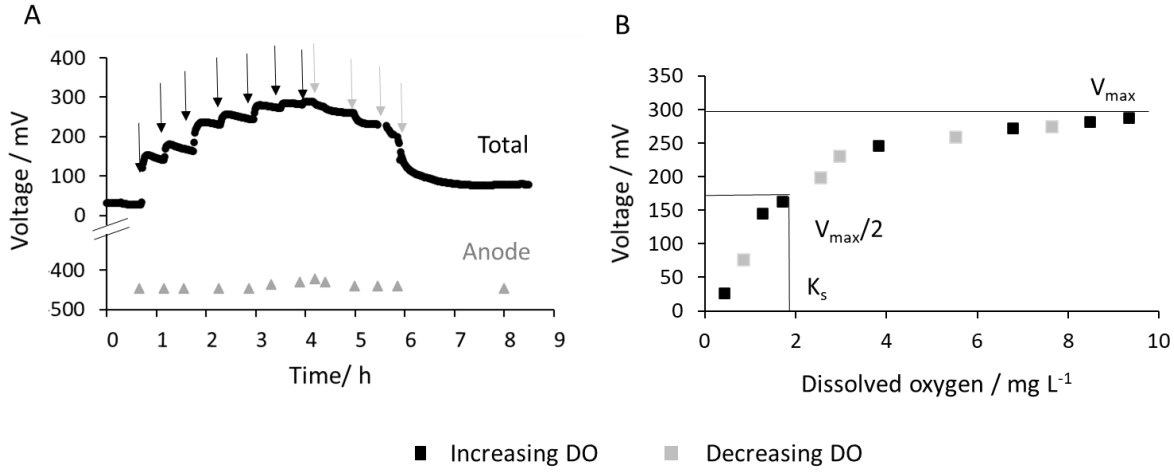

***Figure 7.3**. (A) Response of the CSMFC sensor to increasing (black arrows) and decreasing (grey arrows) concentration of dissolved oxygen (T=20 ℃; pH=; conductivity=1.65 mS cm^{-1}) and anodic electrode potential (grey triangles). (B) Calibration curve of the sensor, showing response, in terms of voltage output, to increasing (black squares) and decreasing (grey squares) concentrations of DO. Each point in (B) correspond to the steady-state value of the output voltage after each step change in the*

catholyte DO in (A). K_s is the half saturation constant (mg L^{-1}) and V_{max} is the maximum voltage at the saturation point, in mV. Data corresponds to one representative replicate, Results from another replicate are shown in Figure S7.2.

7.3.2 Investigating the effect of environmental factors on the CSMFC sensor response. OFAT approach

The response of the CSMFC sensor to pH, conductivity and temperature was evaluated to assess the performance in real scenarios. These factors were selected since they are the most representative for water quality [13] and relevant to the electrochemical performance of the CSMFC [10].

The results obtained with the OFAT method (Figure 7.4 and S7.3), show that both the maximum voltage, V_{max} and the saturating value of dissolved oxygen, DO_{sat}, increase with temperature. This result is expected considering that higher temperatures would favour both bacterial metabolism and kinetics [22].

The effect of pH is insignificant with respect to the variability of the data. In theory, both V_{max} and DO_{sat} should be larger at low pH than at high pH, because the oxygen reduction reaction (ORR) proceeds at more favourable potentials in acid media, with the formation of water, as opposed to the production of hydroxyl ions in basic media. For uncatalyzed carbon however, the 2-electron reduction is the predominant pathway due to activation overpotentials [23], and the effect of pH is less evident. The uncertainty in the data could be due to a delay in the response of the system to changes in the pH due to the buffering capacity of the soil.

With regards to salinity, the sensor performs at its best at the mid-range point. At lower salinity, the conductivity decreases, thus increasing ohmic losses, whereas at higher salinity, the anodic bacteria could suffer from osmotic imbalance [24].

Under baseline conditions of temperature (20 ˚C), pH (7) and conductivity (1.65 mS cm^{-1}), the CSMFC shows a saturating voltage of 321 ± 29 mV at a DO of 4.5 ± 1.2 mg L^{-1}, with a sensitivity in the linear range of 53.3 ± 22.6 mV L mg^{-1}. The dependence of both DO and V_{max} on pH, conductivity and temperature demonstrates the need to include all these factors in the calibration of the CSMFC sensor.

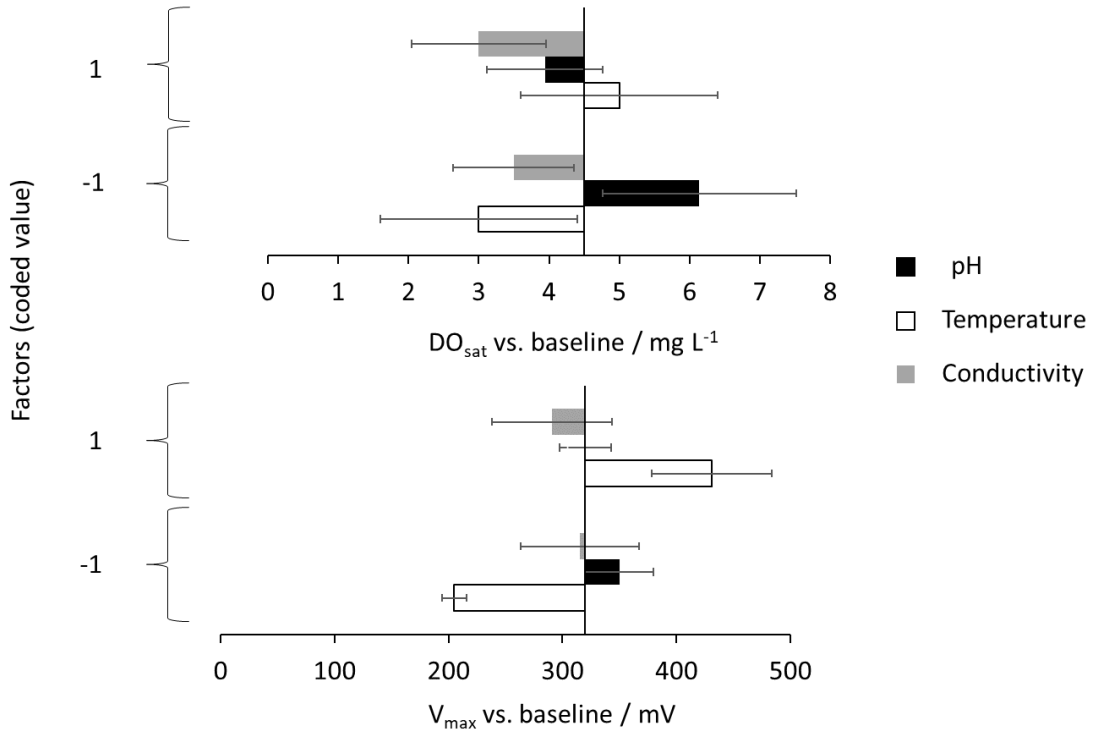

***Figure 7.4**. Effect of T (white), pH (black) and conductivity (grey) on V_{max} and saturating DO of the CSMFC sensor within the range of values of Table 7.1, with respect to the baseline (middle black line). Error bars correspond to the standard deviation of three replicates. Figure S7.3 and Table S7.1 show the fitting on the complete OFAT data set for T, conductivity and pH.*

7.3.3 Investigating the effect of environmental factors on the CSMFC sensor response. Design of experiments

While the OFAT approach is useful to determine the linear range of application of the sensor, it provides limited information on the interactions among the several factors, which is expected to be significant in the CSMFC. To address this issue, a three-level factorial design was performed.

Figure 7.5 shows the result of a 4-factorial design on temperature, conductivity, DO and pH, considering the voltage output as the sensor response. Table S7.2 in the Supplementary Information shows the run order and standard order of the experiments. The significance of each model coefficient is assessed both by comparing the relative importance of the factor effects, using a Pareto Plot, and by analysing the variance of the three replicates [14].

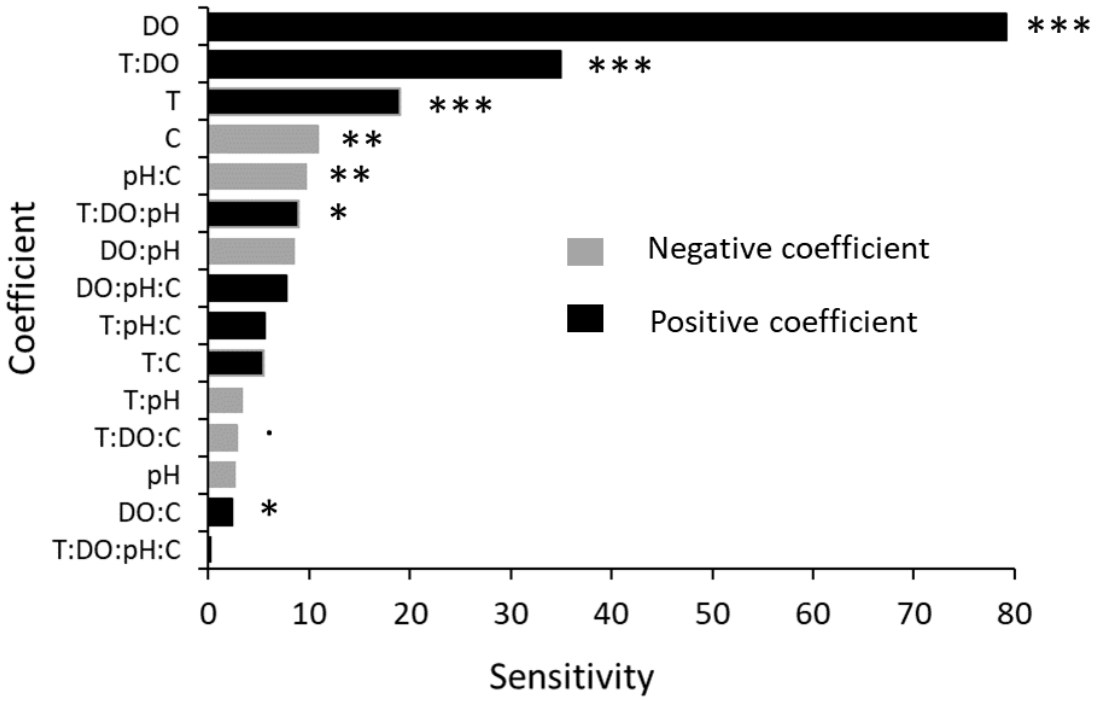

Figure 7.5*. Pareto plot showing the effects of T, pH, conductivity and DO and their interactions on the voltage output generated by the CSMFCs. Values shown are absolute value of the estimates, centred and scaled to remove the intercept. The factorial design was performed in triplicate. t-test significance levels: (***) p < 0.001, (**) p < 0.01, (*) p < 0.05, (.) p < 0.1. Grey bars represent a negative influence and black bars represent a positive influence.*

The model fits the variability of the data well, with a strong positive R^2_{adj} of 0.92. The model is also meaningful, as expressed by the high F-value of 37.5 ($p < 0.001$) [15]. The predictive power of the model is also high, as expressed by the R^2_{pred} in Table 7.2. Figure S7.4 shows that predicted and real data follow a linear correlation close to the unity. Figure S7.4 also shows that the model assumptions (linearity of the data, normal distribution of variance and constant variance) are largely met, however, the residuals are large and scattered with some outliers. This result is probably due to a non-linearity in the correlation between voltage and DO at high concentrations, the experimental error and the possible effect of a factor excluded of the study.

Contrary to what was expected, the conductivity has a negative effect on the output voltage. This outcome may be caused by the detrimental effects of high salinity on

the anodic microorganisms [24]. The estimates in the Pareto plot are calculated as half the effect on the response when the factor increases from minus to plus level, meaning that optimal values between the plus and minus level are not taken into account [14]. On the contrary, the OFAT analysis shows a maximum response at the baseline value (zero level) of conductivity with respect to the low and high levels (Figure 7.4), implying that mid values of conductivity are optimal to maximise the voltage output of the CSMFC. If the conductivity were a main effect, adding quadratic terms to the least squares model would account for this non-linearity of the response.

Based on the relative importance of the several factors investigated, and the significance of their magnitude with respect to the standard deviation, it can be concluded that the effect of both pH and conductivity are insignificant within the ranges tested. The calibration of the CSMFC sensor can, therefore, be simplified as a function of temperature, DO and their reciprocal interaction.

7.3.4 Calibration of the CSMFC using a 2-factor model

Figure 7.6 shows the surface response of the 2-factorial designs on temperature and DO, trained with the OFAT (OFAT model) and the 4-factorial (DOE model) datasets (Table S7.4 and S7.2 respectively). Both models explain the variability of the linear response with T and DO (R^2_{adj}, Table 7.2). Nonetheless, the correlation of the DOE model is less strong than in the complete 4-factorial, possibly due to the effect of removing conductivity and pH as explanatory variables. Yet, the predictive power still high, with an R^2_{pred} of 0.87. The OFAT model shows that temperature is the most influential factor, whereas the DOE model shows a larger impact of DO on the response. According to the F-value, however, which indicates if the data is described by the linear model and the significance of the estimated coefficients, the OFAT model is not significant (Table 7.2). The data for the OFAT model are estimated from the fitted saturation curves and not with direct measurement. In addition, randomisation was not fully achieved on the OFAT experiments, as the saturation curves were obtained at increasing concentrations of DO, which may have introduced the effect of an unknown and uncontrolled variable. The contour plot for the DOE model in Figure 7.6 shows that at low DO the temperature has no impact on the voltage, as the ORR is not taking place due

to a lack of reactant. At high DO concentrations, voltage increases with temperature and the interactions become more important, as shown by the curvature of the contour lines. This is due to the combined positive effect of increasing T and DO on the reaction kinetics.

It is also not surprising that the standard deviation of the coefficients is lower on the DOE model than on the OFAT model (32.6 mV vs. 61.0 mV), considering that this deviation is estimated by using 47 and one degree of freedom respectively. All the experiments carried out in the 4-factorial design were used in the 2-factorial, whereas the values used in the OFAT approach were estimated using the Monod equations (Figure S7.3). The standard error contains the inaccuracy on the measurement of T, DO and V, which the model assumes fixed and known. The results obtained show the self-replication of the DOE methodology and demonstrate its superior efficiency to the OFAT approach, particularly when not all the factors under study are significant.

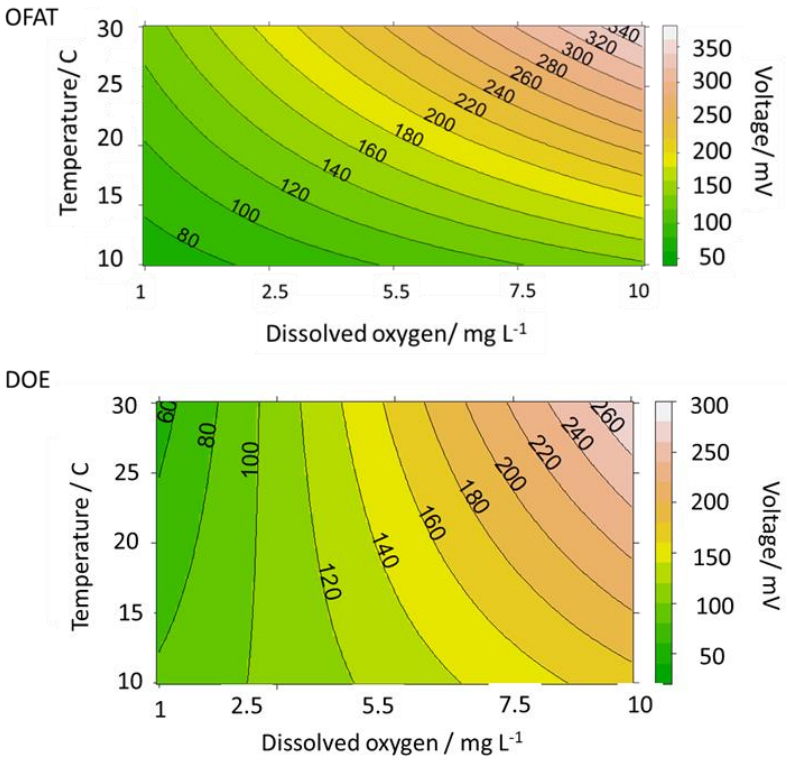

***Figure 7.6**. Surface response of the 2-factorial analysis on T and DO based on the OFAT model-and DOE model.*

Typically, MFC systems show consistent trends among replicates, but the baseline may differ in value in each case [25]. Normalising the data by the sensor baseline, would remove this issue in the calibration model. The coefficients for the calibration model obtained after normalisation are reported in Table 7.2 (DOE_n and OFAT_n models). The intercept of the coefficient should be close to the unit, as it represents the response output at the baseline. This is the case for the DOE model, but not for the OFAT model. The baselines used to normalise the OFAT model were indirectly obtained through the fitting of the experimental data, which could be the reason why the performance of the OFAT models is so poor. In addition, by normalising the data a degree of freedom is used. The OFAT_n model, therefore, does not have any degree of freedom left to calculate the variance. On the other hand, the variance in the DOE_n model is estimated with 44 degrees of freedom. Consequently, the OFAT models were discarded for further analysis (Table 7.2).

Table 7.2*. Multiple linear regression coefficients obtained by least squares where n is the degrees of freedom and the t-test p values are (***) < 0.001; (*) < 0.05, (.) < 0.1 ( ) > 0.1.*

Model	**OFAT (n=1)**				**DOE (n=47)**			
Effect	**Effect (p-value)**	**R^2_{adj}**	**F-value (p-value)**	**R^2_{pred}**	**Effect (p-value)**	**R^2_{adj}**	**F-value (p-value)**	**R^2_{pred}**
Intercept	173 (.)	0.7	4.3 (0.33)	-4.77	146 (***)	0.87	118 (0.00)	0.90
DO	71.1 ( )				79.2(***)			
T	74.3( )				19(***)			
DO:T	39.8( )				35(***)			
Model	**OFAT_n (n=0)**				**DOE_n (n=44)**			
Effect	0.70 ( )	NA	NA	NA	0.90 (***)	0.75	49.8 (0.00)	0.88
Intercept	0.31 ( )				0.47 (***)			
DO	0.33 ( )				0.12 (*)			
T	0.17 ( )				0.20 (***)			
DO:T	0.70 ( )				0.90 (***)			

The resulting equations for the calibration derived from the least squares models [14] using the coefficients of Table 7.2 are:

$$DO_{DOE} = \frac{y-146-19*T}{79.2+35*T} \quad (7.8)$$

$$DO_{DOE\_n} = \frac{y\_n-0.9-0.12*T}{0.46+0.20*T} \quad (7.9)$$

Where y is voltage output (mV), y_n is the normalised by the intercept voltage output and is adimensional, T is temperature in coded value temperature and DO is dissolved oxygen in coded value. T and DO must be transformed into real values using Equations 7.2 - 7.4.

Since negative values of DO lack physical meaning, a constraint was imposed to the model to limit the lower limit of DO to zero.

7.3.5 Testing and validating the calibration models

The DOE and DOE_n models were tested on freshly enriched CSMFCs under the experimental set up shown in Figure 7.1B. A drift in the sensors steady state voltage of 30 ± 19% (n=3) over three months was observed, which, considering the stability over time of the anode potential and the dependence on the cell voltage on the cathode potential (Figure S7.6), is attributed to changes in cathodic performance over time [26, 27]. Since the saturating value of DO at 20 ˚C is 5 mg L^{-1}, which is close to the baseline value, continuous determination of the baseline can be easily done by measuring the signal output in tap water.

The coefficients on Equation 7.9 were therefore recalculated by using the new baseline (Table 7.3). The performance of the models is assessed by the RMSE (Equation 7.7), which measures the discrepancy between the real and predicted value of DO [14]. Table 7.3 shows that when the baseline is close to the one used for calibration (170 mV in CSMFC II vs. 146 mV in DOE model), both the DOE and DOE_n models show a similar performance. When the baseline differs from that used for calibration, as is the case of CSMFC I and CSMFCIII, the DOE_n is the best performing model, as demonstrated by the lower RMSE. An accurate determination of the baseline is therefore a must to successfully apply the DOE_n model. Table 7.3 also shows that the error of the model is lower at DO < 6 mg L^{-1} (CSMFC I and III), because of the non-linearity of the model at higher DO.

The performance of the DOE_n model is independent of the CSMFC used, thus extending the use of this calibration equation to any CSMFC device.

***Table 7.3**. Summary of the calibration models performance for CSMFC.*

Device	Range of measured DO / mg L^{-1}	N	Baseline / mV	RMSE / mg L^{-1}	
				DOE	DOE_n
CSMFC I	0.2-4.6	9	270	5.4	0.7
CSMFC II	3.9-9.6	21	170	1.5	1.0
CSMFC III	0-6.44	12	260	4.3	0.6

The DOE_n model was further validated in real water. The value of the conductivity of the collected water was below the lower limit chosen in the calibration study, which could challenge the use of the model outside the calibration conditions. Equation 7.9 was modified with the actual voltage output baseline (247 mV) generated by CSMFC III, to determine the predicted DO value of the water sample, as shown in Figure 7.7. The baseline difference of 13 mV with the previous reading is within the standard deviation.

Figure 7.7 shows the DO prediction of the CSMFC III sensor under uncontrolled DO and T over a 30 min period. The goodness of fit of the model, assessed by the RMSE, is as low as, 0.05 mg L^{-1}. This deviation is comparable to the nominal accuracy of 0.1 mg L^{-1} of commercial electrochemical DO sensors [3]. It is also better than the 0.5 mg L^{-1} reported for a reported submersible MFC-based DO sensor in lake water [10]. The low RMSE is due to a DO value close to the narrower area of the model confident interval [14]. Nonetheless, further work should be performed to assess the model accuracy under several values of temperature, pH and conductivity. The sensor validation in the field should also be better investigated.

While effective for hypoxic events, this linear model poorly predicts DO values higher than 6 mg L^{-1}. To address this limitation, and account for the non-linear behaviour after the saturation value of DO, quadratic terms could be introduced into Equations 7.8 and 7.9. This strategy would, however, complicate the transformation of Equation 7.5 in Equation 7.6. An extended analysis to improve the accuracy of the model at high DO values would, however, be important to

monitor also high DO events, such as environmental algal growth. Alternatively, redefining the upper level of DO factor as the saturating DO value would constraint the study to the linear region of dependency of the sensor voltage output with DO. The practicality of the selected range of DO in this study relies on the simplicity of calculating the baseline. As the CSMFC saturates at ca. 5 mg L^{-1}, any water with DO > 5 mg L^{-1} saturates the signal and provides the value of the baseline. A practical and easy determination of the baseline is particularly useful in low-income regions with limited equipment for accurate measurements of DO and T.

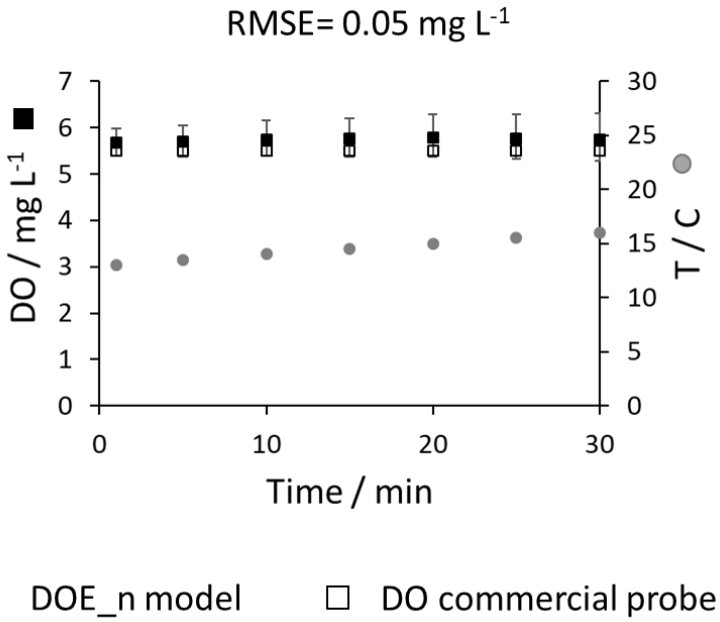

Figure 7.7. *Validation of the model in real water samples with CSMFC III. Black squares refer to the predicted DO obtained with the model. White squares refer to the DO of the water measured with a DO probe. Error bars represent the 95% confident interval.*

Based on these results, the calibration model DOE_n obtained with a 2-factorial design of experiments on temperature and DO can be used to successfully predict the DO value of an unknown water sample. Remarkably, the model can be corrected with the sensor voltage baseline, thus becoming independent of the CSMFC device used. To our knowledge, this is the first time that the calibration model of a MFC sensor is successfully demonstrated by using a design of experiments.

7.4 Conclusions

In this work, we report an innovative and low-cost ceramic soil microbial fuel cell and successfully demonstrate its use as sensor for dissolved oxygen in water. A large ratio of anode/cathode electrode area ensures that the sensor signal correlates well with the dissolved oxygen in the catholyte. Water saturation of the soil, maintained thanks to the permeability of terracotta to water, allows for high stability of the anode performance under unattended operation, which is a key advantage for field applications. OFAT tests identify the linear range of detection of the CSMFC system under varying conditions of pH, temperature and conductivity. While the OFAT approach is largely reported in the literature it presents several limitations. Design of experiments is instead an efficient tool to understand the influence that multiple factors can have on the CSMFC response and to properly calibrate the sensor. Based on the results of a 4-factorial DoE, both pH and conductivity had a negligible effect on the sensor response compared to DO and T and their interaction, within the tested ranges. The calibration model can be easily adapted to other CSMFC devices by simply normalising the model coefficients to the voltage baseline. This important feature reduces the need for recalibration of the sensor over time, enhancing its autonomy and hence its use for in-field applications. In conclusion, this work not only demonstrates the development of a low-cost DO sensor, suitable for in field monitoring with minimal to no maintenance requirements, but it also pioneers the use of design of experiments as a necessary tool for the effective calibration of microbial fuel cell-based sensors.

7.5 Acknowledgements

This work was supported by the UK Engineering and Physical Sciences Research Council (EP/L016214/1) and the Society of Spanish Researchers in the United Kingdom (SRUK). The authors thank Laura Forfar (Paul Murray Catalysis Consulting) for the support on the experimental design and Andrew Chapman (University of Bath) for the support in statistical analysis.

7.6 Supplementary information

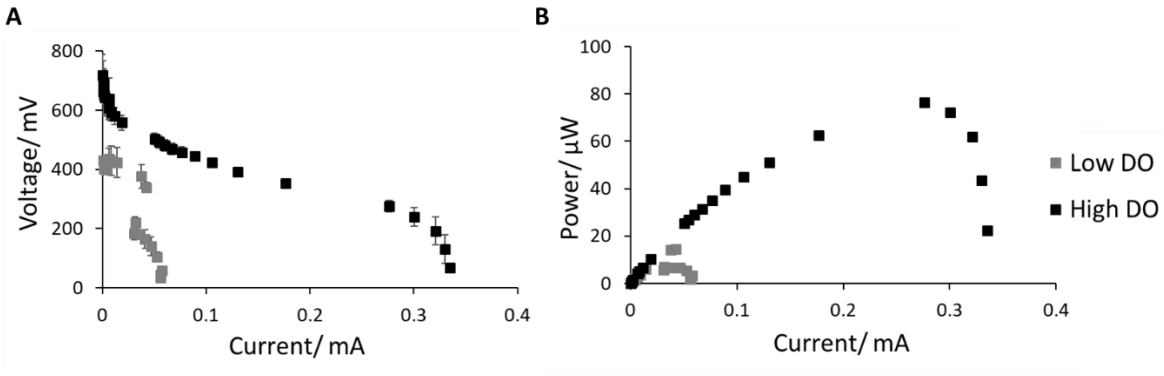

Figure S7.1. *Polarisation curves (A) and power curves (B) of the CSMFC under low (1 mg L^{-1}, grey squares) and high (10 mg L^{-1}, black squares) concentration of DO in the catholyte. Error bars represent the standard deviation of three replicates.*

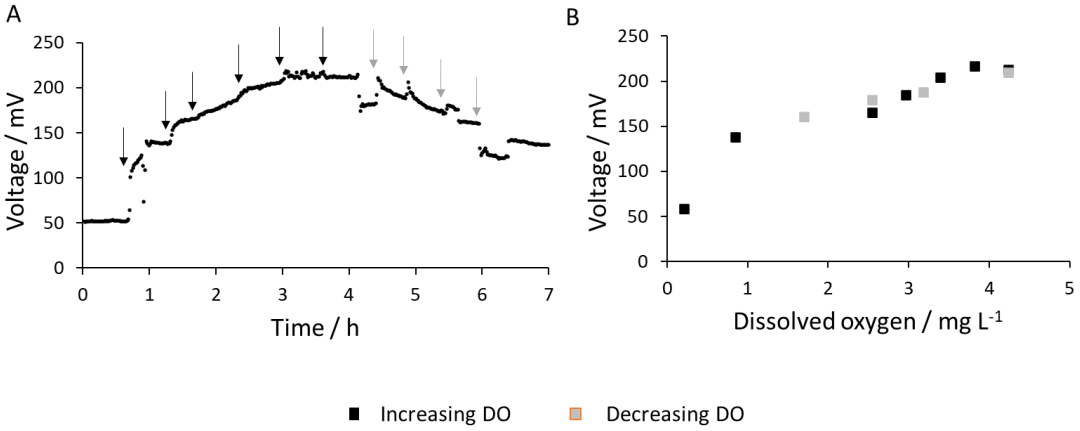

Figure S7.2. *(A) Response of the CSMFC sensor to increasing (black arrows) and decreasing (grey arrows) concentration of dissolved oxygen (T=20 ℃; pH=; conductivity=1.65 mS cm^{-1} in the catholyte) with time. (B) Correlation of voltage output and dissolved oxygen for the 7 h period shown in (A). Each point corresponds to the average steady state value of the output voltage after each step change in the D, with black squares for increasing DO and grey squares for decreasing DO. Data corresponds to one representative replicate. Results from another replicate are shown in Figure 7.3.*

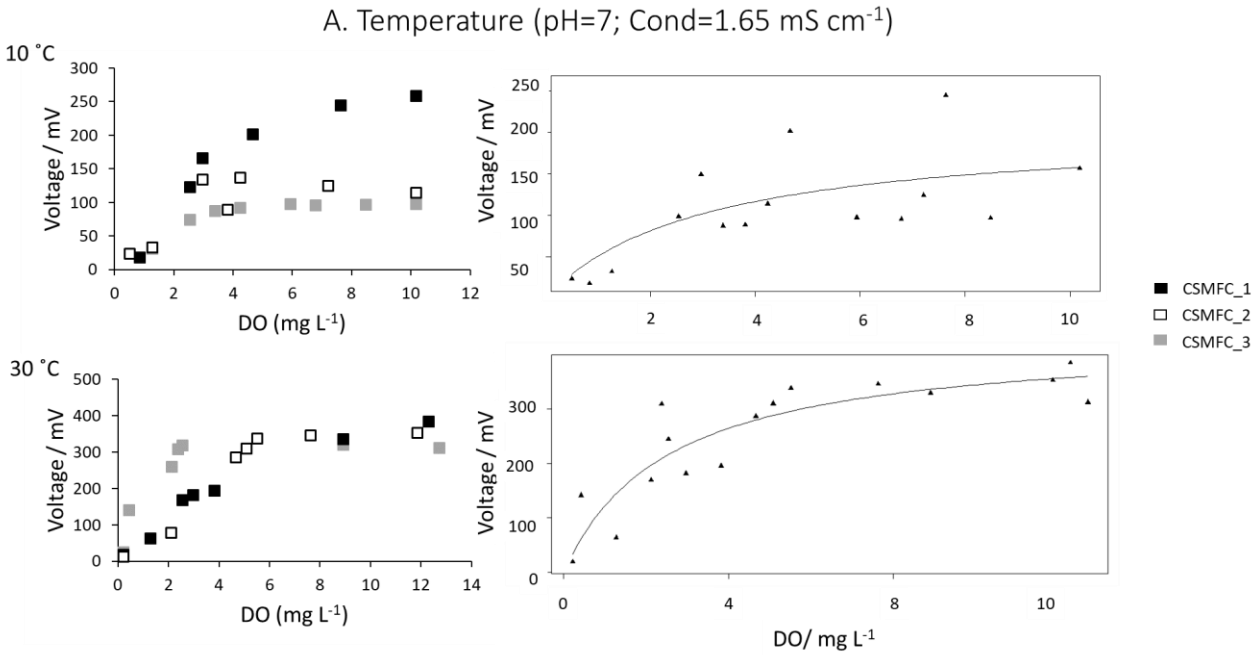
A. Temperature (pH=7; Cond=1.65 mS cm-1)
10 ˚C
30 ˚C
Voltage / mV
DO (mg L-1)
DO/ mg L-1
CSMFC_1
CSMFC_2
CSMFC_3

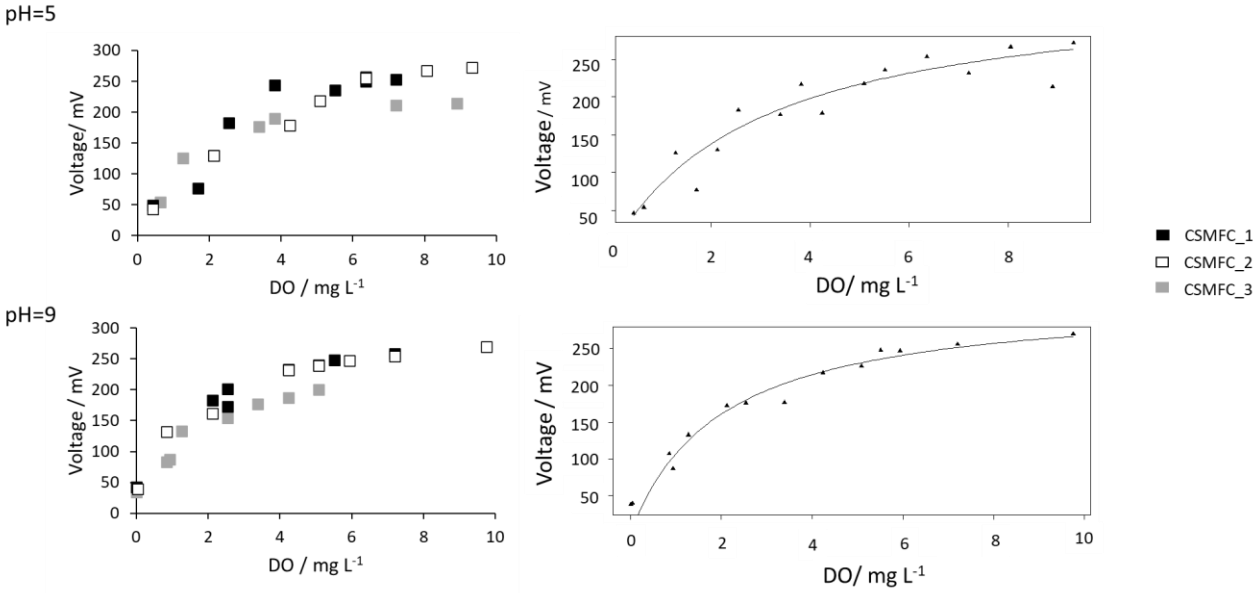
B: pH (T=20 ˚C; Cond=1.65 mS cm-1)
pH=5
pH=9
Voltage/ mV
Voltage / mV
DO / mg L-1
DO/ mg L-1
CSMFC_1
CSMFC_2
CSMFC_3

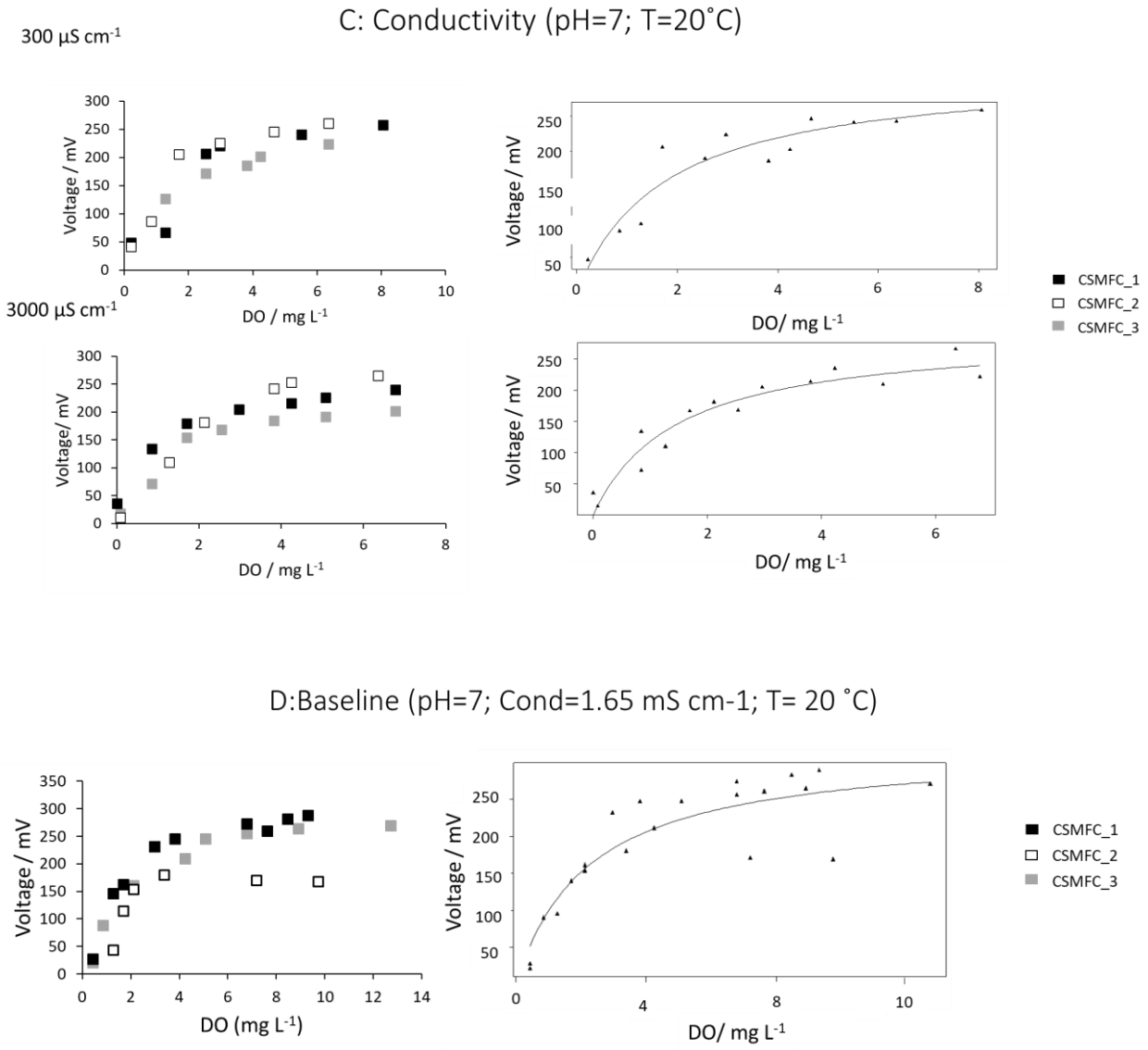

Figure S7.3*. Assessing the impact of temperature (A), pH (B) conductivity (C) and determination of the baseline (D) on the response of three CSMFC sensors (black, grey and white squares) to DO following the OFAT method. Experimental curves (left) and fitted saturation curve (right). The saturation curves were obtained fitting the Monod model on the three replicates.*

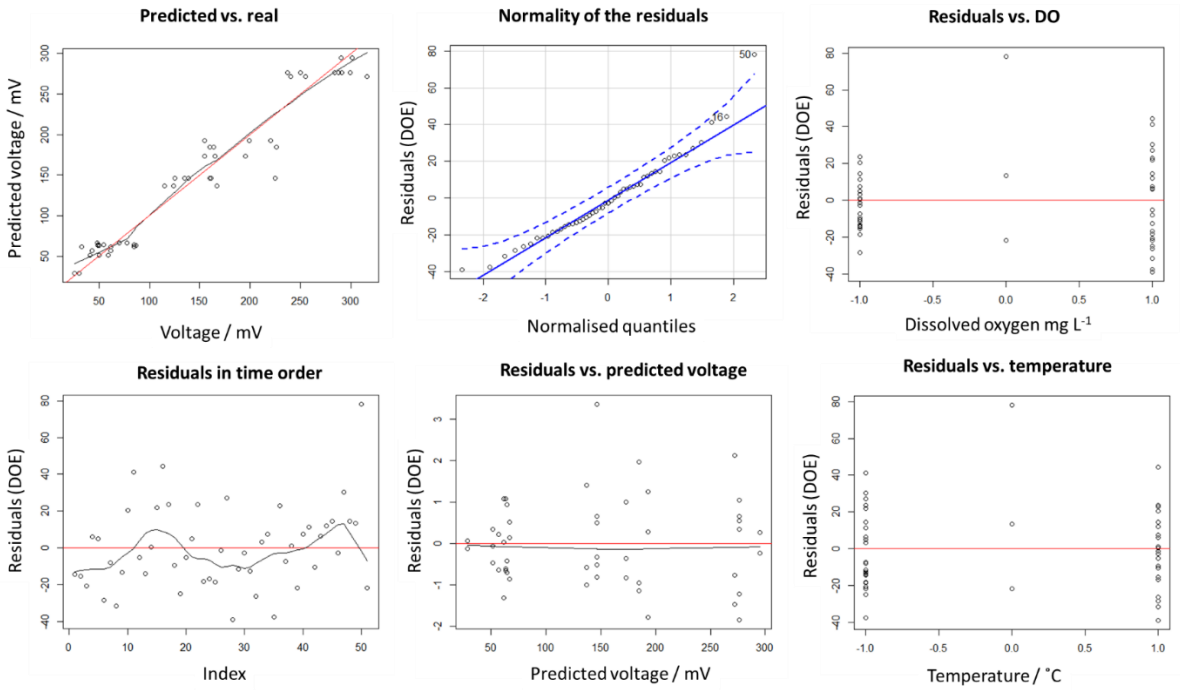

***Figure S7.4**. Power of prediction of the training data (predicted vs. real) and diagnosis of the assumptions of the model.*

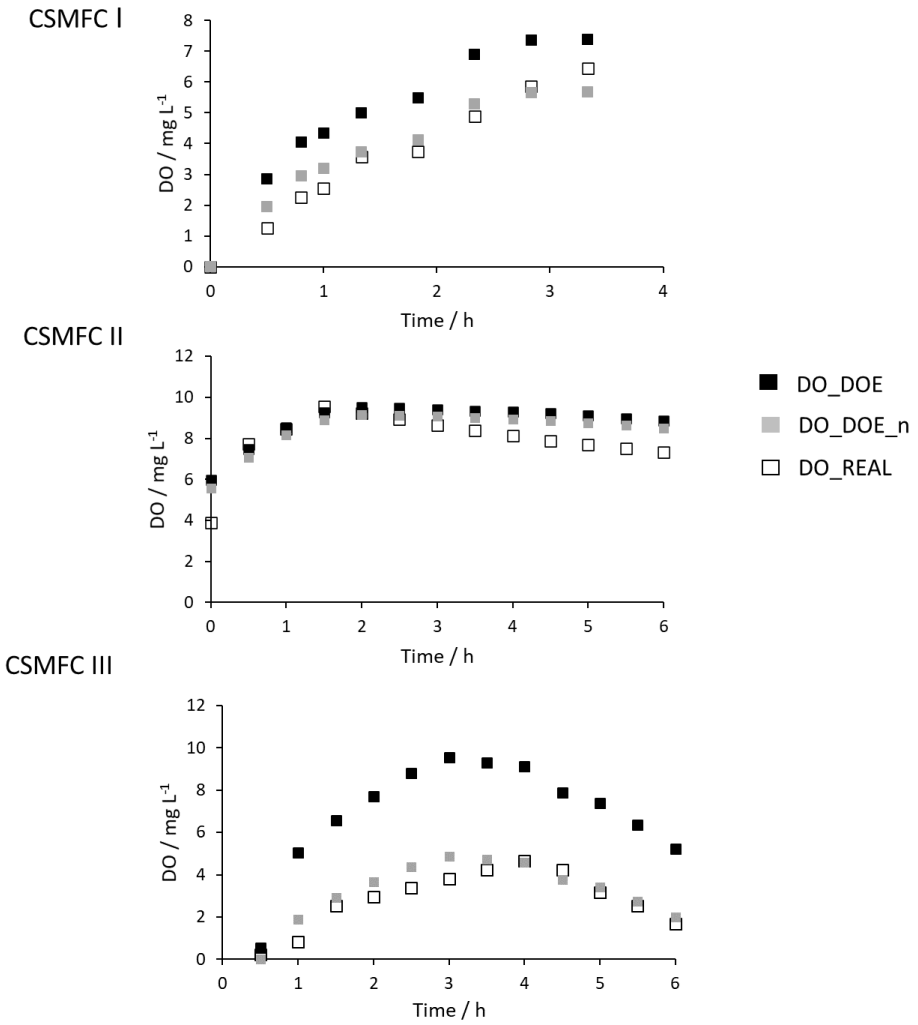

***Figure S7.5**. Comparison of the prediction of DO using the DOE and DOE_n calibration models. CSMFC I, CSMFC II and CSMFC III are replicates enriched in the same conditions where DO was varied arbitrarily. Figures are complementary to Table 7.3.*

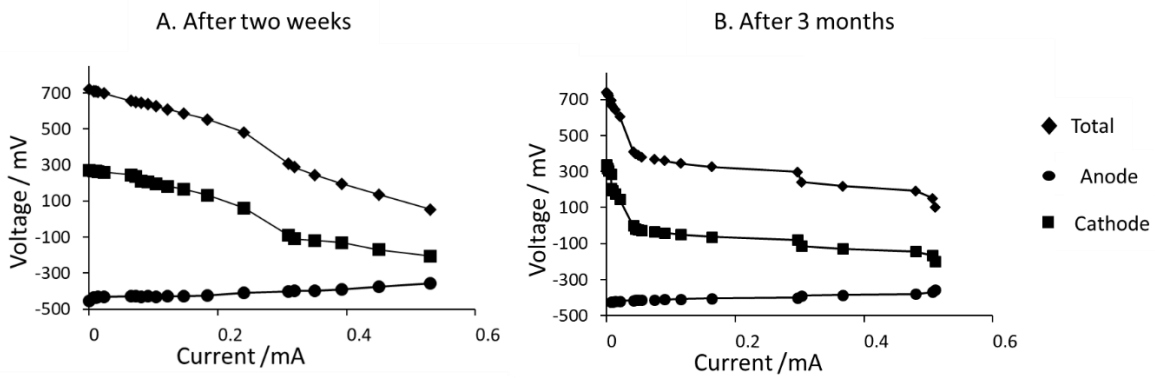

***Figure S7.6**. Comparison of polarisation curves of the CSMFC used for calibration after two weeks (A) and three months of operation (B).*

***Table S7.1**. V_{max} and saturated DO obtained with the fitting curves shown in Figure S5.3. T-test p values (***) < 0.001; (**) <0.01, (*) < 0.1, ( ) > 0.1.*

Factor	Value	Factor coded	Vmax mV	p-value	DO sat mg L^{-}	p-value
T / ˚C	10	-1	205 ± 52	***	6.0 ± 4.0	
	30	1	431 ± 53	***	5.0 ± 1.8	*
pH	5	-1	351 ± 23	***	6.1 ± 1.4	***
	9	1	321 ± 21	***	3.9 ± 0.8	***
Conductivity / µS cm^{-1}	300	-1	315 ± 30	***	3.5 ± 1.0	**
	3000	1	291 ± 24	***	3.0 ±0.9	**
Baseline						
Conductivity / µS cm^{-1}	1650	0	321 ± 29	***	4.5 ± 1.2	**
pH	7	0				
T / ˚C	20	0				

***Table S7.2**. Run and standard order table for the 4 and 2-factorial design.*

Run order	Standing order	A=T	B=DO	C=pH	D=ABC=Cond	y_1	y_2	y_3
		˚C	mg L^{-1}	pH	mS cm^{-1}	mV	mV	mV
8	1	-	-	-	-	49	50	87
6	2	+	-	-	+	48	85	55
4	3	-	+	-	+	164	226	160
5	4	+	+	-	-	301	290	290
7	5	-	-	+	+	62	43	62
2	6	+	-	+	-	33	62	64
3	7	-	+	+	-	165	195	155
1	8	+	+	+	+	240	316	368
12	9	-	-	-	+	48	70	78
10	10	+	-	-	-	50	59	70
16	11	-	+	-	-	220	155	199
15	12	+	+	-	+	237	299	288
11	13	-	-	+	-	135	139	139
9	14	+	-	+	+	26	30	26
13	15	-	+	+	+	124	115	167
14	16	+	+	+	-	228	284	291
17	17	0	0	0	0	160	228	224

***Table S7.3**. Standard order table for the 2-factorial design used in the calibration.*

Experiment	A=T / ˚C	B=DO / mg L^{-1}
1	+	+
2	-	+
3	+	-
4	-	-
5	0	0

Table S7.4. *OFAT dataset the 2-factorial design used in the calibration.*

Experiment	A=T / ˚C	B=DO / mg L^{-1}	y / mV
1	+	+	345
2	-	+	117
3	+	-	123
4	-	-	54
5	0	0	228

R Summary of models

Factors:

A=T

B=DO

C=pH

D=Conductivity

OFAT model

```
Temp<- c( -1, +1, -1, +1, 0)

DO<- c(+1, +1, -1, -1, 0)

y<- c(116.52, 344.8,  53.9, 123, 227.8) #All values obtained through Monod fit of real data in R files

model <-lm(y~ DO*Temp)

summary (OFAT)

anova(OFAT)

confint(OFAT)

library(pid)

paretoPlot(OFAT)

#Checking the assumptions for calculation of SE

#Normality of the residuals:

library(car)

qqPlot(OFAT)          # uses studentized residuals

qqPlot(resid(OFAT))     # uses raw residuals


# Visualize the surface

N <- 100  # resolution of surface (higher values give smoother plots)
```

```
# The lower and upper bounds, in coded units, over which we want
# to visualize the surface
bound <- 1
Temp_plot <- seq(-1, 1 ,length=N)
DO_plot <- seq(-1, 1, length=N)
grd <- expand.grid(Temp=Temp_plot, DO=DO_plot)

# Predict directly from least squares model
grd$y <- predict(model, grd)

library(lattice)

contourplot(y ~ Temp*DO ,
        data = grd,
        cuts = 20,
        region = TRUE,
        pretty=TRUE,
        col.regions = terrain.colors,
        ylab=list(label="Temperaure",cex=2),
        xlab=list(label="Dissolved oxygen / mg L-1", cex=2),
        labels=list(cex=2),
        scales=list(cex=2))
```

OFAT_n model

Same as OFAT with the data:

```
y<- c(0.51, 1.51, 0.237, 0.54) #All values obtained through Monod fit of real data
```

DOE 4-factorial model

```
A<- c( -1,+1, -1, +1, -1, +1, -1, +1,
     -1,+1, -1, +1, -1, +1, -1, +1,
```

```
      -1,+1, -1, +1, -1, +1, -1, +1,
      -1,+1, -1, +1, -1, +1, -1, +1,
      -1,+1, -1, +1, -1, +1, -1, +1,
      -1,+1, -1, +1, -1, +1, -1, +1,
      0,0,0)

B<- c(-1, -1, +1, +1, -1, -1, +1, +1,
     -1, -1, +1, +1, -1, -1, +1, +1,
     -1, -1, +1, +1, -1, -1, +1, +1,
     -1, -1, +1, +1, -1, -1, +1, +1,
     -1, -1, +1, +1, -1, -1, +1, +1,
     -1, -1, +1, +1, -1, -1, +1, +1,
     0,0,0)

C<- c( -1, -1, -1, -1, 1, 1, 1, 1,
      -1, -1, -1, -1, 1, 1, 1, 1,
      -1, -1, -1, -1, 1, 1, 1, 1,
      -1, -1, -1, -1, 1, 1, 1, 1,
      -1, -1, -1, -1, 1, 1, 1, 1,
      -1, -1, -1, -1, 1, 1, 1, 1,
      0,0,0)

D<- c(-1, 1, 1, -1, 1, -1, -1, 1,
    -1, 1, 1, -1, 1, -1, -1, 1,
    -1, 1, 1, -1, 1, -1, -1, 1,
    1, -1, -1, 1, -1 , 1, 1, -1,
    1, -1, -1, 1, -1 , 1, 1, -1,
    1, -1, -1, 1, -1 , 1, 1, -1,
    0,0,0)

y <- c(49, 49, 164, 301, 62, 33, 165, 240,
```

```
    50, 85, 226, 290, 43, 62, 195, 316,
    87, 55, 160, 290, 62, 85, 155, 255,
    48, 50, 220, 237, 135, 26, 124, 250,
    70, 59, 155, 299, 139, 30, 115, 284,
    78,41, 199, 288, 161, 26, 167, 291,
    160, 260, 125)

# Built the least squares model using the centred and normalised data set.
model_comp <-lm(y ~ A*B*C*D)

summary(model_comp)
anova(model_comp)

# Calculate the confident intervals at 95%.
confint(model_comp)

# Pareto Plot
library(pid)
paretoPlot(model_comp)

#Checking the assumptions for calculation of SE:
#Normality of the residuals:

library(car)
qqPlot(model_comp)          # uses studentized residuals
qqPlot(resid(model_comp))   # uses raw residuals

#plot residuals against x to see trends on the residuals
plot(A, resid(model_comp))
abline(h=0, col="red")
```

```
plot(B, resid(model_comp))
abline(h=0, col="red")

#plot residuals in time order
plot(resid(model_comp))
abline(h=0, col="red")
lines(lowess(resid(model_comp), f=0.2))   # use a shorter smoothing span

plot(predict(model_comp), rstudent(model_comp))
lines(lowess(predict(model_comp), rstudent(model_comp)))
abline(h=0, col="red")
```

DOE 2-factorial model

Same as DOE 4-factorial with the model: mod_2f <-lm(y ~ A*B)

DOE_n

Same as DOE 2-factorial with the data:

```
A<- c( -1,+1, -1, +1, -1, +1, -1, +1,
       -1,+1, -1, +1, -1, +1, -1, +1,
       -1,+1, -1, +1, -1, +1, -1, +1,
       -1,+1, -1, +1, -1, +1, -1, +1,
       -1,+1, -1, +1, -1, +1, -1, +1,
       -1,+1, -1, +1, -1, +1, -1, +1)

B<- c(-1, -1, +1, +1, -1, -1, +1, +1,
      -1, -1, +1, +1, -1, -1, +1, +1,
      -1, -1, +1, +1, -1, -1, +1, +1,
      -1, -1, +1, +1, -1, -1, +1, +1,
      -1, -1, +1, +1, -1, -1, +1, +1,
      -1, -1, +1, +1, -1, -1, +1, +1)
```

```
C<- c( -1, -1, -1, -1, 1, 1, 1, 1,
       -1, -1, -1, -1, 1, 1, 1, 1,
       -1, -1, -1, -1, 1, 1, 1, 1,
       -1, -1, -1, -1, 1, 1, 1, 1,
       -1, -1, -1, -1, 1, 1, 1, 1,
       -1, -1, -1, -1, 1, 1, 1, 1)


D<-c(-1, 1, 1, -1, 1, -1, -1, 1,
     -1, 1, 1, -1, 1, -1, -1, 1,
     -1, 1, 1, -1, 1, -1, -1, 1,
     1, -1, -1, 1, -1 , 1, 1, -1,
     1, -1, -1, 1, -1 , 1, 1, -1,
     1, -1, -1, 1, -1 , 1, 1, -1)

# Values are normalised by the baseline of each sensor.
y<- c(0.31, 0.31, 1.09, 1.88, 0.27, 0.21, 1.03, 1.5,
      0.22, 0.37, 0.99, 1.65, 0.19, 0.27, 0.85, 1.51,
      0.68, 0.43, 1.25, 2.27, 0.48, 0.50, 1.21, 2.88,
      0.3, 0.31, 1.38, 1.48, 0.84, 0.16, 0.78, 1.56,
      0.26, 0.26, 0.68, 1.31, 0.71, 0.13, 0.50, 1.24,
      0.61,0.55,1.55,2.25,1.09,0.20,1.30,2.27)
```

7.7 References

[1] R. J. Diaz and A. Solow, “Ecological and economical consequences of hypoxia,” *Decis. Anal.*, no. 16, 1999.

[2] Y. Wei, Y. Jiao, D. An, D. Li, W. Li, and Q. Wei, “Review of dissolved oxygen detection technology: From laboratory analysis to online intelligent detection,” *Sensors (Switzerland)*, vol. 19, no. 18. 2019. DOI: 10.3390/s19183995.

[3] The Dissolved Oxygen Handbook a practical guide to dissolved oxygen measurements Y S I . c o m/w e k n o wDO [accessed October 2019] ,pp. 1-43, 2009.

[4] J. Chouler, M. Di Lorenzo Water quality monitoring in developing countries; Can microbial fuel cells be the answer?, *Biosensors*, vol. 5, no. 3, pp. 450-470, 2015.DOI: 10.3390/bios5030450.

[5] L. Gonzalez Olias, P. J. Cameron, and M. Di Lorenzo, “Effect of Electrode Properties on the Performance of a Photosynthetic Microbial Fuel Cell for Atrazine Detection,” *Front. Energy Res.*, vol. 7, no. October, pp. 1–11, 2019.DOI: 10.3389/fenrg.2019.00105.

[6] T. Ewing, T. Ha, and H. Beyenal, “Evaluation of long-term performance of sediment microbial fuel cells and the role of natural resources,” *Appl. Energy*, vol. 192, pp. 490–497, 2017.DOI: 10.1016/j.apenergy.2016.08.177.

[7] K. Kubota, T. Watanabe, H. Maki, G. Kanaya, H. Higashi, and K. Syutsubo, “Operation of sediment microbial fuel cells in Tokyo Bay, an extremely eutrophicated coastal sea,” *Bioresour. Technol. Reports*, vol. 6, pp. 39–45, 2019.DOI: 10.1016/j.biteb.2019.02.001.

[8] S. B. Velasquez-Orta, D. Werner, J. C. Varia, and S. Mgana, “Microbial fuel cells for inexpensive continuous in-situ monitoring of groundwater quality,” *Water Res.*, vol. 117, pp. 9–17, 2017.DOI: 10.1016/j.watres.2017.03.040.

[9] F. Fang, G. L. Zang, M. Sun, and H. Q. Yu, “Optimizing multi-variables of microbial fuel cell for electricity generation with an integrated modeling and experimental approach,” *Appl. Energy*, vol. 110, pp. 98–103, 2013.DOI: 10.1016/j.apenergy.2013.04.017.

[10] Y. Zhang and I. Angelidaki, “A simple and rapid method for monitoring dissolved oxygen in water with a submersible microbial fuel cell (SBMFC),” *Biosens. Bioelectron.*, vol. 38, no. 1, pp. 189–194, 2012.DOI: 10.1016/j.bios.2012.05.032.

[11] M. H. McCrady, “STANDARD METHODS FOR THE EXAMINATION OF WATER AND WASTE-WATER (12th ed.),” *Am. J. Public Heal. Nations Heal.*, vol. 56, no. 4, pp. 684–684, 2008.DOI: 10.2105/ajph.56.4.684-a.

[12] S. M. Martinez and M. Di Lorenzo, “Electricity generation from untreated fresh digestate with a cost-effective array of floating microbial fuel cells,” *Chem. Eng. Sci.*, vol. 198, pp. 108–116, 2019.DOI: 10.1016/j.ces.2018.12.039.

[13] U.S EPA, “Online source water quality monitoring for water quality surveillance and response systems,” *U.S.Environmental Prot. Agency*, no. September, p. 114, 2016.

[14] K. G. Dunn, “Process Improvement using Data,” *http://learnche.org/pid*, 2019. [accessed October 2019]. Available: learnche.mcmaster.ca/pid.

[15] M. J. Salar-García, A. de Ramón-Fernández, V.M. Ortiz-Martínez, D. Ruiz-Fernández, I. Ieropoulos, Towards the optimisation of ceramic-based microbial fuel cells: A three-factor three-level response surface analysis design” Biochem. Eng. J. 144 pp. 119–124, 2019. DOI: 10.1016/j.bej.2019.01.015.

[16] N. Song , Z. Yan, H. Xu, Z. Yao, C. Wang, M. CHen, Z. Zhao., “Development of a sediment microbial fuel cell-based biosensor for simultaneous online monitoring of dissolved oxygen concentrations along various depths in lake water” Sci. Total Environ., vol. 673, no. April, pp. 272–280, 2019.DOI:10.1016/j.scitotenv.2019.04.032.

[17] J. Menicucci, H. Beyenal, E. Marsili, R. A. Veluchamy, G. Demir, and Z. Lewandowski, “Procedure for determining maximum sustainable power generated by microbial fuel cells,” *Environ. Sci. Technol.*, vol. 40, no. 3, pp. 1062–1068, 2006.DOI: 10.1021/es051180l.

[18] F. F. Ajayi and P. R. Weigele, “A terracotta bio-battery,” *Bioresour. Technol.*, vol. 116, pp. 86–91, 2012.DOI: 10.1016/j.biortech.2012.04.019.

[19] V. Yousefi, D. Mohebbi-Kalhori, and A. Samimi, “Ceramic-based microbial fuel cells (MFCs): A review,” 2017.DOI: 10.1016/j.ijhydene.2016.06.054.

[20] J. Winfield, L. D. Chambers, J. Rossiter, I. Ieropoulos, "Comparing the short and long term stability of biodegradable, ceramic and cation exchange membranes in microbial fuel cells", *Biores. Tech.* vol. 148, pp.480-486, 2013. DOI: 10.1016/j.biortech.2013.08.163.

[21] R. Vaquer-Sunyer and C. M. Duarte, “Thresholds of hypoxia for marine biodiversity,” *Proc. Natl. Acad. Sci. U. S. A.*, vol. 105, no. 40, pp. 15452–15457, 2008.DOI:

10.1073/pnas.0803833105.

[22] B. S. Razavi, E. Blagodatskaya, and Y. Kuzyakov, “Nonlinear temperature sensitivity of enzyme kinetics explains canceling effect — a case study on loamy haplic Luvisol,” vol. 6, no. October, pp. 1–13, 2015. DOI: 10.3389/fmicb.2015.01126.

[23] H. Zhang, C. Lin, L. Sepunaru, C. Batchelor-McAuley, and R. G. Compton, “Oxygen reduction in alkaline solution at glassy carbon surfaces and the role of adsorbed intermediates”, *J. Electroanal. Chem.*, vol. 799, pp. 53–60, 2017.DOI: 10.1016/j.jelechem.2017.05.037.

[24] M. Miyahara, A. Kouzuma, and K. Watanabe, “Effects of NaCl concentration on anode microbes in microbial fuel cells”, *AMB Express*, 2015.DOI: 10.1186/s13568-015-0123-6.

[25] N. E. Stein, H. V. M. Hamelers, and C. N. J. Buisman, “Bioelectrochemistry Stabilizing the baseline current of a microbial fuel cell-based biosensor through overpotential control under non-toxic conditions” *Bioelectrochemistry*, vol. 78, no. 1, pp. 87–91, 2010.DOI: 10.1016/j.bioelechem.2009.09.009.

[26] Y. Yang, L. Yan, J. Song, and M. Xu, “Optimizing the electrode surface area of sediment microbial fuel cells,” *RSC Adv.*, vol. 8, no. 45, pp. 25319–25324, 2018. DOI: 10.1039/c8ra05069d.

[27] F. Zhao, F. Harnisch, U. Schröder, F. Scholz, P. Bogdanoff, and I. Herrmann, “Challenges and constraints of using oxygen cathodes in microbial fuel cells,” *Environ. Sci. Technol.*, vol. 40, no. 17, pp. 5193–5199, 2006. DOI: 10.1021/es060332p.

Chapter 8

In Chapter 7, the CSMFC was tested for early detection of hypoxic events in water bodies. A holistic approach, based on a DoE, was also proposed to simultaneously study the influence of several environmental factors in the signal response. It was concluded that, in a system with variations in conductivity, pH, DO and temperature, the signal of the CSMFC correlated mainly with the oxygen content in water, temperature and the interaction between them. The DoE proved to be an efficient method to characterise the system and calibrate the sensor.

With the aim to expand the use of the CSMFC sensors for environmental water monitoring, Chapter 8 explores its use as early warning system for eutrophic events in water bodies. The presence of algae in water produces a characteristic cyclic signal with DO increasing in the day and decreasing in the night that can be used as a proxy to detect the occurrence of algae in surface waters.

In Chapter 8, the use of design of experiments to understand the system's behaviour is further explored. A screening design is performed to identify the main environmental factors, including nitrates. Nitrates are found in high concentrations in eutrophic water and are a competitor to oxygen for the cathodic reduction reaction, which could affect the sensititvity of the CSMFC sensors to dissolved oxygen. Design factors such as the external resistance and the cathode material are also included in the screening design to optimise the sensor's configuration. The external resistance influences the reaction rate and hence the sensitivity, response time and long-term stability. The influence of the cathode material in the sensor's performance was evaluated in Chapter 6 for an algal biocathode. In the present study, the cathode is abiotic but could be colonised with algae over time. Therefore carbon felt and carbon cloth are chosen as the most durable and cost-effective materials for the CSMFC sensor.

To mimic an eutrophic environment, in this study the catholyte is enriched from real freshwater pond instead of a pure culture.

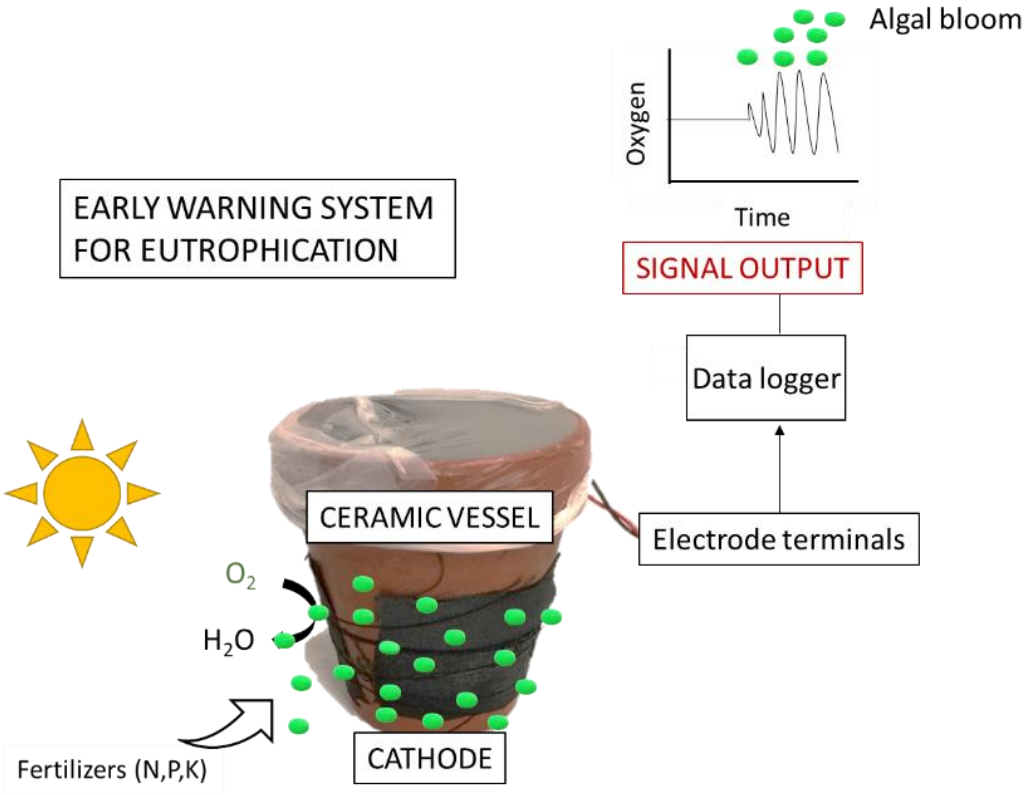

This chapter is published as a proceedings paper, with details on the following page. Amendments have been made to account for stylistic consistency in this thesis.

Statement of authorship

This declaration concerns the article entitled:

"Ceramic soil microbial fuel cells sensors for in situ and early detection of eutrophication"

Publication status: Published in the "1st International Electronic Conference on Biosensors (IECB 2020)". Proceedings (MDPI).

Authorship contributions:

Original ideal, conceptualization and sensor design: L.G. Experimental design: L.G., M.D.L. and P.J.C. Experimentation: L.G. and A.R. Manuscript writing: L.G., M.D.L. and P.J.C. Supervision: M.D.L. and P.J.C.

Statement from candidate: This paper reports on original research I conducted during the period of my Higher Degree by Research candidature. In line with the regulations in QA7 Appendix 6 of the University of Bath, the abovementioned article has been stylistically integrated into the thesis, including: sections' and figures' numbering, typeface, margins and pagination.

Signed:

Date:

8. Ceramic soil microbial fuel cells sensors for *in situ* and early detection of eutrophication

Lola Gonzalez Olias,[1,2] Alba Rodríguez Otero[1], Petra J. Cameron,[3] Mirella Di Lorenzo[1,]*

[1] Centre for Biosensors, Bioelectronics and Biodevices (C3Bio) and Department of Chemical Engineering, University of Bath, Bath BA2 7AY, United Kingdom

[2] Water Innovation Research Centre (WIRC), University of Bath, Bath BA2 7AY, United Kingdom

[3] Department of Chemistry, University of Bath, Bath BA2 7AY, United Kingdom

The growing use of fertilisers increases the risk of eutrophication that seriously damages ecosystems due to critical oxygen depletion. Continuous monitoring of oxygen in environmental water could improve the detection of eutrophication and prevent anoxic conditions. However, online and *in situ* dissolved oxygen sensors are yet to be implemented due to poor portability and power requirements. Here, we propose a ceramic soil microbial fuel cell as a self-powered sensor for algal growth detection *via* monitoring of dissolved oxygen in water. The sensor signal follows the characteristic photosynthetic cycle, with a maximum day current of 0.18 ± 0.2 mA and a minimum night current of 0.06 ± 0.34 mA, which correlates with dissolved oxygen (R^2 = 0.85 (day); R^2= 0.5 (night)) and the algal concentration (R^2=0.63). A saturated design of experiments on seven factors suggests that temperature, dissolved oxygen, nitrates and pH are the most influential operational factors in the voltage output. Moreover, operating the system at the maximum power point (R_{ext}= 2 kΩ) improves the sensor sensitivity. To the best of our knowledge, this is the first self-contained, floating MFC-based biosensor proposed for in field, early detection of eutrophic events.

Keywords: Biosensor, Eutrophication, Microbial Fuel Cell, Photosynthesis, Water quality.

8.1 Introduction

Climate change and the excessive use of fertilisers in agriculture is intensifying eutrophication of water bodies worldwide. High concentration of nitrates and phosphates in water, promote rapid growth of microalgae on surface waters that excrete harmful toxins and produce hypoxia in the subsurface waters, leading to the irreversible loss of biodiversity [1]. Early detection of sudden growth of algae could help implementing proactive approaches to control the use of fertilisers, reducing the risk of eutrophication [2]. Eutrophication involves rapid growth of algal biomass that causes oxygen supersaturation during the day, and depletion during the night on surface waters, as a consequence of photosynthetic production of oxygen [1].

Current monitoring techniques for detection of algal blooms, based on remote sensing technologies such as radar or satellite, are effective in open sea but have limited efficacy in inland waters, where the risk of eutrophication is higher, due to interferences from vegetation and urbanization [3]. These systems are, in addition, costly and data analysis is slow, hence not effective as early warning systems (EWS) [4]. Continuous, *in situ* and online sensors to monitor algae growth are not readily available yet, due to shortcomings in portability, autonomy and long-term stability [5].

Microbial Fuel Cell (MFC)-based biosensors are a type of electrochemical biosensor that have been proposed as an alternative to overcome some of these issues, due to simplicity of the design and low power requirements [6]. Recently, a ceramic, soil-based MFC (CSMFC) sensor was proposed by our group as a portable device for online, in-situ and real time readings of dissolved oxygen (DO) in water [7]. In this study, we propose to use CSMFC technology as an early warning system for eutrophic events by monitoring the distinctive photosynthetic day/night patterns of dissolved oxygen in water.

To effectively calibrate the sensor, a preliminary analysis on a wide range of possible influential factors should be done to account for all important variables. This analysis is rarely performed because it involves a large number of experiments, especially when the “one factor at the time” approach is followed. In

contrast, Design of Experiments (DoE) is an efficient tool that maximises the knowledge of a system with minimum number of experiments [8]. Within DoE designs, a Resolution III saturated fractional design (RIII) is commonly employed as a preliminary screening to identify the most influential factors on a novel design. In a RIII, the main factors are confounded with second order interactions, meaning that the accuracy of the design is low for prediction purposes. Resolution designs constitute, however, an effective first step to identify the most influential operational and design variables in the response of the system [8].

In this study, the effect of temperature, DO, nitrates, conductivity, pH, external resistance and cathode material on the voltage output is investigated following a RIII design methodology.

8.2 Materials and methods

8.2.1 Materials

All chemicals were purchased from Sigma Aldrich without further purification. Aqueous solutions were prepared with reverse osmosis purified water.

Soil was collected at the outskirts of the University of Bath campus and cleared of branches and leaves prior to be used. The organic content of the soil, measured with the loss of ignition method [9] right after collection, was 16.88 ± 0.91 %

Water with algae was collected from a pond at the University of Bath (51.378294, -2.328439) on the 4th of January of 2019 at 10 am and filtered with a sieve to remove grit and debris. Aliquots of 50 mL of pond water were inoculated for ten days in 250 mL of Bold Basal Medium (BBM) [10]. The mixture was sub-cultured three times for ten days each time in 250 mL of BBM, to select for photosynthetic species. The resulting mixture was maintained in 1L bottles at an OD_{750nm} between 0.7 and 1. All algal cultures were grown in an incubator at 12h/12h light cycle under white light at 5 lm m^{-1} intensity, at 25 ˚C and agitation of 180 rpm. The cultures were inoculated in 25 mL Erlenmeyer and maintained in containers with natural airflow.

The pH was measured with a pH-meter (Thermo Scientific Orion ROSS Ultra pH/ATC Triode, USA). Conductivity was measured with a conductivity benchtop

cell (Orion, Thermo Scientific). Dissolved oxygen was measured with a DO portable meter (RDO Orion 7003, Singapore). Nitrates were measured by using a commercial reagent for high range samples (0-14000 ppm, HANNA Instruments HI 839800 COD reactor).

8.2.2 Operation of the CSMFC in eutrophic water

The CSMFCs consist of terracotta vessels (Little Bug Crafts, UK) of dimensions 7.4 cm (height) x 8 cm (upper diameter) x 4.8 cm (bottom diameter) x 0.4 cm (thickness). The anode is made of four pieces (3 x 3 x 0.7 cm^3) of graphite felt (GF, Online Furnace Services Ltd.), acid treated as previously described [11], woven together with Ti wire (25 mm, Advent Research Materials, Oxford, UK). This was done to increase the anode/cathode surface area ratio. The cathodes (6 x 4 cm^2) are made of two pieces of carbon cloth (Plain carbon cloth, Etek Cloth A, Fuel Cell Earth US) and one piece of 0.7 x 4 x 6 cm^3 of graphite felt. The CSMFC were assembled as described in our previous study (Figure 8.1). Anode and cathode terminals were connected to an external resistance (R_{ext}) of 1 kΩ and to a data logger (PicoLog High Resolution Data Logger, Pico Technology) to monitor the voltage every minute. During enrichment, the CSMFCs were placed inside a 250 mL glass vessel containing 200 mL of an algae solution of $OD_{750\ nm}$=0.06 in BBM with a final pH = 6.4 and conductivity of 750 µS cm^{-1}. The vessels were covered with parafilm to prevent contamination while allowing transportation of gases. The set-up was operated in a black box on a 12h/12h light regime with 60 W adjustable blue and red LEDs (light intensity of 40 mW cm^{-1}). Experiments were run at room temperature, i.e. 20 ± 3 ˚C.

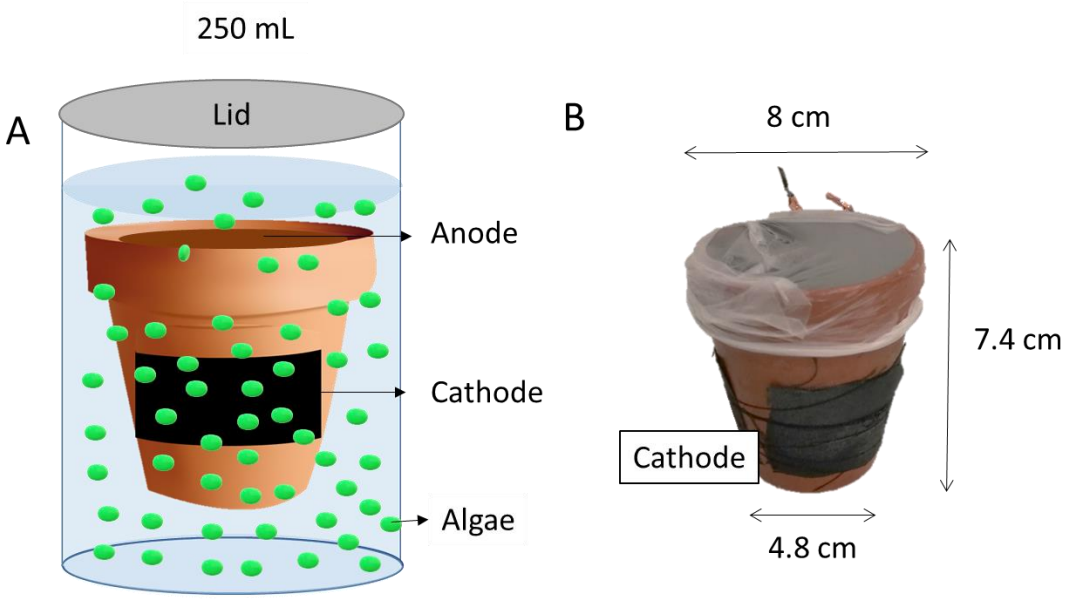

Figure 8.1. *Sketch of the set up. (A) CSMFC in a 250 mL beaker with algal (green circles) solution, held in the middle with a plastic frame (not shown). (B) Dimensions of the CSMFC device.*

8.2.3 Electrochemical characterisation

Polarisation tests were conducted to evaluate the effect of two cathode materials, carbon felt and carbon cloth, hereafter referred as CSMFC-CF and CSMFC-CC respectively. The polarisation tests were not performed in the algal solution, because variable DO due to photosynthesis produces an unstable baseline. Instead, new CSMFC were enriched and operated in tap water (Figure S8.1) at DO= 8.6 mg L^{-1}, following the procedure reported in our previous study [7]. Tap water was left open to air 10 min before addition, to reduce the chlorine content. The tests were performed by applying an external load within the range of 10 MΩ - 100 Ω with a resistance box (RS Components, UK), starting from Open Circuit Voltage (OCV) and and switching to the next value, following pseudo-steady states. The range was chosen based on preliminary tests. The current (I) was calculated according to *Ohm's Law* (I = V/ Rext) and power (P) was calculated as P = I x V. Tests were performed in triplicate.

Drifts in cathodic performance over time were assessed with cyclic voltammetry (CV) using a potentiostat (PalmSens4, Palmsense) and a 3-electrode system,

where the algal cathode served as the working electrode, an array of four stainless steel meshes (4 x 4 cm^2) as counter electrode and a Ag/AgCl (3 M KCl sat) as reference electrode. The CVs were run at a scan rate of 1 mV s^{-1} sweeping from 0.6 V to - 0.6 V vs Ag/AgCl with 5 seconds of stabilisation. Duplicated experiments were performed in a 250 mL beaker with 200 mL of BBM as electrolyte to maintain the biofilm in optimal conditions, without agitation, at approximately five hours after the start of the light period.

8.2.4 Influence of factors on the CSMFC response

A saturated fractional design on seven factors and eight experiments was performed in duplicate, to test the effect of DO, nitrates, conductivity, pH, temperature, external resistance, electrode material, on the sensor voltage output. For this, new CSMFCs were enriched as previously described, in the absence of algae [7]. Table 8.1 shows the treatment levels chosen for each factor, which are selected based on typical values for environmental water bodies ([12]) including high conductivity to mimic operation in seawater. The external resistance was chosen as the optimum value for power generation (R_{ext}=2 kΩ) and a higher value of 5 kΩ, to slow down the kinetics of organic matter oxidation and extend the sensors lifetime [13]. Carbon cloth, CC, and carbon felt, CF, were chosen as electrode materials due to proven stability in biological systems. Table 8.2 shows the standard order table for the DoE and Equations 8.1-8.6 show the confounding pattern of main factors with second order interactions in this screening design. Higher order interactions are assumed negligible. The detailed aliasing procedure of the factors to obtain the confounding pattern is described in specialised DoE references [8]. In this case, the aliasing pattern, ignoring third and fourth order interactions, is:

$$M=C \times NO_3=DO \times pH=T \times Rext \quad (8.1)$$

$$C=M \times NO_3=DO \times T=pH \times Rext \quad (8.2)$$

$$DO=M \times pH=C \times T= NO_3 \times Rext \quad (8.3)$$

$$NO_3=M \times C=DO \times Rext=pH \times T \quad (8.4)$$

$$T=C \times DO=Mx\ Rext= NO_3 \times T \quad (8.5)$$

$$Rext=DO \times NO_3=C \times pH=M \times T \quad (8.6)$$

Coding of factor levels and the experimental runs (Table 8.2) were performed following the methodology described in our previous study and using the same set up. The statistical analyses, model assumptions and Pareto Plots were performed by using the R software (www.r-project.com), using the code provided in our previous study [7].

Table 8.1. *Range of study of the factors.*

Factors	**Level**	
	+	-
Temperature, T / ˚C	30	10
Dissolved oxygen, DO / mg L^{-1}	10	1
pH / -	9	5
Conductivity, C/ µS cm^{-1}	3000	150
Electrode material, M	GF	CC
Rext / Ω	5000	2000
NO_3 / mg L^{-1}	10	1

8.3 Results and discussion

8.3.1 Enrichment and operation of CSMFC as DO sensor in eutrophic waters

Figure 8.2A shows the enrichment period of the CSMFCs in the algal solution. This is the time when microorganisms colonise the electrodes and form electroactive biofilms. The lag period, during which an output current is not yet detectable, extends up to 10 days, longer than reported in other types of MFCs with algal cathodes [14]–[17]. This delay could be a consequence of oxygen crossover from the catholyte into the anode chamber that impedes the growth of strict anaerobic electroactive bacteria [18]. Oxygen crossover is indeed an issue in algal assisted sediment MFCs where current is inversely proportional to DO and algal concentration due to the negative effect of oxygen on the coulombic efficiency [16], [19]. Figure 8.2B shows that DO and voltage are positively correlated, suggesting that the performance of the anode is not compromised. Despite the proximity of the electrodes (electrode distance: 3 cm), oxygen crossover is reduced in the CSMFC by the higher organic content of soil. The soil in fact promotes microbial activity and oxygen uptake, preventing diffusion of oxygen towards the anode. Oxygen

diffusion is further impeded because the soil is water saturated, enhancing anaerobic conditions at the anode. In addition, the higher ratio anode to cathode electrode area, ensures that the cathode rate limits the signal output, which is therefore independent on the anode potential at the operating conditions ([7, 20]).

From day 10, the output current follows the typical photosynthetic cycle, with current increasing during the day and decreasing in the night (inset in Figure 8.2A), as shown in previous studies [15, 21]. The steady state is reached after 17 days, with a maximum day voltage of 182.8 ± 27.8 mV (0.18 ± 0.2 mA) and a minimum night voltage of 60.0 ± 34.2 mV (0.06 ± 0.34 mA). The day/night cycle is not observed in CSMFCs enriched in the absence of algae (Figure S8.1), which suggests that, in the experimental conditions, oxygen reduction is the rate-limiting reaction and dominates the sensor signal.

The pH of the catholyte increases over time (Figure 8.2B), possibly due to production of hydroxyl ions and in the electrolyte. The energy gain in the ORR in basic media is lower than acid media [22], hence the power output of the CSMFC is lower than reported elsewhere on buffered algal assisted cathodes, operated at neutral pH. Buffer control is nonetheless not practical for field applications [23]. Consequently, the catholyte pH shifts to alkaline enhancing the peroxide pathway, reducing the sensitivity of the sensor to DO [24]. Additionally, the production of reactive oxygen species induces stress on algal metabolism, which could trigger an unwanted metabolic response [25]. Alkaline conditions are often inevitable in eutrophic waters [21] and should be taken into consideration in the evaluating the sensor performance.

The slow increase in conductivity, observed in Figure 8.2B is probably due to crossover of ions from the soil to the catholyte (Figure S8.2). The high conductivity of soil improves migration of ions, particularly relevant in freshwater environments. Algal growth could not be assessed after 11 days due to clumping and aggregation of algae in the catholyte.

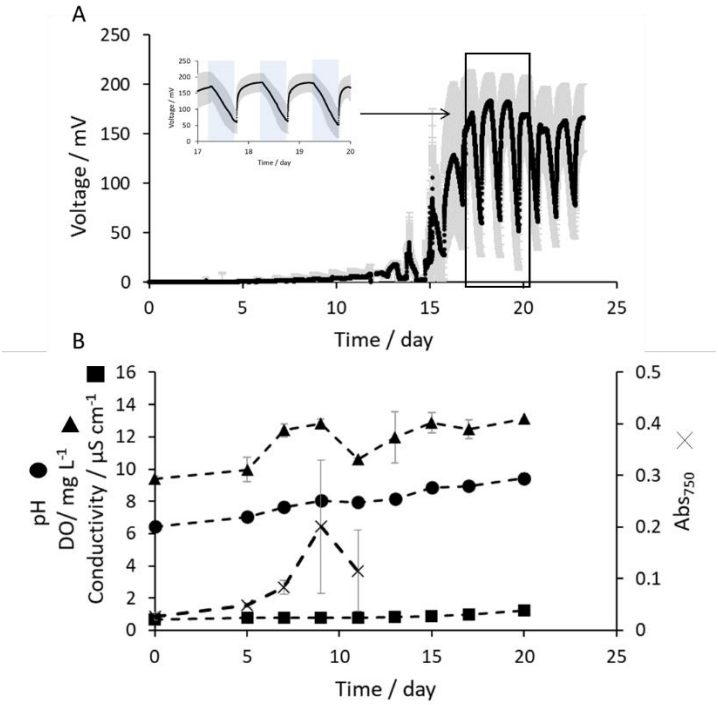

***Figure 8.2**. (A) Enrichment of the CSMFC-GF in algal catholyte (R_{ext} = 1kΩ). Shadowed areas correspond to the standard deviation of the mean and the blue areas in the inset correspond to the dark cycle. (B) Evolution of pH (circles), DO (triangles), conductivity (squares) and absorbance (crosses) during the enrichment period. Error bars correspond to the standard deviation of the mean. Data refer to three replicates.*

Figure 8.3 shows a correlation between the signal and DO variations, with a correlation factor of R^2 = 0.66 over a time span of ten hours (R^2 = 0.85 in night period and R^2 = 0.5 during the day period). The correlation factor is lower than reported in a soil MFC sensor monitoring DO in tap water [7]. Possibly, the high DO during the day, up to 13 mg L^{-1} improves both oxygen crossover and the oxidation reaction rate, turning the anode into the limiting electrode under light.

The correlation coefficient is likely to differ in field applications. Algal activity varies throughout the year due to changes in light intensity, temperature and nutrient availability, which affect the photosynthetic activity of algae and the concentration of oxygen produced [26].

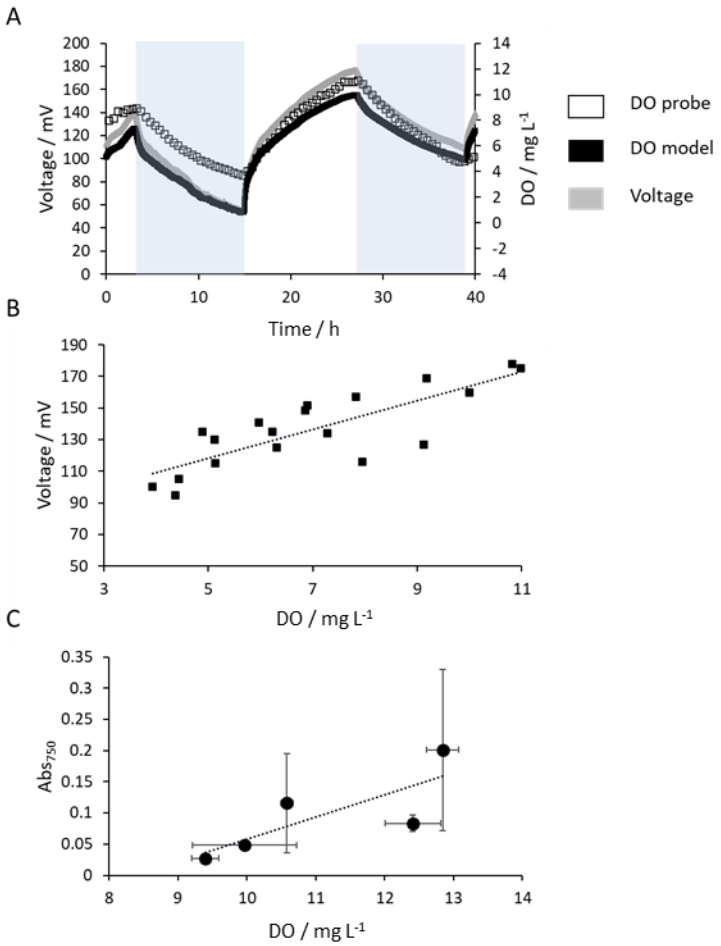

***Figure 8.3**. (A) Comparison of DO predicted with the CSMFC (black line) and commercial probe (white squares) over time. The CSMFC DO is predicted from the CSMFC voltage output (grey line) using the calibration model from* [7]*) during the dark/light cycle. (B) Correlation of DO and voltage in the time span presented in (A) (R^2=0.66). (C) Correlation of algal concentration and voltage during the first 11 days of operation (R^2= 0.63). Error bars correspond to the standard deviation of the mean of three replicates.*

8.3.2 Calibration of the CSMFC sensor

The CSMFC voltage output could help assess the degree of eutrophication based on algal concentration (given by the R^2=0.65 of Abs_{750} and DO, Figure 8.3C). A general calibration model for a CSMFC-based sensor developed in a previous study [7] (Equation 8.7) is applied to this specific case by multiplying the model coefficients to the baseline voltage output at DO= 5.5 mg L^{-1}. Interpolation of the curve in Figure 8.3 gives a baseline of 130 mV, leading to Equation 8.8.

$$DO_{CSMFC} = \frac{y\_n - 1.07 - 0.18 * T}{0.6 + 0.28 * T} \quad (8.7)$$

$$DO_{Algal\ CSMFC} = \frac{y - 139.1 - 23.4 * T}{78 + 36.4 * T} \quad (8.8)$$

Where y_n is the signal voltage output normalised by the baseline, y is the absolute signal output, in mV, T and DO are temperature and dissolved oxygen in coded values.

The RMSE, defined as the root square of the quadratic sum of distances from each point to the mean [7], is 1.98 mg L^{-1}, which is a low accuracy in comparison with commercial electrochemical sensors (± 0.2 mg L^{-1} or 2 % of reading [27]). Nonetheless, it allows capturing the distinctive photosynthetic pattern of eutrophic events. Moreover, the signal response to changes in DO is instantaneous, which is an essential requirement for early detection devices.

Based on these results, the voltage output generated by the CSMFC is correlated with the presence of algae in water. The CSMFC sensor could therefore be used as an early warning system for eutrophic events. The lower correlation coefficient obtained in the SCMFC model operated in algal solution in comparison with tap water, could be caused by an overlooked factor in the algal system. The variability caused by factors not included in the study is attributed to the modelling error. It may be possible that nitrates compete as electron acceptor, weakening the correlation between oxygen and the signal output.

8.3.3 Evaluation of relevant factors on CSMFC performance

A RIII saturated factorial DoE on temperature (T), dissolved oxygen (DO), nitrates (NO_3), conductivity (C), pH, external resistance (R_{ext}) and material (M) was performed according to Tables 8.1 and 8.2.

The Pareto Plot in Figure 8.4 is a representation of the relative importance of factors [8]. Dissolved oxygen, temperature and nitrates are the most influential and statistically significant factors. High values of DO improve the reaction rate of oxygen reduction, whereas temperature enhances both kinetics and microbial

activity, suggesting that DO mainly affects the cathodic performance, and anodic activity is governed by temperature [28].

***Table 8.2**. Standard order table for the RIII experimental design. V_1 and V_2 are the normalised by the baseline (pH=7; DO=5.5 mg L^{-1}; T=20 ˚C).*

Run	M	C	DO	NO_3=MxC	pH=MxDO	T=CxDO	Rext=MxCxDO	V_1	V_2
1	CC	300	1	10	9	30	2000	1.06	0.60
2	CF	300	1	1	5	30	5000	0.96	0.95
3	CC	3000	1	1	9	10	5000	0.70	0.99
4	CF	3000	1	10	5	10	2000	0.73	0.74
5	CC	300	10	10	5	10	5000	0.88	1.05
6	CF	300	10	1	9	10	2000	1.24	1.01
7	CC	3000	10	1	5	30	2000	1.47	2.13
8	CF	3000	10	10	9	30	5000	1.08	0.96

Increasing pH from 5 to 9, shifts the cathodic reaction to hydroxyl ions and hydrogen peroxide production, decreasing the magnitude of the signal [22]. Increasing conductivity has a positive impact, probably because of the reduced ohmic resistance, which is important in the system, as concluded from the symmetrical semicircle obtained in the power curves in Figure 8.5 [29].

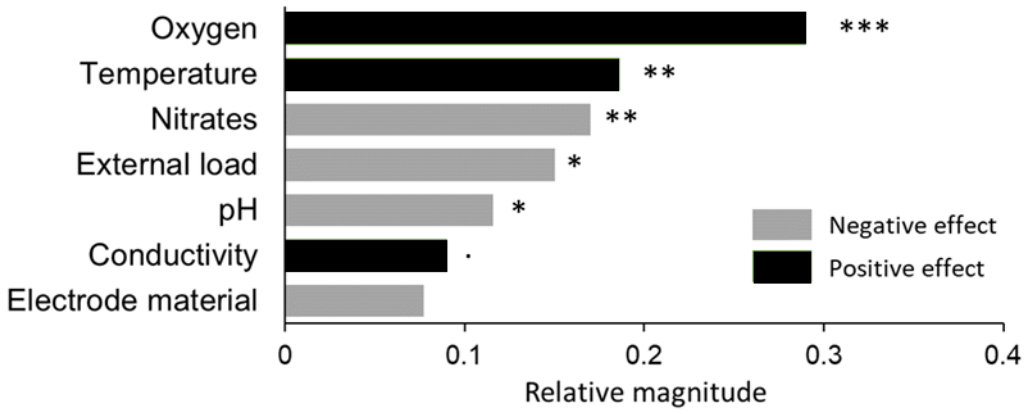

Figure 8.4**. Pareto Plot representing the coefficients, centred and scaled, of the factors studied with the resolution III saturated DoE. Significant codes: p<0 ''p< 0.001 '**' p<0.01 '*' p<0.05 '.'p< 0.1 ' '.*

Regarding the design factors, an external resistance of 2 kΩ generates a larger signal than 5 kΩ, relative to their respective baseline. The comparison of absolute

values would mislead the results interpretation because, according to Ohm's law, the signal increases with R_{ext} and therefore will always be higher at higher R_{ext}, in the tested timeframe. Any trend caused by the factors under study would be within the signal variance. These trends can be detected by reducing the magnitude of the signal in steady state conditions. Normalising the signal by its baseline narrows the output range from 0 to 1, and enhances the sensitivity of the sensor [30].

The effect of the electrode material in the signal output is relatively low. Yet, the higher voltage output of CSMFC-CC over CSMFC-GF suggests that the former has better energy efficiency. This result is not statistically significant but is in agreement with the maximum power output and internal resistance trends obtained by polarisation, with maximum power of 103.6 ± 27.2 μW in CSMFC-CC and 70.5 ± 3.1 μW in CSMFC-GF, and ohmic resistances of 1150 Ω and 1970 Ω respectively (Figure 8.5). The power production in CSMFC is similar to other ceramic [31] and membrane-less sediment MFC [24 , 32] in freshwater, but lower than in seawater [33], further indicating that ohmic limitations are important in the system. Despite having different exposed electrode areas, similar values would be expected with both materials, as the specific surface area is larger for graphite felt (22100–22700 m^{-1} [34]) than carbon cloth (675.14 m^{-2} [35]). The porosity of graphite felt could have facilitated bacterial attachment that would block the electrode active sites and consume oxygen.

Comparing the DO coefficient of 0.26 in this study to the DO coefficient in a similar study without nitrates, of 0.46 [7], shows that the difference in values corresponds to the nitrates coefficient determined in this study, suggesting that nitrates are a competing oxidant for the cathodic reduction [12]. The effect of nitrates is negative because nitrate reduction produces lower current than oxygen reduction reaction [36]. This is because the redox potential of nitrate reduction is lower than oxygen reduction [36]. Nitrate reduction would increase the current if the system was operated in anaerobic conditions. The relative effect of nitrates has implications for the CSMFC signal operating in the dark, when the oxygen level is < 2 mg L^{-1} (Figure 8.3A) which weakens the correlation of the signal voltage with DO.

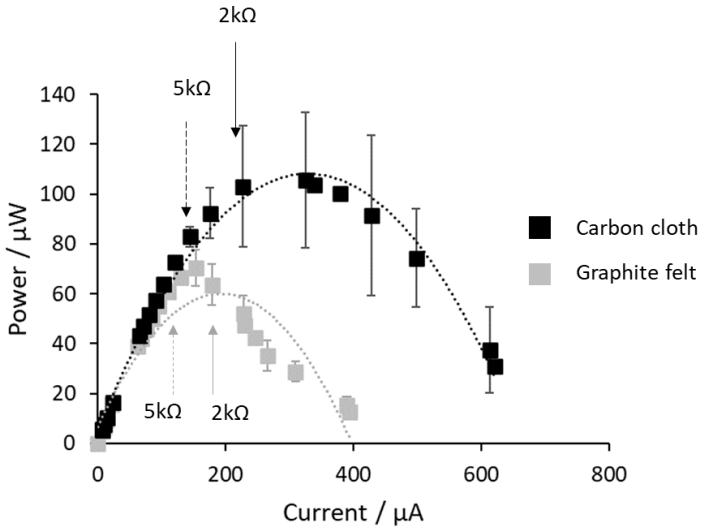

***Figure 8.5**. Power density curves of CSMFC with graphite felt cathode (CSMFC-GF, grey squares) and with carbon cloth cathode (CSMFC-CC, black squares). Error bars represent the standard deviation of the mean of three replicates.*

The significance of factor coefficients indicates that the calibration of the CSMFC for eutrophic environments should, at least, include terms for DO, temperature and nitrates.

Equation 8.10 shows the complete least squares model resulting from the RIII DoE analysis (R^2_{adj}=0.86). The independent term, or intercept, corresponds to the centre point, calculated at the mid values of the factor ranges (level zero). Normalising the sensor response by the baseline values means that the intercept should be close to the unity, which indeed is 1.07.

$$y = 1.07 + 0.29DO + 0.19T - 0.15R_{ext} - 0.17NO_3 + 0.1TDO - 0.07TR_{ext} - 0.11TNO_3 \quad (8.\ 10)$$

The model coefficients agree with previous studies and theoretical trends [7,12], suggesting that the DoE results in this study are robust. In addition, the assumptions of the model are not heavily violated, except for the constant variance (Figure S8.3C and D) which is seldom achieved in biological systems. The model should not be used as a prediction tool but provides meaningful information on the behaviour of the system.

8.3.4 Cyclic voltammetry

The electrochemical performance of the cathode electrodes in algal solution was evaluated after three months of operation, to detect any influence of the biofilm in the reaction (Figure 8.6). A stable onset potential of -0.2 V over time suggests that the presence of the algae does not reduce the activation energy of the reduction reaction. The capacitance on the other hand increases, probably because of growth of non-electroactive species onto the electrode, or adsorption of dissolved species on the electrode surface [37]. A redox couple is observed in the initial voltammogram and develops over time with a formal potential of around 0.2 V vs Ag/AgCl (pH=7). This activity could be related to redox compounds in BBM, endogenous redox mediators excreted by the biofilm ([38]), or soil components like humic acids [39]). In both cases, the limiting current, around 1 mA, is obtained at -0.4 V vs. Ag/AgCl, when the rate of oxygen reduction exceeds the rate of atmospheric oxygen diffusion to the cathode. This suggests that the biofilm is not providing oxygen or increasing diffusion limitations to the electrode.

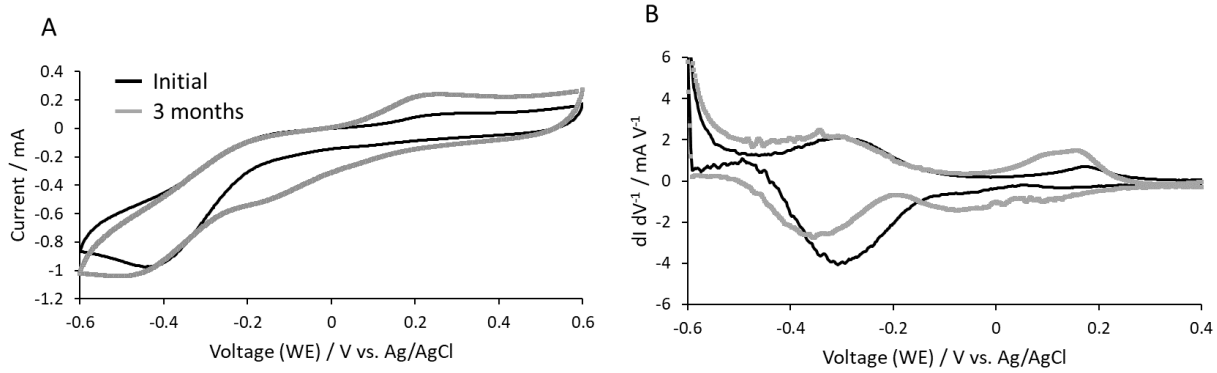

***Figure 8.6**. (A) Cyclic voltammograms of the carbon cloth cathode at the beginning of the experiment (black line) and after three months of operation in an algal catholyte (grey line). (B) First derivative of current with voltage vs. voltage for data shown in (A).*

8.4 Conclusions

Eutrophication of environmental water bodies can seriously compromise ecosystems and could be greatly reduced with early detection of algal blooms. The ceramic soil microbial fuel cell biosensor presented in this study could provide a real time, *in situ* and early detection system of eutrophic events. The sensor signal correlates with dissolved oxygen in water. The development of a cyclic day/night signal, with voltage increasing in the day and decreasing in the night is a straightforward indication of algal activity. Nitrates, oxygen and temperature are the most relevant variables affecting the signal output and optimal resistances improve the sensitivity of the sensor to changes in DO. Biofouling or electrode degradation over three months is not significant, which suggests long-term stability of the sensor signal. This work, therefore, sets the ground for unattended, real time, continuous monitoring of algal blooms *via* electrochemical oxygen reduction. Further work is needed to address the autonomy of the sensor in the field (data logging, transmission and storage).

8.5 Acknowledgments

This work was supported by the UK Engineering and Physical Sciences Research Council (EP/L016214/1) and the Society of Spanish Researchers in the United Kingdom (SRUK). The authors thank Andrew Chapman (University of Bath) for the support in statistical analysis.

8.6 Supplementary information

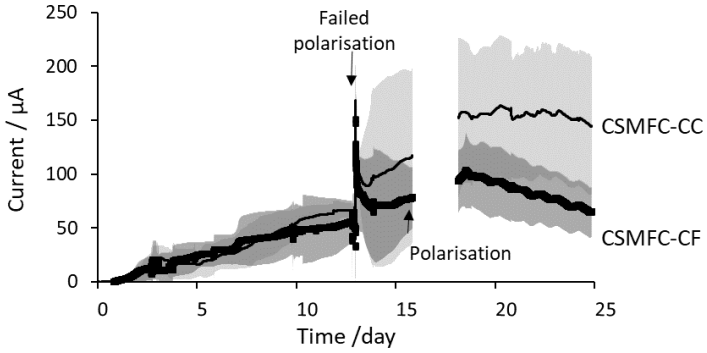

***Figure S8.1**. Enrichment period of the CSMFC operated in tap water with carbon cloth cathode electrodes (CSMFC-CC) and carbon felt cathode electrodes (CSMFC-CF). Shadowed areas correspond to the standard deviation of the mean of three replicates.*

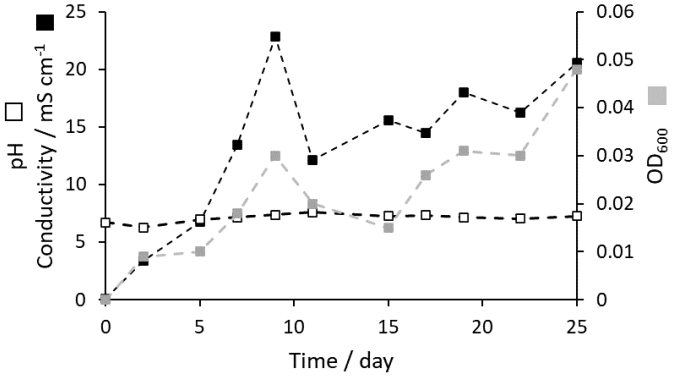

***Figure S8.2**. Crossover of species from the anode to the catholyte over time. pH (white squares), optical density (grey squares) and conductivity (black squares). Results are one replicate.*

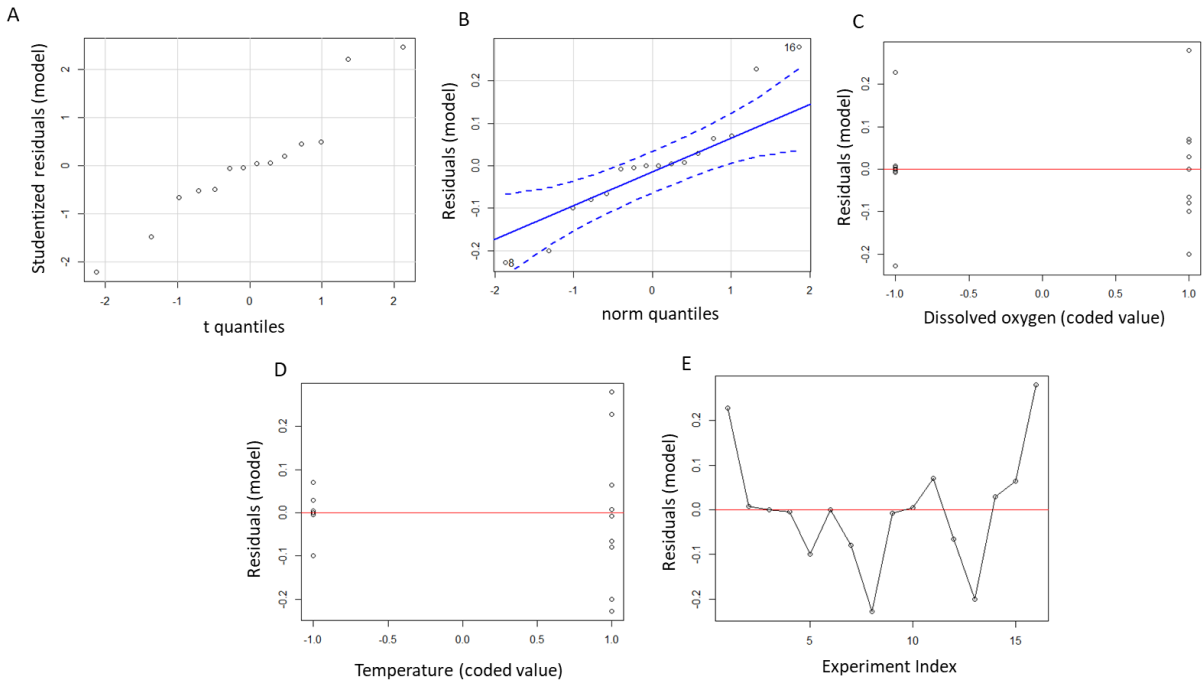

***Figure S8.3**. Resolution III saturated design model assumptions (A) Normality of residuals (B) Independence of residuals. (C and D) Constancy of variance (E) Independence of data.*

8.7 References

[1] EEA, *Nutrient enrichment and eutrophication in Europe's seas*, no. 14. 2019.

[2] M. Lürling and M. Mucci, "Mitigating eutrophication nuisance: in-lake measures are becoming inevitable in eutrophic waters in the Netherlands," *Hydrobiologia*, vol. 9, 2020.

[3] NOWPAP, "Eutrophication Monitoring Guidelines by Remote Sensing for the NOWPAP Region," *CEARAC Rep. 2007. UNEP Reg. Seas*, p. 62, 2007.

[4] Z. Dai *et al.*, "In-situ oil presence sensor using simple-structured upward open-channel microbial fuel cell (UOC-MFC)," *Biosens. Bioelectron. X*, vol. 1, no. 2, p. 100014, 2019.

[5] J. Chouler and M. Di Lorenzo, "Water quality monitoring in developing countries; Can microbial fuel cells be the answer?," *Biosensors*, vol. 5, no. 3. MDPI AG, pp. 450–470, 2015.

[6] K. Kubota, T. Watanabe, H. Maki, G. Kanaya, H. Higashi, and K. Syutsubo, "Operation of sediment microbial fuel cells in Tokyo Bay, an extremely eutrophicated coastal sea," *Bioresour. Technol. Reports*, vol. 6, pp. 39–45, 2019.

[7] L. G. Olias, A. Rodr, P. J. Cameron, and M. Di Lorenzo, "A soil microbial fuel cell-based biosensor for dissolved oxygen," *Electrochim. Acta*, p. 137108, 2020.

[8] K. G. Dunn, "Process Improvement using Data," *http://learnche.org/pid*, 2019. [Online]. Available: learnche.mcmaster.ca/pid.

[9] M. H. McCrady, "STANDARD METHODS FOR THE EXAMINATION OF WATER AND WASTE-WATER (12th ed.)," *Am. J. Public Heal. Nations Heal.*, vol. 56, no. 4, pp. 684–684, 2008.

[10] R. Kakarla and B. Min, "Photoautotrophic microalgae Scenedesmus obliquus attached on a cathode as oxygen producers for microbial fuel cell (MFC) operation," *Int. J. Hydrogen Energy*, vol. 39, no. 19, pp. 10275–10283, Jun. 2014.

[11] S. M. Martinez and M. Di Lorenzo, "Electricity generation from untreated fresh digestate with a cost-effective array of floating microbial fuel cells," *Chem. Eng. Sci.*, vol. 198, pp. 108–116, 2019.

[12] Y. Zhang and I. Angelidaki, "A simple and rapid method for monitoring dissolved oxygen in water with a submersible microbial fuel cell (SBMFC)," *Biosens. Bioelectron.*, vol. 38, no. 1, pp. 189–194, 2012.

[13] G. Pasternak, J. Greenman, and I. Ieropoulos, "Self-powered, autonomous Biological Oxygen Demand biosensor for online water quality monitoring," *Sensors Actuators, B Chem.*, vol. 244, pp. 815–822, 2017.

[14] A. González *et al.*, "Microbial fuel cell with an algae-assisted cathode : A preliminary assessment," *J. Power Sources*, vol. 242, pp. 638–645, 2013.

[15] J. Lobato, A. González del Campo, F. J. Fernández, P. Cañizares, and M. A. Rodrigo, "Lagooning microbial fuel cells: A first approach by coupling electricity-producing microorganisms and algae," *Appl. Energy*, vol. 110, pp. 220–226, 2013.

[16] Z. He, J. Kan, F. Mansfeld, L. T. Angenent, and K. H. Nealson, "Self-sustained phototrophic microbial fuel cells based on the synergistic cooperation between photosynthetic microorganisms and heterotrophic bacteria," *Environ. Sci. Technol.*,

vol. 43, no. 5, pp. 1648–1654, 2009.

[17] X. Y. Wu, T. S. Song, X. J. Zhu, P. Wei, and C. C. Zhou, “Construction and operation of microbial fuel cell with Chlorella vulgaris biocathode for electricity generation,” *Appl. Biochem. Biotechnol.*, vol. 171, no. 8, pp. 2082–2092, 2013.

[18] S. Yousaf, M. Anam, S. Saeed, and N. Ali, “Environmental Technology Reviews Electricigens: source, enrichment and limitations Electricigens: source, enrichment and limitations,” *Environ. Technol. Rev.*, vol. 6, no. 1, pp. 117–134, 2017.

[19] X. Song *et al.*, “Chlorella vulgaris on the cathode promoted the performance of sediment microbial fuel cells for electrogenesis and pollutant removal,” *Sci. Total Environ.*, vol. 728, p. 138011, 2020.

[20] N. Song *et al.*, “Development of a sediment microbial fuel cell-based biosensor for simultaneous online monitoring of dissolved oxygen concentrations along various depths in lake water Science of the Total Environment Development of a sediment microbial fuel cell-based bio,” *Sci. Total Environ.*, vol. 673, no. April, pp. 272–280, 2019.

[21] L. Gonzalez Olias, P. J. Cameron, and M. Di Lorenzo, “Effect of Electrode Properties on the Performance of a Photosynthetic Microbial Fuel Cell for Atrazine Detection,” *Front. Energy Res.*, vol. 7, no. October, pp. 1–11, 2019.

[22] J. Mao, “Oxygen Reduction Reaction Electrocatalysis †,” vol. 1, no. 9, pp. 8785–8789, 2019.

[23] C. T. Wang *et al.*, “Novel bufferless photosynthetic microbial fuel cell (PMFCs) for enhanced electrochemical performance,” *Bioresour. Technol.*, vol. 255, pp. 83–87, 2018.

[24] L. Fu, S. J. You, F. L. Yang, M. M. Gao, X. H. Fang, and G. Q. Zhang, “Synthesis of hydrogen peroxide inmicrobial fuel cell,” *J. Chem. Technol. Biotechnol.*, vol. 85, no. 5, pp. 715–719, 2010.

[25] M. Rezayian, V. Niknam, and H. Ebrahimzadeh, “Oxidative damage and antioxidative system in algae,” *Toxicology Reports*, vol. 6. Elsevier Inc., pp. 1309–1313, 01-Jan-2019.

[26] S. Venkata Mohan, S. Srikanth, P. Chiranjeevi, S. Arora, and R. Chandra, “Algal biocathode for in situ terminal electron acceptor (TEA) production: Synergetic association of bacteria-microalgae metabolism for the functioning of biofuel cell,” *Bioresour. Technol.*, vol. 166, pp. 566–574, 2014.

[27] YSI, “The Dissolved Oxygen Handbook,” *Ysi*, p. 43, 2009.

[28] A. S. Commault, G. Lear, P. Novis, and R. J. Weld, “Photosynthetic biocathode enhances the power output of a sediment-type microbial fuel cell,” *New Zeal. J. Bot.*, vol. 52, no. 1, pp. 48–59, Jan. 2014.

[29] B. E. Logan *et al.*, “Microbial fuel cells: Methodology and technology,” *Environmental Science and Technology*, vol. 40, no. 17. pp. 5181–5192, 2006.

[30] C. Liao *et al.*, “Optimal set of electrode potential enhances the toxicity response of biocathode to formaldehyde,” *Sci. Total Environ.*, vol. 644, pp. 1485–1492, Dec. 2018.

[31] F. F. Ajayi and P. R. Weigele, “A terracotta bio-battery,” *Bioresour. Technol.*, vol. 116, pp. 86–91, 2012.

[32] I. Bardarov, M. Mitov, D. Ivanova, and Y. Hubenova, “Light-dependent processes

on the cathode enhance the electrical outputs of sediment microbial fuel cells ☆," *Bioelectrochemistry*, vol. 122, pp. 1–10, 2018.

[33] S. M. Strycharz-Glaven, R. H. Glaven, Z. Wang, J. Zhou, G. J. Vora, and L. M. Tender, "Electrochemical investigation of a microbial solar cell reveals a nonphotosynthetic biocathode catalyst," *Appl. Environ. Microbiol.*, vol. 79, no. 13, pp. 3933–3942, 2013.

[34] J. González-García, P. Bonete, E. Expósito, V. Montiel, A. Aldaz, and R. Torregrosa-Maciá, "Characterization of a carbon felt electrode: Structural and physical properties," *J. Mater. Chem.*, vol. 9, no. 2, pp. 419–426, 1999.

[35] A. Thamilselvan, A. Samson Nesaraj, M. Noel, and E. J. James, "Effect of chemically treated / untreated carbon cloth: Potential use as electrode materialsin the capacitive deionization process of desalination of aqueous salt solution," *J. Electrochem. Sci. Technol.*, vol. 6, no. 4, pp. 139–145, 2015.

[36] D. Ucar, Y. Zhang, and I. Angelidaki, "An overview of electron acceptors in microbial fuel cells," *Front. Microbiol.*, vol. 8, no. APR, pp. 1–14, 2017.

[37] E. Labelle and D. R. Bond, "Cyclic voltammetry of electrode-attached bacteria.," in *Bio-electrochemical Systems: from extracellular electron transfer to biotechnological application.*, Wiley-VCH Verlag, 2005, pp. 1–15.

[38] E. Marsili, D. B. Baron, I. D. Shikhare, D. Coursolle, J. A. Gralnick, and D. R. Bond, "Shewanella secretes flavins that mediate extracellular electron transfer," vol. 105, no. 10, pp. 6–11, 2008.

[39] Z. Struyk and G. Sposito, "Redox properties of humic acids," *Geoderma*, vol. 102, no. 3–4, pp. 329–346, 2001.

Chapter 9

This Thesis has demonstrated the use of CSMFC sensors to monitor dissolved oxygen in water bodies. The signal output of the CSMFC correlates with the DO in water when the cathodic reduction reaction of oxygen limits the overall electrochemical process. To do so the anode electrode must be larger than the cathode, and oxygen crossover from cathode to anode must be minimised.

In a CSMFC however, the organic matter in the soil would eventually be depleted. A passive and sustained supply of organic matter is therefore necessary to maintain the anodic activity over time. In Chapter 6 it was observed that the algal biomass in the catholyte diffuse into the anode chamber, possibly enriching the soil in organic matter.

Chapter 9 is a preliminary study to evaluate the increase in organic matter in the soil when the catholyte provides algal biomass. In this study, the electrical output of a single-chamber, membrane-less, soil MFC with an algal catholyte was monitored for a year, along with the organic enrichment of the soil, measured as chemical oxygen demand (COD).

The minimum thickness of soil between electrodes to prevent oxygen crossover from affecting the anodic activity is determined by the open circuit voltage (OCV). The OCV indicates the amount of electron donors available for the electrochemical reaction to take place at the anode electrode. In anaerobic conditions, oxygen is not available as an alternative electron acceptor to the electrode, and the OCV is high.

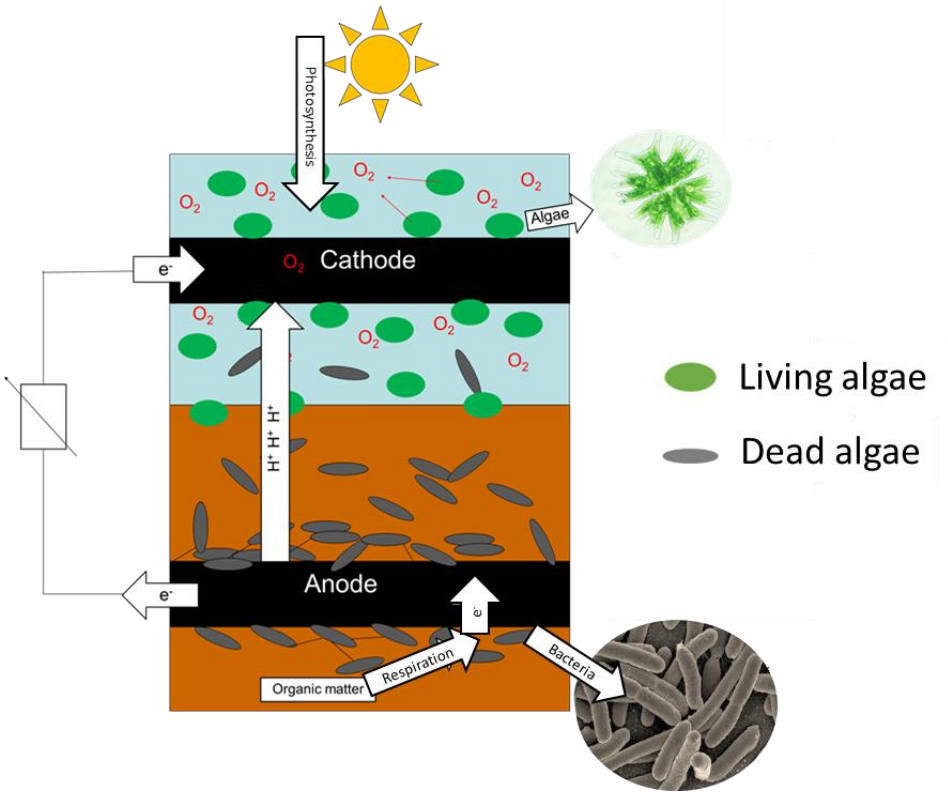
Photosynthesis
O_2
Algae
O_2 Cathode
e⁻
H^+ H^+ H^+
Anode
e⁻
e⁻
Respiration
Organic matter
Bacteria
Living algae
Dead algae

9. Assessment of long-term stability of Photosynthetic Soil Microbial Fuel Cells

Lola Gonzalez Olías, Mirella Di Lorenzo[*]

Centre for Biosensors Bioelectronics and Biodevices (C3Bio) and Department of Chemical Engineering, University of Bath, Claverton Down, BA2 7AY, Bath, UK

Soil MFC sensors are a promising technology for continuous, *in situ* and real time monitoring of water quality. In these, the electrical output, that serves as sensor signal, depends on the rate of anodic bacterial oxidation of organic matter in the soil. A steady supply of organic matter to the soil is therefore required to maintain a stable sensor signal over time. To do so, this study proposes a single-chamber, photosynthetic soil MFC, where algae present in the water enrich the soil in biomass, that provides a steady supply of electron donors to the anode. Despite the adverse effect of photosynthetic oxygen in the anodic activity, the signal output increased steadily over a year, from 1 to 15 mV along with an increase in the soil chemical oxygen demand from 12 to 46 %. Increasing the thickness of the soil between electrodes increases the signal baseline, probably due to reduced oxygen diffusion into the anodic chamber. Soil MFC without algae could not sustain the signal beyond 60 days, stressing the importance of a steady supply of organic matter in soil MFC sensors for long-term monitoring of water quality.

Keywords: Microalgae, Photosynthesis, Soil microbial fuel cell, Water quality monitoring.

9.1 Introduction

Soil Microbial Fuel Cells (MFC) have shown great potential as online sensors for *in situ* monitoring of water quality. A key advantage of these devices over other sensors for environmental applications, is the autonomy of the signal output, self-generated through the anaerobic oxidation of organic matter by electroactive bacteria at the anode [1]. Among soil MFCs, floating soil MFC sensors are particularly interesting for unattended monitoring in field conditions [2]. In a floating soil MFC, the anode is contained in a relatively small quantity of soil [3] where the organic content is eventually consumed, limiting the operational lifetime of the sensor. Ensuring a steady, passive supply of organic matter to the soil over time is therefore key to provide sufficient autonomy for unattended water quality monitoring. A constant load of biomass could be supplied by adding photosynthetic organisms into the system. Algal assisted MFCs have shown great durability and stability over time, thanks to the slow decomposition of algal biomass that provides electron donors to the anode [4, 5].

Nonetheless, the presence of algae also increases the dissolved oxygen concentration, promoting oxygen diffusion to the anode that could poison the electroactive biofilm and decrease the coulombic efficiency. Electrode distance [4] and depth of the anode [6] greatly influence the extent of oxygen crossover.

The long-term stability of algal assisted MFCs has been assessed using large volumes of soil or sediment but, to date, there is no evidence of long-term stability for small self-contained floating soil MFCs [7]. With the aim to improve the long-term operation of soil MFC sensors in the field, this study investigates the effect of algae on the long-term performance of a soil MFC and the influence of anode depth on oxygen crossover into the anode.

9.2 Materials and methods

9.2.1 Materials

All chemicals were purchased from Sigma Aldrich unless otherwise stated and used without further purification. All aqueous solutions were prepared with Millipore denoised water (conductivity= 56 µS cm^{-1}, pH=6.99).

Soil was collected at the margins of the Avon River in Bristol, UK (51°26'47.4"N 2°37'25.1"W), on the 17th of July 2017, around 15 cm below the surface. The sample was stored at 4 ˚C in anaerobic conditions until further use. At the moment of use, the soil had an organic content of 6.72 ± 3.15 % by loss of ignition method (LOI) [8], a pH of 8.04 ± 0.12 and a conductivity of 4.53 ± 0.24 mS cm^{-1}.

Artificial wastewater (AWW) was used as electrolyte and prepared as follows: 270 mg L^{-1} of $(NH_4)_2SO_4$, 60 mg L^{-1} of $MgSO_4 \cdot 7H_2O$, 6 mg L^{-1} of $MnSO_4 \cdot H_2O$, 130 mg L^{-1} of $NaHCO_3$, 3 mg L^{-1} of $FeCl_3 \cdot 6H_2O$ and 4 mg L^{-1} of $MgCl_2$, adjusted to a final pH of 7.56 ± 0.21 with HCl or NaOH 0.1 M and conductivity =1.46 ± 0.35 mS cm^{-1}.

The green microalga *Scenedesmus obliquus* (Dept. of Biology and Biochemistry, University of Bath, UK) was used as the photosynthetic organism. A scooped sample was transferred from an agar plate (1.5% agar in Bold Basal's Medium [9]) into 100 mL of autoclaved AWW. The culture was grown for two weeks in an incubator at 25 ˚C and 12h/12h cycle with white light (5 lm m^{-1}) and natural airflow, under agitation of 180 rpm.

To prepare the catholytes, 75 mL of the algal culture was transferred into a 1 L bottle of AWW to a final cell concentration of 4.5 x 10^5 cells mL^{-1} (Guava Easy Cyte, Millipore). The final pH of the catholyte was 6.75 ± 0.28 and the conductivity 0.97 ± 0.15 mS cm^{-1}.

9.2.2 Soil Microbial Fuel Cells design and operation

To construct the soil MFCs, two acid-treated [6] graphite felt electrodes (Online Furnace Services Ltd., 4 x 4 x 0.7 cm^3; 43.2 cm^2 of total exposed area) were attached to a plastic frame with a fixed electrode distance of 6.4 cm and placed into a 250 mL glass beaker (Figure 9.1A). Soil was added on top of the bottom electrode, operated as the anode. For the long-term stability test, the anode was placed on top of 1 cm and covered by 3 cm of soil (Figure 9.1B). The soil portion of the beaker was covered with tape to prevent light penetration. Then, a volume of 75 mL of catholyte was added on top of the soil, up to the level of the cathode electrode, to ensure both fluidic conductance between the electrodes and access of the cathode to air. Control soil MFCs were constructed in the same conditions but adding 75 mL of AWW as catholyte instead of the algal solution.

To evaluate the effect of anode depth, two soil MFCs were constructed, one with 1 cm (Figure 9.1C) and the other with 3 cm (Figure 9.1D) of soil on top of the anode, named $SMFC_{1cm}$ and $SMFC_{3cm}$. The catholyte volumes were 125 and 75 mL respectively. Tap water was periodically added to compensate for evaporation losses and keep the volume constant.

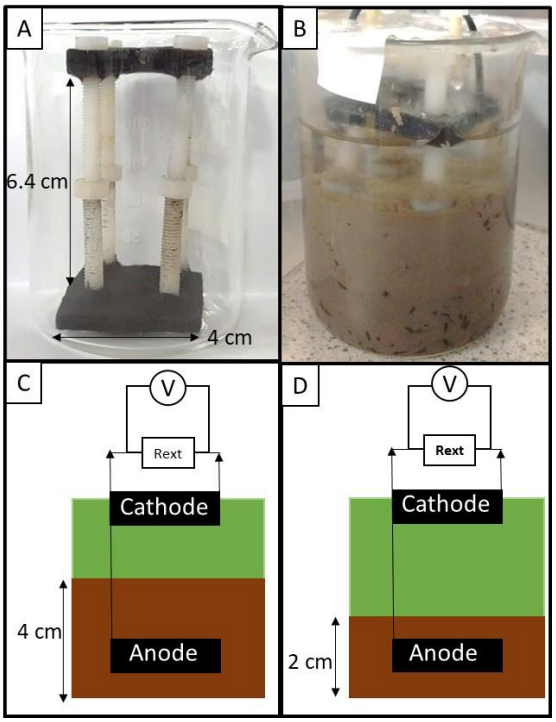

***Figure 9.1**. Set-up of the soil MFC used in this study. (A) Electrodes attached to the plastic frame. (B) Soil MFC with artificial wastewater. (C) and (D) Soil MFC to assess oxygen crossover.*

The electrodes were connected with Ti wires (25 mm, Advent Research Materials, Oxford, UK) to a fixed external resistance (R_{ext}) of 510 Ω and to a data logger (PicoLog High Resolution Data Logger, Pico Technology) to monitor the fuel cell voltage over time. The influence of anode depth, the cells was studied under open circuit voltage (OCV) to assess the influence of alternative electron acceptors like oxygen in the anode.

The soil MFCs were operated in a black box under a 12h/12h light/dark cycles with LED lights (4.8 Wm^{-3} Warm White, 6000K, Lighting Ever, UK). All experiments were carried out at a temperature of 25 ± 3 ℃, open to air.

9.2.3 Methods

Over the course of the experiment, the organic content of the soil was determined with the soluble chemical oxygen demand (sCOD) method. To ensure that the sCOD was not saturated, one gram of the dry soil (dried at 105 ˚C for 24h) was diluted into 5, 10 and 20 mL of DI water, sonicated for 5 min and vacuum filtered with a 0.2 µm Whatman paper. The COD was determined by adding 0.2 mL of the resulting solutions into the commercial vials and digesting it for 2h at 450 ˚C (0-14000 ppm, HANNA Instruments HI 839800 COD reactor). The COD content was then optically determined (HANNA Instruments HI 83224 Wastewater Treatment photometer). The pH was measured with a pH-meter (Thermo Scientific Orion ROSS Ultra pH/ATC Triode, USA), the conductivity was measured with a conductivity cell (Orion, Thermo Scientific) and the dissolved oxygen (DO) of the electrolytes was measured with a DO probe (RDO Orion 7003, Singapore).

9.3 Results and discussion

9.3.1 Influence of algal catholyte in the long-term stability of soil MFCs

Figure 9.2 shows the enrichment curves of the algal assisted soil MFCs, $SMFC_{Algae}$, and the control soil MFCs without algae, $SMFC_{Control}$. The initial voltage is likely a consequence of electron transport from planktonic cells *via* redox mediators, rather an electroactive biofilm, which takes longer to form [10]. From the beginning of the operation, the signal in both systems follows a dark/light cycle, with voltage increasing in the light and decreasing in the dark. This trend is probably caused by a day/night shift in temperature rather than the effect of photosynthetic oxygen in the cathodic reaction, as the cathode surface is exposed to air. During the first days, the DO drops in the catholyte from 12 to 8 mg L^{-1} in $SMFC_{Algae}$ and 8 to 3 mg L^{-1} in $SMFC_{Control.}$, possibly as a result of microbial activity in the soil consuming oxygen in the catholyte. The relatively high DO in the algal catholyte with respect to the control could adversely affect the anode, slowing down the rate of signal increase in $SMFC_{Algae}$ with respect to $SMFC_{Control}$ (0.27 and 1.1 mV d^{-1} respectively) during start up. The maximum voltage is reached after 9 days at 12.9 ± 4.2 mV for $SMFC_{Control}$ and after 12 days at 5.1 ± 2.4 mV for $SMFC_{Algae}$ after which the signal

decays, in both cases, likely due to diffusion limitations. The voltage gradually decays in the $SMFC_{Control}$ over the next month as the diffusion layer thickens at the anode. The rate of decay is faster for the $SMFC_{Algae}$, due to combined diffusion and oxygen crossover limitations [11] (Figure 9.2A).

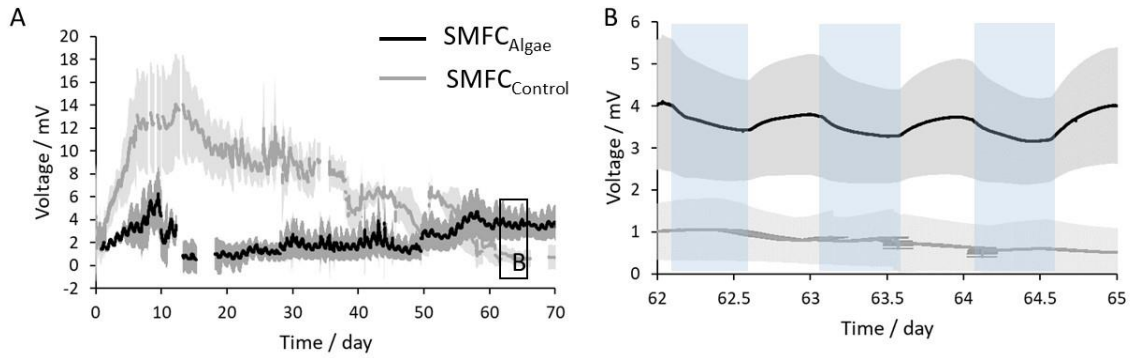

***Figure 9.2**. (A) Signal output over the first three months of operation. (B) Detail of voltage after two months. Grey line and black line correspond to $SMFC_{Control}$, $SMFC_{Algae}$, respectively. Blue areas represent the dark period. Shadowed areas correspond to the standard deviations of two replicates.*

After two months, the signal of the $SMFC_{Control}$ decays to less than 1 mV and losses the signal. The $SMFC_{Algae}$ signal on the other hand reaches 4 mV (Figure 9.2B) and increases steadily up to 15 mV after a year (Figure 9.3A), possibly because the accumulation of algal biomass on the soil surface reduces oxygen crossover and increases the soil organic content, improving the anodic reaction (Figure 9.3B). The sCOD in fact increases from 12.81 ± 9.75 mg_{COD} g^{-1} to 49.46 ± 17.91 mg_{COD} g^{-1} in the $SMFC_{Algae}$ while the sCOD in the $SMFC_{Control}$ was below the limit of detection of the test kit after three months. The sCOD does not indicate the biodegradable fraction of total carbon, but it can be assumed that is partially available for bacterial oxidation [12, 13]. The ability of anodic biofilms to use algal biomass as substrate for electricity production has been widely reported [14, 15]. In $SMFC_{Algae}$, the photosynthetic microorganisms in the catholyte produce oxygen, available for the cathodic reactions. The algal biomass precipitates on the soil surface (Figure 9.3B), enriching it in nutrients over time. Slow decomposition of biomass at the anode releases CO_2 which is again reduced by the algae at the cathode to produce biomass through photosynthesis [16]. As a result, the system enters a synergistic closed loop operation [16]-[18]. Since algae biomass is a

continuous source of organic matter, the $SMFC_{Algae}$ is potentially suitable for long-term deployment in remote locations.

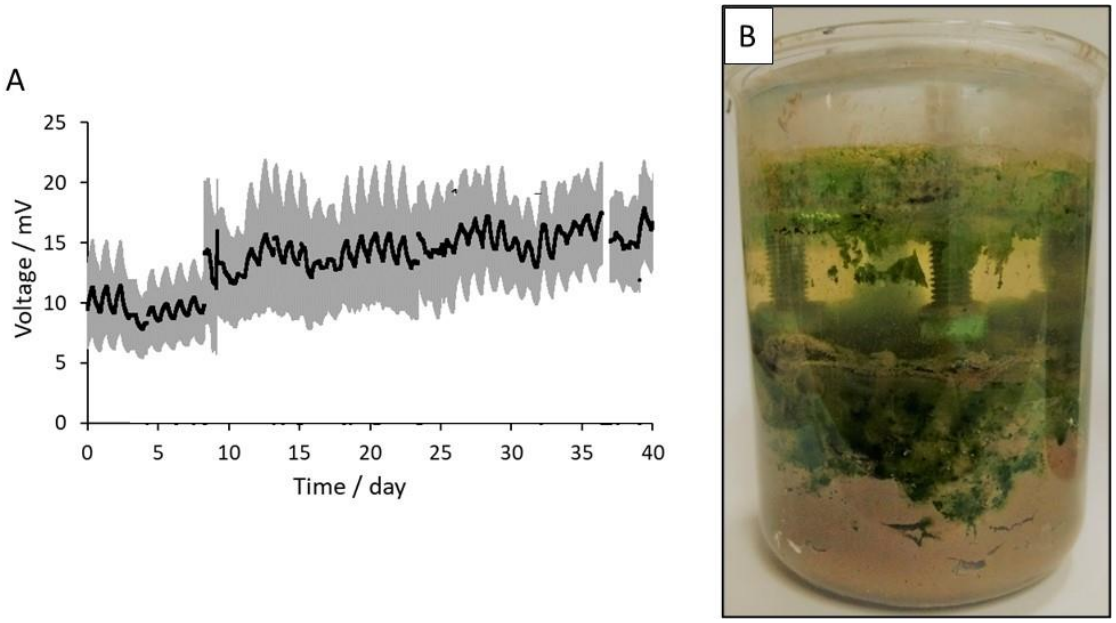

***Figure 9.3**. (A) Voltage output of the $SMFC_{Algae}$ after 10 months of continuous operation. Shadowed areas correspond to the standard deviation of three replicates. (B) Image of the $SMFC_{Algae}$ after a year of operation with a thick layer of algal biomass covering the soil.*

However, the signal stability is low due to changes in the anodic activity. Increasing the anode to cathode electrode area [19], operating the system in intermittent OCV to reduce diffusion limitations, or using a high external resistance [20] could help stabilise the anodic activity and hence, the signal output.

9.3.2 Influence of soil depth

To evaluate the impact of anode depth on the signal output, two CSMFCs were buried below 1 cm and 3 cm of soil ($SMFC_{1cm}$ and $SMFC_{3cm}$). The OCV is an indicator of oxygen crossover into the anode. When oxygen is present in soil, it is consumed in non-electroactive bacterial oxidation, reducing the availability electron donors for the anode in the soil and hence the OCV [21]. Indeed, there is a drastic drop in the OCV when the thickness is reduced from 3 to 1 cm, with 805 mV for the $SMFC_{3cm}$ and 38 mV for the $SMFC_{1cm}$ (Figure 9.4). In $SMFC_{3cm}$, the OCV rises in the day and drops in the night, with a difference of 5 mV between light/dark periods. In $SMFC_{1cm}$ the trend is reversed, with OCV dropping during the

day and rising during the night by a value of 10 mV. The reverse in the trend may be a consequence of oxygen crossover into the anode. The difference seems rather drastic for the small change in thickness, but it agrees with other reports were the current decreased in the light period with a sediment layer of 0.5 cm [22], but increased with 5 cm [23]. An et al. [11] obtained a current density 3.5 times higher when the anode was buried at a depth of 5 cm than 1 cm. Hence, increasing the anode depth improves the overall performance of the soil MFC.

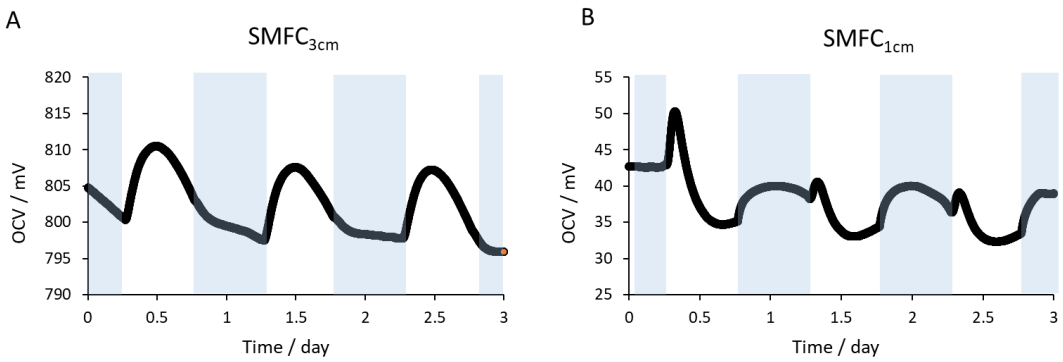

***Figure 9.4**. Influence of thickness layer of soil in the OCV. (A) 3 cm of soil on top of the anode ($SMFC_{3cm}$) and (B) 1 cm of soil on top of the anode ($SMFC_{1cm}$). Shadowed areas represent the night shift. Data is from one replicate.*

9.4 Conclusions

This preliminary assessment reveals that a steady supply of organic matter to the anode is required to sustain unattended and continuous operation of small-scale soil MFC sensors. The addition of living algae in the catholyte provides a source of biomass to the soil (and electron donors to the anode) that maintains a signal for a year, increasing in magnitude over time along with an increase in COD in the soil. In the absence of algae, the signal in the soil MFC drops to zero after two months. The thickness of soil on top of the anode strongly influences the signal pattern, possibly due to oxygen crossover to the anode. These results indicate that 3 cm of soil would be enough to prevent oxygen crossover. The determination of the minimum thickness should be however evaluated in each case as may depend on electrode size, soil characteristics and electrode distance.

9.5 References

[1] J. Babauta, R. Renslow, Z. Lewandowski, and H. Beyenal, “Electrochemically active biofilms: Facts and fiction. A review,” *Biofouling*, vol. 28, no. 8. pp. 789–812, 2012.

[2] A. Schievano *et al.*, “Floating microbial fuel cells as energy harvesters for signal transmission from natural water bodies,” *J. Power Sources*, vol. 340, pp. 80–88, 2017.

[3] L. G. Olias, A. Rodriguez, P. J. Cameron, and M. Di Lorenzo, “A soil microbial fuel cell-based biosensor for dissolved oxygen,” *Electrochim. Acta*, p. 137108, 2020.

[4] Z. He, J. Kan, F. Mansfeld, L. T. Angenent, and K. H. Nealson, “Self-sustained phototrophic microbial fuel cells based on the synergistic cooperation between photosynthetic microorganisms and heterotrophic bacteria,” *Environ. Sci. Technol.*, vol. 43, no. 5, pp. 1648–1654, 2009.

[5] C. Xu, K. Poon, M. M. F. Choi, and R. Wang, “Using live algae at the anode of a microbial fuel cell to generate electricity,” *Environ. Sci. Pollut. Res.*, vol. 22, no. 20, pp. 15621–15635, 2015.

[6] J. An, B. Kim, J. Nam, H. Y. Ng, and I. S. Chang, “Comparison in performance of sediment microbial fuel cells according to depth of embedded anode,” *Bioresour. Technol.*, vol. 127, pp. 138–142, 2013.

[7] T. Ewing, T. Ha, and H. Beyenal, “Evaluation of long-term performance of sediment microbial fuel cells and the role of natural resources,” *Appl. Energy*, vol. 192, pp. 490–497, 2017.

[8] M. H. McCrady, “STANDARD METHODS FOR THE EXAMINATION OF WATER AND WASTE-WATER (12th ed.),” *Am. J. Public Heal. Nations Heal.*, vol. 56, no. 4, pp. 684–684, 2008.

[9] R. Kakarla and B. Min, “Photoautotrophic microalgae Scenedesmus obliquus attached on a cathode as oxygen producers for microbial fuel cell (MFC) operation,” *Int. J. Hydrogen Energy*, vol. 39, no. 19, pp. 10275–10283, Jun. 2014.

[10] Y. Cao *et al.*, “Electricigens in the anode of microbial fuel cells: pure cultures versus mixed communities,” *Microb. Cell Fact.*

[11] J. An, B. Kim, J. Nam, H. Y. Ng, and I. S. Chang, “Comparison in performance of sediment microbial fuel cells according to depth of embedded anode,” *Bioresour. Technol.*, vol. 127, pp. 138–142, Jan. 2013.

[12] B. Neethu and M. M. Ghangrekar, “Electricity generation through a photo sediment microbial fuel cell using algae at the cathode,” *Water Sci. Technol.*, pp. 1–9, 2017.

[13] N. Rashid, Y.-F. Cui, M. Saif, U. Rehman, and J. Han, “Enhanced electricity generation by using algae biomass and activated sludge in microbial fuel cell,” *Sci. Total Environ.*, vol. 456–457, pp. 91–94, 2013.

[14] S. B. Velasquez-Orta, T. P. Curtis, and B. E. Logan, “Energy from algae using microbial fuel cells,” *Biotechnol. Bioeng.*, vol. 103, no. 6, pp. 1068–1076, 2009.

[15] M. J. Salar-García *et al.*, “Microalgae as substrate in low cost terracotta-based

microbial fuel cells: Novel application of the catholyte produced," *Bioresour. Technol.*, vol. 209, pp. 380–385, 2016.

[16] B. Saba, A. D. Christy, Z. Yu, and A. C. Co, "Sustainable power generation from bacterio-algal microbial fuel cells (MFCs): An overview," *Renewable and Sustainable Energy Reviews*, vol. 73. pp. 75–84, 2017.

[17] M. Rosenbaum, F. Aulenta, M. Villano, and L. T. Angenent, "Cathodes as electron donors for microbial metabolism: Which extracellular electron transfer mechanisms are involved?," *Bioresource Technology*, vol. 102, no. 1. Elsevier Ltd, pp. 324–333, 2011.

[18] Z. H. E N H E , † , ‡ J I N J U N K A N , † F L O R I A N M A N S F E L D, "Self-Sustained Phototrophic Microbial Fuel Cells Based on the Synergistic Cooperation between Photosynthetic Microorganisms and Heterotrophic Bacteria."

[19] M. Di, K. Scott, T. P. Curtis, and I. M. Head, "Effect of increasing anode surface area on the performance of a single chamber microbial fuel cell," vol. 156, pp. 40–48, 2010.

[20] G. Pasternak, J. Greenman, and I. Ieropoulos, "Self-powered, autonomous Biological Oxygen Demand biosensor for online water quality monitoring," *Sensors Actuators, B Chem.*, vol. 244, pp. 815–822, 2017.

[21] D. Wang *et al.*, "Open external circuit for microbial fuel cell sensor to monitor the nitrate in aquatic environment," *Biosens. Bioelectron.*, vol. 111, no. March, pp. 97–101, 2018.

[22] Z. He, J. Kan, F. Mansfeld, L. T. Angenent, and K. H. Nealson, "Self-sustained phototrophic microbial fuel cells based on the synergistic cooperation between photosynthetic microorganisms and heterotrophic bacteria," *Environ. Sci. Technol.*, vol. 43, no. 5, pp. 1648–1654, 2009.

[23] I. Bardarov, M. Mitov, D. Ivanova, and Y. Hubenova, "Light-dependent processes on the cathode enhance the electrical outputs of sediment microbial fuel cells ☆," *Bioelectrochemistry*, vol. 122, pp. 1–10, 2018.

Chapter 10

10. General discussion and future work

10.1 Discussion

The aim of this Thesis is to design an affordable, durable sensor for continuous and online monitoring of water quality in environmental waters. Microbial Fuel Cell based sensors are chosen as the most promising technology to this end due to their durability, resilience, cost-effectiveness of the materials and potential autonomy to operate in remote areas. The main improvements needed in MFC sensor technology to realise *in situ*, unattended and online monitoring of water quality in the environment are identified in Chapter 2. These are to: optimise the sensing element/bioreceptor configuration to enhance selectivity and minimise false warnings in field conditions; design portable and autonomous sensors made of robust and cost-effective materials; improve the analysis of the sensor signal to account for a non-steady baseline during operation; and minimise re-calibration and maintenance of the sensor after site deployment. All these aspects have been addressed in this Thesis and will be discussed in this section.

10.1.1 Choice of sensing element/bioreceptor

Toxic events like sewage spills or agricultural leaching are often accompanied by changes in BOD, conductivity and pH. The literature review in Chapter 2 shows that most studies in MFC sensors rely on the anodic biofilm as sensing element. This is because any change in the bacterial electroactivity is rapidly

traduced into a disturbance in the sensor electrical signal. The high sensitivity of bacteria to environmental conditions can however lead to false warnings in field sensors.

When the anode is the sensing element, an increase in BOD in the anolyte improves the anodic oxidation rate of organic matter, subsequently increasing the signal output. In contrast, a toxic compound in contact with the anodic biofilm generally decreases the magnitude of the signal output, as it disrupts the bacterial metabolic pathways associated with electricity generation. These opposite trends could cancel each other, rising the likelihood of overlooking a toxic event (Error Type II). As such, most of the studies in MFC sensors are performed in controlled environmental conditions. When real field conditions are considered, discerning the contribution of the toxic compound from the total signal output becomes challenging. Attempts to solve this issue are to: use a cascade of MFCs where the sequential profile relates to the BOD content and presence of toxicants [1]; use a sequential anode/cathode sensing element to classify the compounds based on the distinctive effect at the anode and cathode [2]; or use a cathode/biocathode as sensing element [3].

The advantages of using the cathode as sensing element are firstly, that the disturbances produced by BOD and toxicants in the signal output follow a trend in the same direction and secondly, that the signal is less sensitive to variations in the environmental conditions. For example, when a heterotrophic biocathode is used, the organic matter acts as an alternative electron donor to the cathodic biofilm, decreasing the signal magnitude. Toxicants disrupt the electrogenic activity of the cathodic biofilm further decreasing the magnitude of the signal. The effects are therefore additive, increasing the chance of Error Type I but decreasing the chance of Error Type II.

As discussed in Chapter 2, the selectivity of the cathodic reduction reaction to a target redox compound can be maximised by selecting an external resistance that matches the reduction potential of the target compound. The specificity of the cathodic sensing element can be further improved by using a selective biofilm. Algal biocathodes are particularly interesting because they rely on

ubiquitous CO_2, are representative organisms of most water bodies and are very sensitive to heavy metals and pesticides.

Hence, Chapter 5 presents the proof of concept of a MFC sensor with an algal biocathode to detect pesticides in water (Objective 1). This work validates the hypothesis that a toxicant affects the biofilm's photosynthetic activity, inducing a measurable change in the sensor signal output. To maximise the sensor sensitivity, the system must be rate limited by the cathode electrode. Two materials, ITO and carbon felt are compared in terms of sensitivity, long-term stability and energy performance of the sensors. The results show an improved sensitivity using carbon felt electrodes, due to enhanced biofilm formation on carbon felt than ITO. The higher surface area and porous microstructure of carbon felt probably facilitated algal attachment to the electrode. However, the energy performance of the sensor is greater for ITO, relative to the electroactive surface area of the electrodes.

10.1.2 Suitable designs for in field water quality monitoring

In Chapter 5, the effect of pesticides in an algal biofilm is evaluated using a lab-based double chamber configuration, known as H-cell. Whether useful for controlled experiments, this configuration is not suitable for real applications: the polymeric membrane is short lived, prone to biofouling and expensive; and the system requires active feeding of electrolytes and nutrients.

To overcome these drawbacks, Chapter 6 presents a novel floating soil ceramic based MFC (CSMFC) sensor (Objective 3). Firstly, the polymeric membrane is replaced by a terracotta vessel, that serves both as separator and container for the anode chamber. Terracotta is a clay-based material widely used in MFC systems for in field applications, thanks to its robustness and low cost [4]. The separation properties of the membrane such as porosity or the cation exchange capacity depend on the composition and thickness of the terracotta [5]. Secondly, the liquid anolyte is replaced by soil, rich in organic matter. Soil provides both the electroactive bacteria to form the anodic biofilm and a slow release of organic matter, that sustains the anodic activity over time. In

addition, bacterial activity in the soil consumes the oxygen infiltrating through the terracotta, keeping the anode biofilm anaerobic.

In Chapter 7, the CSMFC design is tested as an early warning system for hypoxic events. The CSMFC sensors operated autonomously for 3 months, rapidly responding to changes in oxygen, up to a concentration of 6 mg L^{-1} with an error of 0.05 mg L^{-1}. This value is higher than the critical value of DO for aquatic life, around 2 mg L^{-1} and therefore the linear range was sufficient to detect hypoxic events in water bodies [7].

In Chapter 8, the floating CSMFC sensor was further challenged to detect eutrophication, by monitoring changes in the oxygen produced during algal photosynthesis. In this case, the sensor output followed a day/night cycle caused by variations in the photosynthetic oxygen produced by algae. The signal output correlated with DO (R^2=0.66) and algal concentration (R^2=0.63) in the first 11 days of algal growth (Abs_{750}=0.2). The algal concentration could not be estimated at higher values due to agglomeration of microorganisms.

The CSMFC design has the advantages of sediment MFCs with the added benefit of minimal electrode spacing and portability. While the performance of sediment MFCs depends on site conditions (water conductivity, pH, DO and soil BOD), the performance of the CSMFC is independent of the properties of the site under study, which expands the use of sensor in water bodies with different characteristics and facilitates the comparison of results from site to site.

10.1.3 Enhancing the stability of the signal in the field

The stability of the CSMFC signal output to changes in conductivity, pH and DO in environmental waters is enhanced by embedding the anode electrode in soil, inside the terracotta vessel. In this work, soil acts as a solid electrolyte with high conductivity, buffer capacity and high bacterial activity that helps maintaining anaerobic conditions at the anode interface by consuming the oxygen diffusing from the cathode. In addition, the high organic content in soil stabilises the signal output to the BOD content in the tested water. The results in Chapter 6 show that increasing the BOD of the tested water to 20 mg L^{-1}

does not influence the anodic activity in the first 4 h. In contrast, the results of Chapters 6 and 7 show that presence of toxicants or sudden variations in DO, produce rapid disturbances in the signal output.

The CSMFC prototype is thus an efficient tool to detect toxicants in environmental waters.

10.1.4 Effect of oxygen crossover

A catholyte with high DO could negatively affect the performance of the anode. In Chapter 6, the CSMFC sensing element is a cathodic algal biofilm. This study concludes that the small volume of the terracotta vessel, together with the high oxygen content at the algal cathode-terracotta interface increases the oxygen content in the anode chamber. Anodic aerobic conditions affect the electricity generation both by acting as an alternative electron acceptor to the anode electrode and altering the metabolism of strict electroactive bacteria. Consequently, at DO > 9 mg L^{-1} the correlation of the signal output with oxygen reverses from positive to negative. This issue is solved in Chapter 7, by increasing the anode chamber volume (terracotta vessel) and eliminating the algal cathodic biofilm, which reduces the interfacial DO and oxygen flux towards the inside of the vessel.

In Chapter 9 the minimum distance between electrodes to prevent oxygen crossover with an algal catholyte in a membrane-less soil MFC is assessed in terms of the OCV. The OCV indicates the availability of electron donors for the electrochemical oxidation, like acetate or glucose. Oxygen acts as an alternative electron acceptor to the anode, decreasing the OCV [6]. A 4 cm electrode spacing showed an increase in the OCV during the day and a decrease during the night, while 2 cm spacing between electrodes showed the opposite trend and the maximum OCV was reduced from 800 mV to 50 mV, due to the effect of oxygen in the anode.

10.1.5 Linear range: anode to cathode area ratio

In CSMFC sensors, the sensing activity is performed by the cathode electrode, therefore the signal output must be independent of the anodic activity. This

implies that the electrochemical reaction is cathode limited. The linear range of the sensor is therefore the window of current where the cathode dominates the signal. The polarisation curves in Chapter 5 show that the linear range depends on the capacity of the anode, therefore increasing at higher anode to cathode area ratios.

In Chapter 5, the electron flow rate produced by the anodic biofilm is not fast enough to cope with the maximum level of DO under measurement (> 20 mg L^{-1} in photosynthetic systems and 8 mg L^{-1} in freshwater). The signal output saturates, reaching a plateau after which the correlation between the DO and the signal output decreases. In a photosynthetic cathode, the minimum anode/cathode area ratio is achieved when the sinusoidal signal output does not reach a plateau and the correlation value between DO and the voltage output is constant in the range of photosynthetic DO. The minimum anode to cathode area ratio can be also determined from the polarisation curves.

10.1.6 External resistance

The choice of external resistance influences the long-term stability of the signal, power efficiency, likelihood of voltage reversal, sensitivity and response time. The choice is case specific. The procedure developed in this Thesis to select the optimum value of R_{ext} is as follows: firstly, the polarisation curves of the system in steady state indicate the range of current where the cathode potential dominates the cell voltage. The response time and sensitivity of the sensor to changes in the cathodic reaction are maximised when the anode potential is constant throughout the whole window of current.

Secondly, the choice of external resistance depends on the DO at the cathode interface. In photosynthetic systems, oxygen is generated continuously at the cathode. To avoid excessive accumulation of oxygen at the interface that could delay the detection of changes in oxygen production, the external resistance must promote a fast reaction rate. Low values of external resistance are therefore optimal to monitor DO *via* the cathodic reduction of oxygen with an algal biocathode.

In CSMFCs monitoring DO in freshwater, the DO in the bulk water is constant and the double layer thickness increases when oxygen is consumed at the cathode interface. The larger the double layer thickness the less accurate the DO readings. This case is similar to commercial galvanic DO sensors, where stirring of the water under measurement is required to obtain accurate measurements. In this situation, the optimal R_{ext} is close to the maximum power point, to the left of the curve. A high R_{ext} is detrimental for the response time and sensitivity but improves the durability of the anode substrate.

10.1.7 Using algae to replenish organic matter at the anode chamber

The continuous and passive supply of organic matter to the anode is addressed in Chapter 9 (Objective 6). The addition of algae to the soil MFC, enriches it in organic matter and provides oxygen for the cathodic oxidation, improving the electrochemical performance of the sensor. When operating at a fixed external resistance, the soil MFCs with an algal catholyte generates a continuous electrical signal for a year, while in the absence of algae, the soil MFCs lost activity after two months of operation. The increase in COD in soil correlated with an increase of 14 mV in the baseline during a year of operation.

10.1.8 Signal analysis

10.1.8.1 Non-steady baseline

The baseline in a MFC depends on the bacterial activity as well as on the operational factors, being generally unstable in real scenarios. To circumvent this issue, baseline independent performance indicators are required (Objective 2).

Several baseline independent indicators have been evaluated in this Thesis. In Chapter 5, toxicity was assessed in terms of the inhibition ratio, in the short and long term. In Chapter 6, the legal discharge limit concentration of the herbicides Diuron and glyphosate was significantly ($p < 0.01$) detected, based on the change in accumulated charge and accumulated variance before and after the toxic event.

Another approach to deal with unsteady baselines is based on the hypothesis that even if the baseline changes over time, the trends in the signal with respect to variations in the environmental factors are maintained. A model based on Design of Experiments is proposed in Chapter 7 to understand the contribution of each factor and their interferences to the signal response (Objective 4). Chapter 4 describes the fundamentals of the statistical DoE method. In Chapter 7 a fractional DoE in the most relevant environmental factors (temperature, conductivity, pH and dissolved oxygen) is developed to obtain a prediction model for the sensor's electrical response. The results show that the signal output is mostly sensitive to dissolved oxygen, temperature and their mutual interference (Objective 4), while pH and conductivity are comparatively not significant, in the tested conditions. The comparison of the DoE with the one factor at the time (OFAT) method concludes that the model obtained with DoE is more descriptive, based on R^2, RMSE and F-value; due to the better estimation of the variance given by the larger degrees of freedom in the DoE approach over the OFAT method.

10.1.8.2 Calibration model

The predictive model of the factorial design in Chapter 7 is traduced into a calibration model to estimate the DO concentration (Objective 5). Importantly, the calibration model takes into account baseline sifts due to changes in environmental conditions and energy performance. The coefficients of the calibration expression, which are baseline-independent, can be referred to the new baseline with a single-point calibration method, that simply requires measuring the voltage output of the MFC sensor in tap water at 20 ˚C.

10.2 Future work

The findings of this PhD thesis constitute a step towards practical implementation of MFC sensors. Further improvements are still needed to realise long-term, unattended operation. With the aim to provide guidance for future studies, this section indicates strategies to improve the performance of floating MFC sensors with a cathode bioreceptor.

10.2.1 Anode stability

In floating MFCs operating in environmental waters, the anode is often exposed to high concentrations of oxygen, detrimental for energy generation. The use of a solid anolyte would reduce the diffusion of oxygen into the anode, maintaining anaerobic conditions at the biofilm that prevents the non-electrogenic oxidation of organic matter [8]. Alternatively, a large anode to cathode area greatly reduces the sensitivity of the MFC signal to the anodic activity when operated at non-limiting organic content [9].

10.2.2 Organic matter supply

Continuous operation requires a steady supply of electron donors to the anode. Soild anolytes, like growth medium immobilised in agar, can be customised to provide a steady and saturating concentration of organics to the anodic bacteria. By controlling the anolyte composition, the sensors signal can be independent of any varation in the organic content in the water under evaluation. A simple solution would be to integrate a plant in the floating MFC sensor, which continuously excretes organic molecules through the roots. A floating plant ceramic MFC would be a robust, easy to use and cost effective design that could potentially detect a wide range of contaminants, including herbicides and acid rain [10].

10.2.3 Selectivity

Discerning amongst multiple analytes is a challenge in MFC sensors, due to the unspecific response of bacterial metabiolism to toxicity. Combining biofilms with different properties could improve the selective detection of compounds. For example, an anaerobic biofilm inoculated in soil, in the dark, would be sensitive to most contaminants, except herbicides and those specifically targeting photosynthesis. A multi-receptor array could be used to compare the effect of a toxicant on biofilms of different nature, giving information on the compounds porperties based on the distinctive signal response of each sensor in the array. Alternatively, an MFC with a dual anode/cathode bioreceptors would produce a signal with two components, one for each bioreceptor. The signal components could be diffferentiated by introducing a time lag between electrode responses.

Different potentials and operational conditions between electrodes, could promote a shift in the metabolic capabilities of each bioreceptor, improving the selectivity.

10.2.4 Long-term operation

A main limitation of MFC sensors for long-term operation is the irreversible damage of bioreceptors exposed to accute toxicity. Shifts in biofilm population from electroactive to toxicant tolerant bacteria would reduce sensitivity, increase response time and limit of detection and affect baseline stability. The deployment of “latent” sensors, where the bioreceptor is protected from the environment with a solid electrolyte, could improve the long-term unattended operation of single-use MFC sensors. The protective layer would dissolve over time, exposing the bioreceptor to the target water some time after the sensors deployment. The time lag could be controlled with the layer thickness, that would determine the starting time of exposure of the bioreceptor to the water.

10.2.5 Signal treatment

The complexity of the sensors output operating under non-controlled conditions needs efficient signal analysis. Machine learning techniques like multiple regression [11], artificial neural networks [12] or logic gates [13] are statistical models that can describe a moving baseline as a function of changes in the environment. Most environmental parameters follow a circadian pattern, and therefore can be identified and substracted from the signal. Likewise, calibration procedures must identify baseline shifts due to changes in pH, temperature and conductivity. These parameters are frequently monitored in current water quality stations, and can be therefore correlated with shifts in the baseline. A Definitive Saturated Design of Experiments would efficienty determine the major factors impacting the system in a holistic manner, and optimise the predictive power of the calibration model [14].

10.3 Novel designs

The following designs are suggestions to implement some of the future trends identified in the previous section.

10.3.1 Sequential anode/cathode sensing element

A MFC where the analyte contacts the anode and cathode electrode at different times could help distinguishing single electrode signals from the overall sensor output. Figure 10.1 shows a floating soil MFC, immersed in the water under evaluation. Here, analytes in solution touch the cathode, then diffuse across the ceramic and into the soil, finally reaching the anode. The time taken for the analyte to diffuse into the soil produces a sequential signal with a first cathodic component and a time lagged anodic component. The minimum electrode spacing to separate the signals should be used to avoid soil bacteria degrading the pollutant before it reaches the anode.

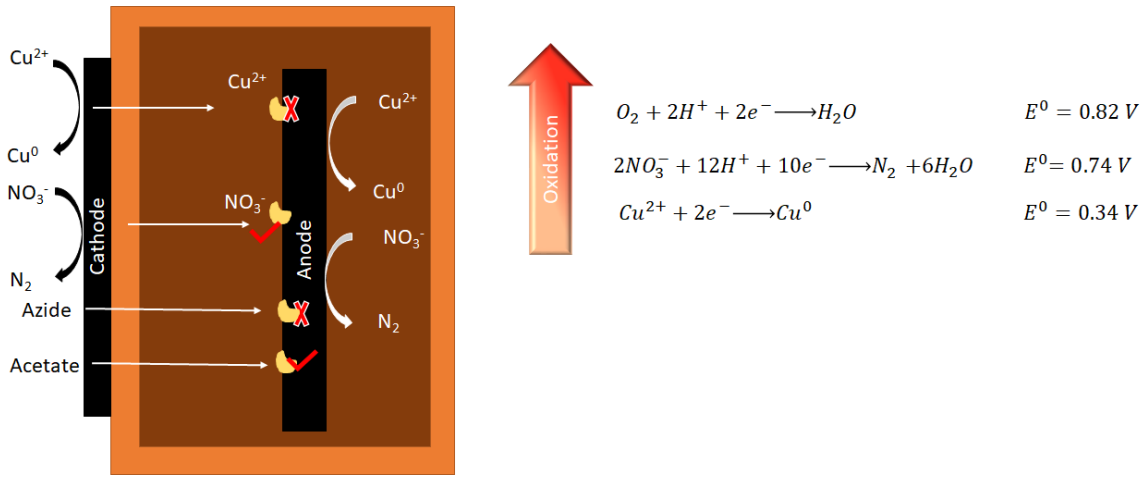

***Figure 10.1**. Example of a floating MFC sensor with dual bioreceptor and ceramic support for selective detection of compounds based on redox properties and bacterial inhibition pathway.*

The response of each electrode could be used to quantify the toxicant redox properties, its biodegradability and effect on the bioreceptor (Table 10.1).

For example, if the analyte is first reduced at the cathode and then inhibits the anodic activity, the signal will display an initial increase in current followed by a decrease. If the redox potential of the toxicant is lower than oxygen it will not be reduced at the cathode, producing a single decrease in the signal. The magnitude of the perturbations would be proportional to the concentration and contact time of the toxicant. Additionally the reversiblitiy of the toxic effect can be based on the short and long- term signal output. The sensitivity of the signal to each component can be modified with the external resistance and relative surface area of each electrode.

Table 10.1. *Possible response of the signal to pollutants in a CSMFC sensor with dual bioreceptor.*

Analyte		Anode oxidation		Abiotic cathode reduction	
		Abiotic	**Biotic**	**Aerobic**	**Anaerobic**
Non-toxic	COD	No	Increase	No	No
	NO3	Decrease	Decrease	No	Increase
Toxic	Cu (II)	Increase	Decrease	No	Increase
	Azide	Increase	Decrease	No	No
	Chromium(VI)	Increase	Decrease	Increase	Increase

10.3.2 Ceramic printed MFC sensors

Paper MFC sensors are a promising technology for single-use testing. Screen-printed sensors are small, portable and easy to handle. Paper substrates degrade fast and the sustainablity is questionable. Ceramic substrates, made of clay, would otherwise provide a stable and porous structure, ideal to improve the robustness of screen printed MFC sensors. The high content of iron in clays would also enhance the reaction rate, improving the performance. The extensive research on the use of ceramic as separators can be put into use for the optimisation of these sensors, in terms of porosity, mechanical strength, electrode modification and composition.

This work presents an MFC sensor to monitor oxygen in water. The sensor is simple in design and can be made with local, natural materials, thus is available to most people. The sensor is self-powered, can operate in most water bodies and does not need complex re-calibration, thanks to the DoE methodology. The affordability of the sensors facilitates the implementation of spatially distributed monitoring networks to provide a geograpical distribution and transport profiles of water pollutants over time. Introducing the idea of “dormant sensor” could improve the long-term unattended operation of environmental water quality.

This Thesis illustrates the importance to use DoE in developing a MFC sensor and provides a new approach to calibrate the sensor efficiently. I hope this work becomes a valuable tool for future studies in environmental water quality monitoring.

10.4 References

[1] M. W. A. Spurr, E. H. Yu, K. Scott, and I. M. Head, “A microbial fuel cell sensor for unambiguous measurement of organic loading and definitive identification of toxic influents,” *Environ. Sci. Water Res. Technol.*, vol. 6, no. 3, pp. 612–621, 2020.

[2] T. Zhao, B. Xie, Y. Yi, and H. Liu, “Sequential flowing membrane-less microbial fuel cell using bioanode and biocathode as sensing elements for toxicity monitoring,” *Bioresour. Technol.*, vol. 276, no. January, pp. 276–280, 2019.

[3] Y. Jiang, P. Liang, P. Liu, D. Wang, B. Miao, and X. Huang, “Biosensors and Bioelectronics A novel microbial fuel cell sensor with biocathode sensing element,” *Biosens. Bioelectron.*, vol. 94, no. February, pp. 344–350, Aug. 2017.

[4] J. Winfield, I. Gajda, J. Greenman, and I. Ieropoulos, “A review into the use of ceramics in microbial fuel cells,” *Bioresour. Technol.*, vol. 215, pp. 296–303, Sep. 2016.

[5] A. N. Ghadge, M. Sreemannarayana, N. Duteanu, and M. M. Ghangrekar, “Influence of ceramic separator’s characteristics on microbial fuel cell

performance," *J. Electrochem. Sci. Eng.*, vol. 4, no. 4, pp. 315–326, Dec. 2014.

[6] D. Wang *et al.*, "Open external circuit for microbial fuel cell sensor to monitor the nitrate in aquatic environment," *Biosens. Bioelectron.*, vol. 111, no. March, pp. 97–101, 2018.

[7] S. S. Hale, G. Cicchetti, and C. F. Deacutis, "Eutrophication and hypoxia diminish ecosystem functions of benthic communities in a New England Estuary," *Front. Mar. Sci.*, vol. 3, no. NOV, pp. 1–14, 2016.

[8] G. Massaglia *et al.*, "In situ continuous current production from marine fl oating microbial fuel cells," *Appl. Energy*, vol. 230, no. July, pp. 78–85, 2018.

[9] Y. Yang, L. Yan, J. Song, and M. Xu, "Optimizing the electrode surface area of sediment microbial fuel cells," *RSC Adv.*, vol. 8, no. 45, pp. 25319–25324, 2018.

[10] T. Li *et al.*, "Swift Acid Rain Sensing by Synergistic Rhizospheric Bioelectrochemical Responses," *ACS Sensors*, vol. 3, no. 7, pp. 1424–1430, 2018.

[11] L. G. Olias, A. R. Otero, P. J. Cameron, and M. Di Lorenzo, "A soil microbial fuel cell-based biosensor for dissolved oxygen monitoring in water," *Electrochim. Acta*, vol. 362, 2020.

[12] Y. Feng, O. Kayode, and W. F. Harper, "Using microbial fuel cell output metrics and nonlinear modeling techniques for smart biosensing," *Sci. Total Environ.*, vol. 449, pp. 223–228, 2013.

[13] Z. Li, M. A. Rosenbaum, A. Venkataraman, T. K. Tam, E. Katz, and L. T. Angenent, "Bacteria-based AND logic gate: a decision-making and self-powered biosensor," *Chem. Commun.*, vol. 47, no. 11, p. 3060, 2011.

[14] D. C. Montgomery, *Design and Analysis of Experiments*, 10th ed. Wiley-VCH Verlag, 2019.